

# Low-Cost and High-Impact Environmental Solutions for Military Composite Structures

PP-1271

*FINAL REPORT*

A Report for  
the SERDP office by



Army Research Laboratory and Drexel University

December 15, 2005





This report was prepared under contract to the Department of Defense Strategic Environmental Research and Development Program (SERDP). The publication of this report does not indicate endorsement by the Department of Defense, nor should the contents be construed as reflecting the official policy or position of the Department of Defense. Reference herein to any specific commercial product, process, or service by trade name, trademark, manufacturer, or otherwise, does not necessarily constitute or imply its endorsement, recommendation, or favoring by the Department of Defense.

# FINAL REPORT

## ESTCP Project: WP-1271

### TABLE OF CONTENTS

		Page
1.0	EXECUTIVE SUMMARY .....	1
2.0	SYNOPSIS OF THE PROGRAM .....	3
3.0	TECHNICAL PROGRESS.....	7
3.1	INTRODUCTION .....	7
3.2	TECHNOLOGY DEVELOPMENT.....	7
3.2.1	Experimental Techniques .....	7
3.2.1.1	Preparation of Vinyl Ester Monomers .....	7
3.2.1.1.1	Epoxy Titration .....	7
3.2.1.1.2	VE Preparation .....	8
3.2.1.1.3	FTIR Characterization of VE Monomers.....	9
3.2.1.1.4	Size Exclusion Chromatography of VE .....	9
3.2.1.1.5	Nuclear Magnetic Resonance Spectroscopy of VE .....	12
3.2.1.2	Rheological Characterization .....	14
3.2.1.3	Cure of VE Resins.....	14
3.2.1.4	Cure Kinetics of VE Resins .....	14
3.2.1.5	Thermal and Mechanical Characterization .....	16
3.2.2	Baseline Measurements .....	16
3.2.2.1	Molecular Weights and Composition.....	16
3.2.2.2	Viscosity of Commercial Resins .....	18
3.2.2.3	Polymer Properties of Commercial Resins .....	18
3.2.2.4	Baseline Styrene Emissions .....	19
3.2.2.4.1	Emissions Mass Loss Measurements.....	19
3.2.2.4.2	Effect of Styrene Content on Emissions .....	21
3.2.2.4.3	Variation in Temperature (T) of the Resin.....	23
3.2.2.4.4	Variation in Depth (D) of the Resin in Test Container .....	24
3.2.2.5	Monitoring of Resin Conditions during Cure .....	25
3.2.2.6	Mechanisms of Styrene Emission .....	28
3.2.2.7	Emissions Modeling.....	29
3.2.2.7.1	Theory .....	29
3.2.2.7.2	Variation in Styrene Content (S) of the Resin ..	32
3.2.2.7.3	Effect of Temperature on Styrene Emissions....	38
3.2.2.7.4	Effect of Aspect Ratio on Styrene Emissions ...	40
3.2.2.7.5	Complete Emissions Modeling from Liquid Vinyl Ester Resins.....	40

**TABLE OF CONTENTS (continued)**

		<b>Page</b>
3.2.3	Reduce Styrene Content in Raw Materials Systems by Use of a Bimodal Molecular Weight Distribution of Vinyl Ester Monomer .....	41
3.2.3.1	Material Properties of Monodisperse VE Resins .....	41
3.2.3.2	Preparation of Bimodal Blends of VE Monomers .....	44
3.2.3.3	Resin Viscosity of Bimodal Blends .....	45
3.2.3.3.1	Effect of Vinyl Ester Molecular Weight and Styrene Content.....	45
3.2.3.3.2	Effect of Temperature .....	52
3.2.3.3.3	Complete Viscosity Model for Vinyl Ester/Styrene Resins .....	55
3.2.3.4	Cure Kinetics and Morphology of Bimodal Blends.....	56
3.2.3.5	Polymer Properties of Bimodal Blends.....	61
3.2.3.6	Styrene Emissions from Bimodal Blends.....	63
3.2.3.6.1	Total Styrene Emission .....	63
3.2.3.6.2	Evaporation Rate.....	64
3.2.3.6.3	Diffusion Coefficient .....	65
3.2.3.6.4	Modeling of Emissions from Bimodal Blends..	66
3.2.3.7	Bimodal VE Conclusions .....	67
3.2.4	Replacing Styrene with Other Reactive Diluents.....	68
3.2.4.1	Di-functional Vs. Monofunctional Reactive Diluents.....	68
3.2.4.2	Petroleum-Based Comonomers.....	69
3.2.4.2.1	Resin Viscosity and Gelation.....	71
3.2.4.2.2	Resin Cure Kinetics.....	74
3.2.4.2.3	Polymer Properties.....	74
3.2.4.2.4	Petroleum-Based Comonomer Conclusions .....	77
3.2.4.3	Fatty Acid-Based Comonomers .....	77
3.2.4.3.1	Synthetic Routes .....	77
3.2.4.3.2	Synthesis .....	80
3.2.4.3.3	Monomer Viscosity and the Effect of Fatty Acid Structure .....	89
3.2.4.3.4	Phase Separation and Cure of Mixtures of Fatty Acid Monomers and Vinyl Ester .....	92
3.2.4.3.5	Resin Viscosity and Gelation.....	99
3.2.4.3.6	Effect of Temperature on Resin Viscosity.....	103
3.2.4.3.7	Complete Viscosity Model for Fatty Acid-Based Vinyl Ester Resins.....	105
3.2.4.3.8	Viscosity of Vinyl Ester Resins Using Both Fatty Acid Monomers and Styrene as Reactive Diluents .....	106
3.2.4.3.9	Viscosity Conclusions.....	109
3.2.4.3.10	Cure Kinetics.....	110
3.2.4.3.11	Polymer Properties.....	112
3.2.4.3.12	E-Beam of Fatty acid-Based Vinyl Esters .....	121
3.2.4.3.13	VE/MFA/Styrene Blends .....	123

**TABLE OF CONTENTS (continued)**

		<b>Page</b>
	3.2.4.3.14 VE 828 MOA- Br-MSA Styrene Polymer Properties .....	134
	3.2.4.3.15 Morphology of Fatty Acid-Based Vinyl Esters.....	136
	3.2.4.3.16 Improvements to Low VOC Fatty Acid Resins .....	144
	3.2.4.3.17 VE/MFA/Petroleum Monomer/Styrene Blends.....	146
	3.2.4.3.18 Cyclized Fatty Acids.....	154
	3.2.4.3.19 Di-Functional Fatty Acid Monomers.....	154
3.2.4.4	VOC Emissions from Fatty Acid-Based Resins .....	154
3.2.4.5	Kinetic Modeling of Fatty Acid Methacrylation Using Glycidyl Methacrylate.....	156
	3.2.4.5.1 Experimental .....	156
	3.2.4.5.2 Results and Discussion.....	157
	3.2.4.5.3 Conclusions.....	161
3.2.4.6	Scale-Up of MFA Production .....	161
	3.2.4.6.1 Introduction.....	161
	3.2.4.6.2 Experimental Procedure.....	161
	3.2.4.6.3 Results/Discussion .....	163
	3.2.4.6.4 Conclusions.....	163
3.2.4.7	Unsaturated Polyester Resins.....	163
	3.2.4.7.1 Introduction.....	163
	3.2.4.7.2 Resin Formulation.....	163
	3.2.4.7.3 Liquid Resin Properties.....	164
	3.2.4.7.4 Polymer Properties.....	166
	3.2.4.7.5 Conclusions.....	171
3.2.4.8	Novalac Type Vinyl Ester (VE 160) - MOA-Br-MSA – Styrene Liquid Resin and Polymer Properties .....	172
	3.2.4.8.1 Introduction.....	172
	3.2.4.8.2 VE 160 - MOA-Br-MSA – Experimental.....	173
	3.2.4.8.3 VE 160 - MOA-Br-MSA – Liquid Resin Properties .....	174
	3.2.4.8.4 VE 160 – Polymer Properties.....	175
	3.2.4.8.5 Comparison of VE 160 and VE 828 Polymer Properties .....	177
	3.2.4.8.6 Conclusions.....	181
3.2.4.9	Fatty Acid Monomer Conclusions .....	182
3.2.5	Low VOC Composites .....	183
	3.2.5.1 Exploratory Composite Work .....	183
	3.2.5.1.1 Resin Formulation.....	183
	3.2.5.1.2 Composite Fabrication .....	183
3.2.5.2	Gel Times .....	186
3.2.5.3	Composite Testing.....	188

## TABLE OF CONTENTS (continued)

		Page
	3.2.5.3.1	Glass Fiber Composites – Preparation and Testing.....188
	3.2.5.3.2	Glass Fiber Composites – Results.....189
	3.2.5.3.3	Carbon Fiber Composites – Preparation .....191
	3.2.5.3.4	Carbon Fiber Composites – Results.....191
	3.2.5.3.5	Effect of MFA Type and Chain Length on Composite Properties .....192
	3.2.5.4	Composite Truck Hood .....193
	3.2.5.4.1	Fiber Lay-Up.....195
	3.2.5.4.2	Resin Infusion .....199
	3.2.5.4.3	Demolding.....200
	3.2.5.4.4	M35-A3 Truck Hood Conclusions.....202
	3.2.5.5	Navy Composite Fabrication.....202
3.2.6		Novel Styrene Suppressant Systems .....205
	3.2.6.1	Commercial Petroleum-Based Dendritic Systems .....206
	3.2.6.1.1	Synthetic Routes .....206
	3.2.6.1.2	Modification of Hyperbranched Polyethyleneimines .....209
	3.2.6.1.3	Modification of Hyperbranched Polyesters ....211
	3.2.6.1.4	Styrene Suppression Efforts.....213
	3.2.6.2	Triglyceride-Based Dendritic Systems.....221
	3.2.6.2.1	Preparation of Fluorinated, Acrylated Triglycerides .....221
	3.2.6.2.2	Triglyceride-Based Dendritic Polymers.....222
3.3		ENVIRONMENTAL IMPACT AND COST SAVINGS ANALYSIS.....224
	3.3.1	Direct Cost.....224
	3.3.1.1	Raw Material Costs .....225
	3.3.1.2	Estimated Resin Costs.....226
	3.3.1.2.1	Fatty Acid-Based Resin Costs.....226
	3.3.1.2.2	Bimodal Blend Resin Costs .....228
	3.3.2	Indirect Cost Analysis .....229
3.4		CONCLUSIONS.....231
4.0		PERFORMANCE ASSESSMENT .....233
	4.1	PERFORMANCE DATA.....233
	4.2	PERFORMANCE CRITERIA .....235
	4.3	DATA EVALUATION .....237
	4.3.1	TF33 Tests I at Barksdale Air Force Base.....237
	4.3.1.1	Particulate Matter Emissions.....237
	4.3.2	T-43 Tests at Randolph Air Force Base .....237
	4.3.2.1	Particulate Emissions .....237
	4.3.3	TF33 Tests II at Barksdale Air Force Base .....238
	4.3.3.1	Particle Emissions .....238
	4.3.4	T63 Tests at Wright-Patterson Air Force Base.....239

## TABLE OF CONTENTS (continued)

	<b>Page</b>
4.3.4.1 Particle Emissions .....	239
4.4 TECHNOLOGY COMPARISON .....	239
5.0 COST ASSESSMENT .....	241
5.1 COST REPORTING .....	241
5.2 COST ANALYSIS .....	241
5.2.1 Implementation Costs for B-52 Aircraft at Barksdale AFB .....	242
5.2.2 Implementation Costs for T-43 Aircraft at Randolph AFB .....	242
5.3 COST COMPARISON .....	242
6.0 IMPLEMENTATION ISSUES .....	243
6.1 COST OBSERVATIONS .....	243
6.2 PERFORMANCE OBSERVATIONS .....	243
6.3 SCALE-UP .....	243
6.4 OTHER SIGNIFICANT OBSERVATIONS .....	243
6.5 LESSONS LEARNED .....	243
6.6 END-USER/ORIGINAL EQUIPMENT MANUFACTURER (OEM) ISSUES .....	243
6.7 APPROACH TO REGULATORY COMPLIANCE AND ACCEPTANCE .....	244
7.0 REFERENCES .....	245
APPENDIX A POINTS OF CONTACT .....	A1

*This page left blank intentionally.*

## FIGURES

		<b>Page</b>
Figure 1.	Lifecycle sources of pollution associated with composite materials processing. Impact originates from initial fabrication, repair, and potential during service. ....	3
Figure 2.	Technical Approach for reducing VOC emissions in vinyl ester resins. ....	4
Figure 3.	Program timeline and completion level. ....	5
Figure 4.	The reaction of methacrylic acid with Epon to form vinyl ester monomer. ....	7
Figure 5.	The FTIR spectra of Epon/methacrylic acid and the resulting vinyl ester formed after complete reaction. ....	9
Figure 6.	The SEC traces for Epon 834 and VE 834. ....	10
Figure 7.	SEC Calibration curve for resin MBBn BBas a function of retention time. ....	11
Figure 8.	Calibration curve relating styrene content measured using SEC to the actual styrene content in the sample. ....	12
Figure 9.	The NMR spectrum of VE 828 with 50 wt% styrene (A) with the peaks labeled to correspond to chemical groups of VE monomer (B) and styrene (C) [1]. Note the definition of m (m=1 represents the lowest possible value of m for DGEBA-based resins). ....	13
Figure 10.	The FTIR spectrum of VE/styrene as a function of cure time. ....	15
Figure 11.	Emissions measurement setup used to measure VOC mass loss as a function of time and temperature. ....	19
Figure 12.	Reproducibility of macro-TGA analysis, 40°C, Derakane 470-300 resin. ....	21
Figure 13.	Mass loss of styrene in the VE 828 resin system as a function of time under 40°C isothermal conditions for four different initial styrene contents. ....	22
Figure 14.	Volatile normalized mass as a function of time. ....	22
Figure 15.	Percentage of styrene as a function of emission time. ....	23
Figure 16.	Fractional mass loss of styrene in the VE 828 resin system having 50% styrene under different isothermal conditions in the study of temperature variation. ....	24
Figure 17.	Fractional mass loss of styrene in the VE 828 resin system under 40°C isothermal conditions in the study of depth variation. ....	25
Figure 18.	Percent volatiles and temperature as a function of cure time. ....	27
Figure 19.	Styrene emission curve for a generalized VE resin system showing the three different regions. ....	28
Figure 20.	An illustration of a VE system initially (left) and the VE after a long time (right). ....	30
Figure 21.	The slope of this plot, $s$ , is used to calculate diffusivity. ....	33
Figure 22.	Plot of evaporation flux and diffusion flux for VE 828/Styrene 50/50 as a function of time under 40°C isothermal conditions for finding the cross-over point. ....	34

## FIGURES (continued)

		Page
Figure 23.	Plot of evaporation flux and diffusion flux with time for finding cross-over point (for $\beta_{10}$ ) in the study of styrene variation of VE 828 resin system under 40°C isothermal conditions. Suffix ‘_Evap’ designates the curves corresponding to evaporation flux. Suffix ‘_Diffusion_C_B10’ designates the curves corresponding to diffusion flux obtained by considering first ten terms ( $\beta_1$ through $\beta_{10}$ ) of the expansion series.....	35
Figure 24.	Comparison of model and experimental values of mass loss behavior of styrene through VE 828/Styrene 50/50 resin system under 40°C isothermal conditions.....	36
Figure 25.	The length-scale modified Crank model accurately models the diffusion regime, as shown for VE 828/Styrene 50/50 at 40°C isothermal conditions. ....	37
Figure 26.	Effect of styrene percentage on evaporation coefficient in the study of temperature variation of VE 828 resin having 50% styrene. ....	38
Figure 27.	Effect of styrene percentage on diffusion coefficient in the study of temperature variation of VE 828 resin having 50 % styrene. ....	39
Figure 28.	The emission profile from VE/Styrene 50/50 at 60°C as measured experimentally and as predicted from the modified Crank model.....	39
Figure 29.	The normalized mass loss as a function of normalized time for different aspect ratios.....	40
Figure 30.	Model predictions vs. experimental results for styrene emissions from VE/styrene 50/50 at 60°C for an aspect ratio of $l_0/D$ of 0.037. ....	41
Figure 31.	The viscosity of vinyl ester resins as a function of the molecular weight of the VE monomer.....	42
Figure 32.	The viscosity of vinyl ester 828 resin as a function of styrene content. ....	42
Figure 33.	The fracture toughness as a function of VE molecular weight for vinyl esters with 40 wt% styrene. ....	43
Figure 34.	The fracture toughness as a function of styrene content for VE 834 and VE 828. ....	43
Figure 35.	$T_g$ as a function of vinyl ester molecular weight for samples with 35% styrene. ....	44
Figure 36.	The resin viscosity as a function of styrene composition for various bimodal VE compositions of VE 828/1007F.....	46
Figure 37.	The resin viscosity as a function of VE $M_n$ and styrene content, showing that resin viscosity is normalized by VE $M_n$ .....	47
Figure 38.	The resin viscosity as a function of VE $M_w$ for resins containing 20 wt.% styrene, showing that resin viscosity is not normalized by VE $M_w$ .....	47
Figure 39.	The bulk viscosities of C5-C16 alkanes and alcohols at 25°C dependence on molecular weight [26]. ....	48
Figure 40.	The resin viscosity as a function of styrene content at constant $M_n$ . Styrene content affects the resin viscosity to the same extent for all bimodal resins with the same $M_n$ , and the effect of styrene content on resin viscosity decreases as $M_n$ decreases.....	49
Figure 41.	The dependence of $M_c(S)$ on the styrene weight fraction in bimodal blends of VE resins.....	50

## FIGURES (continued)

		Page
Figure 42.	The viscosity-temperature dependence is Arrhenius for VE resins with 20 wt% styrene.....	52
Figure 43.	The activation energy for viscous flow as a function of styrene content in VE resins.....	53
Figure 44.	The pre-factor as a function of styrene content in VE resins.....	54
Figure 45.	The activation energy for viscous flow as a function of VE molecular weight....	54
Figure 46.	The conversion as a function of time for Derakane 411-350 resins at 30°C and 90°C.....	57
Figure 47.	The styrene and VE monomer conversions as a function of cure time at 90°C for VE 828-1007F 65/35 with $M_n = 780$ g/mol with 25 wt% and 55 wt% styrene.....	58
Figure 48.	The styrene and VE monomer conversions as a function of cure time at 30°C for monodisperse VE 828 with 30 wt% styrene and 50 wt% styrene. ....	58
Figure 49.	The styrene and VE monomer conversions as a function of cure time at 30°C for VE 828/1004F 43/57 with 30 wt% styrene and 50 wt% styrene. ....	59
Figure 50.	Microgel morphology of vinyl ester resins [8]. ....	60
Figure 51.	$T_g$ and $M_c$ as a function of $M_n$ of bimodal VE blends with 45 wt.% styrene. ....	61
Figure 52.	$T_g$ and $M_c$ as a function of styrene content for bimodal VE 828/1001F 48/52 ( $M_n = 710$ g/mol) and VE 828/1009F 84.9/15.1 ( $M_n = 630$ g/mol).....	62
Figure 53.	Total styrene emission curve for bimodal vinyl ester systems. ....	64
Figure 54.	The diffusivity as a function of vinyl ester molecular weight for bimodal systems.....	65
Figure 55.	Model vs. experimental emissions profile for VE 828/1004F 43/57 + 30% styrene.....	66
Figure 56.	The molecular structure of tested petroleum-derived styrene replacements for VE resins. ....	70
Figure 57.	The vapor pressure of styrene, cyclohexyl methacrylate, and isobornyl methacrylate as a function of temperature as calculated with the Antoine Equation. ....	71
Figure 58.	The viscosity of VE resins as a function of gel time and comonomer. VE/HDDA results are very similar to VE/HDDMA results and are omitted for clarity.....	72
Figure 59.	The viscosity of VE 828 resins as a function of styrene and HDDMA content at 30°C.....	73
Figure 60.	The viscosity as a function of gel time for VE/HDDMA/styrene blends at 30°C.....	73
Figure 61.	The overall conversion as a function of time for CHMA-based vinyl esters relative to styrene-based vinyl esters. ....	74
Figure 62.	The storage modulus as a function of temperature for VE/HDDMA/styrene blends. ....	75
Figure 63.	The loss modulus as a function of temperature for VE/HDDMA/styrene blends. ....	75
Figure 64.	The loss modulus as a function of temperature for VE/HDDA relative to VE/HDDMA and VE/styrene. ....	76

## FIGURES (continued)

		Page
Figure 65.	The DMA behavior of VE/CHMA and VE/IBMA resins relative to VE/styrene.....	76
Figure 66.	The proposed synthetic routes to produce fatty acid-based monomers [43]. .....	79
Figure 67.	The mid IR spectra of MOA (oleic acid) after reaction.....	80
Figure 68.	Acid number measurements during reaction at 90°C for the synthesis of Methacrylated Lauric Acid (MLau).....	82
Figure 69.	Reaction of Lauric Acid with Glycidyl Methacrylate to form MLau. Methacrylated lauric acid (MLau) (●) 0 min, (■) 90 min ( ), Glycidyl methacrylate, ( ) Pure lauric acid. ....	83
Figure 70.	Shift of the peak of the ( ) Pure lauric acid to ( ) Methacrylated lauric acid.....	83
Figure 71.	The peak shift of the Methacrylated fatty acids (MFA) with increasing chain length of fatty acids, methacrylated Myristic acid (●), methacrylated lauric acid (■), methacrylated capric acid (▲), methacrylated caprylic acid ( ), methacrylated caproic acid ( ), methacrylated butyric acid( ). .....	84
Figure 72.	The reaction scheme for the synthesis of 9-10 di-bromo stearic acid glycidyl methacrylate (Di-Br MSA) from oleic acid.....	85
Figure 73.	The <sup>1</sup> H-NMR spectra of (a) oleic acid (b) 9,10 di-bromo stearic acid(Di-BrSA).....	86
Figure 74.	The <sup>1</sup> H-NMR spectrum of dibromo stearyl glycidyl methacrylate (Di-BrMSA).....	87
Figure 75.	The viscosities of the Di-BrOA and Di-BrMSA as a function of temperature.....	91
Figure 76.	Viscosity of MFA monomers as a function of fatty acid chain length. ....	92
Figure 77.	The FTIR spectra of VE/AOH-SBO with CoNap at t=0 and t=6 days.....	93
Figure 78.	The molecular structure of acrylated soybean oil. ....	94
Figure 79.	The FTIR spectra at t=0 and t=12 days for the induced cure of VE in the presence of FAME and CoNap. ....	95
Figure 80.	The extent of cure of VE as a function of time in the mixture of VE, FAME, and CoNap. There are two x-axes in order to show both the short-term VE cure and the long-term VE cure.....	96
Figure 81.	The molecular structure of epoxidized fatty acid methyl esters. ....	96
Figure 82.	The viscosity of VE/GM-OA resins as a function of cure time.....	100
Figure 83.	The viscosity of VE/MFA as a function of fatty acid chain length at 25°C. ....	100
Figure 84.	Viscosity of VE resin as a function of MFA content for MLau fatty acids, showing the exponential fit to the data. ....	101
Figure 85.	Viscosity of VE resin as a function of MLau content, showing the exponential fit to the data.....	102
Figure 86.	The MFA coefficient in Eq. 18 is a linear function of MFA viscosity.....	103
Figure 87.	The activation energy as a function of diluent content and fatty acid type. ....	104
Figure 88.	The pre-exponential constant as a function of diluent content and fatty acid type.....	105

## FIGURES (continued)

		Page
Figure 89.	The minimum MFA content required to achieve VE resin viscosities below 500 cP as a function of temperature, fatty acid chain length, and unsaturation level. The operating window is any MFA content above the curve. Legend: [Carbon atoms:Unsaturation sites].....	106
Figure 90.	The viscosity of VE/MHex/styrene as a function of styrene content in the resin for resins containing 55 wt% and 65 wt% VE 828, along with model predictions.....	107
Figure 91.	The experimental and model viscosities of VE/MHex/Styrene as a function of VE molecular weight and VE content for resins containing 20 wt% styrene.....	108
Figure 92.	The experimental and model viscosities of VE/MLau/Styrene as a function of temperature.....	108
Figure 93.	The minimum styrene content required to achieve VE resin viscosities below 500 cP as a function of fatty acid chain length, VE content, and VE molecular weight at 30°C. The operating window is any styrene content above the curve for any molecular weight along the curve. Legend: [Carbon atoms: Unsaturation sites]. .....	109
Figure 94.	The conversion as a function of time for the homopolymerization at 90°C of MFA with 0, 1, and 2 residual unsaturation sites and their autocatalytic fit.....	110
Figure 95.	The overall conversion as a function of time for the cure of VE/MFA relative to VE/styrene and their autocatalytic fits using 45% reactive diluent. Samples were cured at 90°C and post-cured at 120°C once the cure reaction stopped.....	111
Figure 96.	The individual cure kinetics of the components of VE/styrene and VE/MLau, each containing 45% reactive diluent.....	112
Figure 97.	Normalized Loss (a) and storage modulus (b) behavior of Methacrylated Fatty Acids (MFA) as a function of fatty acid chain length. Methacrylated Palmitic acid (●), Methacrylated Myristic acid (□), Methacrylated Lauric acid (▲), Methacrylated Decanoic acid ( ), Methacrylated Octanoic acid ( ), Methacrylated Hexanoic acid(Δ), Methacrylated Butyric acid ( O ).....	114
Figure 98.	Major (●) and Minor (□) Glass Transition Temperatures (T <sub>g</sub> ) of the Methacrylated Fatty Acids (MFA).....	116
Figure 99.	Loss (a) and Storage (b) modulus of 55 wt% VE with 45 wt% MFA. MBut (x), MHex (●), MOct (□), MLau (▲), MMyr(■).....	117
Figure 100.	Glass transition temperature behavior changes with increasing chain length of VE samples with 45 wt% MFA as determined by experiment and as predicted by the Fox Model.....	118
Figure 101.	The fracture toughness of the 55%VE/25% MFA/20% Styrene ternary blends at increasing fatty acid chain lengths.....	120
Figure 102.	The fracture toughness of VE/MBut/Styrene ternary blends containing 55% VE as a function of styrene content.....	121
Figure 103.	The extent of cure of fatty acid-based vinyl esters, comparing thermal cure to E-beam.....	122

## FIGURES (continued)

		Page
Figure 104.	The effect of post-cure on the conversion of E-beam cured VE/MFA polymers.....	122
Figure 105.	The storage modulus and $T_g$ of fatty acid-based vinyl esters cured thermally and via E-beam. ....	123
Figure 106.	The viscosity of VE/MLau/styrene as a function of styrene content in the resin for resins containing 55 wt% and 65 wt% VE 828. ....	124
Figure 107.	Viscosity of methacrylated butyric acid ( $\times$ ), methacrylated caproic acid ( $\circ$ ), methacrylated caprylic acid ( $\Delta$ ), methacrylated lauric acid ( $\blacksquare$ ) changes with increasing styrene content from 0 weight % to 45 weight % and 55 weight % vinyl ester monomer, at 24°C .....	125
Figure 108.	The conversion as a function of time for the cure of VE/MLau/Styrene 65/15/20 relative to VE/MLau 65/35 and VE/styrene 65/35. Samples were cured at 90°C.....	126
Figure 109.	DMA behavior of VE/MOA/styrene with 65 wt% VE 828.....	127
Figure 110.	The storage modulus as a function of styrene content for VE/MOA/styrene blends. ....	127
Figure 111.	$T_g$ as a function of styrene content for VE/MOA/styrene blends. ....	128
Figure 112.	The Fox equation can be used to predict $T_g$ of blends of VE, MLau, and styrene. ....	129
Figure 113.	Loss modulus (MPa) behavior of 55 weight% VE and 45 weight% of methacrylated butyric acid and styrene combination. 45 wt% MBut ( $\blacktriangle$ ), 35 wt% MBut & 10 wt% Styrene ( $\circ$ ), 30 wt% MBut 15 wt% Styrene ( $\Delta$ ), 25 wt% MBut & 20 wt% Styrene ( $\blacksquare$ ), 45 wt% Styrene ( $\bullet$ ). ....	130
Figure 114.	Loss modulus (MPa) behavior of 55 weight% VE and 45 weight% of methacrylated lauric acid and styrene combination. 45 wt% MLau ( $\Delta$ ), 35 wt% MLau & 10 wt% Styrene ( $\blacksquare$ ), 30 wt% MLau 15 wt% Styrene ( $\circ$ ), 25 wt% MLau & 20 wt% Styrene ( $\blacktriangle$ ), 45 wt% Styrene ( $\bullet$ ). ....	130
Figure 115.	Loss modulus (MPa) behavior of 55 weight% VE and 45 weight% of methacrylated caproic acid and styrene combination. 45 wt% MHex ( $\Delta$ ), 35 wt% MHex & 10 wt% Styrene ( $\blacktriangle$ ), 30 wt% MHex 15 wt% Styrene ( $\circ$ ), 25 wt% MHex & 20 wt% Styrene ( $\bullet$ ), 45 wt% Styrene ( $\blacksquare$ ).....	131
Figure 116.	Glass transition temperature ( $T_g$ ) of 55 weight% vinyl ester and 45 weight% of acids with styrene. MBut ternary blends ( $\circ$ ), MHex ternary blends ( $\times$ ), MOct ternary blends ( $\Delta$ ), MLau ternary blends ( $\blacksquare$ ). ....	132
Figure 117.	The flexural properties as a function of styrene content for resins containing 55% VE and using MLau and styrene as the reactive diluent. The open points show the results for Derakane 411-350.....	133
Figure 118.	$G_{IC}$ of VE/MLau/styrene as a function of styrene content in the resin for resins containing 55 wt% and 65 wt% VE 828.....	134
Figure 119.	The chemical structure of ortho- tetra bromo-diglycidyl ether of Bisphenol A (DGEBA). ....	135
Figure 120.	The loss modulus as a function of temperature for MLau, MLin, and styrene based vinyl esters using 35% reactive diluent. ....	137

## FIGURES (continued)

		Page
Figure 121.	The loss modulus as a function of temperature for ternary blends of VE/MLau/Styrene and VE/MLin/Styrene with weight ratios of 65/15/20. ....	137
Figure 122.	The width of the $\tan \delta$ peak at half-height for VE and VEA resins using 45% reactive diluent (MLau and styrene) as a function of styrene content. ....	138
Figure 123.	The loss modulus as a function temperature for VE/MLau/Sty and VEA 55/15/30. ....	139
Figure 124.	The molecular weight between cross-links for VE/MLau, VEA/MLau, and VE/styrene polymers. ....	139
Figure 125.	The overall conversion of VE/MLau is similar to that of VEA/MLau for resins containing 45 wt% MLau. ....	140
Figure 126.	The component and overall cure of VEA/MFA/Styrene 65/15/20. ....	140
Figure 127.	Component and overall cure of VE/MFA/Styrene 65/15/20. ....	141
Figure 128.	Optical image of VEA/MLau 65/35 at 50x magnification. ....	142
Figure 129.	Optical image of VEA/MLin 65/35 at 50x magnification. ....	142
Figure 130.	The flexural strength as a function of styrene content for MHex and MLau-based resins. ....	145
Figure 131.	The flexural modulus as a function of styrene content for MHex and MLau-based resins. ....	146
Figure 132.	Viscosity as a function of mono-functional resin formulation for resins with 65% CN151. ....	148
Figure 133.	Viscosity as a function of di-functional resin formulation for resins with 55% CN151. ....	149
Figure 134.	The storage modulus and loss modulus as a function of temperature for VE/MLau/Styrene/CHMA 55/15/15/15 and VE/MLau/Styrene/CD550. ....	151
Figure 135.	Storage modulus as a function of mono-functional monomers for resins with 55% CN151, 15% MLau, 10% low VOC petroleum monmomer, and 15% Styrene. ....	151
Figure 136.	$T_g$ as a function of low VOC mono-functional monomers for resins with 55% CN151, 15% MLau, 10% low VOC petroleum monmomer, and 15% Styrene. ....	152
Figure 137.	Modulus as a function of low VOC di-functional monomer for resins containing 55% CN151, 15% MLau, 10% low VOC petroleum monomer, and 20% styrene. ....	152
Figure 138.	$T_g$ as a function of resin formulation for of low VOC di-functional monomers containing 55% CN151, 15% MLau, 10% low VOC petroleum monomer, and 20% styrene. ....	153
Figure 139.	The percentage mass change as a function of time for MFA monomers. ....	155
Figure 140.	The normalized mass loss as a function of time for vinyl esters containing 50 wt% vinyl ester monomers and 50 wt% reactive diluent. ....	156
Figure 141.	Methacrylated fatty acid synthesized from lauric acid and glycidyl methacrylate with AMC-2 catalyst. ....	157
Figure 142.	Representative plots of $\ln(dE/dt)$ vs. $[E]$ for experiments conducted at 80°C for four catalyst concentrations. ....	158
Figure 143.	Plot of $\ln[k']$ versus $\ln[C]$ for the four temperatures investigated. ....	159

## FIGURES (continued)

		Page
Figure 144.	Plot of $\ln(k)$ versus $1/T$ used to determine $E_a$ and $A_0$ .....	159
Figure 145.	Plot showing a change in concentration $[E]$ as a function of time for both model and experimental data at varying $[C]$ for data obtained at $60^\circ\text{C}$ .....	160
Figure 146.	Plot showing a change in concentration $[E]$ as a function of time for both model and experimental data at varying $[C]$ for data obtained at $80^\circ\text{C}$ .....	161
Figure 147.	The viscosity of the of the 45 wt.% MOA-55 wt.% UP resin as a function of temperature. ....	165
Figure 148.	The viscosity of the of the 20 wt.% Br-MSA-15wt% Styrene-55wt% UPE resin and the 30 wt.% Br-MSA-15wt% Styrene-55wt% UP Eas a function of temperature. ....	166
Figure 149.	The tan delta curves of Viapal-MOA-Styrene polymers at 10-30 wt.% MOA content. (45 wt.% total comonomer content).....	168
Figure 150.	The tan delta curves of Viapal-MOA-Styrene and Viapal-Br-MSA-Styrene Polymers at (a) 20 wt.% and (b) 30 wt.% fatty acid comonomer content. ....	169
Figure 151.	The tan delta curves of Viapal-MOA-Styrene polymers at 10-20 wt.% MOA content. (35 wt.% total comonomer content).....	171
Figure 152.	The tan delta curves of Viapal-MOA-Styrene and Viapal-Br-MSA-Styrene Polymers at 15 wt.% fatty acid comonomer content. ....	171
Figure 153.	The synthesis of VE 160 from Epon 160 and methacrylic acid. ....	173
Figure 154.	(a) The change in the viscosity of VE 160-MOA and VE 160-Br-MSA resins with increasing temperature (b) magnified in the 0-5000 cP viscosity range.....	175
Figure 155.	The loss modulus curves of the (a) 35 wt.% styrene (b) 35 wt.% MOA and Br-MSA-VE 160 polymers. ....	178
Figure 156.	Comparison of (a)the $T_{gs}$ (tan delta max)and (b) $E'(30^\circ\text{C})$ of the post-cured VE 160 and VE 828 resins containing MOA, Br-MSA, and Styrene as reactive diluents. ....	179
Figure 157.	Comparison of (a) the $T_{gs}$ (tan delta max) and (b) $E'(30^\circ\text{C})$ of the post-cured MBut, MHex-VE 160 and VE 828 resins. ....	180
Figure 158.	Schematic representation of the VARTM process used to fabricate composites in this work. ....	184
Figure 159.	Photographs of the VARTM process.....	184
Figure 160.	Photograph of the composites produced from VARTM.....	185
Figure 161.	The gel time for CN-151/MLau/Sty 65/15/20 as a function of cure temperature, inhibitor, initiator, and catalyst contents.....	187
Figure 162.	Flexural modulus for commercial resins and low VOC formulations using 9 oz glass fiber reinforcement. ....	189
Figure 163.	Flexural strength for commercial resins and low VOC formulations using 9 oz glass fiber reinforcement. ....	190
Figure 164.	Short bean shear strength for commercial resins and low VOC formulations using 9 oz glass fiber reinforcement. ....	190
Figure 165.	DMA scans of composites with $G'$ -sized AS4 carbon composites with low VOC resins and Derakane 411-C50.....	192
Figure 166.	Commercial hood fabricated by Sioux Manufacturing Corp. mounted on M35-A3 truck.....	194

## FIGURES (continued)

		Page
Figure 167.	Bottom view of the hood with the stiffeners.....	195
Figure 168.	The tool used for fabricating the composite hood. ....	195
Figure 169.	Photograph showing the two rows of tacky tape, the breather cloth, and the method with which the inlet and outlet lines enter the inner mold area. ....	196
Figure 170.	The schematics of the composite hood. ....	197
Figure 171:	The composite hood lay-up showing the three inlet lines and two vacuum lines. ...	198
Figure 172.	Photograph of the mold after bagging. ....	199
Figure 173.	The resin infused fairly uniformly except that it race-tracked at the foam stiffeners.....	200
Figure 174.	The completed low VOC composite hood.....	201
Figure 175.	Photograph of the inside of the low VOC truck hood after painting with the low VOC CARC. ....	202
Figure 176.	Lay-up of hat-stiffened structure showing the PVC foam hats and the E-glass woven roving mats. ....	203
Figure 177.	Lay-up of hat-stiffened structure showing the complex bagging geometry and multiple feed ports and vacuum lines used. ....	204
Figure 178.	Hat-stiffened structure showing the final hat-stiffened structure and a close-up of the hat-stiffened area. ....	205
Figure 179.	Potential methods of end-group modification. Routes I (Michael addition) and II (epoxide opening) are more suited to the PEI end-groups, while routes III (acyl condensation) and IV (halide displacement) should be applicable to either system. ....	207
Figure 180.	Synthetic scheme for modification of branched PEIs.....	209
Figure 181.	Preparation of PEI-PDMS suppressants. ....	211
Figure 182.	Melt condensation for modified hyperbranched polyesters. Boltorn HBP is first functionalized with dodecanoic and perfluorooctanoic acids. Thioacetic acid may be added to incorporate thiol end groups, or the polymer may be isolated and functionalized with ring-opened succinic anhydride in a second step to generate acid end groups. ....	212
Figure 183.	VOC Suppression as a function of Styrid concentration in 1:1 styrene-VE formulation.....	214
Figure 184.	PEI-based suppressant candidates.....	215
Figure 185.	Emissions performance of polyester based suppressant candidates at 2% loading. ....	217
Figure 186.	New end groups for PEI scaffolds. ....	218
Figure 187.	Emissions as a function of time from a VE/Styrene 50/50 resin showing that HB-polypropylene is not an effective suppressant and temperature control is paramount. ....	219
Figure 188.	Results of two component suppressant efforts. Trials with 2 component additives showed greater dependence upon oven temperature than additive composition (e.g. component A molecular weight variation).....	220
Figure 189.	Disulfide bond formation (top) and carboxylic acid.....	221

## FIGURES (continued)

	<b>Page</b>
Figure 190. Potential methods of producing AB <sub>2</sub> monomers from triglycerides and fatty acids. In Route 1, epoxidized triglycerides are modified with cyclohexyl amine. In Route 2, linoleic acid is reacted to form epoxidized linoleic acid.....	223
Figure 191. The SEC traces of epoxidized linoleic acid compared to that of hyperbranched polymers derived from epoxidized linoleic acid and epoxidized soybean oil.....	224
Figure 192. PND as a Function of Power Setting for T-43 Engines 608 and 636. ....	234
Figure 193. PND as a Function of Power Setting for T-43 Engines 607 and 613. ....	235

## TABLES

		<b>Page</b>
Table 1.	Low VOC composites team members .....	6
Table 2.	Epoxy equivalent weight as determined by epoxy titration and literature values. .	8
Table 3.	The literature/known and experimentally determined (NMR) VE molecular weights and styrene contents for VE resins. ....	17
Table 4.	Styrene content in commercial resins as measured using HPLC.....	17
Table 5.	The molecular weight of commercial resins calculated using SEC.....	18
Table 6.	The viscosity of commercial resins at 30°C. ....	18
Table 7.	The polymer properties of postcured and non-postcured Derakane neat resins. .	19
Table 8.	Cases Considered to Study the Effect of Variation in Depth of Resin on Emission Behavior of Styrene. ....	24
Table 9.	Resin compositions for emissions measurements during cure experiments. ....	26
Table 10.	The calculation variables for VE 828 resin system tested under 40°C isothermal conditions in the study of styrene variation. ....	32
Table 11.	The experimentally determined VE molecular weights and styrene contents. The styrene contents are the experimentally determined and the initial weight fraction styrene (prepared) in the reaction mixture of the prepared VE. The VE $M_n$ was calculated using the epoxy titration molecular weight results.....	45
Table 12.	The minimum allowable styrene content to achieve a viscosity of 500 cP or lower for various values of the number average molecular weight of the VE monomers.....	51
Table 13.	The calculated styrene content as a function of VE molecular weight and temperature that is required to achieve $\eta = 500$ cP for DGEBA-based vinyl esters. ....	56
Table 14.	The reactivity ratios of vinyl ester and styrene for monodisperse VE resins and bimodal resins. ....	60
Table 15.	The fracture toughness of bimodal blends. Fracture toughness for blends with the same VE monomer formulation but with different styrene compositions are listed with the styrene composition in parenthesis. ....	63
Table 16.	Monodisperse and bimodal molecular weight and styrene content for VE resin systems.....	64
Table 17.	Calculated Evaporation and Diffusion Coefficients .....	65
Table 18.	Promising resin formulations that have low styrene contents (low VOCs), viscosities below 500 cP, good $T_g$ , and good fracture properties. ....	68
Table 19.	The vapor pressure, viscosity, and cost of potential styrene replacements for VE resins. ....	70
Table 20.	Initial viscosity of VE 828 resins at 30°C using various comonomers. ....	72
Table 21.	The fracture toughness of vinyl ester 828 resins using styrene and CHMA as reactive diluents. ....	77
Table 22.	The reaction conditions tested to produce MFA and the resulting reaction times and extents of reaction.....	81
Table 23.	The molecular structure differences of the fatty acids used to prepare MFA monomers.....	81

## TABLES (continued)

		Page
Table 24.	The viscosity of fatty acid-based monomers and precursors.....	89
Table 25.	The viscosity of the starting materials/reactants for fatty acid monomers. ....	90
Table 26.	The RT viscosities of Di-BrMSA and MOA monomers and their precursors. ....	90
Table 27.	The viscosities of Di-BrMSA monomer with MOA and styrene. ....	91
Table 28.	The initial viscosity of fatty acid-based VE resins at 30°C. ....	99
Table 29.	The properties of styrene and fatty acid based vinyl esters cured at room temperature and post-cured with a temperature ramp from room temperature to 200°C at 5°C/min. ....	113
Table 30.	The properties of MFA-based vinyl esters cured at 90°C and then post-cured with a temperature ramp from room temperature to 200°C at 5°C/min. ....	113
Table 31.	Glass transition temperature behavior ( $T_g$ ) of the Methacrylated Fatty Acids (MFA).....	115
Table 32.	The viscosities and mechanical properties of the VE/MFA/Styrene ternary blends.....	119
Table 33.	The storage modulus values $E'$ (30°C) and the $T_g$ s of the post cured VE 828 resins. ....	135
Table 34.	The reactivity ratios of the binary blends of vinyl ester, MFA, and styrene measured at 90°C. ....	141
Table 35.	The composition of the phase regions in VE/Mlin/Styrene 65/15/20. ....	143
Table 36.	Flexural properties of modified resins relative to DVB resins. ....	144
Table 37.	Viscosity of resin formulations containing mono-functional petroleum monomers.....	148
Table 38.	The viscosity of mono-functional monomers [www.sartomer.com]. ....	149
Table 39.	Viscosity of resin formulations containing di-functional petroleum monomers.....	150
Table 40.	Viscosity of di-functional monomers [www.sartomer.com]. ....	150
Table 41.	DMA properties of mono-functional low VOC petroleum monomer formulations. ....	153
Table 42.	DMA properties of di-functional low VOC petroleum monomer formulations. ....	153
Table 43.	The viscosities of the Viopal 575G, MOA, Br-MSA, styrene blends.....	164
Table 44.	$E'$ , $E''$ and $T_g$ values of the post cured Viopal UPE resins at 45 wt.% total comonomer concentration.....	168
Table 45.	$E'$ , $E''$ and $T_g$ values of the high temperature cured Viopal UPE resins at 35 wt.% total comonomer concentration. ....	170
Table 46.	$E'$ , $E''$ and $T_g$ values of the post-cured Viopal UPE resins (2 <sup>nd</sup> run DMA) at 35 wt.% total comonomer concentration. ....	170
Table 47.	The viscosities of the Epon 160, MOA, Br-MSA, styrene blends.....	174
Table 48.	The modulus $E'$ (30°C) and the temperatures of $E''$ maximum and the tan delta maximum of the post-cured VE 160 resins.....	177
Table 49.	The cross-link densities and the effective molecular weight values, $M_c$ , of the post-cured VE 160 and VE 828 resins.....	181
Table 50.	VE formulations using fatty acid monomers and styrene with optimum polymer properties. ....	182

## TABLES (continued)

		<b>Page</b>
Table 51.	Viscosity measurements (using spindle 21 and a speed of 50 RPM) for ternary blends.....	183
Table 52.	Gel time as a function of resin, CoNap content, and trigonox content at room temperature. ....	187
Table 53.	Fiber fraction of the E-glass composites.....	189
Table 54.	The composite properties of composites with G'-sized AS4 carbon composites with low VOC resins and Derakane 411-C50.....	192
Table 55.	The mechanical properties of the composites prepared using VE/MFA/Styrene ternary blends and the 9 oz glass fiber mats.....	193
Table 56.	Composition of PEI-based suppressant candidates. A (+) indicates styrene suppression, (++) indicates better styrene suppression, and (-) indicates a formulation that increases styrene emissions.....	214
Table 57.	Composition of polyester based suppressant candidates .....	216
Table 58.	The quoted price for a given volume scale for various chemicals relevant to the production of bimodal vinyl esters ad fatty acid-based vinyl esters. ....	225
Table 59.	The projected cost of MFA monomers on the small production scale. ....	226
Table 60.	The estimated prices for VE/MFA/Sty 65/15/20 resins as produced from a small scale manufacturer.....	227
Table 61.	The estimated prices for VE/MFA/Sty 65/15/20 resins as produced from a large scale VE manufacturer for a number of assumptions of the economy of scale.....	228
Table 62.	Lower bound estimate (large scale manufacturer) for the cost of bimodal vinyl ester resins. ....	228
Table 63.	Upper bound estimate (small scale manufacturer) for the cost of bimodal vinyl ester resins. ....	229
Table 64.	Costs over 10 years for epoxy resins for production of HMMWV hoods (~100,000 lbs resin/yr) relative to using low VOC resins. ....	230
Table 65.	Costs over 10 years for standard VE resins for production of HMMWV hoods (~100,000 lbs resin/yr) relative to using low VOC resins.....	230
Table 66.	Particle Number Density Data for TF33 Test I.....	233
Table 67.	Particle Mean Diameter for T-43 Aircraft Engines Using JP-8 and JP-8+100... ..	234
Table 68.	Particle Number Density ( $10^6$ ) for Different Power Settings TF33 Tests II.....	235
Table 69.	Performance Criteria.....	236
Table 70.	Actual versus Expected Performance. ....	236
Table 71.	+100 Additive Operational and Implementation Costs for T-43 and B-52 Aircraft.....	241

*This page left blank intentionally.*

## ACRONYMS AND ABBREVIATIONS

---

°C	degrees Celcius
µm	
<sup>1</sup> H-NMR	proton nuclear magnetic resonance spectroscopy
<sup>19</sup> F NMR	
AEM/S	
AFB	Air Force Base
AFPET	Air Force Petroleum Office
AHOSO-ME	
AMC-2	
AME	
AOH-SBO	Allyl Alcohol Modified Soybean Oil
ARL	U.S. Army Research Laboratory
ASTM	
Br <sub>2</sub>	bromine
Br-SAGAMA	
C-Br	
C-H	
CARC	chemical agent resistant coating
CCM	
CD550	methoxy PEG 350 methacrylate
CD612	ethoxy (4) nonyl phenol methacrylate
CHMA	Cyclohexyl methacrylate
cm	centimeters
CN151 or CN-151	
CNC	condensation nuclei counter
CoNap	cobalt naphthanate
cP	
DCC	dicyclohexylcarbodiimide
DCU	dicyclohexyl urea
DDX	
DGC-MS	desorption gas chromatography-mass spectrometry
DGEBA	diglycidyl ether of bisphenol
Di-Br	di-bromo stearyl glycidyl methacrylate
Di-BrSA	di-bromo stearic acid
DMA	dynamic mechanical analysis
DoD	Department of Defense
DPTS	4-(dimethylamino)pyridinium 4-toluenesulfonate
DSC	
DVB	divinyl benzene
E-beam	Electron beam

## ACRONYMS AND ABBREVIATIONS (continued)

---

EEQ	epoxy equivalent weight
EHOSO-FAME	epoxidized oils
EPA	Environmental Protection Agency
ESO	epoxidized soybean oil
ESTCP	Environmental Security Technology Certification Program
FA	fatty acids
FAME	fatty acid methyl esters
FCS	
FTIR	Fourier transform infrared spectroscopy
g	grams
g/mol	
$G_{IC}$	fracture energy
GM	glycidyl methacrylate
GPa	
GPC	
HAP	hazardous air pollutant
HBP	
HDDA	1,6-hexanediol diacrylate
HDDMA	1,6-hexanediol dimethacrylate
HMMWV	
HPLC	
HOSO	
HQ	
Hz	
Hz/pt	
IBMA	isobornyl methacrylate
in.	inches
IR	
IRGACURE	
$J/m^2$	
K	
$K_{IC}$	fracture toughness
Lau	lauric acid
Lin	linoleic acid
LM	lauryl methacrylate
macro-TGA	macro-thermogravimetric analyzer
MAP-MURI	Macromolecular Architecture for Performance MURI

## ACRONYMS AND ABBREVIATIONS (continued)

---

MBut	methacrylated butyric acid
MEHQ	
MEKP	methyl-ethyl-ketone peroxide
MFA	methacrylated fatty acids
MHex	methacrylated hexanoic acid
MHz	
micro-TGA	micro-thermogravometric analyzer
min.	Minute
mL	milliliter
MLau	
MLin	
mm	millimeter
MOA	oleic acid glycidyl methacrylate
MOct	
MPa	
MSA	
MURI	Multi-University Research Initiative
MW	molecular weight
N KOH	
NESHAP	
NIR	
NMR	nuclear magnetic resonance spectroscopy
NSWC	Naval Surface Warfare Center
OA	oleic acid
OEM	Original Equipment Manufacturer
PAH	
PDMS	poly(dimethylsiloxane)
PEI	polyethyleneimine
PI	
PM	
PMCs	
PND	
POC	
ppm	
PVC	
RT	
SA	stearic acid
SBO	
SbPh <sub>3</sub> /PPh <sub>3</sub>	triphenyl antimony/triphenyl phosphine
SEC	size exclusion chromatography

## ACRONYMS AND ABBREVIATIONS (continued)

---

SENB	single-edge notch bend
SERDP	Strategic Environmental Research and Development Program
SPO	
SR239	1,6-hexanediol dimethacrylate
SR252	PEG 600 dimethacrylate
SR259	PEG 200 diacrylate
SR480	ethox. (10) bis A dimethacrylate
T <sub>g</sub>	glass transition temperature
TGA	thermal gravimetric analysis
THF	tetrahydrofuran
UHC	unburned hydrocarbons
UP	
UPE	unsaturated polyester
UV	
VARTM	vacuum assisted resin transfer molding
VE	vinyl ester
VE 160	Bisphenol F type Novalac resin
VE 828	Bisphenol A type VE resins
VEA	acrylated vinyl ester
VOC	volatile organic compound

wt% or wt.%

## 1.0 EXECUTIVE SUMMARY

This document reports the results from a four year program funded by the Strategic Environmental Research and Development Program (SERDP) to research, develop, and demonstrate affordable, low volatile organic compound (VOC) emission vinyl ester resins for composite applications.

The Federal Environmental Protection Agency increased legislation to address hazardous emissions from composite manufacturing and repair by enacting new emission standards through the “National Emission Standards for Hazardous Air Pollutants: Reinforced Plastic Composites Production,” which specifically targets styrene as a regulated hazardous air pollutant (HAP). VOC emissions are liberated during all phases of composite fabrication. Three means of reducing the styrene emissions have been proposed. First, styrene emissions can be reduced by using a bimodal blend of vinyl ester (VE) monomers. Second, some or all of the styrene monomer in VE and unsaturated polyester (UPE) resins can be replaced with low-volatile petroleum or fatty acid-based monomers. Lastly, the use of a self-assembling vapor barrier using surface-active dendritic polymers to suppress styrene emissions was investigated.

Characterization techniques, including FTIR and GPC, show that VE monomers with narrow molecular weight distributions and bimodal blends of these monomers have been successfully prepared. These bimodal blends have low resin viscosities while having high fracture and thermal properties. Furthermore, these bimodal blends can be used to reduce the VOC emissions from vinyl esters by ~20%.

Out of all the petroleum-based comonomers studied as styrene replacements, cyclohexyl methacrylate has shown to be the most successful because its VE resins have low vapor pressure, good thermo-mechanical, and acceptable viscosities. A number of synthetic procedures have been developed to produce fatty acid-based monomers. These monomers are inexpensive, have very low volatilities, and improved global sustainability. Results have shown that low molecular weight and saturated fatty acid monomers yield resins with the lowest viscosities and highest thermo-mechanical properties. However, thermal cure of fatty acid-based vinyl esters resulted in polymers with properties inferior to that of commercial resins. Electron beam cure was used to increase the performance of fatty acid-based vinyl esters. In addition, fatty acid monomers can be blended with styrene to reduce the styrene content in VE resins while maintaining good thermo-mechanical, fracture, and rheological properties relative to commercial vinyl ester resins. The VOC emissions are reduced by 50-78% in these blends of VE, fatty acid monomers, and styrene.

Composites have been prepared from these low VOC resins. The properties of fiberglass-reinforced composites were similar or superior for these newly developed low VOC formulations relative to commercial resins. Furthermore, large-scale composite structures have been fabricated successfully using standard resin infusion techniques.

A macro-thermogravimetric analyzer (macro-TGA) was developed to measure the styrene emissions from vinyl ester resins because the results from more conventional techniques, such as desorption gas chromatography and micro-TGA, had low reproducibility due to the small masses

involved. Emissions studies from the bimodal blends of vinyl ester monomers and commercial VE resins display a characteristic elbow where the initial emission rate of styrene suddenly drops to a much lower emission rate. The position of this elbow moved to higher volatile content remaining as the number average molecular weight of the vinyl ester monomers increased. The initial rate of emission was only dependent on the styrene content in the resin. However, overall emissions were reduced by increasing the molecular weight of the vinyl esters used, as in the bimodal blends. Overall, this technique shows that bimodal blends of vinyl esters and fatty acid-based vinyl esters reduce emissions significantly relative to commercial resins.

Commercial dendritic polymers and triglycerides were investigated in their ability to form a self-assembling vapor barrier to suppress styrene emissions. These dendritic polymers were successfully modified with fluorine groups and vinyl functionality to induce surface migration to reduce styrene emissions and to allow them to react into the polymer network. Although these resins do reduce styrene emissions, their effect is small and takes a long time to reduce emissions. In fact, commercial styrene suppressants also fail for this long time scale for styrene emissions reductions, but these additives reduce styrene emissions to a much greater degree at that point.

Overall, the program has been successful at identifying critical Department of Defense (DoD) environmental needs, developing practical solutions to these requirements, and developing candidate resins for reducing VOC emissions from VE resins for military applications. Future work must still be done to validate the ability of these resins to produce high performance large-scale materials for the DoD.

## 2.0 SYNOPSIS OF THE PROGRAM

Recently, the Federal Environmental Protection Agency increased legislation to address hazardous emissions from composite manufacturing and repair by enacting new emission standards through the “National Emission Standards for Hazardous Air Pollutants: Reinforced Plastic Composites Production,” which specifically targets styrene, methyl methacrylate, and methylene chloride as regulated hazardous air pollutants (HAP). Volatile organic compound (VOC) emissions are liberated during all of the phases of composite fabrication (Figure 1). Styrene emissions occur during the mixing of diluents, catalysts, and initiators into the system. Composite parts typically have very large surface to volume ratios, which allows up to 20% of the styrene content to be lost during the molding stage. During cure, elevated temperatures increase the vapor pressure of styrene and thus increase the rate of VOC emissions. Unfortunately, even after cure during the lifetime of the part, styrene emissions can be substantial. Past work has shown that up to 40% of the styrene is unreacted after cure [1]. Therefore, liberation of VOC emissions must be mitigated not only during composite processing, but also during curing and fielding of the composite part.

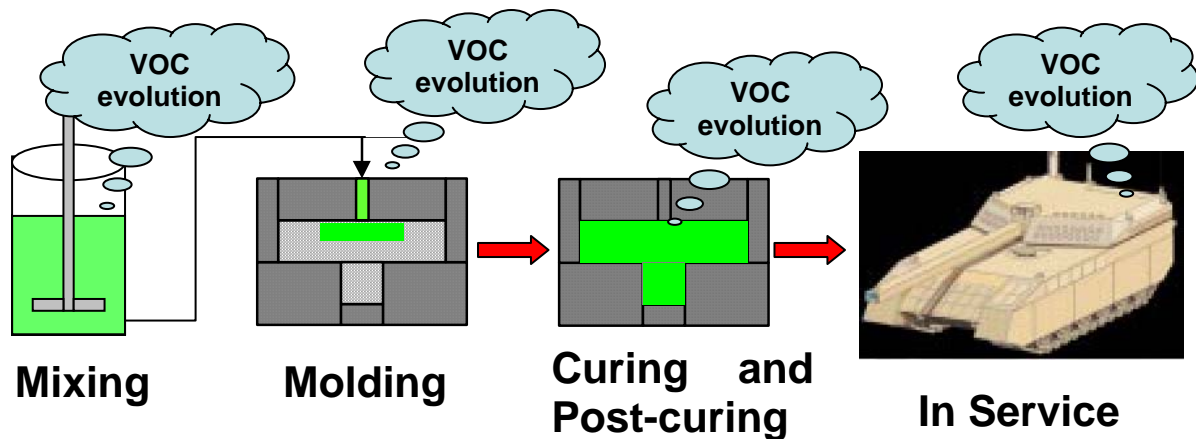


**Figure 1. Lifecycle sources of pollution associated with composite materials processing. Impact originates from initial fabrication, repair, and potential during service.**

The technical objective of the program was to research, develop, and demonstrate low VOC emission, high performance vinyl ester resins to comply with the new EPA regulations. Three methods were formulated for reducing VOC emissions in vinyl ester resins (Figure 2):

1. Reduction of styrene content by use of bimodal molecular weight distribution of vinyl ester monomers
2. Substitution of styrene with low molecular weight alternatives
3. Suppression of emissions with in-situ formed vapor barrier\*.

In the first method, the styrene content of VE resins was reduced using high molecular weight VE monomers to improve toughness and low molecular weight VE monomers to reduce the resin

viscosity to acceptable levels. The key to this work was to be able to prepare vinyl ester (VE) monomers with narrow molecular weight distributions. In the second method, methacrylate-based reactive diluents with low vapor pressures are studied as replacements for styrene in VE and unsaturated polyester (UPE) resins. Various monomers, including di-functional, aliphatic, cyclic, and aromatic monomers were tested to not only determine possible styrene replacements, but to more successfully understand the effect of monomer structure on resin rheology, cure kinetics, and polymer properties. In addition, fatty acid-based monomers were prepared and assessed as replacements for styrene. Fatty acids have very low volatilities and are derived from renewable resources, further improving the potential environmental impact of this project. In the third method, small amounts of multi-functional dendritic polymers were added to VE resins to suppress VOC emissions. In this work, we first examined and determined methods for inducing surface-segregation of these dendrimers. Means for incorporating these dendrimers into polymer networks were derived to insure the formation of good interfaces for adhesive applications and to insure that these dendrimers do not plasticize the polymer. Lastly, we studied the effects of dendrimer molecular weight, architecture, functionality, etc. on the thermodynamics and kinetics of surface segregation to provide an effective barrier to styrene evaporation. Unfortunately, styrene suppression was not successful. As a result, another objective was established to replace the styrene suppression effort:

4. Develop a mathematical model to predict styrene emissions from vinyl ester resins.

In this effort, the styrene emissions were measured for various resin formulations. The effect of temperature, styrene content, and vinyl ester molecular weight were determined in order to model styrene emissions. The emissions modeling was based on Fick's Law and was compared to the experimental emissions modeling.

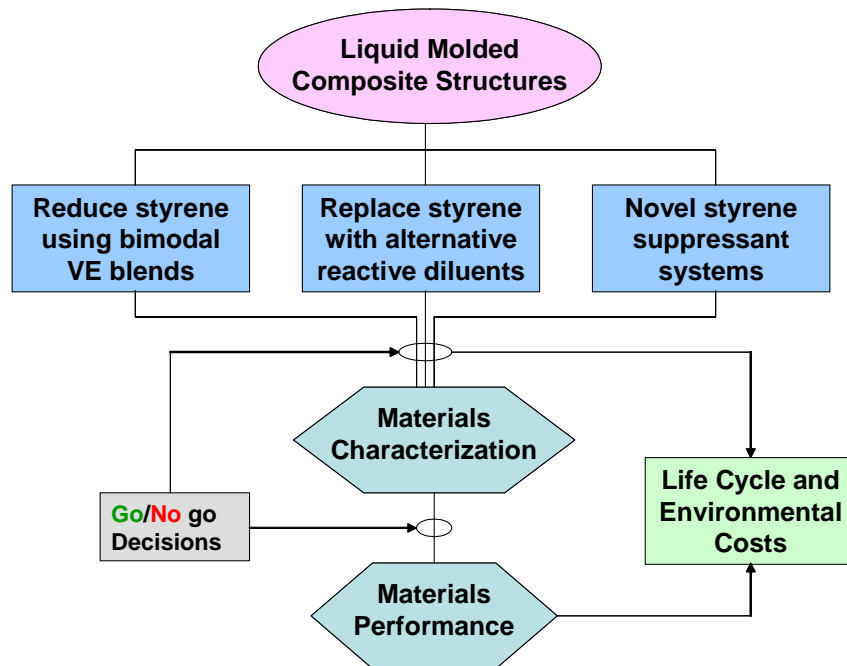


**Figure 2. Technical Approach for reducing VOC emissions in vinyl ester resins.**

This project was subdivided into tasks. The first task was to develop and study methods for reducing the VOC emissions from vinyl ester resins. Another important task of this work was to measure the properties and emissions of commercial VE resins in order to accurately assess alternative VE resin formulations. The third task of this work was to assess the environmental impact and cost savings of low VOC VE resins. The timeline for these tasks is shown in Figure 3. Tasks 1 and 2 constitute the resin design and performance testing, respectively, and continue through the project lifetime. Tasks 3 and 4 occurred intermittently throughout the program. The program was complete by December, 2005, and low VOC vinyl ester and unsaturated polyester resins with good polymer properties were established and proven.

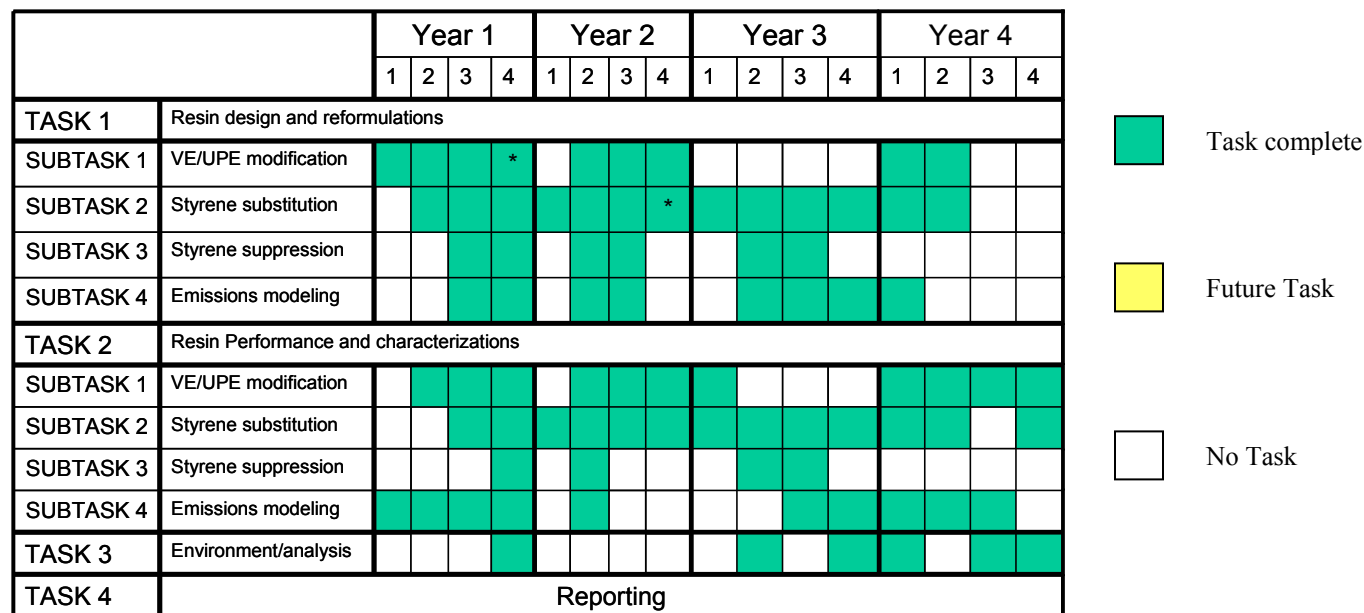


**Figure 3. Program timeline and completion level.**

Go/ No go decision points:

\* Yr1 and Yr2 – 10-20% reduction in styrene emission expected based on subtasks 1 and 2.

# Yr3 – at least 10% reduction in styrene emissions and significant emissions reductions with 30 minutes.

† Yr3 – 20-30% reduction in styrene emission expected based on combination of technologies in TASK 1.

‡ Yr4 – 40-50% reduction in styrene emission and commercial transition prospects for Subtask areas 1-3.

The current research team was made up of researchers from government and academia with expertise in monomer synthesis and characterization, specialized resin formulation, rheology, cure kinetics, and polymer property testing and evaluation. Table 1 shows the primary team members and contributors to the effort.

**Table 1. Low VOC composites team members.**

Organization	Team Members	Activities
U. S. Army Research Laboratory (ARL)	Mr. John Brown Mr. Dan DeSchepper Dr. John J. La Scala Dr. Steven H. McKnight Dr. Joshua Orlicki Dr. James M. Sands (PI) Ms. Cherise Winston	Evaluate styrene emissions from VE resins. Preparation of petroleum-based dendritic polymers as styrene suppressants. Characterization of surface-active nature of styrene suppressants. Economic and environmental impact. VOC emission modeling and characterizations
Drexel University	Mr. Jeremy Baer Dr. Erde Can Mr. Chad Cavan Dr. Tania Dey Ms. Amuta Jeyarajasingam Ms. Ji-Hean Lee Dr. Giuseppe R. Palmese (POC) Mr. Justin Robertson Mr. E. Jason Robinette	Preparation of VE with narrow MW and bimodal VE blends. Preparation of fatty acid monomers. Screening and evaluation of styrene replacements. Preparation of triglyceride-based dendritic styrene suppressants.
University of Alabama	Mr. Rahul Jain Mr. Chad A. Ulven Dr. Uday K. Vaidya	Baseline materials testing, mechanical testing, VOC emissions characterization
C. Milton Wright High School	Ms. Priya Kamath Ms. Anita Sahu	Resin formulation and testing
University of Delaware, Center for Composite Materials	Mr. Matthew Logan	Composite fabrication and testing
Naval Surface Warfare Center (NSWC), Carderock Division	Dr. Roger M. Crane	Composite fabrication, testing, and evaluation

## 3.0 TECHNICAL PROGRESS

### 3.1 INTRODUCTION

This report comprises three major subsections covering (1) measuring styrene emissions and baseline assessment for commercial VE resins, (2) synthesis, characterization, and development of vinyl esters with low VOC emissions, and (3) environmental impact and cost savings analysis. Overall, the program to date has been successful at identifying critical Department of Defense (DoD) environmental needs, gaining a fundamental understanding of VE resin systems, and developing practical solutions to reduce styrene emissions from VE resins. This work will be used to produce inexpensive, low-VOC VE resins for Army (composite replacement parts, FCS platforms, sheet metal substitutes) and Navy (DDX surface vessels, AEM/S, high contour rudders, high corrosion replacements) applications. We present results acquired during the first three years of this Strategic Environmental Research and Development Program (SERDP) program.

### 3.2 TECHNOLOGY DEVELOPMENT

#### 3.2.1 Experimental Techniques

In this section, general experimental techniques that are used in all aspects of the work are presented.

##### 3.2.1.1 Preparation of Vinyl Ester Monomers

Vinyl ester monomers were prepared via methacrylation of diglycidyl ether of bisphenol (DGEBA) (Figure 4) [2].

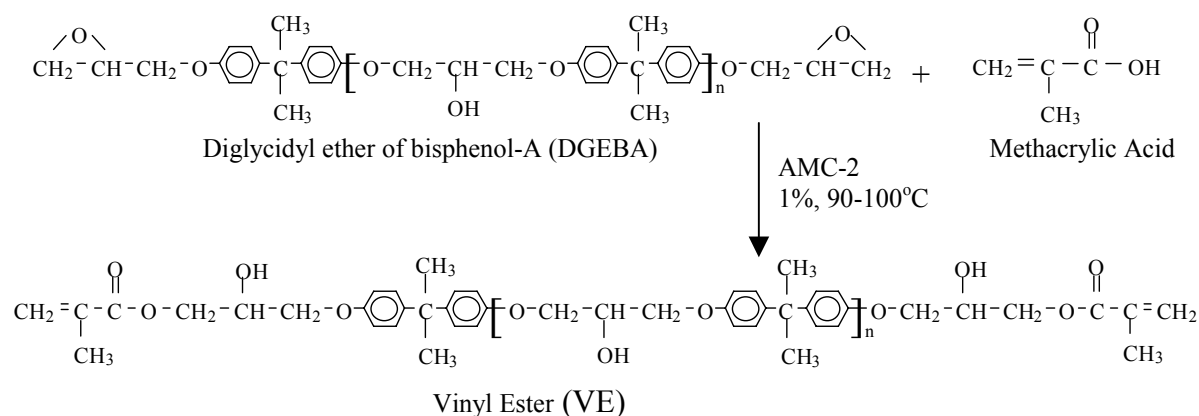


**Figure 4. The reaction of methacrylic acid with Epon to form vinyl ester monomer.**

##### 3.2.1.1.1 Epoxy Titration

To determine the epoxy equivalent weight of the Epon resins, epoxy titration was performed as per ASTM D1652-90, Procedure B. The epoxy resin was dissolved in 10-15 milliliter (mL)

methylene chloride, and 10 mL tetraethylammonium bromide solution was then added to the mixture. The sample was titrated with the perchloric acid/peracetic acid solution until the indicator changed color from blue to green. Epon 828, 1001F, 1004F, 1007F, and 1009F (Miller-Stephenson, Danbury, CT) were used as the source of DGEBA. The epoxy titration results agreed well with literature values for the epoxy equivalent weight (EEQ) (Table 2).

**Table 2. Epoxy equivalent weight as determined by epoxy titration and literature values.**

<b>Epon Resin</b>	<b>Literature EEQ (g/mol)</b>	<b>Experimental EEQ (g/mol)</b>	<b>Calculated MW* (g/mol)</b>
828	185-192	186	372
1001F	525-550	548	1096
1004F	800-950	900	1800
1007F	1700-2300	1990	3980
1009F	2300-3800	2770	5550

\* The calculated MW is simply twice the experimental EEQ with the assumption that each molecule has exactly two epoxide groups.

### 3.2.1.1.2 VE Preparation

VE 828 was prepared via methacrylation of Epon 828. Approximately 500 grams (g) Epon resin was reacted with 1.01 times the stoichiometric amount of methacrylic acid (i.e. as determined through epoxy titration). AMC-2 (Aerojet Chemicals, Rancho Cordova, CA), which is a mixture of 50% trivalent organic chromium complexes and 50% phthalate esters, was used as a catalyst for the reaction and to prevent epoxy homopolymerization [4] in the amount of 1 wt.%. The reaction was run at ~90PPoPPC, but because of the exothermicity of this reaction, water was periodically flowed through cooling coils within the reactor to keep the temperature below 95PPoPPC. Acid number titration was used during the course of the reaction to measure the amount of free (unreacted) acid in the VE system. The acid number tests were performed in accordance with ASTM D1980-87. Approximately 1 g of the VE reaction mixture was dissolved in 5 g acetone. Three drops of 0.5 wt% phenolphthalein in 50% ethanol were added to the mixture to determine the neutralization point. The solution was then titrated with 0.5 N sodium hydroxide until the solution remained slightly pink in color for 30 seconds. An acid number (mg NaOH/g VE) of 5, corresponding to ~2% free acid, was the maximum allowable acid number. The acid number of the VE mixture was then calculated (Eq. 1):

$$AcidNumber = \frac{mg \cdot NaOH}{g \cdot VE} = \frac{V \cdot N \cdot MW_{NaOH}}{m} \quad (1)$$

where V is the volume in mL of NaOH solution used, N is the normality of the NaOH solution, and m is the VE mass in grams. If the acid number was too high, the methacrylation reaction was allowed to continue until future acid numbers were below 5.

In previous work, 1% of a catalyst mixture containing 1 part triphenyl phosphine and 3 parts triphenyl antimony was used to catalyze the methacrylation of vinyl esters while preventing epoxy homopolymerization [2]. Although this catalyst worked well, the reaction required

approximately 5 hours to run. Previous work with triglyceride-based systems has shown that the acrylation of epoxidized triglycerides can be selectively catalyzed using AMC-2 [4]. Studies with the AMC-2 catalyst show that the resulting VE is the same in all aspects to VE produced using the older catalyst system (triphenyl phosphine/triphenyl antimony), except that the AMC-2 reduces the reaction duration from 5 hours to 1.5 hours. For this reason, the AMC-2 catalyst was used exclusively throughout the rest of this work to prepare VE monomers of various molecular weights.

### 3.2.1.1.3 FTIR Characterization of VE Monomers

FTIR was used to measure the concentration of unreacted epoxides and attached methacrylate groups. A Thermo Nicolet Nexus 670 FTIR was used in absorbance mode, taking 16 scans per spectrum with a resolution of  $4\text{ cm}^{-1}$ . The FTIR spectra of these resins indicated that all of the epoxide groups ( $917\text{ cm}^{-1}$ ) reacted, and methacrylate groups ( $942\text{ cm}^{-1}$ ) [2] were present in the resin (Figure 5).

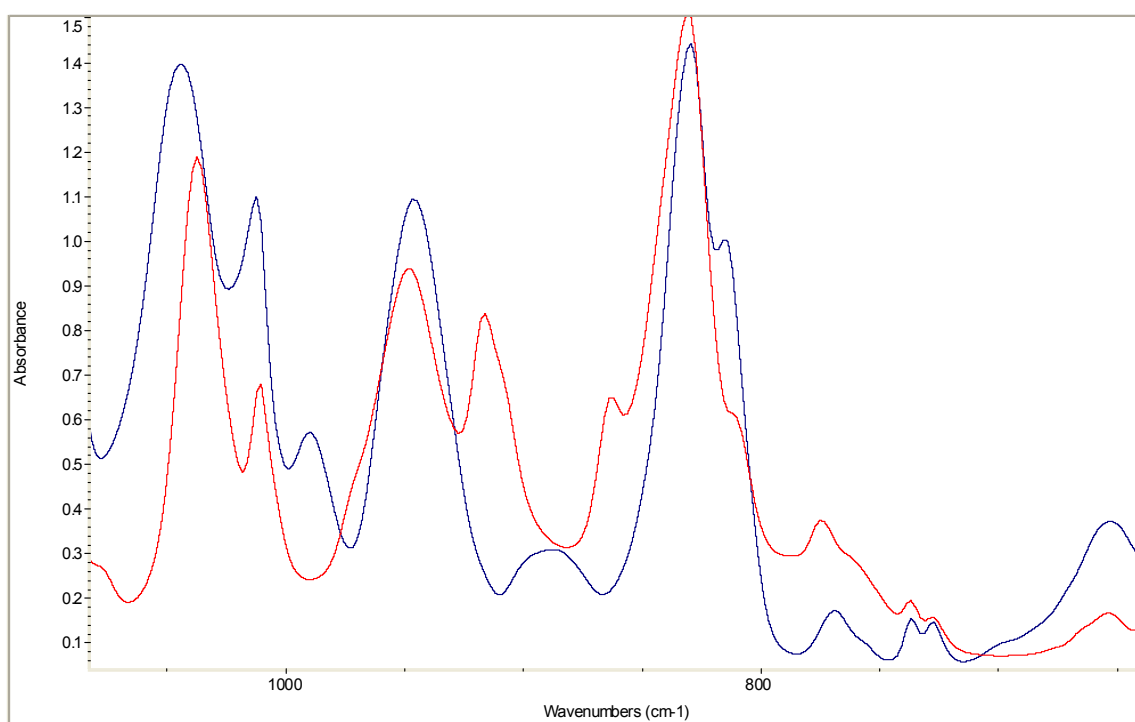


**Figure 5. The FTIR spectra of Epon/methacrylic acid and the resulting vinyl ester formed after complete reaction.**

### 3.2.1.1.4 Size Exclusion Chromatography of VE

Size exclusion chromatography (SEC) was run on the VE samples to determine VE molecular weight and styrene content. A Waters 515 GPC was used with two  $5\text{ }\mu\text{m}$  styrene-divinyl benzene columns in series. The columns were equilibrated and run at  $45^\circ\text{C}$  using tetrahydrofuran (THF) as the elution solvent at a flow rate of  $1\text{ ml/minute}$ . The column effluent was monitored by two detectors operating at  $25^\circ\text{C}$ : a Waters 2410 refractive index detector and a Waters 2487 dual absorbance detector operating at  $270\text{ nm}$  and  $254\text{ nm}$  (absorbed by phenyl rings). Samples

were prepared by dissolving 2 mg sample in 1 ml THF. Because high molecular weight species cannot diffuse into the packing, they elute first from the column, while lower molecular weight species elute later [5, 6]. Previous work has shown that if a significant amount of epoxy homopolymerization occurred, a broad peak appearing at 10 minutes and lower elution times would appear [6, 7]. Because no such peak appeared in our prepared vinyl esters, we conclude that no epoxy homopolymerization occurred. In addition, these results conclusively show that Epon reacted with the methacrylic acid to form higher molecular weight vinyl ester monomers. Figure 6 shows the SEC traces for a representative Epon (834) and the vinyl ester formed after complete reaction with methacrylic acid. There are four peaks, 15.66 min, 13.90 min, 13.20 min (peak shoulder), and 11.40 min (small peak) representing Epon with 0, 1, 2, and 3 repeat units, respectively. Most of the individual peaks still appear in the VE, but they are shifted to shorter elution times (14.48 min, 13.55 min, and 11.18 min) because the VE molecular weight is approximately 172 g/mol greater than the Epon. The peak representing the n=2 monomer is coincident with the peak representing the n=1 monomer and the individual peaks cannot be resolved. Previous work has shown that if a significant amount of epoxy homopolymerization occurred, a broad peak appearing at 10 minutes and lower elution times would appear [2, 5]. Because no such peak appeared in our prepared vinyl esters, we conclude that no epoxy homopolymerization occurred. In addition, these results conclusively show that Epon reacted with the methacrylic acid to form higher molecular weight vinyl ester monomers.

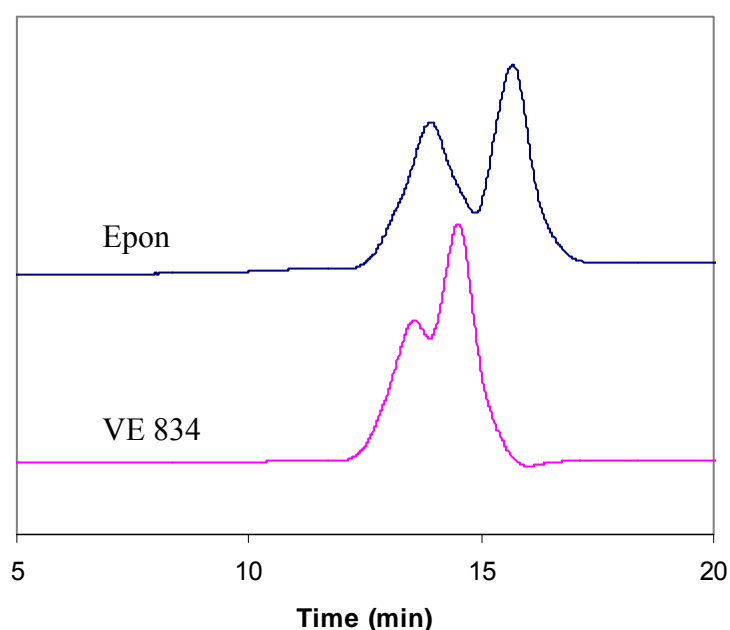


**Figure 6. The SEC traces for Epon 834 and VE 834.**

To measure the molecular weights of VE resins using SEC, the molecular weight as a function of retention time was calibrated using Epon resin samples. The molecular weight of the Epon 100XF resins was known through epoxy titration results. However, 1001F and 1004F resins have two peaks: one is the result of n=0 species while the other peak is the result of higher molecular weight species. The n=0 peak can be simply identified from its retention time, and the molecular weight of 340 g/mol was assigned to this peak. The relative areas of these two peaks

were calculated. Then,  $M_n$  of the lower retention time peak was determined by equating the area-weighted number average molecular weights of both peaks to  $M_n$  overall of the Epon resin (determined from Epoxy titration results). The calibration curve relating peak retention time to molecular weight is shown in Figure 7.

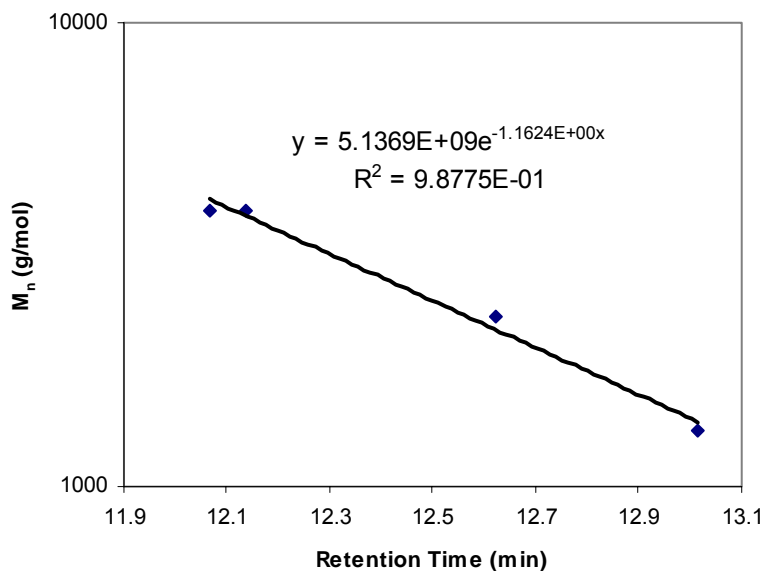


**Figure 7. SEC Calibration curve for resin MBBn BBAs a function of retention time.**

The styrene content of VE resins can also be measured using SEC. VE 828 standards with 30 wt%, 40 wt% and 50 wt% styrene were prepared and tested to calibrate SEC results. Using this calibration curve, the styrene content in commercial resins was measured. The styrene content was calculated by measuring the area of the low molecular weight peak at 18 min relative to the area of the VE peaks from 12-16 min. The calibration curve for these results (Figure 8) shows that the measured styrene content is similar (although slightly higher) than the actual styrene content.

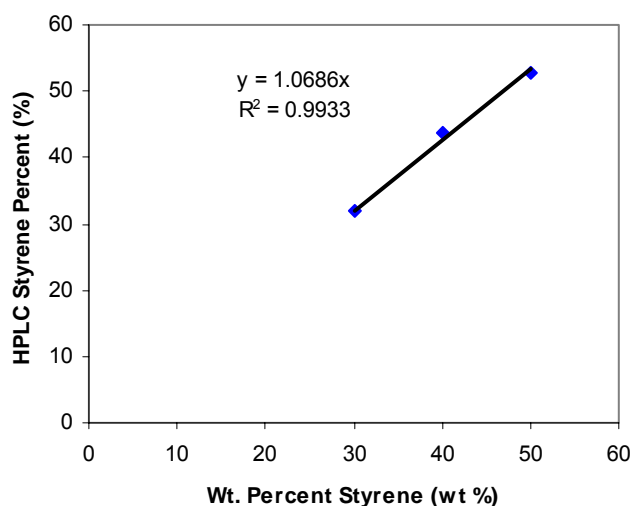


**Figure 8.** Calibration curve relating styrene content measured using SEC to the actual styrene content in the sample.

#### 3.2.1.1.5 Nuclear Magnetic Resonance Spectroscopy of VE

Nuclear magnetic resonance spectroscopy (NMR) was run on commercial VE resins to verify the styrene content and VE molecular weight. The NMR spectrum of VE 828 with known styrene content was also measured to determine the accuracy of this method. In general, a Bruker AM250 spectrometer (250.13 MHz, spectral window of  $\pm 2000$  Hz, 0.427 Hz/pt digital resolution, 16 scans at 293 K, 90° pulse width) was used. Figure 9a shows the NMR spectrum of VE 828 with 50 wt. % styrene using a Bruker 600 MHz Spectrometer. The method used is described in the literature [1, 8]. The internal standards for VE are the 4 methylene protons at 5.63 ppm and 6.18 ppm (peak *e*) and the 6 methyl protons of the methacrylate groups at 1.99 ppm (peak *b*) per VE. The area per proton for these standards should be in agreement. The value of *m* for the VE (Figure 9b) is calculated based on the area of the  $5m+5$  isopropyl protons at 3.8-4.4 ppm (peak *c*), the 8 phenyl protons at 6.8 ppm and 7.13 ppm (peak *g*) per *m*, or the 6 DGEBA methyl protons at 1.67 ppm (peak *a*) per *m*. These values of *m* resulting from all three standards should be in agreement. The styrene content is calculated by measuring the relative area of the styrene methylene protons at 5.25 ppm and 5.75 ppm (peak *d*) to the internal standards (Figure 9c).

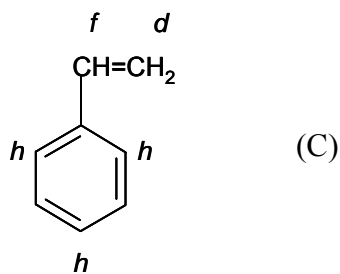
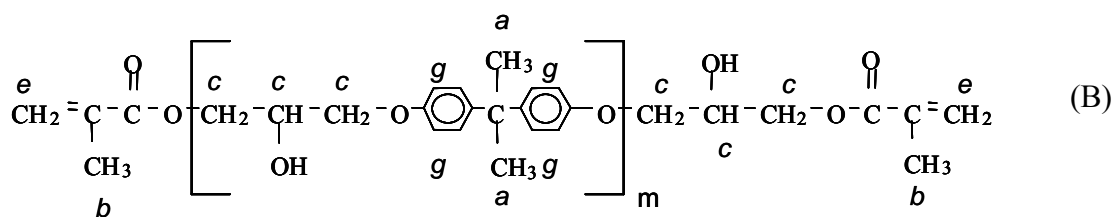
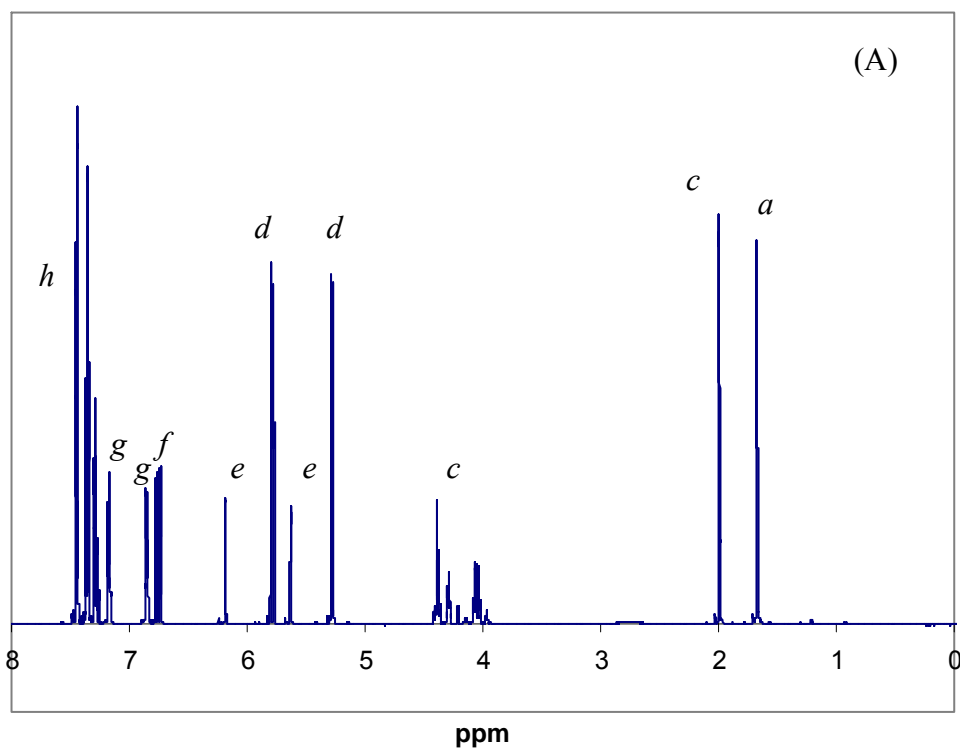


**Figure 9.** The NMR spectrum of VE 828 with 50 wt% styrene (A) with the peaks labeled to correspond to chemical groups of VE monomer (B) and styrene (C) [1]. Note the definition of m (m=1 represents the lowest possible value of m for DGEBA-based resins).

### **3.2.1.2 Rheological Characterization**

The viscosities of the resins were measured using a Brookfield digital viscometer in Couette geometry (concentric cylinders). Approximately 8 ml of the sample were placed into the sample holder. The appropriate spindle and shear rate were selected to maximize the allowable torque. All samples were run at 30°C. The Brookfield viscometer displays the results as a percentage of the maximum torque the instrument can apply. This torque percentage along with the shear rate has been calibrated to the viscosity by the manufacturer. This calibration is verified using silicone oils with a known viscosity.

Viscous forces in liquids are caused by physical and chemical interactions between molecules. Physical interactions, such as chain entanglements, dominate in polymeric melts [9, 10, 11]. For example, as the molecular weight of epoxy monomers increases, the viscosity of the melt increases because of an increase in the entanglements and loss of degrees of freedom [10, 12]. Hydrogen bonding, acid-base interactions, and other such chemical interactions can also greatly affect the viscosity of a substance. As seen with triglyceride-based liquid molding resins, the viscosity of the resin increases exponentially due to increased hydrogen bonding as polar functional groups are added to the triglyceride [13, 14].

### **3.2.1.3 Cure of VE Resins**

Cure conditions significantly affect the microstructure of vinyl ester resins, which in-turn affects the thermal and mechanical of the resulting polymers [1]. For these reasons, cure conditions (temperature, sample thickness, and cure time) were kept constant for all samples, unless otherwise noted.

VE monomer and styrene were mixed in various ratios. Trigonox 239A, containing 45 wt. % cumene hydroperoxide, was used to initiate free radical polymerization of the resin. Cobalt naphthanate (CoNap) was used to catalyze the polymerization at room temperature. The moles of cumene hydroperoxide used were one-hundredth the number of moles of vinyl functionality. A 4:1 weight ratio of trigonox to CoNap was used. The resins were then poured into a mold and allowed to cure. Polymer samples were post-cured *in situ* for dynamic mechanical analysis, but were post-cured for 2 hours at 130°C before thermo-mechanical and fracture tests. These cure conditions are typical for vinyl ester resins, and results in highly cured polymers with good polymer properties [1].

### **3.2.1.4 Cure Kinetics of VE Resins**

The cure kinetics of VE resins containing Trigonox only (no CoNap) were measured using FTIR. A Nicolet Magna 860 Fourier FTIR operating in transmission mode with 4 cm<sup>-1</sup> resolution was used. The set-up of the FTIR cell is explained elsewhere [8]. A drop of the resin was sandwiched between two 25 mm diameter NaCl disks (International Crystal Labs) separated by a 0.025 mm thick Teflon<sup>TM</sup> spacer (International Crystal Labs). One sodium chloride disk was 2 mm thick while the other was 4 mm thick. The salt plate assembly was placed in a cell holder. The temperature of the cell holder can be controlled to within ± 0.1°C of the set-point. When the cell holder equilibrated to 90°C, the salt plate assembly was placed in the holder, and the first

FTIR scan was taken. All resin mixtures were cured at 90°C for 2 hours and post-cured at 120°C for an additional 2 hours. An FTIR spectrum (Figure 10) comprised of 16 scans was taken every 30 seconds during the cure reaction.

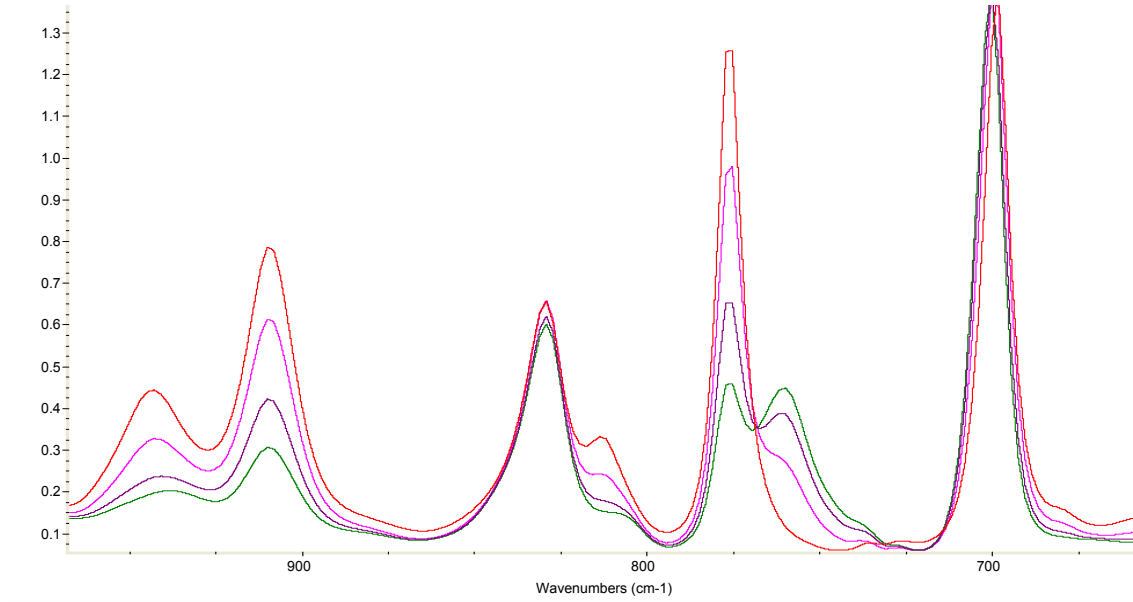


**Figure 10.** The FTIR spectrum of VE/styrene as a function of cure time.

The conversion,  $\alpha$ , was calculated by measuring the height of the peak relative to an internal standard (i.e. a group that is not affected by the reaction) (Eq. 2):

$$\alpha = 1 - \left( \frac{ABS(t)_{peak}}{ABS(t=0)_{peak}} \right) \left( \frac{ABS(t=0)_{standard}}{ABS(t)_{standard}} \right) \quad (2)$$

The cure kinetics was fit to an autocatalytic model (Eq. 3):

$$\frac{d\alpha}{dt} = k\alpha^m (\alpha_u - \alpha)^{2-m} \quad (3)$$

where  $k$  is the rate constant,  $m$  is the reaction order, and  $\alpha_u$  is the ultimate conversion at a given cure temperature [1, 8]. Both VE monomers and MFA contain methacrylate groups that appear at 942  $\text{cm}^{-1}$ . The methacrylate conversion was calculated by measuring the height of the peak relative to the vinyl ester aromatic C-H stretch at 828  $\text{cm}^{-1}$ . The styrene conversion was calculated by measuring the styrene carbon-carbon double bond peak height (910  $\text{cm}^{-1}$ ) relative to the styrene aromatic C-H stretch (700  $\text{cm}^{-1}$ ) [1, 8]. To resolve the cure of VE from the cure of the MFA, acrylated vinyl ester was prepared. Acrylated vinyl ester was prepared in the same way as methacrylated vinyl ester, except acrylic acid was used rather than methacrylic acid in the synthesis procedure (Figure 4). Acrylate groups appear at 990  $\text{cm}^{-1}$  [15]. The disappearance of the acrylate peak and the methacrylate peak relative to the vinyl ester internal standard was used to calculate the cure rate of the individual components. Acrylated VE was cured in the presence

of the 25 wt. %, 35 wt. %, 45 wt. %, and 80 wt. % of the various MFA monomers to allow measurement of reactivity ratios.

### **3.2.1.5 Thermal and Mechanical Characterization**

The thermo-mechanical properties of vinyl esters were measured using dynamic mechanical analysis (DMA). Rectangular samples with approximate dimensions of 25 millimeter (mm) x 9 mm x 3 mm were tested using a TA Instruments DMA 2980 DMA in single cantilever geometry. The samples were tested at 1 Hz with a deflection of 15  $\mu$ m while ramping the temperature from 30°C to 200°C at a rate of 5°C/min. Three temperature ramp experiments were run for each sample. The first ramp usually completely post-cured the polymer, but another ramp was performed to insure this. The temperature at which the peak in the loss modulus occurred in the fully post-cured polymer was considered the glass transition temperature ( $T_g$ ) of the material [15].

Flexural tests, in accordance with ASTM 790M, were performed to determine the modulus of elasticity and flexural strength. The samples had dimensions of 10 x 80 x 64 mm PP3PP and were tested flat-wise on a support span, resulting in a support-to-depth ratio of 16. The samples were tested using an Instron at a crosshead speed of 1.7 mm/min or 0.17 mm/min. A strain gage was applied to each sample to measure the strain of the sample as a function of applied load. Results were analyzed according to ASTM specifications to determine the flexural modulus and the flexural strength.

Three-point single-edge notch bend (SENB) specimens were used for fracture toughness measurements. ASTM 5045-93 specifies that the sample dimensions of approximately 2.00 x 0.50 x 0.25 in. PP3PP to assure plain strain conditions. An initial crack was made by notching the specimens a distance of half their depth. A sharp razor blade was used to initiate a crack at the base of the notches. The samples were tested using an Instron in flexural mode at a crosshead speed of 0.05 in/min. All tests were performed at ambient conditions. When tests were completed, the fracture specimens were examined for signs of plastic deformation. If plastic deformation was apparent, the sample was not used in the reported results. Results were analyzed according to ASTM specifications to determine the fracture energy (GBBICBB) and fracture toughness (KBBICBB).

### **3.2.2 Baseline Measurements**

To determine whether alternative VE formulations have (1) low VOC emissions and (2) comparable material properties to commercial resins, baseline studies on current VE resins are necessary. The results and discussion of some of this work are discussed in the report “Emission and Mechanical Evaluations of Vinyl Ester Resin Systems” located in the Appendix.

#### **3.2.2.1 Molecular Weights and Composition**

NMR was run on commercial VE resins to determine styrene content and VE molecular weight [1, 8]. The NMR spectrum of VE 828 with known styrene content was also measured to determine the accuracy of this method. The Derakane resins used were 411-C50, 411-350, 441-400, and 470-300. Derakane 411-350 is a recent replacement for 411-C50 that is essentially the

same resin, only with a different inhibitor package. 441-400 is a low VOC/HAP resin formulation. Literature lists the molecular weight and styrene contents for 411-C50 and 441-400 resins [1, 8], shown in Table 3. The experimental results for Derakane resins and the VE 828 resin were similar to the literature results. The VE molecular weight was not calculated for 470-300 because there were severe discrepancies between the internal standards. Derakane 470-300 is based on epoxy novolac structure [12] rather than DGEBA like the other vinyl esters used in this work. In addition, the individual peaks representing the area of the phenyl groups (7.0-7.5 ppm) were not clearly resolved and appeared very different from the peaks of other vinyl ester resins. The styrene mol % was calculated using the ratio of the methacrylate groups to the ratio of the styrene methylene group. However, the weight percent styrene in 470-300 could not be calculated because the MW of the vinyl ester molecules was unknown. Table 3 shows that the agreement between literature and experiment was good. Furthermore, VE 828 with 30 wt. % styrene was determined to have 29 wt. % styrene using NMR, proving the validity of this method.

**Table 3. The literature/known and experimentally determined (NMR) VE molecular weights and styrene contents for VE resins.**

Resin	Experimental VE M <sub>n</sub> (g/mol)	Literature VE M <sub>n</sub> (g/mol)	Experimental Styrene Content (wt.%)	Literature Styrene Content (wt.%)
VE 828 + 30% styrene	540	540	29	30
Derakane 411-C50	880	908 <sup>[1]</sup>	43	45-50 <sup>[1, 12]</sup>
Derakane 411-350	960	N.A.	45	45 <sup>[12]</sup>
Derakane 441-400	700	700 <sup>[8]</sup>	27	33 <sup>[8, 12]</sup>
Derakane 470-300	N.A.	N.A.	65 mol%	33 <sup>[12]</sup>

Using SEC, the styrene content in commercial resins was measured. UPE UN1866 is a commercial unsaturated polyester resin. Table 4 shows that the styrene contents measured using SEC are similar to the literature results. The molecular weights of vinyl ester resins were also measured using SEC. Table 5 shows that the experimental values are in good agreement with literature values and the NMR technique (Table 3).

**Table 4. Styrene content in commercial resins as measured using HPLC.**

Resin	HPLC Styrene Content (Raw results) (wt. %)	Calculated Styrene Content (using calibration) (wt. %)	Literature Styrene Content (wt. %)
Derakane 411-C50	48.8	45.7	45-50 <sup>[1, 12]</sup>
Derakane 411-350	42.91	40.2	45 <sup>[12]</sup>
Derakane 441-400	33.53	31.4	33 <sup>[8, 12]</sup>
Derakane 470-300	29.96	28.0	33 <sup>[12]</sup>
UPE UN1866	31.27	29.3	N.A.

**Table 5. The molecular weight of commercial resins calculated using SEC.**

Resin	M <sub>n</sub> of High MW species (g/mol)	VE M <sub>w</sub> (g/mol)	VE M <sub>n</sub> (g/mol)	Literature M <sub>n</sub> (g/mol)
411-C50	1890	1320	920	908 <sup>[1]</sup>
411-350	2070	1540	1050	N.A.
441-400	850	720	690	700 <sup>[8]</sup>
470-300	1330	870	720	N.A.
UPE UN1866	580	550	540	N.A.

**3.2.2.2 Viscosity of Commercial Resins**

The viscosities of selected Derakane resins and a UPE resin were measured and are listed in Table 6. It is clear that both increasing VE M<sub>n</sub> and decreasing styrene content cause increases in the resin viscosity (Table 3-Table 5).

**Table 6. The viscosity of commercial resins at 30°C.**

Resin	Experimental Viscosity (cP)	Literature Viscosity <sup>[12]</sup> (cP)
Derakane 411-C50	150	~100
Derakane 411-350	272	350
Derakane 441-400	312	400
Derakane 470-300	324	300
UPE UN1866	196	N.A.

**3.2.2.3 Polymer Properties of Commercial Resins**

DMA and fracture toughness measurements were run on Derakane 411-C50, 411-350, and 441-400. The polymer properties are summarized in Table 7. Overall, the properties of these resins are good, and are high strength resins with strength values over 100 MPa. The glass transition temperatures are well over 100°C. However, it is obvious that the low VOC formulation, Derakane 441-400 has much lower fracture toughness. Fracture toughness is of paramount importance for DoD applications because low fracture toughness materials are damaged more easily and have poor ballistic performance. Although the Derakane 441-400 could be used to meet the NESHAP regulations for a number of liquid molding applications, its use would mean compromising platform performance.

**Table 7. The polymer properties of postcured and non-postcured Derakane neat resins.**

Resin	Post-cured?	TBB <sub>g</sub> (°C)	Flex. Modulus (GPa)	Flex. Strength (MPa)	GBB <sub>ICBB</sub> (J/m <sup>2</sup> )
411-C50	No	64	N.A.	N.A.	340
411-C50	Yes	124	3.70	133	240
411-350	Yes	124	3.85	130	250
441-400	Yes	138	3.90	128	120

### 3.2.2.4 Baseline Styrene Emissions

#### 3.2.2.4.1 *Emissions Mass Loss Measurements*

An emissions test apparatus and methodology were developed based on the British Standard 2782, Part 4 - Method 432D: Determination of styrene evaporation from unsaturated polyester resins [17]. The apparatus consists of a small convection oven with attached mass balance with the mass being continuously read-out into a computer (Figure 11). This method directly measures VOC mass loss in samples less than 50 g as a function of time at specified temperatures. A direct measurement technique is most applicable for sources that have a large emission rate and fast decay, especially for “wet” materials. A Blue M Stabil-Therm gravity oven was modified by installing an electronic temperature controller (Omega Model: CN137MV-DC-AL1) to maintain specified isothermal conditions. A Mettler (Model: AE 240-S) mass balance was attached to the top of the oven and used to measure the mass as a function of time.

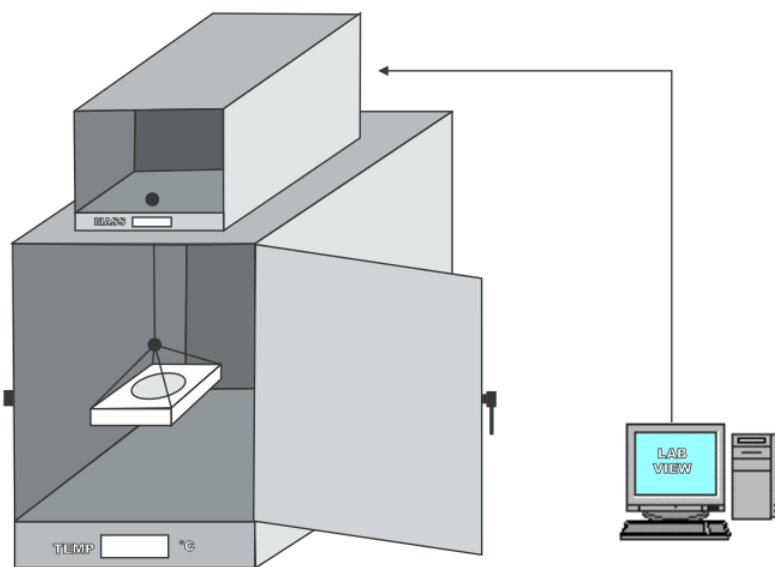


**Figure 11. Emissions measurement setup used to measure VOC mass loss as a function of time and temperature.**

A steel holder, large enough to hold a sample tray, was hung from the bottom of the mass balance through a small hole in the top of the oven. The sample trays used were made of thin

aluminum, with a constant diameter (70 mm) to ensure an equivalent surface area (38.48 cm<sup>2</sup>) for each sample during the experiment. The mass balance was connected to a central processing unit through an eight-pin serial port. A LabVIEW program was created to record mass in grams and time in seconds at specified intervals to a specified file created by the user.

Each VE resin sample tested was dispensed from a large resin batch into the sample tray and inserted into the oven just prior to the start of the test to limit the amount of styrene loss prior to measurement. Each VE system was tested in 40°C isothermal conditions. The total mass recorded in grams was converted to fractional styrene mass loss ( $M_t/M_\infty$ ) by dividing the styrene mass loss at time  $t$  ( $M_t$ ) by the total mass multiplied by the initial styrene weight percentage in the resin system ( $M_\infty$ ). The fractional styrene mass loss was plotted versus time to describe the emissions characteristics.

In order to gauge the effectiveness of a strategy to reduce VOC emissions, an accepted method of measuring VOC emissions was established. Traditional methods of volatiles analysis involve thermal gravimetric analysis (TGA) and desorption gas chromatography-mass spectrometry (DGC-MS). TGA includes a furnace to regulate temperature and a sensitive balance to measure weight changes. Temperature control is very good, but the sample size is quite small (~10-0.1 mg). Self-assembling vapor barriers that suppress styrene emissions are to be used in very small quantities (~1 wt% of resin mass). DGC-MS also uses small masses, but differs from TGA in that it measures the chemical composition of the volatiles emitted from the liquid sample. Preliminary work showed that the reproducibility of TGA and DGC-MS were very poor because of non-homogeneous samples due to the very small masses involved.

As an extension of TGA methodology, we have combined a standard laboratory balance and a temperature controlled oven to permit analysis of weight-loss behavior on a larger scale. The details of the setup and initial calibration of the macro-TGA setup may be found in the published report: “Emission and Mechanical Evaluations of Vinyl Ester Resin Systems,” located in the Appendix. Unlike micro-TGA, macro-TGA uses sample masses on the order of 10 g. The macro-TGA results were found to be mass dependent. Therefore, a standard mass of 10 g was chosen for this work.

We have performed a number of isothermal experiments at 40°C, to provide a baseline reference for our future work. The precision of the macro-TGA was tested by examining a commercial sample (Derakane 470-300) in triplicate. Figure 12 shows the change in mass (normalized to sample size) from three experiments plotted using the square root of time as the independent variable. All of the samples exhibited almost identical behavior, indicating the stability of the macro-TGA arrangement.

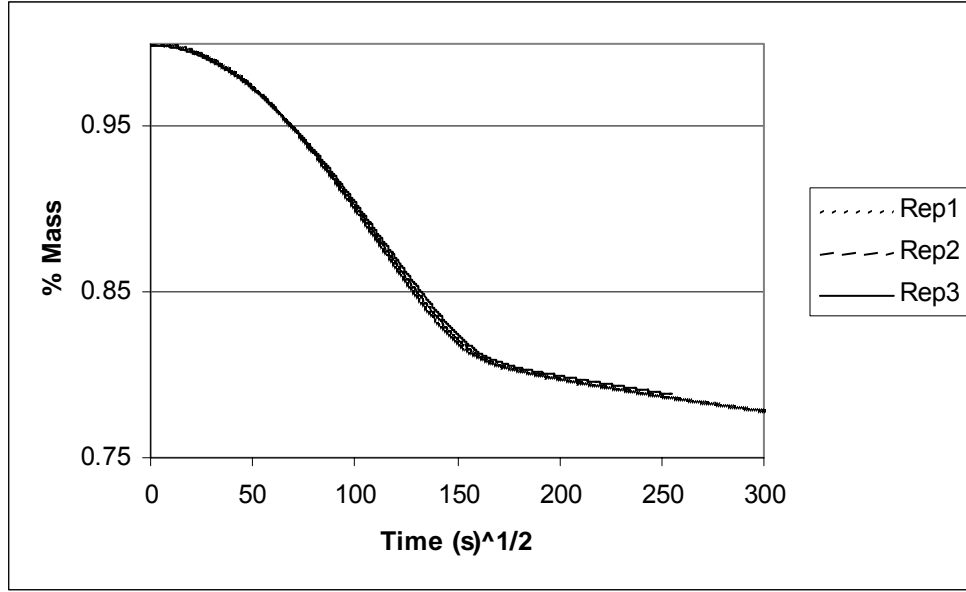


**Figure 12. Reproducibility of macro-TGA analysis, 40°C, Derakane 470-300 resin.**

#### 3.2.2.4.2 Effect of Styrene Content on Emissions

The normalized mass fraction of resin remaining as a function of time is (Eq. 4):

$$NormalizedMass = \frac{m(t)}{m_{initial}} \quad (4)$$

where  $m(t)$  is the resin mass as a function of time and  $m_{initial}$  is the initial resin mass. The transition from short-time to long-time mass loss occurred at greater percent mass loss and time for samples with larger styrene contents, as expected. Pure styrene did not display an elbow (not shown). The resin mass as a function of time was also normalized by the content of volatiles (styrene) using Eq. 5:

$$NormalizedVolatileMass = \frac{m(t) - (\phi_{VE} m_{initial})}{\phi_{styrene} m_{initial}} \quad (5)$$

where  $\phi_{VE}$  and  $\phi_{styrene}$  are the initial mass fractions of vinyl ester monomer and styrene, respectively.

Resin systems based on VE 828 were made with different styrene contents of 20, 30, 40, and 50 wt.% to study the effect of styrene concentration on the emission behavior of styrene. These different resin systems were run through macro TGA under 40°C isothermal conditions. For all cases, aluminum circular dishes of exposed area 38.48 cm<sup>2</sup> were used. Figure 13 plots the normalized mass loss as a function of time. All samples are self-similar, but the mass loss decreased as the styrene content decreased. When normalized by the volatile content, the evaporation rate is the same as shown in Figure 14. Figure 15 shows that the styrene percent becomes similar at about 25 hrs of emissions experiment at 40°C.

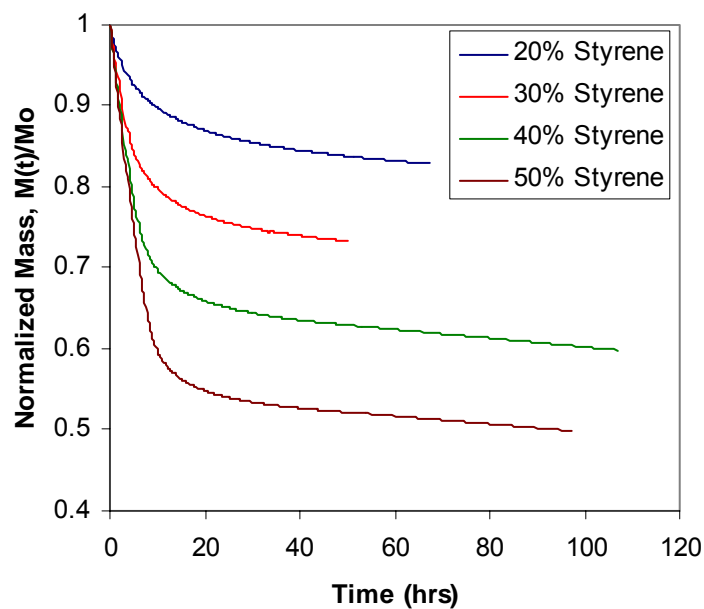


**Figure 13.** Mass loss of styrene in the VE 828 resin system as a function of time under 40°C isothermal conditions for four different initial styrene contents.

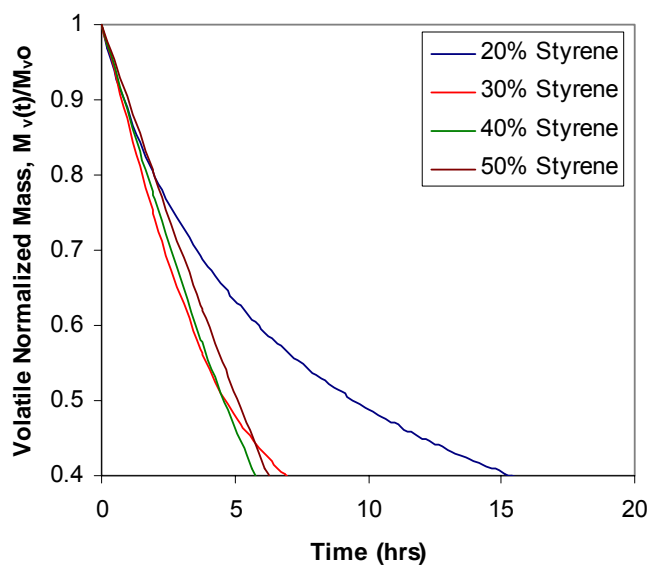


**Figure 14.** Volatile normalized mass as a function of time.

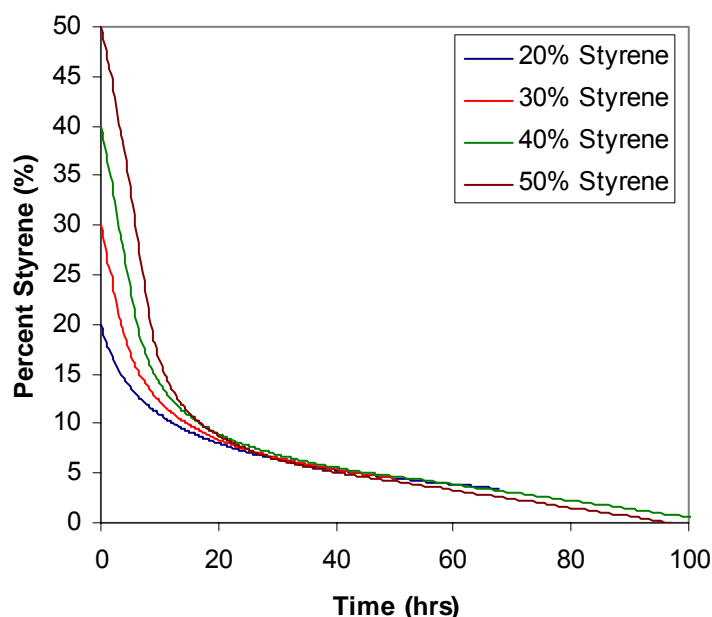


**Figure 15. Percentage of styrene as a function of emission time.**

#### 3.2.2.4.3 Variation in Temperature ( $T$ ) of the Resin

The same resin system VE 828 having 50% styrene was used to examine the effect of temperature on styrene emission. Resin systems at different temperatures (40, 50, 60, and 70°C) were run through macro TGA under isothermal conditions in aluminum circular dishes of exposed area 38.48 cm<sup>2</sup>.

Figure 16 shows the fractional mass loss profiles of VE 828 resin at different test temperatures. The temperature has pronounced effect on emission of styrene from VE resin. This is clearly depicted by the curves in Figure 16, where the slopes decreased and transition regions were shifted to the right with the decreasing test temperature. It was recorded that the time for 90 % styrene loss was increased by 350 % (6.38 h to 28.62 h) when the emission temperature was reduced from 70°C to 40°C. It is evident that the whole emission process is delayed with decrease in temperature. The main reason for this accelerated emission with increasing temperature is that overall viscosity of the resin decreases with increasing temperature, which in turn increases the mobility of styrene in the resin thereby increasing the diffusivity (i.e. styrene molecules can more quickly reach the resin-air interface, which accelerates the emission). In addition, it is hypothesized that an increase in temperature reduces the holding capacity of VE resin (i.e. attractive interaction forces between VE molecules and styrene molecules decrease with increasing temperature, which lead to more free styrene and hence faster emission).

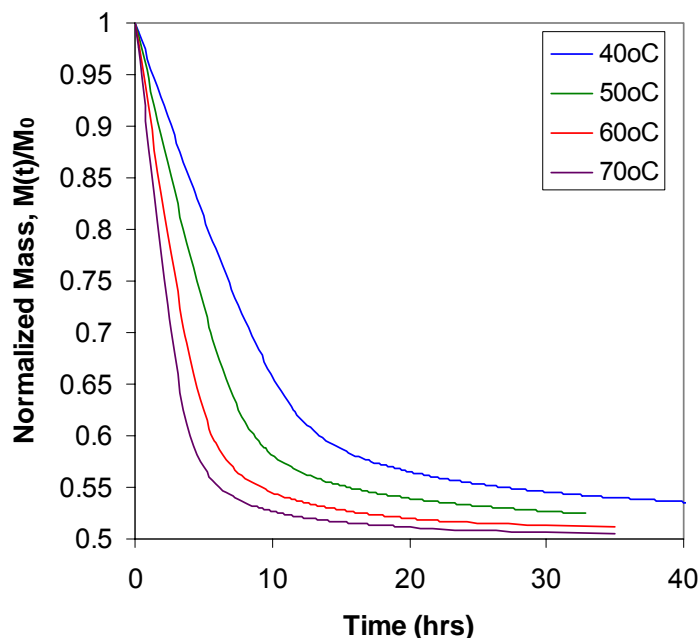


**Figure 16. Fractional mass loss of styrene in the VE 828 resin system having 50% styrene under different isothermal conditions in the study of temperature variation.**

#### 3.2.2.4.4 Variation in Depth ( $D$ ) of the Resin in Test Container

The depth of the VE 828 resin (1.290, 2.572, 11.55, 12.82, 21.91 mm) was varied by adjusting the mass of resin added to the sample pan. These resins were run through the macro TGA at 40°C isothermal conditions. The concentration of styrene in all resin systems was 50%. Details of the different samples tested are listed in Table 8, which have been named as DA, DB, DC, DD, and DE (in increasing order of resin depth). For cases DA through DD, aluminum circular dishes of exposed area 38.48 cm<sup>2</sup> were used, but to avoid the cumbersomeness of using circular dishes with high amount of resin, a glass vial having exposed area 4.5 cm<sup>2</sup> was used for highest depth (2.19 cm) resin system (highlighted cells). Last column in Table 8 shows the  $l_0/D$  ratio (resin thickness to container diameter ratio) for various systems.

**Table 8. Cases Considered to Study the Effect of Variation in Depth of Resin on Emission Behavior of Styrene.**

Case	Depth (mm)	Mass of resin (g)	Surface area (exposed) (cm <sup>2</sup> )	$l_0/D$ ratio (fraction)
DA	1.290	5.0549	38.48	0.0184
DB	2.572	10.0776	38.48	0.036
DC	11.55	45.2313	38.48	0.165
DD	12.82	50.2199	38.48	0.1831
DE	21.91	10.089	4.524	0.4506

Assuming that excess styrene is accumulated at the surface in the beginning, the systems with higher depth (higher amount of resin) will have more styrene at the surface for a longer period. Therefore, systems with higher depth will emit styrene through evaporation-controlled region for a longer period (Figure 17). The fractional mass loss curve of system DE shows that the system was under evaporation regime throughout the experiment. Systems with lower  $l_0/D$  ratio (thickness to diameter ratio), i.e., systems with higher surface area to volume ratio, have more propensity for faster styrene loss (same amount of styrene will be lost in short period). As the thickness increases, the diffusion path of the resin increases, which causes it to take longer for styrene molecule to reach the air-resin interface, thus, slowing the entire emission process (evaporation and diffusion). This is clearly depicted by the curves in Figure 17, where the slope decreased and the transition region shifted to right with the increasing depth of resin.

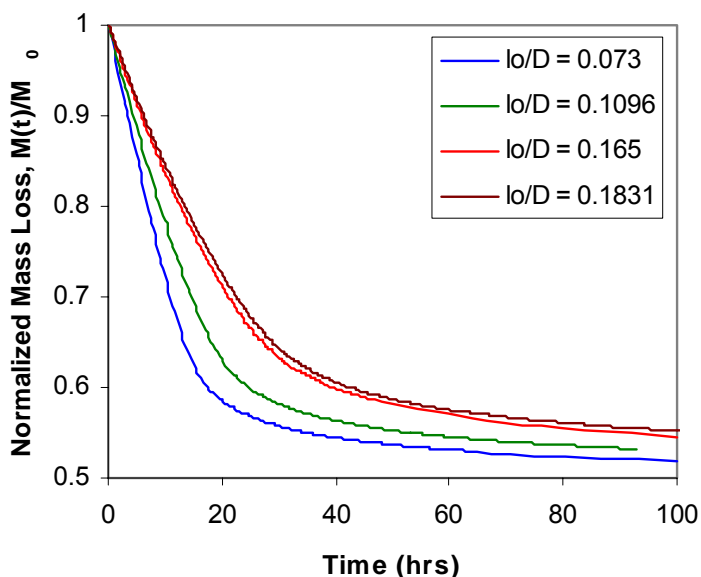


**Figure 17. Fractional mass loss of styrene in the VE 828 resin system under 40°C isothermal conditions in the study of depth variation.**

### **3.2.2.5 Monitoring of Resin Conditions during Cure**

To probe the performance of a model vinyl ester resin system during cure, a set of samples was prepared using standard VE 828 resin diluted to 50% resin with reactive diluent (styrene). The samples were also prepared with a specified amount of cobalt naphthanate. Two samples contained 1 equivalent of CoNap, the remaining sample contained 2 equivalents of CoNap. One of the samples with 1 equivalent of CoNap also contained hydroquinone, a known radical scavenger. Table 9 shows the composition of the resin formulations.

**Table 9. Resin compositions for emissions measurements during cure experiments.**

<b>Sample</b>	<b>VE</b>	<b>Styrene</b>	<b>HQ</b>	<b>CoNap</b>	<b>Trigonox</b>	<b>T<sub>Cure</sub></b>	<b>Temp Δ</b>
<b>1</b>	7g	7g	1.4 mg	15 mg	140 mg	~ 180	6°
<b>2</b>	7g	7g	0	15 mg	140 mg	~ 100	4°
<b>3</b>	7g	7g	0	30 mg	140 mg	~ 75	4°

Sample cure was initiated using Trigonox as a radical source, and similar samples were prepared in duplicate under similar conditions to monitor temperature in the reaction chamber and in the resin. Volatiles loss from 70 mm resin plaques was measured in a convection oven equipped with a platform suspended from an electronically monitored balance (to provide mass change data) and an aluminum plate (to store and radiate heat more evenly, reducing temperature variations). A thermocouple ca. 6 cm above the center of the suspended platform provided temperature information for the oven. To record the temperature in the resin, a thermocouple was inserted into the resin as it cured.

Results are plotted along the axes of time (minutes) and either volatiles content or temperature (Figure 18). The axis representing % VOC is calculated based upon initial styrene composition and indicates the quantity remaining in the resin. The % volatiles remaining in each plot are shown by the solid lines, while the temperatures measured are shown by the dashed lines. All of the “Rep1” samples were taken while measuring temperature in the oven chamber with the suspended thermocouple while the “Rep2” measurements were performed with a thermocouple in contact with the sample (resulting in more scatter in the data).

Trends observed in the cure time for the formulations are as expected—increasing CoNap concentration accelerated the cure rate while the HQ retarded cure. The temperature spike observed in Formulation 1 is higher than that observed for the other formulations, which is counterintuitive. It is possible that a higher population of initiator was generated before propagation began in earnest, resulting in a large exotherm once the HQ was overcome by the radicals.

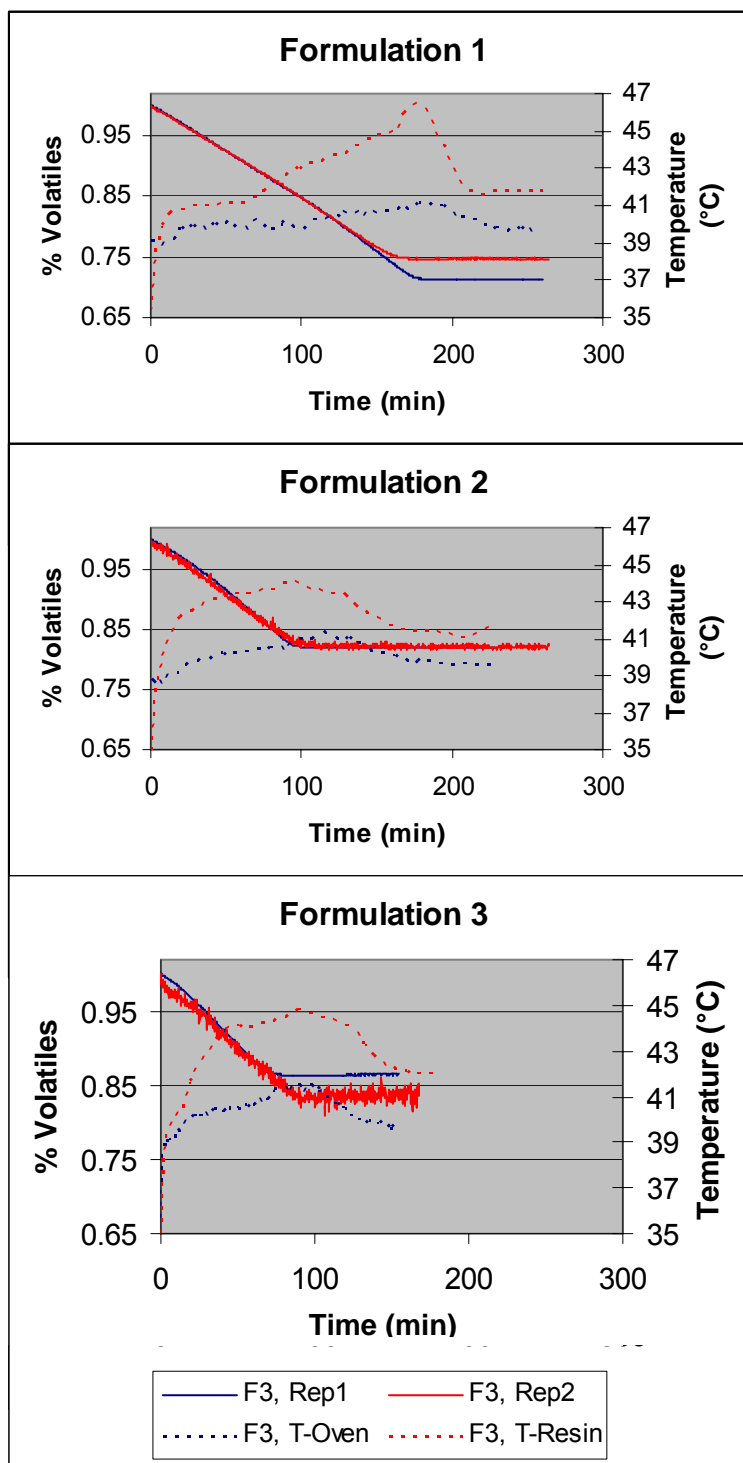
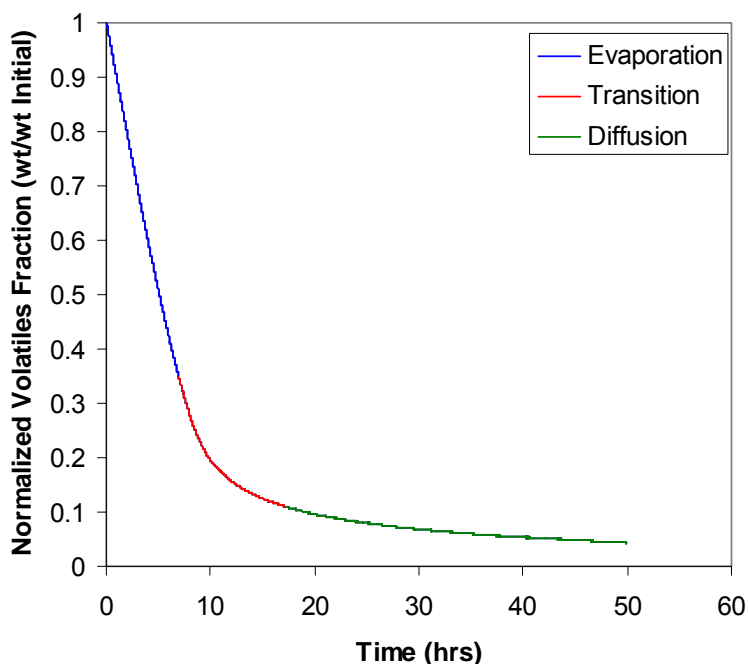


Figure 18. Percent volatiles and temperature as a function of cure time.

### 3.2.2.6 Mechanisms of Styrene Emission

The emission of styrene monomer from a mixture of VE monomer/oligomer and styrene monomer follows well established coupled mass transfer principles. Therefore, mathematical models based on mass transfer theory can be implemented to predict the VOC emission process. There are two main mass transfer mechanisms (i.e. internal and external) which contribute to overall material emissions that occur during the entire process. The diffusion of VOCs from a material is the result of a concentration gradient and interfacial mass transfer that occurs from the interaction of the material surface with the atmosphere [18]. Establishing complete models to describe small-scale emission processes in VE resin systems can be scaled to the prediction of emissions for large VE resin operations.

All of the molecules within the VE monomer/oligomer and styrene monomer mixture interact to a certain extent. The interaction between these molecules can be physical (Van der Waals or dipole-dipole forces), chemical (covalent) interactions, or a combination of types. In the current study, we assume no chemical reactions occur in the VE system. The styrene and vinyl ester monomer components can interact with themselves or each other. To describe the emission process, styrene monomer interacting with VE monomer will be addressed as ‘interacting styrene’ and styrene monomer not interacting with VE monomer will be addressed as ‘free styrene’. During early stages of the emission process, free styrene is released at a fast rate (Figure 19). At later stages, interacting styrene is released at a slower rate (Figure 19). This implies that VE systems which contain a higher percentage of styrene will have relatively higher percentage of free styrene in contrast to interacting styrene.



**Figure 19.** Styrene emission curve for a generalized VE resin system showing the three different regions.

### 3.2.2.7 Emissions Modeling

#### 3.2.2.7.1 Theory

One-dimensional diffusion of styrene through a planar surface of a VE resin bath can be expressed using Fick's Second Law (Eq. 6):

$$\frac{\partial C}{\partial t} = \frac{\partial}{\partial x} \left( D \frac{\partial C}{\partial x} \right) \quad (6)$$

where  $C$  is the concentration of styrene present in the system ( $\text{mg}/\text{m}^3$ ),  $x$  is the VE resin depth in the container,  $t$  is the time, and  $D$  is the diffusion coefficient of styrene present in the VE system ( $\text{m}^2/\text{s}$ ). During a short time period in the emission process, it is assumed that the concentration of styrene is relatively constant and, therefore,  $D$  in Eq. 6 can be assumed constant. Figure 20 illustrates a cylinder filled with VE resin at time equal to zero and after a significant period of time. The following initial and boundary conditions given in Eq. 7-9 are used to solve Eq. 6:

Initial condition:  $C = C_o$  at  $t = 0$  (7)

Boundary conditions (BCs):

BC 1:  $\frac{\partial C}{\partial x} = 0$  at  $x = 0$  (8)

BC 2:  $D \frac{\partial C}{\partial x} = \alpha (C^* - C)$  at  $x = l$  (9)

where  $C_o$  is the initial concentration of styrene present in the system ( $\text{mg}/\text{m}^3$ ),  $C^*$  is the concentration of styrene that would be in equilibrium with the vapor pressure in the atmosphere remote from the surface ( $\text{mg}/\text{m}^3$ ),  $\alpha$  is the evaporation coefficient of styrene ( $\text{m}/\text{h}$ ), and  $l$  is the depth of the VE resin ( $\text{m}$ ) [19]. The initial condition can be obtained independently because styrene concentration,  $C$ , in the beginning is  $C_o$ . The boundary condition BC 1 indicates that there is no mass flow at the bottom of the system, while the boundary condition BC 2 assumes that the mass flux by diffusion is equal to the mass flux by evaporation at the surface of the VE resin bath.

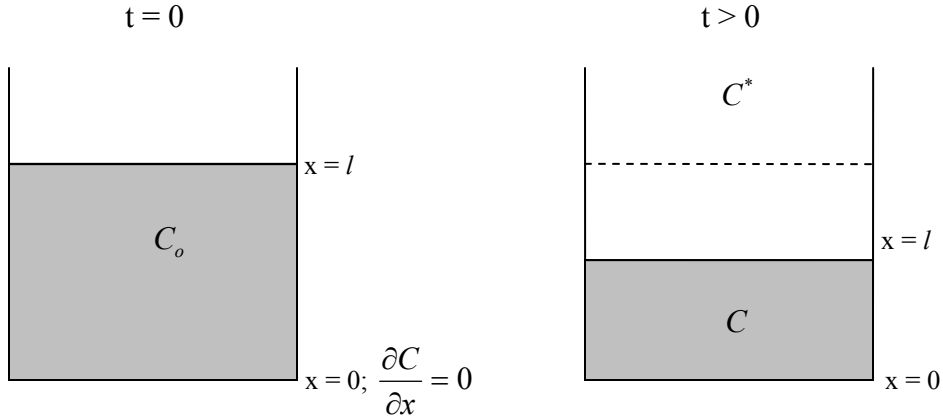


**Figure 20.** An illustration of a VE system initially (left) and the VE after a long time (right).

Solving Eq. 6 using the Laplace transform for the above initial and boundary conditions leads to the Crank solution as shown in Equation 10 [19]:

$$\frac{C - C_o}{C^* - C_o} = 1 - \sum_{n=1}^{\infty} \frac{2L \cos\left(\frac{\beta_n x}{l}\right) \exp\left(\frac{-\beta_n^2 Dt}{l^2}\right)}{(\beta_n^2 + L^2 + L) \cos \beta_n} \quad (10)$$

where the  $\beta_n$  are the positive roots of the following relationship (Eq. 11):

$$\beta_n \tan \beta_n = L = \frac{l\alpha}{D} \quad (11)$$

Based on Eq. 10, the total mass of styrene ( $M_t$ ) that has left the VE system at a particular time  $t$  can be calculated as:

$$\frac{M_t}{M_\infty} = 1 - \sum_{n=1}^{\infty} \frac{2L^2 \exp\left(\frac{-\beta_n^2 Dt}{l^2}\right)}{\beta_n^2 (\beta_n^2 + L^2 + L)} \quad (12)$$

where  $M_t$  is  $M_\infty$  for an infinite  $t$ , or total mass of styrene lost from the system at infinite time. For a large  $t$ , the first term ( $n = 1$ ) of the infinite series in Eq. 12 is usually sufficient to describe the semi-infinite bath [19]. Therefore, Eq. 12 becomes:

$$1 - \frac{M_t}{M_\infty} = \frac{2L^2 \exp\left(\frac{-\beta_1^2 Dt}{l^2}\right)}{\beta_1^2 (\beta_1^2 + L^2 + L)} \quad (13)$$

Taking the natural logarithm (Ln) of the Eq. 13 results in the following linear equation used for calculating D:

$$\text{Ln}\left(1 - \frac{M_t}{M_\infty}\right) = -\frac{\beta_1^2 D}{l^2} t + \ln\left[\frac{2L^2}{\beta_1^2 (\beta_1^2 + L^2 + L)}\right] \quad (14)$$

Plotting the logarithmic term ( $\ln(1 - M_t / M_\infty)$ ) on the left hand side of Eq. 14 versus time results in two regions corresponding to the evaporation controlled (early time) and diffusion controlled (later time) regions of the emission curve. The slope of the latter,  $s$ , is used to calculate  $D$ . In the diffusion controlled region, when only interacting styrene remains,  $D$  is assumed to be constant. Therefore,  $D$  calculated from this region of the emission curve is for interacting styrene only. The slope from the diffusion controlled region is equated to the slope in Eq. 14, leading to the following relationship:

$$s = -\frac{\beta_1^2 D}{l^2} \quad (15)$$

Rearranging the variables in Eq. 15 allows calculation of  $D$  for interacting styrene in the VE system:

$$D = -\frac{sl^2}{\beta_1^2} \quad (16)$$

To calculate  $D$  from the Eq. 16,  $\alpha$  and  $\beta_1$  must be determined first. The evaporation coefficient ( $\alpha$ ) can be calculated using Eq. 17:

$$ER_o = \alpha C_o A \quad (17)$$

when the surrounding air concentration is low (i.e.  $C^* \sim 0$ ). In the chamber experiments, this condition is satisfied at the time the VE system is first placed into the chamber.  $ER_o$  is the initial emission rate (g/h) and  $A$  is the surface area of the resin bath exposed to the atmosphere (m<sup>2</sup>). The initial emission rate ( $ER_o$ ) is evaluated from plotting actual styrene mass loss versus time from early emissions (evaporation controlled region) and using linear regression analysis to find the slope. Therefore,  $\beta_1$  can be calculated from Eq. 18 after manipulating Eq. 11 and 16.

$$\frac{\tan \beta_1}{\beta_1} = -\frac{\alpha}{sl} \quad (18)$$

A tool in Microsoft Excel (Solver) was used to solve Eq. 16, using the Newton-Raphson Method.

Once  $D$  for interacting styrene is calculated, a well known viscosity-diffusion relationship (Hiss-Cussler) can be used to calculate the change in  $D$  with styrene content for the entire emission process [20]. The Hiss-Cussler relationship is valid for the limiting case of a small solute molecule (i.e. styrene) diffusing in a solvent of relatively large molecules (i.e. VE) (Eq. 19):

$$D\mu^{2/3} = H \quad (19)$$

where  $\mu$  is the resin viscosity and  $H$  is a constant. This relationship is valid for liquid resin viscosities from 0.5 to 5000 cP. The determination and complete description of this relationship can be found in [20]. The determination of  $H$  in Eq. 19 is carried out using the calculated  $D$  of interacting styrene in the later stage of the emission process along with the known viscosity at that particular time.  $D$  is then calculated for the variable viscosity throughout the emission process.

### 3.2.2.7.2 Variation in Styrene Content (S) of the Resin

The emission process can be divided into two processes: evaporation followed by diffusion. Initially, when styrene concentration is high, the process is evaporation controlled. Later, the emission process becomes controlled by diffusion. Evaporation being the controlling mechanism during the initial part of emission leads to the formation of a styrene rich layer at the resin surface. This suggests that the more the styrene present in the resin, the greater the styrene rich layer. Therefore, systems with higher styrene content will have more styrene at the top to evaporate. This leads to evaporation as a controlling mechanism for a longer period in higher styrene content systems. For the same reason, systems with lower styrene content will shift to diffusion controlled regime earlier in the emission process.

The evaporation rate constants were calculated from the emission rate measurements and through using Eq. 15. The diffusion rate constant was calculated during the diffusion controlled portion of the emissions curve using Eq. 14, as shown in Figure 21. Table 10 lists the emission rates for resin systems with different styrene contents. The sample masses for all the cases are almost the same. Table 10 also shows the evaporation coefficients and diffusivity of all the systems. The evaporation rate clearly increased with styrene content, indicating that the sample is becoming more volatile. When normalized to the styrene content, it was found that the evaporation rate constant was constant as the initial styrene content was changed. Although the diffusivity increased as the styrene content increased, this result was significantly insignificant because of the error in involved mostly in the liquid resin density. Therefore, the diffusivity of styrene in VE 828 is approximately  $1.7\text{E-}11 \text{ m}^2/\text{s}$ .

**Table 10. The calculation variables for VE 828 resin system tested under 40°C isothermal conditions in the study of styrene variation.**

Styrene Content (wt%)	ER <sub>o</sub> (g/h)	$\alpha$ (m/s)	Density (kg/m <sup>3</sup> )	D (m <sup>2</sup> /s)
20	0.2067	7.6223E-08	1104	1.6E-11
30	0.3553	7.6177E-08	1077	1.7E-11
40	0.4108	7.3064E-08	1048	1.8E-11
50	0.4523	6.7627E-08	1019	2.0E-11

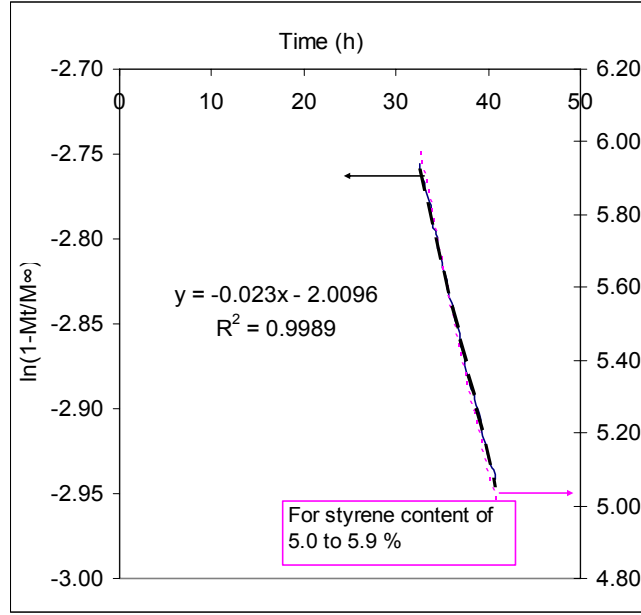


**Figure 21.** The slope of this plot,  $s$ , is used to calculate diffusivity.

Because we are unconcerned with the development of gradients in the system, there is no need to solve the entire diffusion/evaporation model. From the starting mass, we should be able to calculate the mass loss as a function of time using the fluxes alone. In the evaporation controlled region, the evaporation flux is limiting, while in the diffusion controlled region, the diffusion flux is limiting. The diffusion flux is:

$$F(\text{diff}) = D \frac{\partial C}{\partial x} \quad (20)$$

where  $dC/dx$  is:

$$\left. \frac{dC}{dx} \right|_{\beta_1} = \frac{C_o 2L \left( \frac{\beta_1}{l} \right) \tan(\beta_1) \exp\left( \frac{-\beta_1^2 Dt}{l^2} \right)}{(\beta_1^2 + L^2 + L)} = \frac{C_o 2L \left( \frac{\beta_1}{l} \right) \sin \beta_1 \exp\left( \frac{-\beta_1^2 Dt}{l^2} \right)}{(\beta_1^2 + L^2 + L) \cos \beta_1} \quad (21)$$

The evaporation flux is:

$$F(\text{evap}) = \alpha C_s(t) \quad (22)$$

where  $C_s$  is the surface concentration. The surface concentration of styrene is equal to the bulk styrene concentration in the evaporation regime because the high diffusion rates and lower evaporation rates will allow time for the styrene concentration to homogenize.

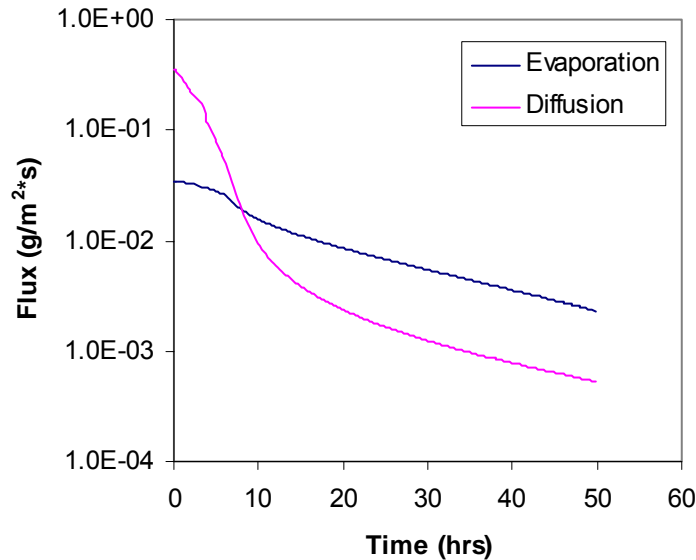
Mass loss due to evaporation flux was calculated using Eq. 23:

$$M_\alpha = \alpha C_o A(\Delta t) \quad (23)$$

Mass loss due to diffusion flux was calculated using Eq. 24,

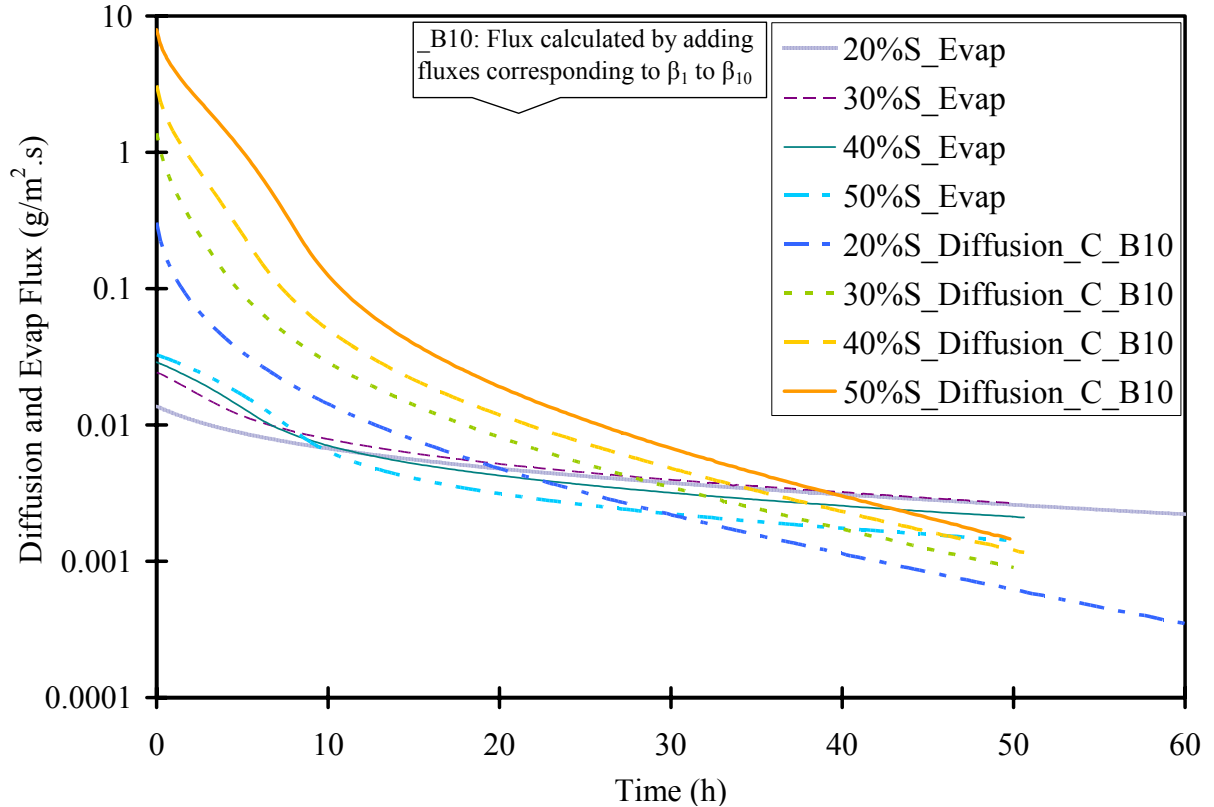
$$M_D = D \frac{dC}{dx} A(\Delta t) \quad (24)$$

The model predictions of the mass as a function of time were obtained by dividing the emission into two processes from the calculation point of view. It is known that the slowest step is the rate-controlling step in any physical or chemical phenomenon. Emission is controlled by both evaporation flux and diffusion flux (these two fluxes are the sole cause of styrene mass loss through the resin system). Therefore, at any instant, the lower flux (be it diffusion flux or evaporation flux) controls the styrene emission. It can be seen from Figure 22 that evaporation (giving lower flux than diffusion flux) is the controlling mechanism during the initial part of styrene emission. The transition was made from evaporation to diffusion flux where the mass loss due to evaporation flux became greater than mass loss due to diffusion flux. Later, when diffusion becomes the controlling mechanism of styrene emission, the values were obtained from the diffusion flux. As said before, as styrene concentration increases, the evaporation-controlled region is increased to over longer periods. For the same reason, cross-over is extended to longer times in systems with higher percentage of styrene. Fast mass loss due to evaporation in the initial region results in curves with very high slopes, followed by very low slopes of diffusion controlling regions.



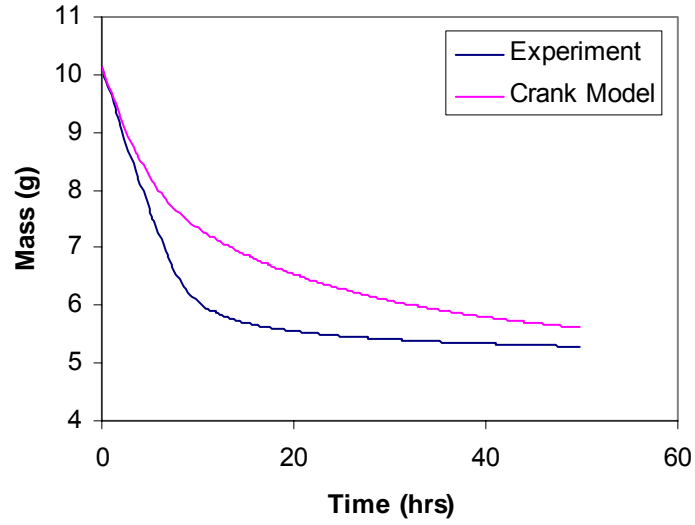
**Figure 22.** Plot of evaporation flux and diffusion flux for VE 828/Styrene 50/50 as a function of time under 40°C isothermal conditions for finding the cross-over point.

Figure 23 shows the evaporation flux and diffusion flux profiles for VE 828/styrene resin systems. The only difference between Figure 22 and Figure 23 is that diffusion flux in Figure 22 was calculated considering only the first term ( $\beta_1$ ) in the series, while diffusion flux in Figure 23 was calculated considering first ten terms of the series ( $\beta_1$  through  $\beta_{10}$ ). No effect can be observed in the cross-over when  $\beta_1$  through  $\beta_{10}$  are considered to calculate the diffusion flux as compared to when only  $\beta_1$  is considered. Therefore, only  $\beta_1$  will be used throughout this report.



**Figure 23. Plot of evaporation flux and diffusion flux with time for finding cross-over point (for  $\beta_{10}$ ) in the study of styrene variation of VE 828 resin system under 40°C isothermal conditions. Suffix ‘\_Evap’ designates the curves corresponding to evaporation flux. Suffix ‘\_Diffusion\_C\_B10’ designates the curves corresponding to diffusion flux obtained by considering first ten terms ( $\beta_1$  through  $\beta_{10}$ ) of the expansion series.**

Figure 24 shows a comparison between the experimental emissions data and the Crank model solution. The experimental values were directly obtained from the macro TGA experiment (recorded mass with time). Under prediction of the evaporation rate caused extensive error between the model and experiment. Over prediction of mass loss by diffusion flux caused extensive variation between the experimental and model results in the diffusion regime. The cause for this problem is the moving boundary associated with mass loss due to styrene evaporation, which is not taken into account in the Crank solution.



**Figure 24. Comparison of model and experimental values of mass loss behavior of styrene through VE 828/Styrene 50/50 resin system under 40°C isothermal conditions.**

The general Crank model assumes the sheet is basically a solid and does not deform during evaporation. This is not the case for the VE/styrene system, which typically loses a significant portion of its height dimension,  $x$ , by the end of the experiment. The Crank model calculates the diffusion flux and evaporation flux assuming no dimension change. This change in dimension must be accounted for in the model. The dimension  $x$  shrinks with time in the VE/styrene system:

$$x = x_{final} \frac{l_0}{l(t)} \quad (25)$$

Therefore, the diffusion flux in our moving boundary system is:

$$F(diff) = D \frac{\partial C}{\partial x} = D \frac{\partial C}{\partial \left( x_{final} \frac{l_0}{l(t)} \right)} = \frac{l(t)}{l_0} D \frac{\partial C}{\partial (x_{final})} \quad (26)$$

The factor of  $l(t)/l_0$  will make the diffusion flux lower, and makes the mass loss due to diffusion more closely match the experimental results. Effectively, the expansion of the length scale as we move backwards from the final mass to the initial sample mass causes this decrease in the diffusion flux for the VE/styrene system.

The evaporation rate is also affected because the evaporation rate constant is related to  $l$ :

$$\alpha = \frac{DL}{l(t)} = \frac{D\beta \tan(\beta)}{l(t)} \quad (27)$$

The length can be written as:

$$l(t) = l_0 \frac{l(t)}{l_0} \quad (28)$$

Substituting this equation into Eq. 27 gives:

$$\alpha = \frac{D\beta \tan(\beta)}{l_0 \frac{l(t)}{l_0}} = \frac{D\beta \tan(\beta)}{l_0} \frac{l_0}{l(t)} = \alpha_0 \frac{l_0}{l(t)} \quad (29)$$

Therefore, the emission rate as a function of time is really:

$$ER(t) = \alpha_0 C(t) A \frac{l_0}{l(t)} \quad (30)$$

Figure 25 shows that the modified Crank model does a much better job of predicting emission rates. Basically, this increase in the evaporation flux is due to compression of the length scale as styrene is emitted from the system. The diffusion flux is decreased for the same reason.

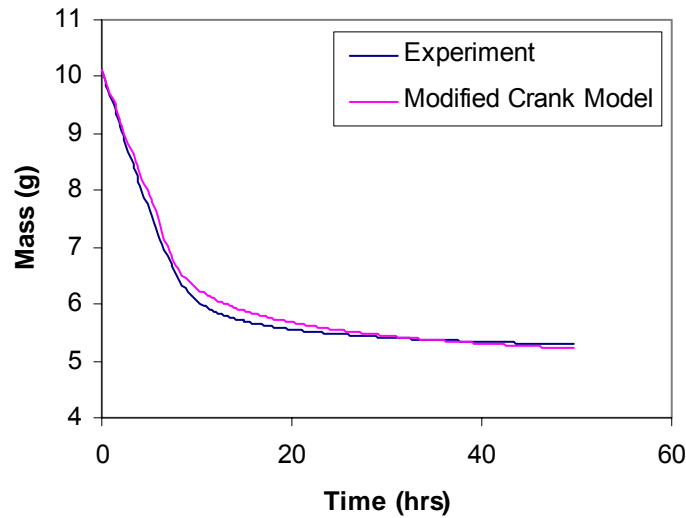


**Figure 25. The length-scale modified Crank model accurately models the diffusion regime, as shown for VE 828/Styrene 50/50 at 40°C isothermal conditions.**

### Summary

1. The straight Crank model does not accurately predict the emission rates in VE/styrene systems
2. Once the Crank model is modified to account for the dimensionality change during the course of styrene evaporation, the predicted results closely match experimental results
3. Evaporation was the controlling mechanism for a longer period as the styrene content increases.
4. Lower styrene content resin reached the diffusion-controlled regime very early in time.
5. Evaporation coefficient remained constant with changing styrene percentage.
6. Diffusivity remained constant with changing styrene percentage.

7. Diffusion flux values calculated for  $\beta_1$ - $\beta_{10}$  converge with diffusion flux values calculated for  $\beta_1$  at higher times. Therefore, higher  $\beta$  terms can be ignored at longer times.

### 3.2.2.7.3 Effect of Temperature on Styrene Emissions

The evaporation coefficient values calculated at different test temperatures have been plotted in Figure 26. An exponential relation between the temperature and evaporation coefficient was observed. The relation can be expressed using Eq. 31:

$$\alpha = 4.1 \times 10^{-5} \left( e^{0.0382T} \right) \quad [\text{m/h}] \quad (31)$$

This result was expected because increasing temperature typically causes an exponential increase in vapor pressure [21].

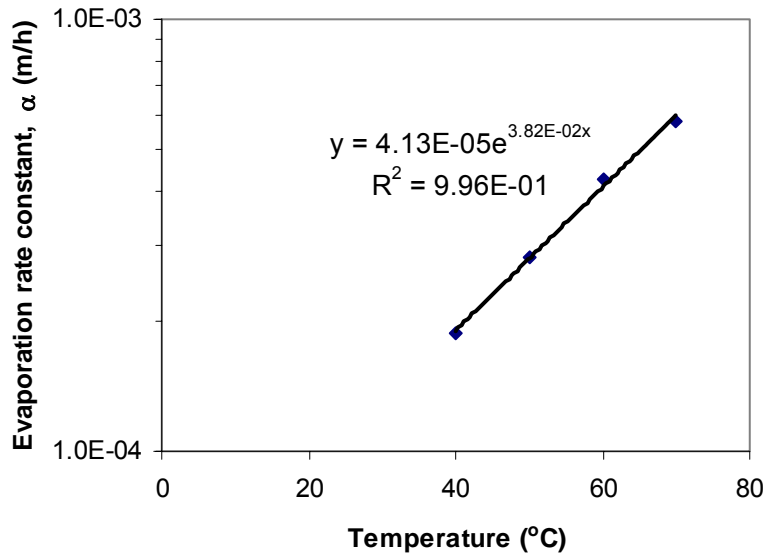


**Figure 26. Effect of styrene percentage on evaporation coefficient in the study of temperature variation of VE 828 resin having 50% styrene.**

As shown in Figure 27, exponential relation between the temperature and diffusivity was observed. The relation can be expressed using Eq. 32:

$$D = 8.0 \times 10^{-13} \left( e^{0.0748T} \right) \quad [\text{m}^2/\text{s}] \quad (32)$$

Again, this exponential behavior is expected because of the exponential decrease in resin viscosity with temperature [9]. These results indicate that temperature affects styrene emission rates in a relatively simple manner.

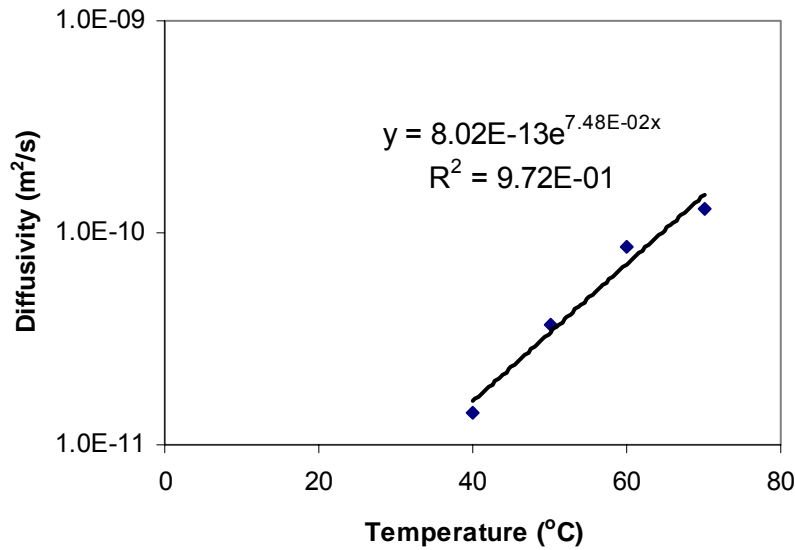


**Figure 27. Effect of styrene percentage on diffusion coefficient in the study of temperature variation of VE 828 resin having 50 % styrene.**

The diffusion model can accurately predict the effect of temperature on the emission profile. Figure 28 compares the experimentally measured emission profile at 50°C vs. the modified Crank model predictions using the measured diffusion constant from the experimental results. The model does a good job of predicting the results, although the characteristic elbow begins too soon and the diffusivity is too high causing mismatched slopes at long times.

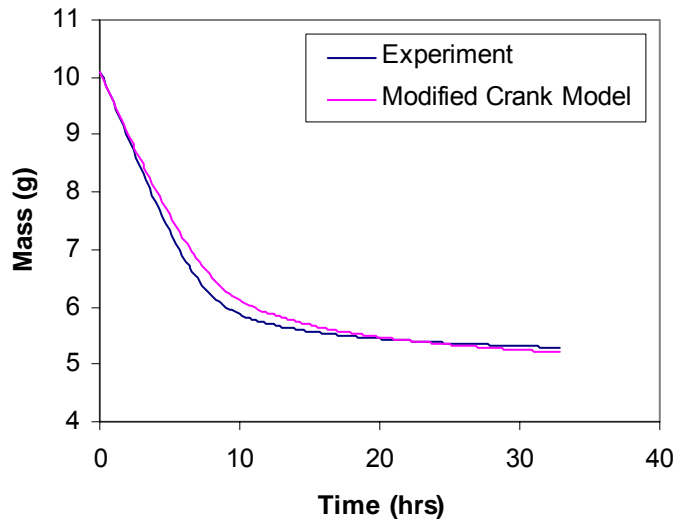


**Figure 28. The emission profile from VE/Styrene 50/50 at 60°C as measured experimentally and as predicted from the modified Crank model.**

#### 3.2.2.7.4 Effect of Aspect Ratio on Styrene Emissions

As shown in Figure 17, the aspect ratio has a significant effect on the emissions profile. However, the emission curves were self-similar. The initial evaporation rate increased as the length/thickness ratio decreased. However, this was a surface area effect, so the evaporation rate constant remained constant at  $\sim 7.5E-8$  m/s. The diffusivity was also unchanged with a value of approximately  $1.7E-11$  m<sup>2</sup>/s. Therefore, only a simple normalization factor is necessary to eliminate the effect of aspect ratio on the emissions profile. The normalization factor chosen was an aspect ratio modification of the emission time (Eq. 33):

$$\text{NormalizedTime} = t * (l / r) \quad (33)$$

where  $l$  is the instantaneous sample thickness and  $r$  is the sample radius. Figure 29 shows that this factor does an excellent job of normalizing the data.

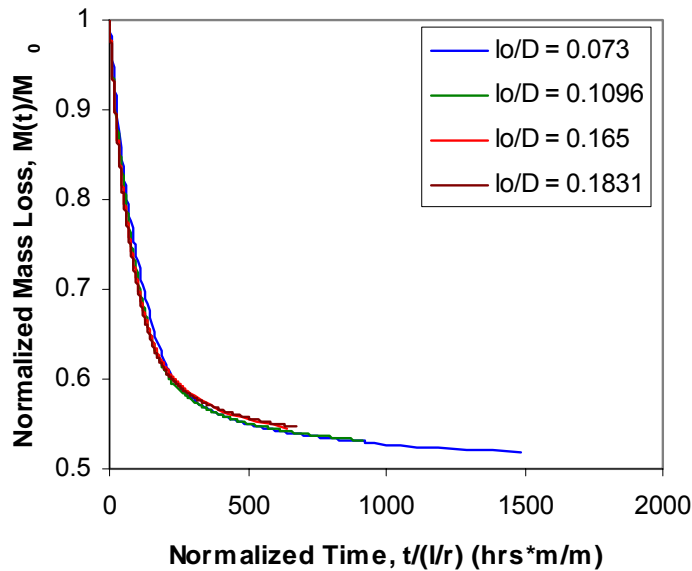


**Figure 29.** The normalized mass loss as a function of normalized time for different aspect ratios.

#### 3.2.2.7.5 Complete Emissions Modeling from Liquid Vinyl Ester Resins

The Crank diffusion model does a fine job of predicting the styrene emission profiles from vinyl ester resins. Essentially, this model requires two material constants ( $\alpha$  and  $D$ ), the temperature, and the aspect ratio (length/diameter). The past few sections have shown that we can quantitatively predict the effect of styrene content, temperature, and aspect ratio on the diffusivity and evaporation coefficient. Therefore, styrene emissions can be predicted with a fair degree of accuracy for any VE 828/styrene composition, any temperature from 40-70°C, and any aspect ratio. Figure 30 shows the model predictions relative for styrene emissions from VE/styrene 50/50 at 60°C based on the diffusion mass transfer rate and evaporation rate as calculated using Eq. 26 and Eq. 30, respectively. In general, the model using the predicted

parameters matches the experimental results as well as the modified Crank model using the experimentally determined parameters.

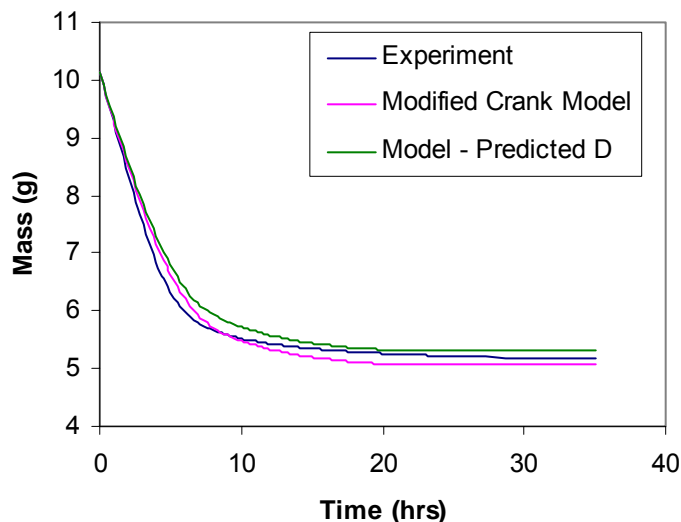


**Figure 30. Model predictions vs. experimental results for styrene emissions from VE/styrene 50/50 at 60°C for an aspect ratio of  $l_0/D$  of 0.037.**

### **3.2.3 Reduce Styrene Content in Raw Materials Systems by Use of a Bimodal Molecular Weight Distribution of Vinyl Ester Monomer**

In this section, we report on the synthetic procedure used to prepare vinyl ester monomers, their rheology, cure, and polymer properties. We first examine the properties of monodisperse VE/styrene blends, and then examine the bimodal blends. We have hypothesized that the styrene content in VE systems can be reduced while maintaining low viscosity and high toughness by using a bimodal distribution of VE molecular weights. Low molecular weight VE is used to maintain low resin viscosity, while high molecular weight VE imparts toughness to the system.

#### **3.2.3.1 Material Properties of Monodisperse VE Resins**

The rheological, mechanical, and thermal properties of vinyl ester resins are dependent on the molecular weight of the vinyl ester monomers and the styrene content. Vinyl ester molecular weight and styrene content had opposite effects on the resin viscosity. Figure 31 shows that the viscosity of VE resins, with constant styrene content, increased with the vinyl ester molecular weight. On the other hand, the resin viscosity decreased exponentially as the styrene content increased (Figure 32). This occurred because styrene acts as a solvent and reduces the interactions (hydrogen bonding and entanglements) among vinyl ester monomers, allowing these large molecules to more easily slide past one another [9, 14].

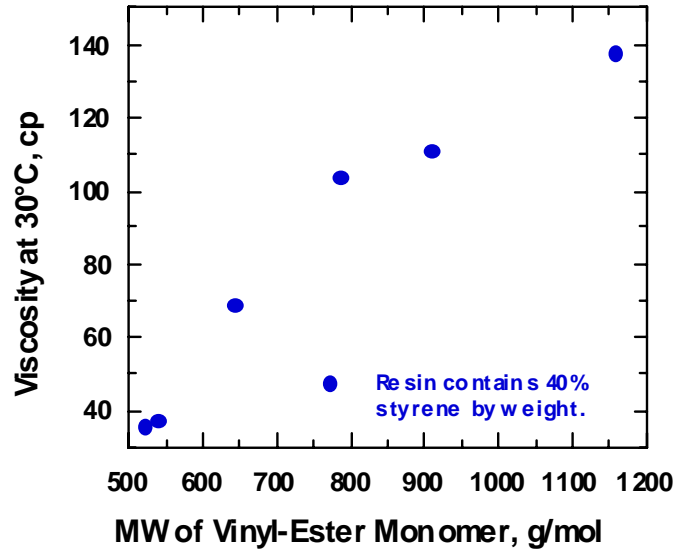


**Figure 31.** The viscosity of vinyl ester resins as a function of the molecular weight of the VE monomer.

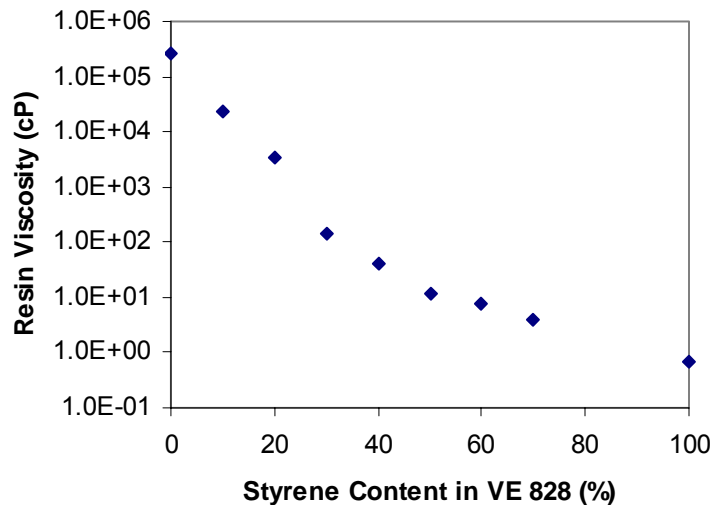


**Figure 32.** The viscosity of vinyl ester 828 resin as a function of styrene content.

The fracture toughness increased with the vinyl ester molecular weight (Figure 33) and with increasing styrene content (Figure 34). This occurred because both of these factors increase the molecular weight between cross-links (i.e. decrease the cross-link density) [22]. The modulus and  $T_g$  are affected in the opposite manner as the fracture toughness with increasing VE molecular weight and styrene content because of decreasing cross-link density [22]. Figure 35 shows that  $T_g$  decreased as the VE molecular weight increased. It is important to note that the fracture toughness is a much larger function of styrene content and VE molecular weight than the modulus and  $T_g$ . In addition, the polymer matrix has only a small effect on the modulus of a composite part, whereas the fracture toughness is highly dependent on the toughness of the polymer [23].

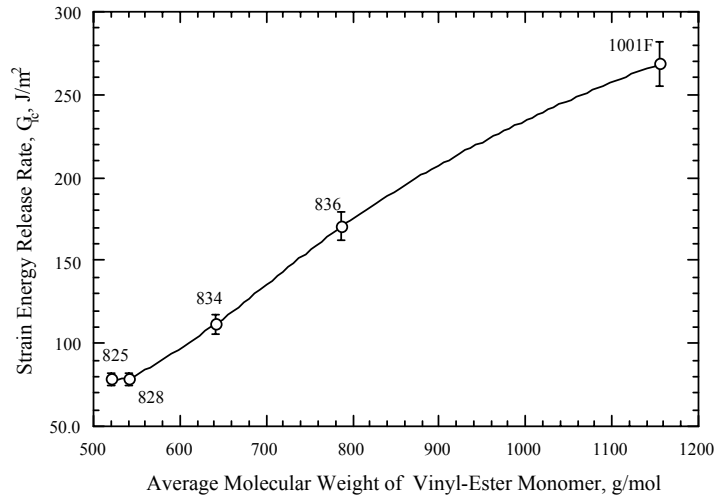


**Figure 33.** The fracture toughness as a function of VE molecular weight for vinyl esters with 40 wt% styrene.

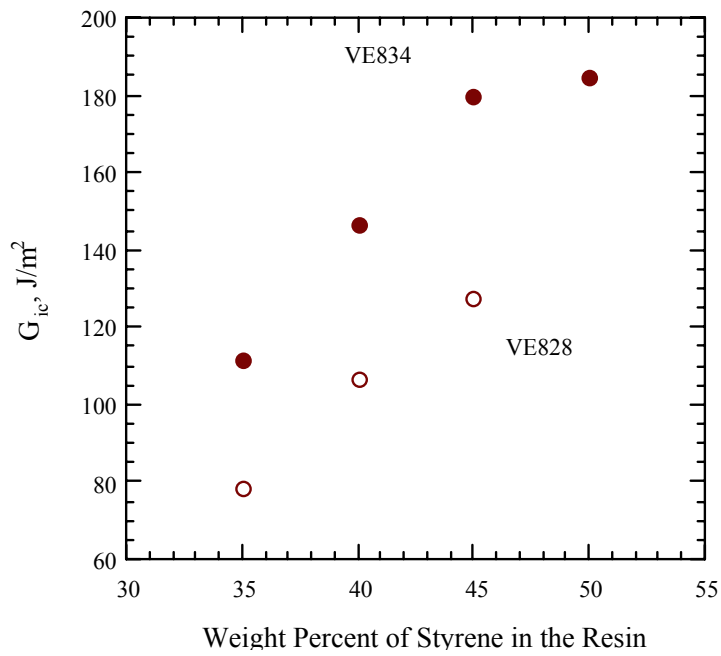


**Figure 34.** The fracture toughness as a function of styrene content for VE 834 and VE 828.

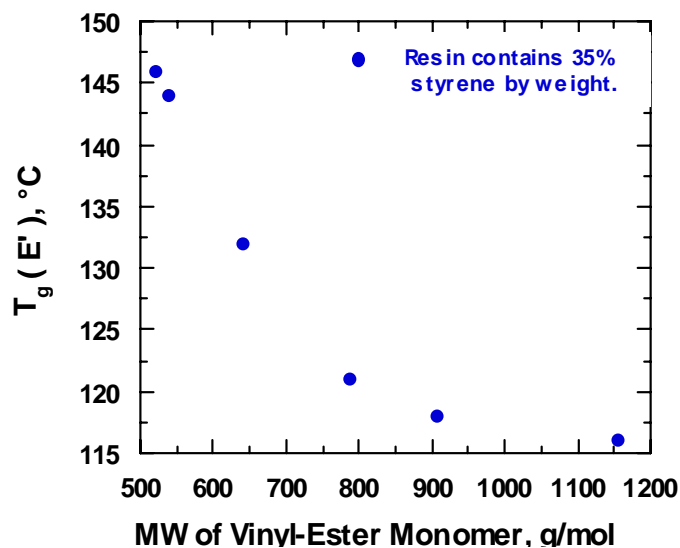


**Figure 35.**  $T_g$  as a function of vinyl ester molecular weight for samples with 35% styrene.

This work shows that a strict reduction in the styrene content of VE resins not only decreases the processability of the resins, but also unacceptably decreases their toughness. Increasing the VE molecular weight can be used to increase the toughness, but requires a greater styrene content to have processable resins. We hypothesize that bimodal blends containing both low and high molecular weight VE monomers would yield resins with low viscosities and high fracture toughness. Therefore, these resins would require less styrene to maintain good fracture properties and acceptable viscosities.

### 3.2.3.2 Preparation of Bimodal Blends of VE Monomers

Bimodal blends of VE monomers were prepared by methacrylation of blends of Epon 828, used as the low molecular weight DGEBA, and 1001F, 1004F, 1007F, or 1009F as the high molecular weight DGEBA. Epon 100XF are solids at room temperature. The viscosities of these resins are too high to effectively mix during the VE reaction, even at 100°C. Therefore, these resins were blended with Epon 828 to prepare bimodal VE blends. Unfortunately, the solid contents were just too high for only Epon 828 and the required amount of methacrylic acid to dissolve, even at the reaction temperature (100°C). Therefore, low styrene contents (< 20 wt.%) were added to completely dissolve the high molecular weight Epon 100XF. Hydroquinone in the amount of 1000 ppm based on the entire reaction contents was added because the addition of styrene during the methacrylation of Epon causes gelation. Bimodal blends of VE were prepared with the specific mass ratios of 828/1001F 29/71, 828/1004F 42/58, 828/1007F 52.5/47.5, and 828/1009F 50/50. These mass fractions were chosen to at least match the molecular weight of Dow Derakane resins. Higher VE 828 weight fractions were achieved by mixing in pure VE 828 to the bimodal blend.

Approximately 200 g Epon 828 was added to the reactor. Approximately 100 g styrene (20 wt.%) was added to the reaction vessel. The reaction vessel was sealed and stirred vigorously with the mechanical mixer. While heating to 100°C, the desired content of Epon 100XF was

added to the reactor in aliquots over the course of ~ 1 hour to prevent excessive clumping of the solid Epon 100XF. In addition, 1.01 times the stoichiometric amount of methacrylic acid along with 1% AMC-2 catalyst (based on Epon and methacrylic acid masses only) was added to the solution. The reaction temperature was kept in the range of 90-95°C, while using the cooling coils for cooling as needed. Once the acid number was approximately 5, the reaction was ended.

For all polymer samples, bimodal blend contents were chosen to match the  $M_n$  and  $M_w$  of Derakane 411-C50. In cases where large gaps in molecular weights occurred, other bimodal compositions were chosen and tested. 45 wt.% styrene was used for all bimodal blends. In addition, the styrene content that equated the resin viscosity to the resin viscosities of Derakane 411-C50 (150 cP) and 441-400 (400 cP) were used.

SEC was used to experimentally measure the molecular weight of VE blends and determine if the oligomerization occurred during VE preparation. No unexpected high molecular weight peaks were visible in the chromatographs, indicating that oligomerization did not occur. The experimental VE  $M_n$  agreed well with the calculated VE molecular weights, based on epoxy titration results (Table 11). Furthermore, the experimental styrene contents closely matched the specific styrene contents that were added to the vinyl ester blends.

**Table 11. The experimentally determined VE molecular weights and styrene contents. The styrene contents are the experimentally determined and the initial weight fraction styrene (prepared) in the reaction mixture of the prepared VE. The VE  $M_n$  was calculated using the epoxy titration molecular weight results.**

Resin	Exp. VE $MBB_w$ (g/mol)	Exp. VE $MBB_n$ (g/mol)	Calculated VE $MBB_n$ (g/mol)	Exp. Styrene Content (wt.%)	Prepared Styrene Content (wt.%)
VE 828 + 30% styrene	550	540	540	29	30
828/1001F 29/71	867	802	800	16.5	16.5
828/1004F 42/58	1370	933	925	16.5	16.5
828/1007F 52.5/47.5	2257	920	930	19.5	19.5
828/1009F 50/50	3130	987	990	19.5	19.5

### 3.2.3.3 Resin Viscosity of Bimodal Blends

#### 3.2.3.3.1 Effect of Vinyl Ester Molecular Weight and Styrene Content

The viscosity decreased exponentially with styrene content for all bimodal blends (Figure 36). In addition, the viscosity decreased as the molecular weight of the bimodal blend decreased. For the most part, the curves appear to be self-similar, with only a shifting in viscosity accounting for any differences among them.

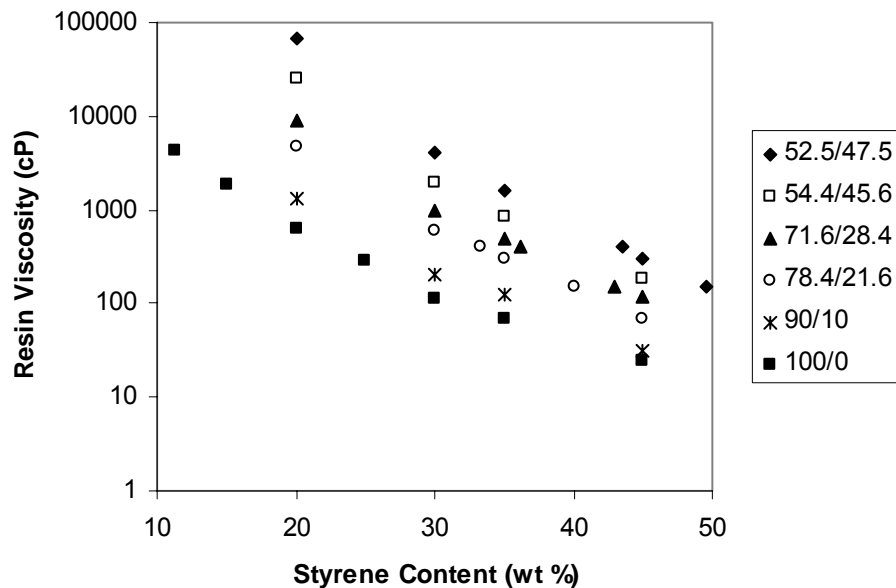


**Figure 36. The resin viscosity as a function of styrene composition for various bimodal VE compositions of VE 828/1007F.**

The number average molecular weight of the VE monomers governs the resin viscosity. For all bimodal blends, the resin viscosity is a single function of the number average molecular weight of the vinyl ester monomers for constant styrene contents (Figure 37). Therefore, number average molecular weight can be used to normalize the resin viscosity for the particular DGEBA used. Similar results were not found when normalizing with the viscosity average or weight average molecular weight (Figure 38).

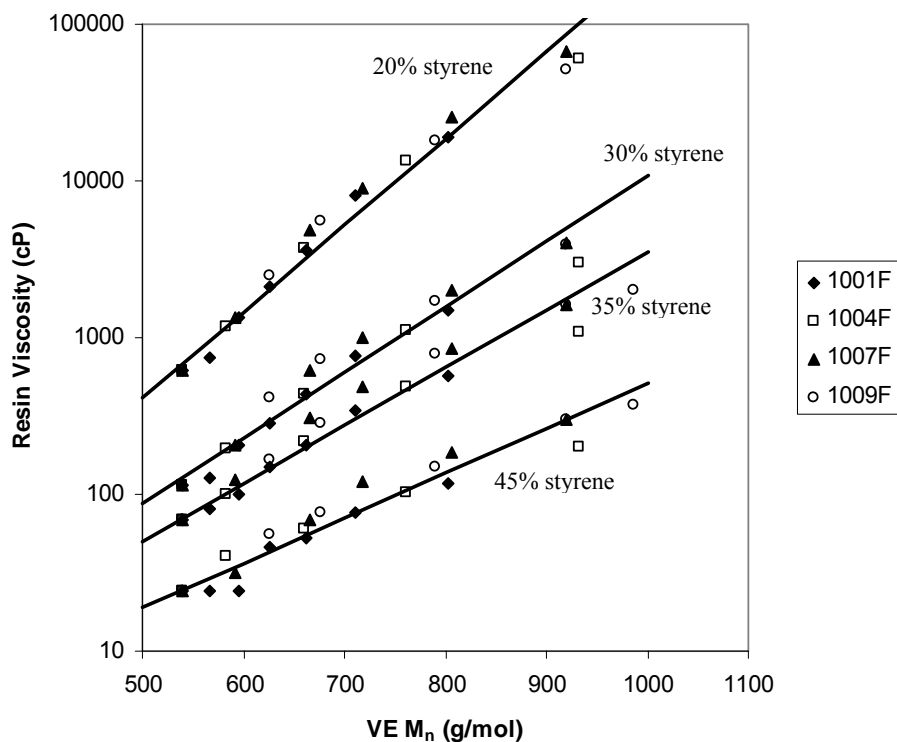


**Figure 37.** The resin viscosity as a function of VE  $M_n$  and styrene content, showing that resin viscosity is normalized by VE  $M_n$ .

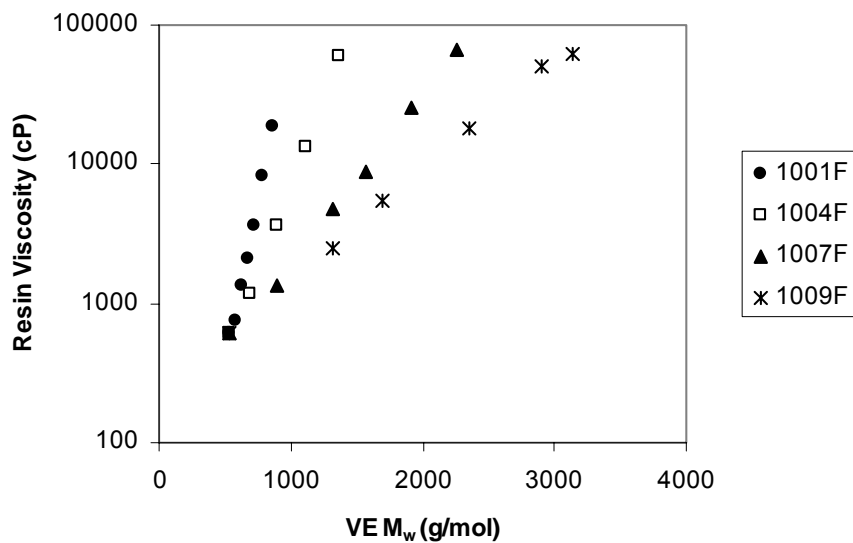


**Figure 38.** The resin viscosity as a function of VE  $M_w$  for resins containing 20 wt.% styrene, showing that resin viscosity is not normalized by VE  $M_w$ .

For polymer melts, the viscosity depends on  $M_w$  in a power-law relationship, as shown by Rouse and Reptation theory [24]. The Mark-Houwink-Sakurada equation shows that the viscosity of dilute polymer solutions depends on the viscosity average molecular weight, which is between the values of  $M_n$  and  $M_w$ , in a power law-fashion [24]. When using a power-law relationship to relate the VE resin viscosity to the molecular weight, the power-law exponent had a value between 5 and 10, which is much higher than that for dilute polymer solutions ( $< 1$ ) and for polymer melts (1 or 3.4) [24]. The resins tested in this work were monomers or small polymers with a very low degree of polymerization, and they were not in dilute solution. In dilute solution theory, the dissolved polymers interact with the solvent only, and increase the viscosity through these interactions. In concentrated VE resins, VE monomers interact with styrene and other vinyl ester monomers to produce frictional forces. Therefore, dilute solution theory is not applicable. The physics and mathematics of concentrated solutions are not well understood [25]. Analysis of literature data shows that the bulk viscosities of C5-C16 alkanes and alcohols at 25°C depend on molecular weight in a power-law relationship with exponents of 2.3 and 1.8, respectively (Figure 9) [26], which are considerably higher than the value of 1 Rouse theory predicts for non-entangled melts. Rouse theory failed for the vinyl esters used in this work because these molecules are Newtonian, and Rouse theory only applies to viscoelastic polymer melts [24, 25]. It is possible that the viscosity of these resins will behave according to Rouse theory when no styrene is present in the resin or for higher molecular weight vinyl esters. Reptation is only valid for entangled polymer melts, and is not appropriate for these low molecular weight VE resins [24]. Furthermore, weight average molecular weights only apply to polymeric molecules, and would not apply to Newtonian VE resins. Therefore, the number average molecular weight should govern the viscosity of vinyl ester resins.

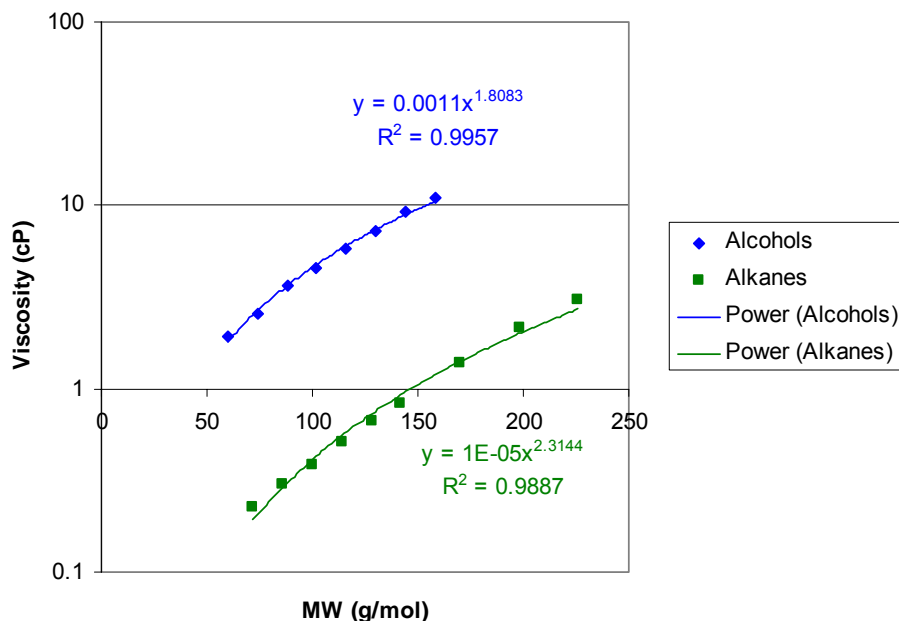


**Figure 39. The bulk viscosities of C5-C16 alkanes and alcohols at 25°C dependence on molecular weight [26].**

Styrene affects the resin viscosity in a consistent manner. For different VE blends with the same number average molecular weight, the normalized resin viscosity is a single decreasing exponential function of styrene content (Figure 40). The normalized resin viscosity,  $\eta_n$ , is simply the viscosity divided by the resin viscosity at 20 wt% styrene (i.e. the maximum tested resin viscosity) (Eq. 34):

$$\eta_n = \frac{\eta}{\eta(20\text{wt}\%St)} \quad (34)$$

This normalization was done to account for slight differences in the molecular weights among the bimodal blends displayed on the same chart, which cause significant differences in the resin viscosity. Therefore, Figure 40 shows that styrene content affects all bimodal blends with similar  $M_n$  to the same extent regardless of the molecular weight of the individual components. However, as the overall number average molecular weight decreases, the effect of styrene content on the viscosity decreases, as shown by a less negative slope (Figure 40).

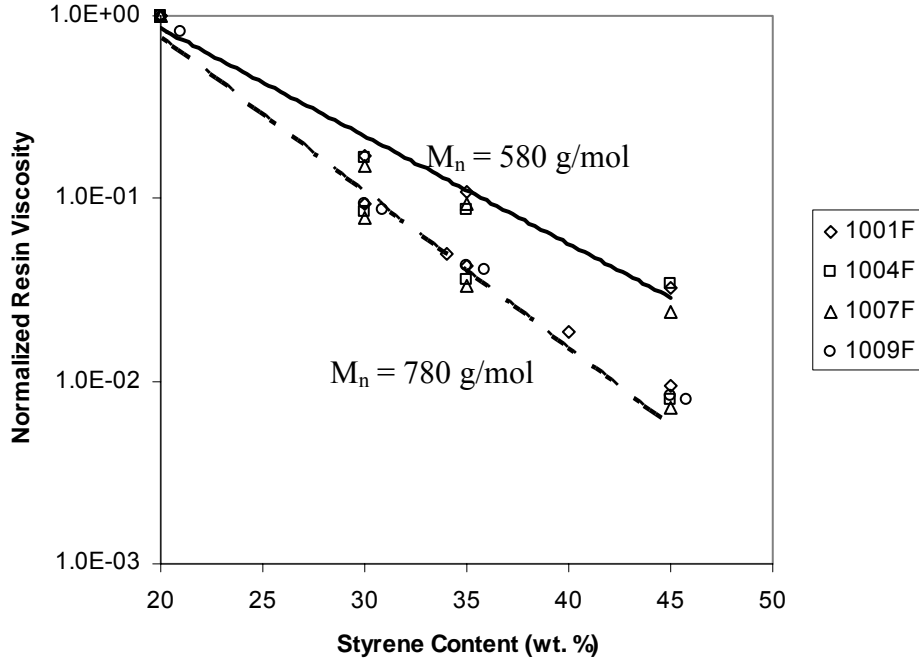


**Figure 40.** The resin viscosity as a function of styrene content at constant  $M_n$ . Styrene content affects the resin viscosity to the same extent for all bimodal resins with the same  $M_n$ , and the effect of styrene content on resin viscosity decreases as  $M_n$  decreases.

The best fit lines in Figure 37 represent a simple expression for the resin viscosity ( $\eta$ ) as a function of number average molecular weight and styrene content. The form of this relationship at 30°C is (Eq. 35):

$$\eta_{VE/Sty}(S, M_n) = \eta_{Sty} \cdot \text{Exp} \left[ \frac{M_n}{M_e(S)} \right] \quad [\text{cP}] \quad (35)$$

$\eta_{\text{Styrene}}$  is the viscosity of styrene (i.e. 0.7 cP, the viscosity when the vinyl ester molecular weight is zero) [26], and  $M_e(S)$  is an effective molecular weight that is a function of styrene content. The form of the relationship implies that we are modeling the effect of the addition of a more viscous, higher molecular weight species on the styrene viscosity. Figure 41 shows that  $M_e(S)$  is an exponential function of the styrene content (Eq. 36):

$$M_e(S) = 46.7 \cdot \text{Exp}[2.63 \cdot S] \quad [\text{g/mol}] \quad (36)$$

where S is the styrene weight fraction. A linear function of styrene weight fraction with a slope of 292.1 g/mol and an intercept of 17.9 g/mol can approximate this function quite well in the range of the collected data. Combining Eq. 35 and 36 shows that the viscosity of bimodal blends is a predictable function of the  $M_n$  of the VE monomers and the styrene weight fraction (Eq. 37):

$$\eta_{VE/Sty}(S, M_n) = \eta_{Sty} \cdot \text{Exp}\left[\frac{M_n}{46.7 \cdot \text{Exp}(2.63 \cdot S)}\right] \quad [\text{cP}] \quad (37)$$

Eq. 37 shows that resin viscosity is proportional to the exponential of the number average molecular weight and proportional the exponential of the inverse of the exponential of the styrene fraction. However, because  $M_e(S)$  can be approximated fairly well by a linear relationship, the viscosity is basically inversely proportional to a single exponential function of styrene content, as shown in Figure 40. In other words, the effect of  $M_n$  on the resin viscosity is modified by a negative exponential function of the styrene content.

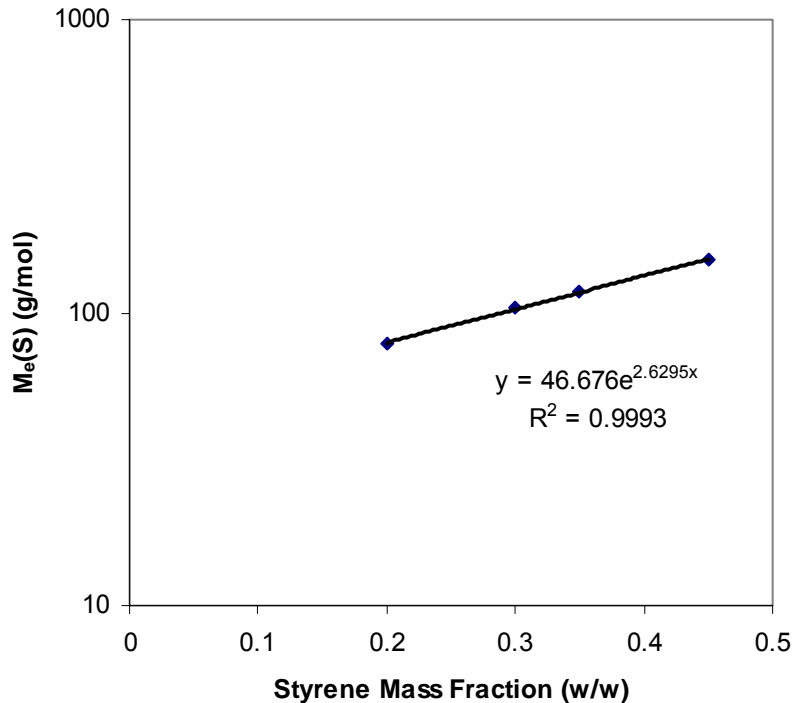


**Figure 41.** The dependence of  $M_e(S)$  on the styrene weight fraction in bimodal blends of VE resins.

Interestingly, styrene's molecular weight (104 g/mol) falls right into the range of values of  $M_e(S)$ , which increased from 46.7 g/mol at ~0% styrene to 648 g/mol at ~100% styrene. Because of the exponential dependence, small changes in styrene content had a larger effect on the resin viscosity for low values of  $M_e(S)$  than they did for high values of  $M_e(S)$  as shown in Figure 36. The numerical coefficients in Eq. 26 and 27 are fitting parameters that physically relate how well styrene can reduce the interactions among VE monomers and represent the ratio of the pure VE viscosity to that of styrene. Rather than examining the effect of polarity, etc.,  $M_e(S)$  allows for an even comparison of VE molecular weight to an effective styrene molecular weight. In other words, at high styrene concentrations, the VE monomers would need to have at least a molecular weight on the order of 650 g/mol to have a significant effect on the viscosity. Because VE monomers are more polar in nature than styrene, the value of  $M_e(S)$  at low styrene concentrations was less than the molecular weight of pure styrene. This means that VE monomers with lower molecular weight than styrene could still raise the viscosity of the resin because of polar interactions.

A viscosity of 500 cP is considered about the maximum for most inexpensive liquid molding techniques [27, 28]. Higher viscosities increase the production time and increase the likelihood of voids in the part. Eq. 37 can be rearranged to solve for the minimum styrene content required to achieve such a viscosity for given values of  $M_n$ . Table 12 shows that the minimum styrene content increased approximately linearly with the number average molecular weight of the VE monomers. The number average molecular weights can be achieved by mixing certain amounts of VE 828 with a corresponding amount of higher molecular weight VE monomer. For example, to formulate a resin with only 30 wt.% styrene, an  $M_n$  of 675 g/mol can be achieved by blending as much as 78 wt.% VE 828 with 22 wt.% VE 1009F or as little as 62 wt.% VE 828 with 38 wt.% 1001F. Table 12 shows that a minimum styrene content of 20 wt.% is necessary to achieve a viscosity of 500 cP for DGEBA-based vinyl ester resins (i.e. the minimum molecular weight of 520 g/mol for DGEBA based vinyl esters occurs when  $n=0$  (Figure 4)).

**Table 12. The minimum allowable styrene content to achieve a viscosity of 500 cP or lower for various values of the number average molecular weight of the VE monomers.**

$M_n$ of VE (g/mol)	Minimum Styrene Content (wt.%)
520	20.0
575	23.9
600	25.5
625	27.0
650	28.5
675	29.9
700	31.3
750	34.0
800	36.4
850	38.7
900	40.9

### 3.2.3.3.2 Effect of Temperature

The viscosity of most chemical species follows an Arrhenius relationship (Eq. 38) [9]:

$$\eta = A \cdot \exp\left(\frac{E}{RT}\right) \quad (38)$$

where  $A$  is the pre-factor,  $E$  is the activation energy for viscous flow,  $R$  is the ideal gas constant, and  $T$  is the absolute temperature. Taking the natural logarithm of both sides of Eq. 38 yields (Eq. 39):

$$\ln(\eta) = \ln(A) + \frac{E}{RT} \quad (39)$$

Therefore, a plot of  $\ln(\eta)$  vs.  $1/T$  should be a line with a slope equal to  $E/R$  and an intercept of  $\ln(A)$ . Figure 11 shows that this plot is indeed linear for vinyl ester resins. When there was viscosity-temperature hysteresis, the viscosity usually deviated from linearity at 55°C or so. These points at 55°C and higher were omitted from analysis because they did not represent the viscosity of the monomeric resin.

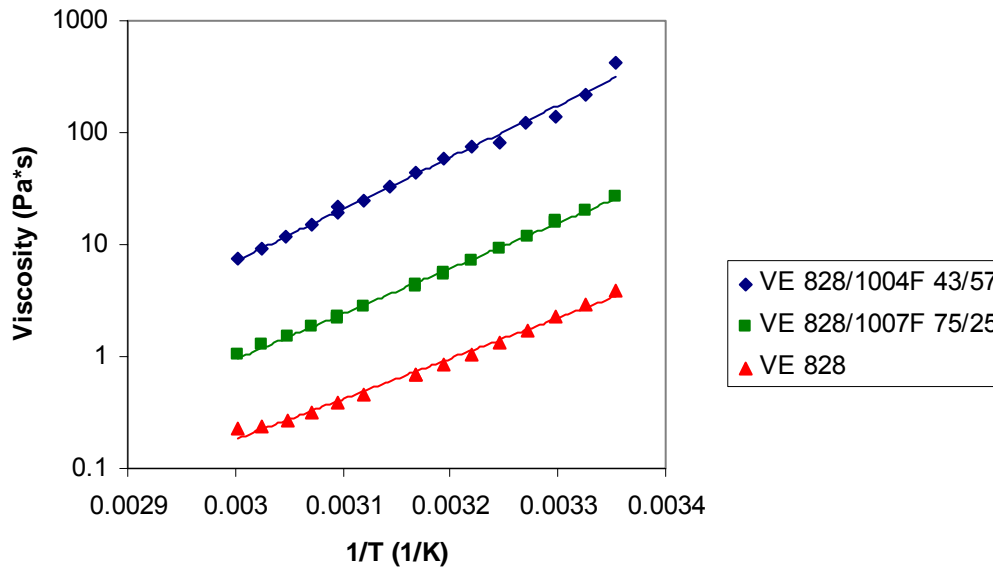


**Figure 42. The viscosity-temperature dependence is Arrhenius for VE resins with 20 wt% styrene.**

The activation energy for viscous flow and the pre-factors were calculated from the Arrhenius plots. The activation energy decreased linearly as a function of styrene content (Figure 43) (Eq. 40):

$$E_{VE/Sty} = -186 * S + 114.5 \quad [\text{kJ}] \quad (40)$$

where  $S$  is the styrene weight fraction. This indicates the sensitivity to temperature decreased as the styrene content increased. This expression is only valid through 50 wt% styrene, considering that over 61 wt.% styrene, the calculated activation energy is negative. This would indicate that the viscosity should become more dependent on styrene content at higher styrene contents, which

is not physically reasonable. The activation energy decreased with styrene content because both styrene and temperature reduce viscosity by disrupting intermolecular interactions. As the styrene content increased, it is easier for molecules to slide by each other, thereby reducing the activation energy for viscous flow. The range of activation energies measured is typical for these monomeric resins [14]. The pre-factor increased exponentially as a function of styrene content in the resin (Figure 44) (Eq. 41):

$$A_{VE/Sty} = 3.67 \cdot 10^{-18} \cdot \text{Exp}(59 \cdot S) \quad [\text{Pa} \cdot \text{s}] \quad (41)$$

This factor was expected to increase because it is related to the frequency of interactions, which should increase given that high styrene contents produce resins with lower viscosities. Calculating  $A$  involves extrapolating to infinite temperature. An accurate measurement of this pre-factor is very difficult, and is the main cause for the scatter in the results. The activation energy and pre-factor were not functions of VE molecular weight (Figure 45). Therefore, vinyl ester molecular weight had no effect on the temperature dependence of the resin, but chemical differences in the resin did affect the temperature dependence of the viscosity [14].

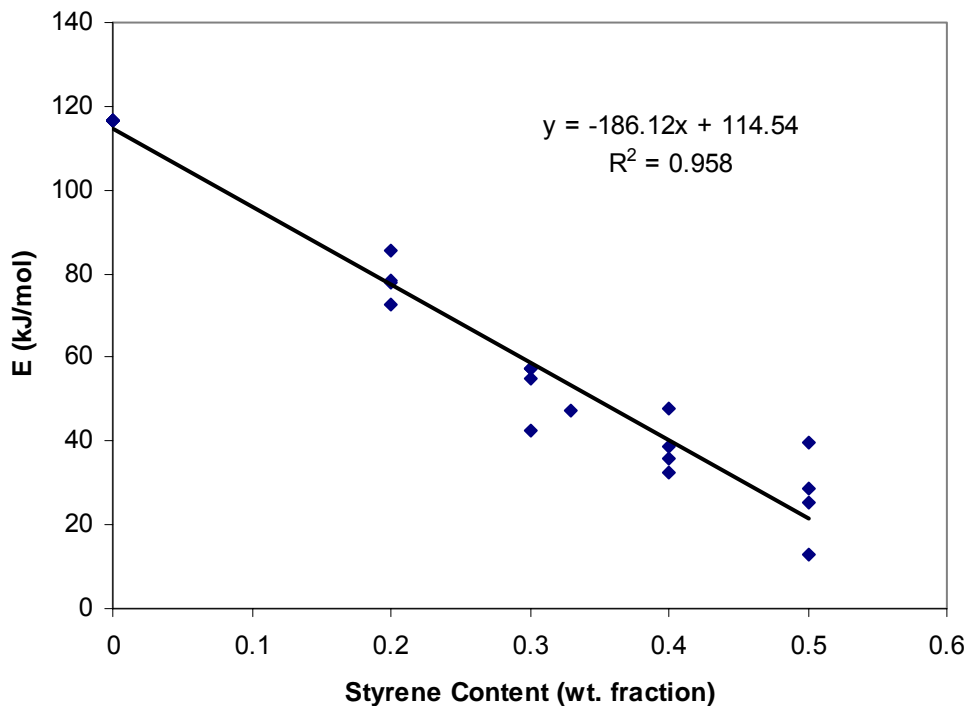


**Figure 43. The activation energy for viscous flow as a function of styrene content in VE resins.**

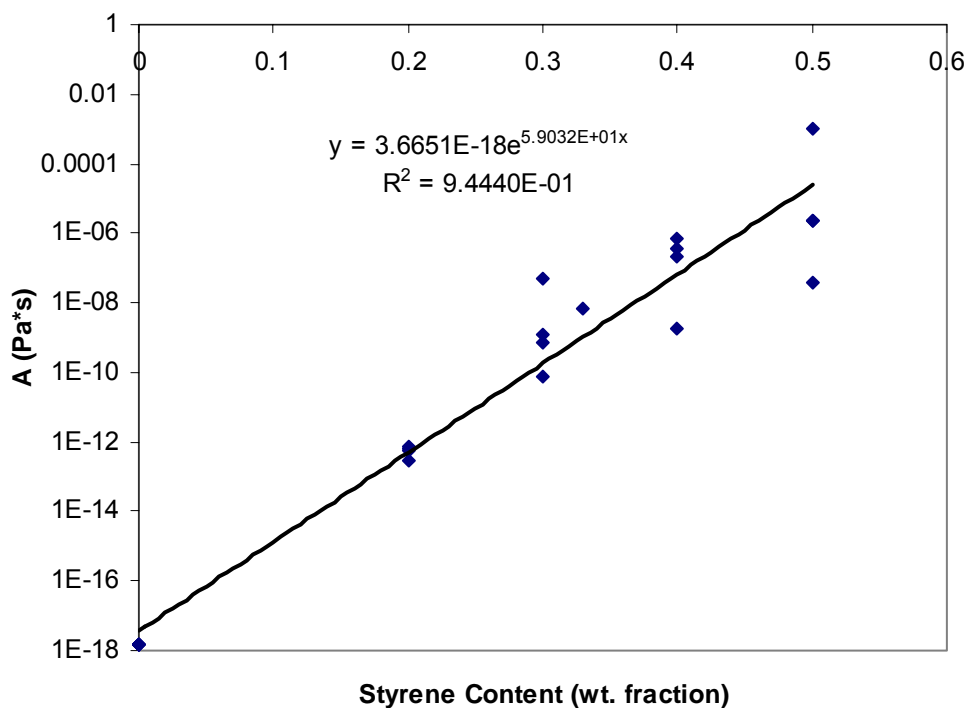


Figure 44. The pre-factor as a function of styrene content in VE resins.

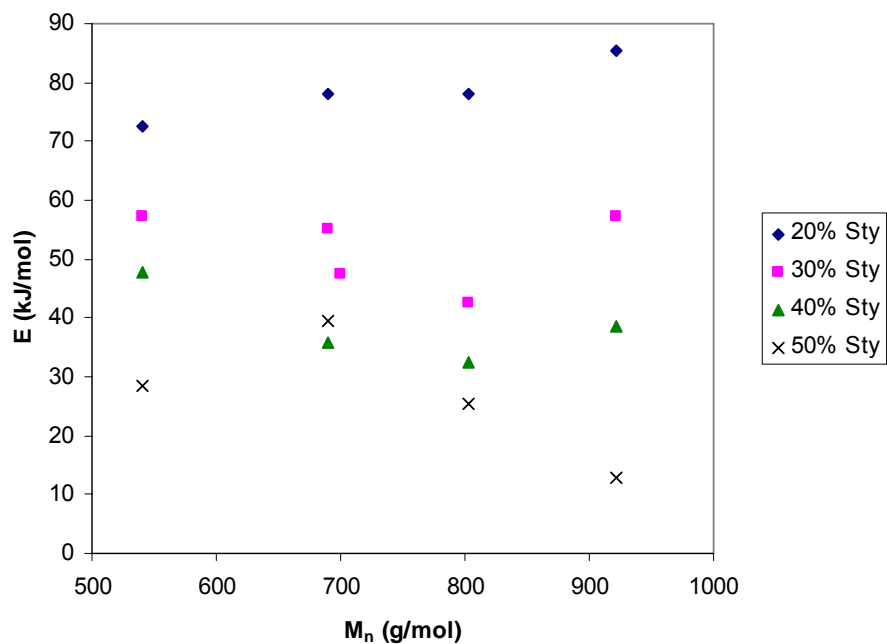


Figure 45. The activation energy for viscous flow as a function of VE molecular weight.

Combining Equations 38, 40, 41 yields the viscosity-temperature model (Eq. 42):

$$\eta_{VE/Sty}(S, T) = 3.67 \cdot 10^{-18} \cdot \text{Exp}\left(\frac{-186120 \cdot S + 114540 + 59 \cdot S \cdot RT}{RT}\right) \text{ [cP]} \quad (42)$$

Therefore, the viscosity-temperature dependence of VE resins was only a function of temperature and styrene content. Specifically, the viscosity was exponentially proportional to the inverse of the temperature. Equation 42 shows the viscosity was both exponentially proportional to the styrene content and to the inverse of the styrene content.

### 3.2.3.3 Complete Viscosity Model for Vinyl Ester/Styrene Resins

We already have an accurate working model to predict resin viscosity as a function of styrene content and VE molecular weight at 30°C (Eq. 37). The viscosity-temperature model only needs to be used to determine the change in viscosity as a result of changing the temperature from 30°C to a higher or lower temperature. The ratio of the viscosities at temperatures 2 and 1 (303 K) is (Eq. 43):

$$\frac{\eta_2}{\eta_{1 \text{ VE/Sty}}}(S, T) = \text{Exp}\left(\frac{-186120 \cdot S + 114540}{RT_2} + \frac{186120 \cdot S - 114540}{RT_1}\right) \text{ [cP]} \quad (43)$$

Given the viscosity at 30°C ( $T_1$ ), the viscosity at an arbitrary temperature 2 is (Eq. 44):

$$\eta_{2 \text{ VE/Sty}}(S, T) = \eta_1 \cdot \text{Exp}\left(\frac{-186120 \cdot S + 114540}{RT_2} + \frac{186120 \cdot S - 114540}{RT_1}\right) \text{ [cP]} \quad (44)$$

Substituting in the viscosity model at 30°C for  $\eta_1$  (Eq. 37) gives the overall viscosity model (Eq. 45):

$$\eta_{VE/Sty}(S, T, M_n) = \eta_{Sty} \cdot \text{Exp}\left[\frac{M_n}{46.7 \cdot \text{Exp}(2.63 \cdot S)}\right] \cdot \text{Exp}\left[\frac{-186120 \cdot S + 114540}{R} \left(\frac{1}{T_2} - \frac{1}{303K}\right)\right] \text{ [cP]} \quad (45)$$

This empirical model allows calculation of the viscosity using only the styrene content, VE  $M_n$ , and temperature. This equation is accurate at temperatures ranging from 25°C to 60°C,  $M_n$  ranging from 540-950 g/mol, and styrene contents ranging from 0-50 wt%. This model probably can be extrapolated to other parameter ranges with a good degree of accuracy, but is not valid at styrene contents approaching and above 60 wt% because of the zero and negative values of the activation energy calculated at these styrene contents. An advantage of using Eq. 45 rather than using Eq. 42 to calculate the resin viscosity as a function of temperature is that the latter equations use the pre-factor, which was calculated with less accuracy than the activation energy or the 30°C viscosity model. This viscosity model for VE/styrene resins can be used to predict the minimum styrene content necessary for a particular liquid molding operation. For example, Table 13 shows the required styrene content for given operation temperatures and vinyl ester molecular weights for a maximum allowable viscosity of 500 cP. Interestingly, 45 wt.% styrene is only necessary for high molecular weight vinyl esters at fairly low operation temperatures.

**Table 13. The calculated styrene content as a function of VE molecular weight and temperature that is required to achieve  $\eta = 500$  cP for DGEBA-based vinyl esters.**

Temperature (°C)	Required Styrene Content to have $\eta = 500$ cP in wt%			
	$M_n = 520$ g/mol	$M_n = 650$ g/mol	$M_n = 800$ g/mol	$M_n = 950$ g/mol
20	25.7	33.0	39.8	45.4
25	22.9	30.8	38.1	44.2
30	20.1	28.5	36.4	43.0
35	17.1	26.2	34.6	41.6

### 3.2.3.4 Cure Kinetics and Morphology of Bimodal Blends

There were differences in the cure kinetics of bimodal blends of vinyl ester relative to monodisperse vinyl ester monomers. The cure kinetics was measured using FTIR at both 30°C and 90°C. VE bimodal blends of 828/1001F, 828/1004F, 828/1007F, and 828/1009F, with three 828/100xF ratios ranging from 29/71 to 85/15 for each, and at least four different styrene contents, ranging from 20 wt.% to 60 wt.%, were prepared. VE 828 with 20-60 wt.% styrene was used as a control along with Derakane 411-350 and Derakane 441-400.

As expected, the cure rate increased with increasing cure temperature (Figure 46). Also, the cure rate of vinyl ester and styrene became more similar as the cure temperature increased, as found in the literature [1]. The styrene cured to a higher extent than the vinyl ester when cured at 90°C, but both reacted to a similar extent when cured at lower temperatures. During post-cure, more styrene reacted into the polymer network than did the VE monomer for resins cured at either temperature (Figure 46), except in the cases where the styrene conversion reached unity. Overall, it appears that cure at elevated temperatures adds polystyrene-rich zones to the material. This could reduce the fracture properties because polystyrene is very brittle. This occurred because styrene has a much lower molecular weight than VE monomers and thus has a higher mobility. Therefore, styrene can more easily diffuse towards growing radicals. Also, some VE monomers are likely to have one functional group reacted into the polymer network, making the other functional group highly unreactive because of diffusion limitations. After post-cure at 120°C (sharp increase in conversion after the plateau at lower times), the extents of cure of each of the components were similar at both cure temperature. Yet, it is expected that the morphology and properties will be different because of the differences in the cure profiles.

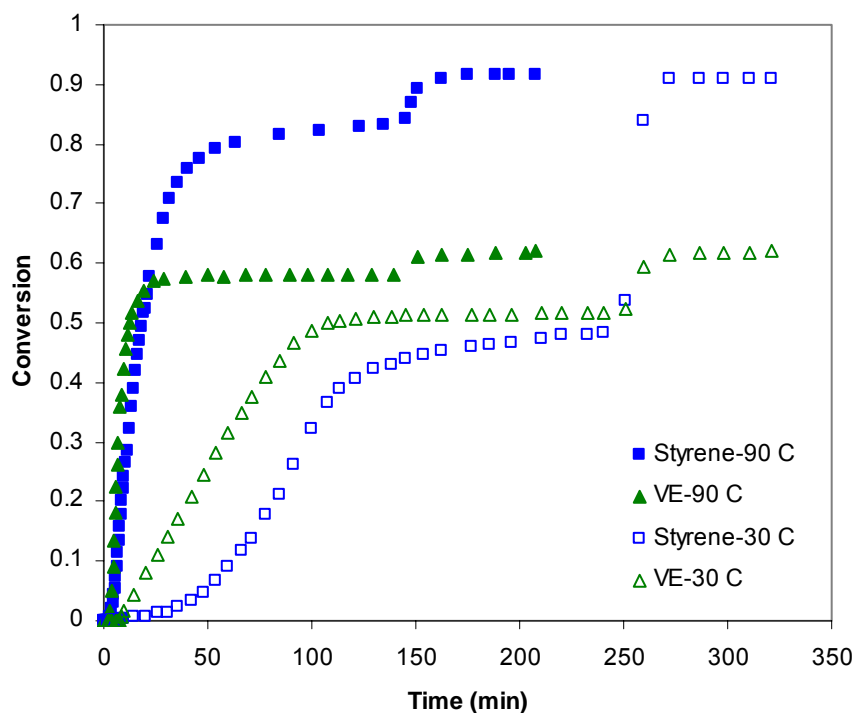


**Figure 46. The conversion as a function of time for Derakane 411-350 resins at 30°C and 90°C.**

Cure of the bimodal blends was affected for resins containing different styrene contents. For example, Figure 47 shows that the extent of cure of styrene monomer was higher but the VE monomer extent of cure was lower in the resin containing low styrene contents. It is well known that styrene facilitates the cure of vinyl ester, a major reason for styrene's wider use in these resins over methyl methacrylate. This indicates that bimodal blends with low styrene contents should have lower than expected cross-link densities based on cure of resins with higher styrene contents. Figure 48 and Figure 49 show the conversion as a function of time at 30°C for monodisperse VE 828 and bimodal blends, respectively. There are a few differences between the conversion profiles. First, the extent of cure of the vinyl ester is always lower in the bimodal blend. Also, the styrene content has more effect on the styrene conversion in monodisperse blends.

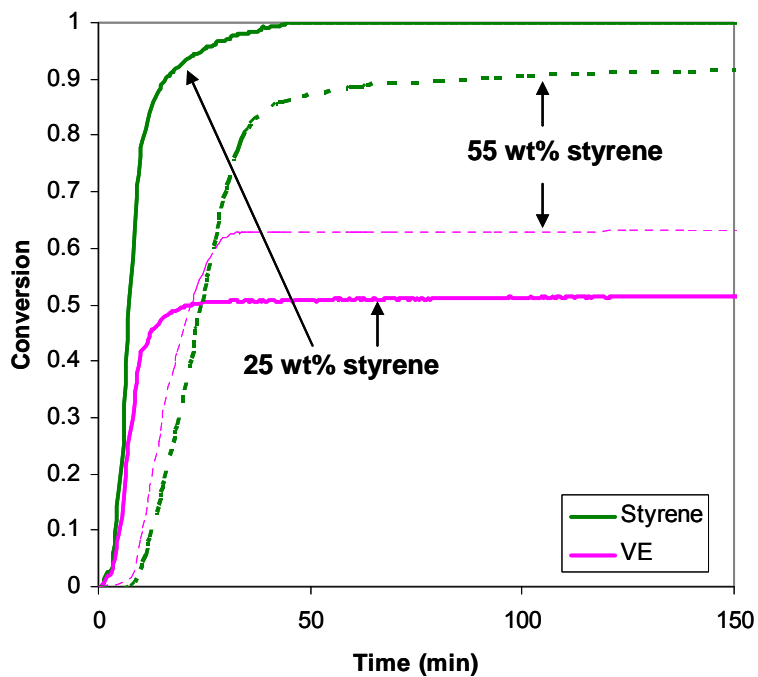


Figure 47. The styrene and VE monomer conversions as a function of cure time at 90°C for VE 828-1007F 65/35 with  $M_n = 780$  g/mol with 25 wt% and 55 wt% styrene.

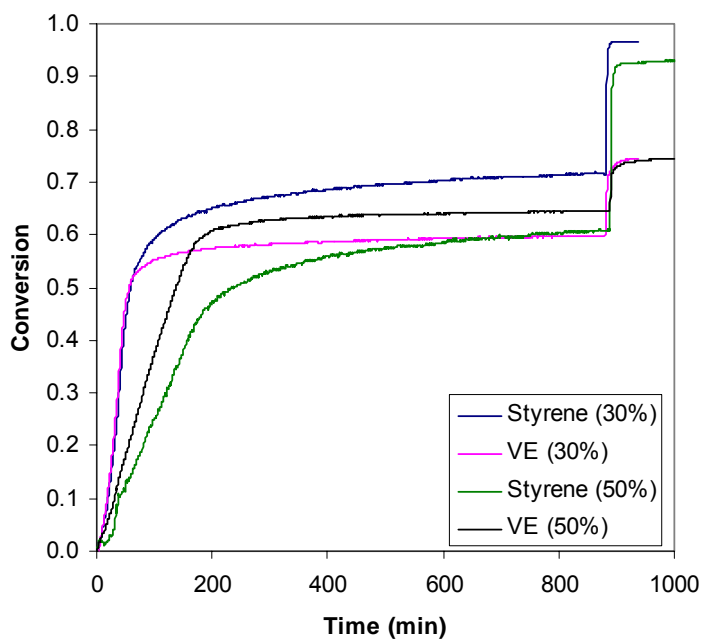
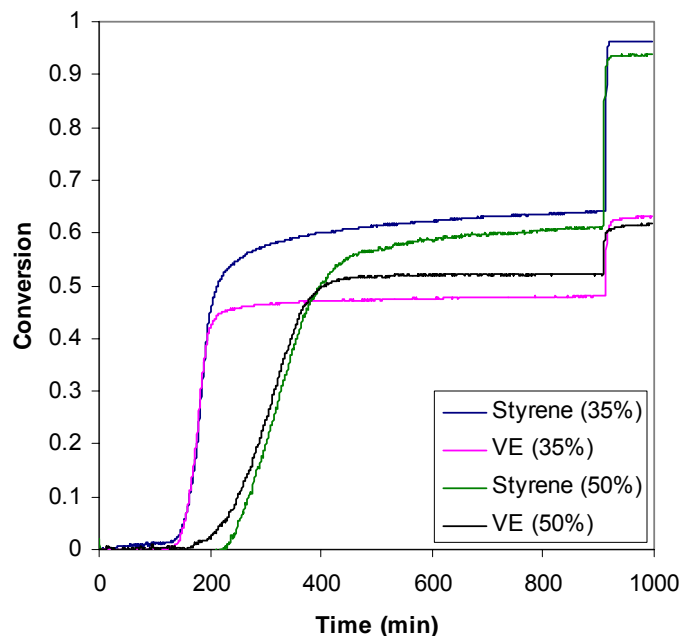


Figure 48. The styrene and VE monomer conversions as a function of cure time at 30°C for monodisperse VE 828 with 30 wt% styrene and 50 wt% styrene.



**Figure 49.** The styrene and VE monomer conversions as a function of cure time at 30°C for VE 828/1004F 43/57 with 30 wt% styrene and 50 wt% styrene.

The differences in the conversion profiles can be explained by the reactivity ratios. Reactivity ratios are a measure of the ratio of the likelihood of one component polymerizing with itself vs. the other component (Eq. 46):

$$r_1 = k_{11}/k_{12} \qquad r_2 = k_{22}/k_{21} \qquad (46)$$

$r_1$  is the reactivity ratio of component 1,  $k_{11}$  is the rate constant for propagation of a radical of type 1 with a monomer of type 1, and  $k_{12}$  is the rate constant for propagation of a radical of type 1 with a monomer of type 2. When  $r_1=0$ , component 1 will only polymerize with monomer 2. When  $r_1=1$ , a radical of component 1 is equally likely to polymerize with either monomer. As  $r_1 \rightarrow \infty$ , radicals of component 1 will only polymerize with monomer 1.

Commercial vinyl esters have a microgel morphology (Figure 50). Microgels are highly cross-linked phase-separated regions of the polymer. These occur when vinyl ester monomers react to a high degree with themselves to produce highly cross-linked regions. It was found that the size of the microgel regions depended on the reactivity ratios and cure temperature [1, 8]. At low cure temperatures, the microgel regions were large and  $r_{VE} > 1$  while  $r_{Styrene} < 1$  [1, 8]. At high cure temperatures, the microgel regions were small and the reactivity ratios of each component was  $\sim 0.5$  [1, 8]. Therefore, it was concluded that microgel morphology is affected by the reactivity ratio of the polymers, and microgels will be more prominent as the reactivity of the VE monomer increases [1, 8]. Furthermore, it was found that the fracture toughness of these polymers increased as the size of the microgel regions increased [1, 8].

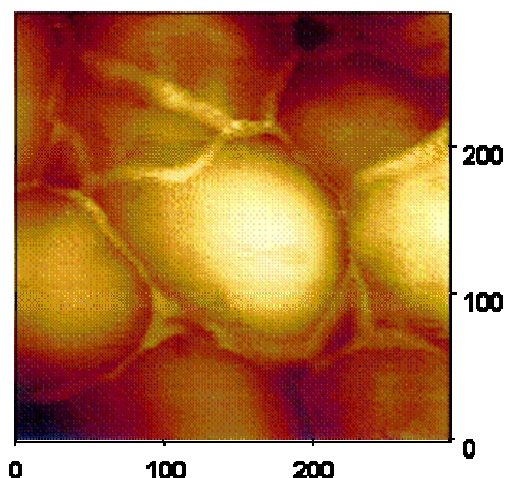


**Figure 50. Microgel morphology of vinyl ester resins [8].**

The reactivity ratios were calculated using the Mayo-Lewis and the Fineman-Ross methods [29]. The results were very similar and were averaged to remove the effect of the calculation method. The reactivity ratios for these systems are listed in Table 14. All of the measured reactivity ratios were below 1, meaning that the initial polymer formed has a propensity to be alternating in nature (i.e. VE prefers to polymerize with styrene and styrene prefers to polymerize with VE). The reactivity of vinyl ester increased relative to styrene as the cure temperature decreased, as was found in the literature. At both temperatures tested, the reactivity ratio of the vinyl ester is near zero for the bimodal blends, while it is higher for styrene. Furthermore, the reactivity ratio of vinyl ester is lower in the bimodal blends and the styrene reactivity ratio is higher in bimodal blends relative to the monodisperse resins. Therefore, the initial polymers formed for the bimodal resins should have a higher percentage of styrene and a lower percentage of vinyl ester than the monodisperse blends. We would therefore expect these bimodal resins to have small microgels. We cannot automatically assume there will be a reduction in the fracture toughness due to decreased microgel size because the cross-link density decreased for the bimodal blends, which should improve the fracture toughness. Furthermore, a direct measurement of the size of the microgels in bimodal blends has yet to be done. The reactivity ratios of vinyl ester and styrene became more similar as the cure temperature increased (as was inferred from Figure 46). This indicates that the microgels decrease in size as cure temperature increases, as was found in the literature [1].

**Table14. The reactivity ratios of vinyl ester and styrene for monodisperse VE resins and bimodal resins.**

Resin type	Cure Temperature (°C)	$r_{VE}$	$r_{Styrene}$
Monodisperse	30	$0.6 \pm 0.1$	$0.4 \pm 0.1$
Bimodal	30	$0.1 \pm 0.1$	$0.6 \pm 0.1$
Monodisperse	90	$0.3 \pm 0.1$	$0.3 \pm 0.1$
Bimodal	90	$0 \pm 0.1$	$0.3 \pm 0.1$

### 3.2.3.5 Polymer Properties of Bimodal Blends

Dynamic mechanical properties were affected by the molecular weight of the bimodal blends and the styrene content. In general, as the number average molecular weight of the bimodal resin increased,  $T_g$  decreased because  $M_c$  increased (Figure 51). In general, samples with the same  $M_n$  and styrene content had  $T_g$  within 3°C of each other. As the molecular weight of the resin increased, the distance between cross-links increased causing the network to become less rigid. However, the effect of bimodal blend molecular weight on polymer properties is fairly small, as  $T_g$  decreased only from 142°C to 125°C as  $M_n$  increased from 540 g/mol to 950 g/mol. For the same reasons,  $T_g$  decreased and  $M_c$  increased as the styrene content increased (Figure 52). As  $M_n$  increased, the effect of styrene content on  $T_g$  was less pronounced. This indicates that  $T_g$  of pure VE with no styrene is a stronger function of VE molecular weight than at 45 wt.% styrene (Figure 51). As shown by the Fox equation [30] and other equations relating  $T_g$  of a miscible blend to that of its components, the blend  $T_g$  is always greater than that of the lower  $T_g$  component. As a result, as the styrene content increases and  $T_g$  of 100°C (styrene) is approached, the effect of increasing styrene content decreases.  $T_g$  and  $M_c$  were not functions of  $M_w$ .

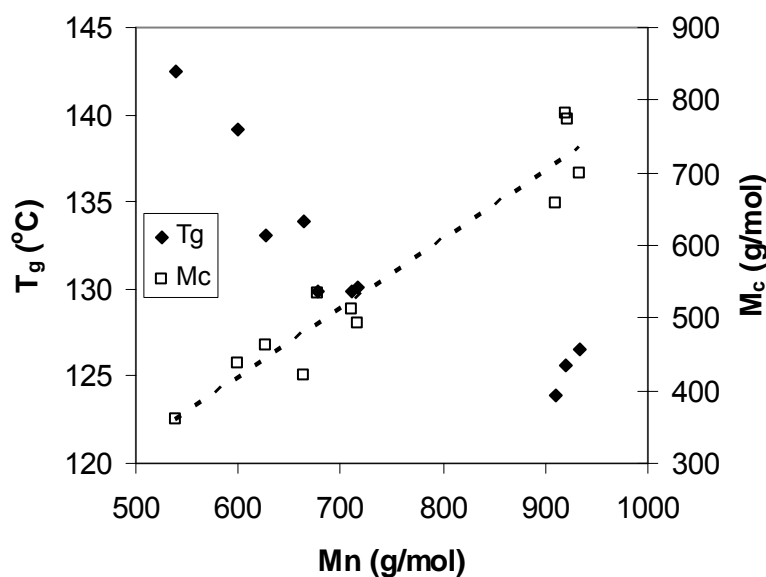
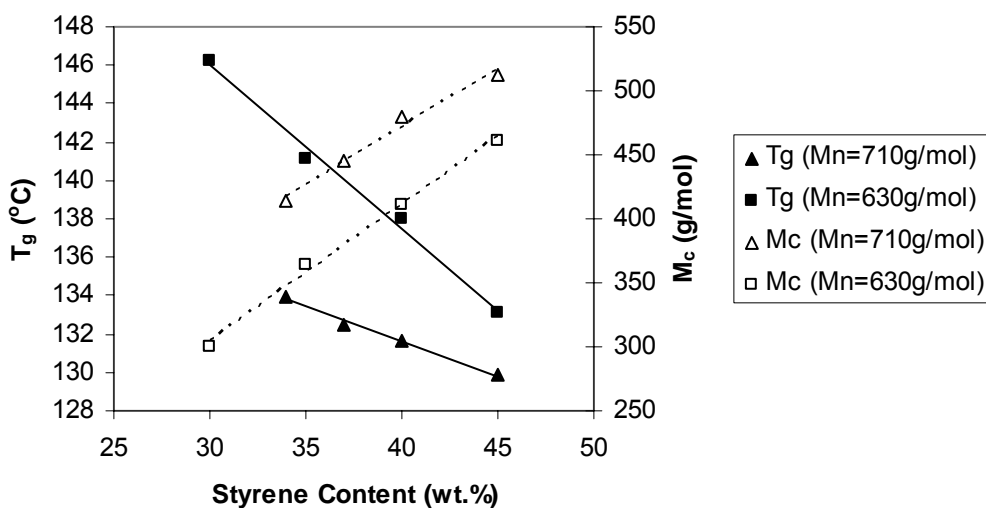


Figure 51.  $T_g$  and  $M_c$  as a function of  $M_n$  of bimodal VE blends with 45 wt.% styrene.



**Figure 52.**  $T_g$  and  $M_c$  as a function of styrene content for bimodal VE 828/1001F 48/52 ( $M_n = 710$  g/mol) and VE 828/1009F 84.9/15.1 ( $M_n = 630$  g/mol).

The fracture toughness of vinyl ester bimodal blends was measured (Table 15). Current results show that fracture toughness did not scale with either vinyl ester molecular weight or styrene content. In most cases, the fracture toughness of the blend exceeds that of monodisperse vinyl esters with similar molecular weights. Furthermore, it is evident that very high fracture toughness values can be achieved, even using fairly low styrene contents. For example, the VE 828/1007F 78/22 with 33 wt.% styrene had a  $G_{IC}$  of  $350 \text{ J/m}^2$ , which is approximately 3 times that of VE 828 with 45 wt.% styrene, while using one-third less styrene. In addition, the fracture toughness of this resin and a few other blends are even higher than that of Derakane 411-C50. Many blends also had higher fracture toughness than Derakane 441-400 while using similar low styrene contents. Therefore, it is possible to tailor vinyl ester molecular weight to achieve good fracture properties, while having low VOC emissions.

Fracture toughness did not scale with styrene content or  $M_n$  of the vinyl ester because a few factors are affecting the fracture properties. First, the results indicated that microgels are smaller in the bimodal blends relative to the monodisperse blends. However, the molecular weight between cross-links is higher for bimodal blends relative to monodisperse blends. Also, cure studies showed that the extent of cure, and therefore the network strength, is affected by the styrene content and  $M_n$  of the vinyl ester. Lastly, polystyrene zones, which are more likely to occur in resins with high styrene contents, are brittle and should reduce the fracture properties. It is possible that the interplay of these factors affected the fracture toughness of the bimodal blends.

**Table 15. The fracture toughness of bimodal blends. Fracture toughness for blends with the same VE monomer formulation but with different styrene compositions are listed with the styrene composition in parenthesis.**

Sample	VE $M_n$ (g/mol)	VE $M_w$ (g/mol)	Fracture Toughness, $G_{IC}$ (J/m <sup>2</sup> )		
			Low styrene content	Mid-styrene content	High styrene content
828	540	540	80 (35)	-	70 (45)
828/1001F 29/71	802	867	250 (37)	510 (43)	350 (45)
828/1001F 48/52	710	779	90 (34)	130 (40)	110 (45)
828/1004F 42/58	933	1371	-	240 (41)	170 (45)
828/1004F 75/25	660	898	130 (31)	120 (38)	140 (45)
828/1007F 53/47	921	2257	-	-	240 (45)
828/1007F 72/28	717	1567	240 (36)	-	220 (45)
828/1007F 78/22	665	1321	350 (33)	220 (40)	200 (45)
828/1009F 54/46	920	2902	-	-	270 (45)
828/1009F 78/22	677	1695	110 (33)	200 (38)	440 (45)
828/1009F 85/15	626	1322	80 (30)	190 (35)	120 (45)

Samples for flexural tests for all bimodal blends with varying styrene contents have been made. The flexural strength and modulus were not significantly affected by the styrene content and vinyl ester molecular weight. The flexural strength was 130 MPa  $\pm$  5 MPa and the flexural modulus was 3.5 GPa  $\pm$  0.2 GPa.

### 3.2.3.6 Styrene Emissions from Bimodal Blends

#### 3.2.3.6.1 *Total Styrene Emission*

The total styrene emission curves for each VE system (Table 16) and pure styrene are shown in Figure 53. All VE systems tested exhibited three distinct regions of evaporation controlled, transitional, and diffusion controlled, previously described. The total styrene emission from VE 828 (97%) was the highest and decreased as the vinyl ester molecular weight increased. This occurred because the viscosity was greater for the higher molecular weight samples, reducing the mobility of styrene in the resin and limiting its ability to diffuse to the surface. For resins with the same styrene content and vinyl ester  $M_n$ , regardless of which bimodal blend (i.e., 828/1001F or 828/1009F) was used, the emission profiles were the same. Therefore, emissions from vinyl ester resins can be reduced by using higher VE  $M_n$  and lower styrene contents, such as in bimodal blends.

**Table 16. Monodisperse and bimodal molecular weight and styrene content for VE resin systems**

VE Resin System	M <sub>n</sub> (g/mol)	M <sub>w</sub> (g/mol)	Styrene Content (wt%)
828	544	544	50
828/1001F 80/20	598	642	50
828/1001F 60/40	670	744	50
828/1001F 29/71	824	902	50
828/1004F 75/25	660	898	50
828/1004F 43/57	933	1371	30
828/1004F 43/57	933	1371	40
828/1004F 43/57	933	1371	50
828/1009F 54.4/45.6	920	2902	50

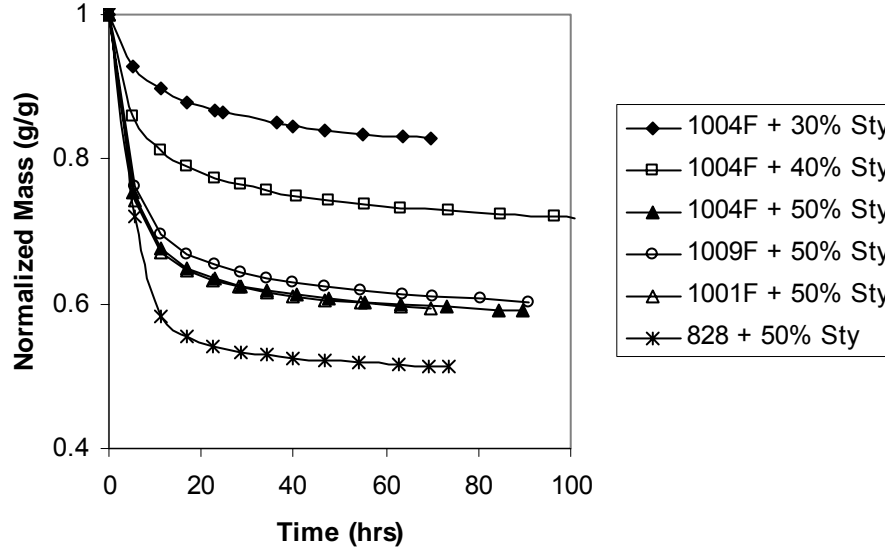


**Figure 53. Total styrene emission curve for bimodal vinyl ester systems.**

### 3.2.3.6.2 Evaporation Rate

The evaporation controlled regions of the styrene emission curves for pure styrene and each VE system are listed in Table 17. The evaporation rate of styrene from the surface is controlled by physical properties such as the heat of evaporation of styrene, styrene vapor pressure, and styrene-air diffusion coefficient [31, 32, 33, 34]. The two latter physical properties change with environmental conditions such as temperature, humidity, velocity of air passing over the surface, turbulence, and styrene concentration in the air. The volatile normalized initial emission rates ( $ER_o$ ) in the evaporation controlled region for each of these samples are the same. Or, as shown in Figure 53, the evaporation rates are identical for all samples with 50 wt% styrene, regardless of the total emissions lost at long times. As a result, the evaporation coefficients are the same for each of these samples. This indicates that VE molecular weight has no effect on styrene emission rates in the evaporation regime. There is considerable error in the measurement of the

evaporation constant as a result of slightly different ambient conditions and the use of different batches of vinyl ester monomers, which could change the volatile content as much as 2% from batch to batch.

**Table 17. Calculated Evaporation and Diffusion Coefficients**

VE Resin System	Evaporation Coefficient (m/h)	Diffusion Coefficient (m <sup>2</sup> /s)
Styrene	2.5E-4	N.A.
828	2.4E-04	1.7E-11
828/1001F 80/20	2.0E-4	1.2E-11
828/1001F 60/40	2.0E-4	1.0E-11
828/1001F 29/71	2.5E-4	4.3E-12
828/1004F 75/25	1.8E-4	1.1E-11
828/1004F 43/57 (30% Sty)	3.1E-4	2.2E-12
828/1004F 43/57 (40% Sty)	2.7E-4	3.2E-12
828/1004F 43/57 (50% Sty)	2.5E-4	3.7E-12
828/1009F 54.4/45.6	2.4E-4	4.3E-12

### 3.2.3.6.3 Diffusion Coefficient

The diffusion controlled regions of  $\ln(1-(M_t/M_\infty))$  versus time were plotted to determine the diffusion coefficients. The diffusion coefficient was definitely affected by using bimodal blends (Table 17). Figure 54 shows that the diffusion coefficient decreased as vinyl ester molecular weight increased. The trend is represented by Eq. 47:

$$D = -3.0 \times 10^{-14} * M_n + 3.1 \times 10^{-11} \quad [\text{m}^2/\text{s}] \quad (47)$$

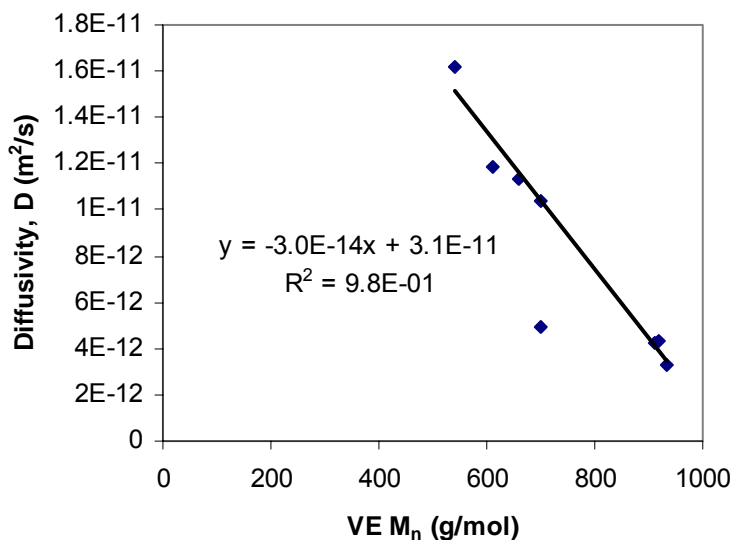


**Figure 54. The diffusivity as a function of vinyl ester molecular weight for bimodal systems.**

Diffusion within the VE system is controlled by the concentration gradient formed when a VE system is exposed to the atmosphere [31-34]. The concentration gradient is a result of differences in physical properties such as molecular size and vapor pressure of VE monomer and styrene monomer as well as the level of physical interaction occurring between the molecules. The larger the difference in molecular size and/or vapor pressure, the greater the concentration gradient formed. The type, length, and amount of the VE monomer present in the system determine the amount and extent of physical interaction between molecules. These physical properties also change with environmental conditions such as temperature, humidity, velocity of air passing over the surface, turbulence, and styrene concentration in the air. An increase in temperature, air velocity, or turbulence and/or a decrease in humidity or styrene concentration in the air induce higher styrene vapor pressure, leading to a higher concentration gradient. An increase in temperature also decreases the physical interaction forces between molecules, leading to a higher concentration gradient.

#### 3.2.3.6.4 Modeling of Emissions from Bimodal Blends

The modified Crank model was used to predict the emissions profiles from bimodal blends of vinyl ester monomers. The model does a fair job of predicting the emissions from bimodal blends as shown in Figure 55. However, the model under-predicts the mass loss in the evaporation regime and over-predicts the mass loss in the diffusion regime. The over-predicted mass loss in the diffusion regime occurred because of the sharp elbow that occurs in bimodal systems that is not apparent in VE 828 systems. The reason for the under-prediction in the evaporation regime is unknown. Future work is necessary to improve the model fit to the experimental data, but the current fit is a good first order estimate of the emissions profiles.

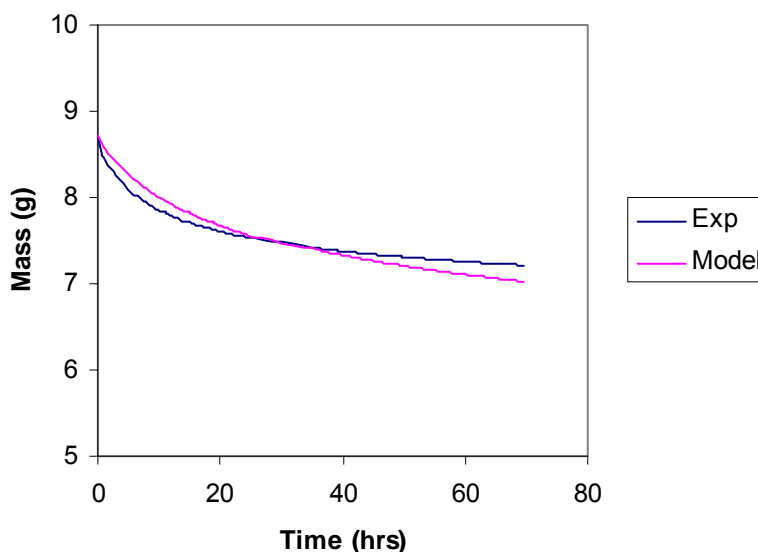


**Figure 55. Model vs. experimental emissions profile for VE 828/1004F 43/57 + 30% styrene.**

### **3.2.3.7 Bimodal VE Conclusions**

It is apparent that we are able to make bimodal VE resins that have low VOC emissions, low resin viscosities, and good thermal and fracture properties. Table 18 lists a few such resin formulations and their key properties.

**Table 18. Promising resin formulations that have low styrene contents (low VOCs), viscosities below 500 cP, good  $T_g$ , and good fracture properties.**

Sample	Styrene Content	Viscosity (cP)	$T_g$ ( $^{\circ}$ C)	$G_{IC}$ (J/m <sup>2</sup> )
VE 828/1001F 29/71	37	500	129	250
VE 828/1007F 78/22	33	400	144	350
VE 828/1009F 85/15	35	165	141	190
VE 828/1009F 78/22	37	200	137	210

### 3.2.4 Replacing Styrene with Other Reactive Diluents

One possible way to reduce the VOC emissions from VE systems is to replace some or all of the styrene with a low viscosity, low volatility monomer. Ideally, replacement monomers should not be much more expensive than styrene; however, the replacement monomer is acceptable as long as the VE resin is still less expensive than epoxy resins (\$6-\$10/lb).

Two types of diluents were tested: petroleum-based diluents and fatty acid-based diluents. Petroleum-based diluents are advantageous in that they are already being manufactured on large-scales and cost estimates are well known. Fatty acid-based monomers are simply derived from plant oils, which are composed of triglyceride molecules. Although fatty acid-based monomers are not currently being manufactured, their cost estimates show that they are inexpensive, and they are advantageous to improved global sustainability because they are derived from renewable resources. A paper published in Polymer entitled “Fatty Acid Monomers as Styrene Replacements for Liquid Molding Resins” is attached in the Appendix.

#### 3.2.4.1 Di-functional Vs. Monofunctional Reactive Diluents

Mono-functional comonomers and di-functional comonomers as replacements for styrene have been proposed. Previous work has shown that a large percentage of styrene remains unreacted in a room temperature cure of VE resins [1]. Therefore, di-functional comonomers can be advantageous because they are likely to have a lower vapor pressure, and therefore would have lower levels of hazardous emissions. In addition, the conversion necessary to bind all of the monomers into the matrix is reduced. A simple analysis was done to determine the necessary conversion of monomer in di-functional resins that would result in lower free-monomer content in the cured VE polymer. This analysis does not factor in the effect of reduced vapor pressures, and therefore represents a worst-case-scenario for di-functional monomers.

If a binomial distribution of unsaturation sites is assumed, the probability of having  $m$  reacted groups on an  $N$ -functional monomer is (Eq. 48):

$$P(N, m, x) = C \binom{N}{m} x^m (1-x)^{N-m} \quad (48)$$

where  $x$  is the conversion and  $C \binom{N}{m}$  is the combinatorial function (i.e. the number of ways of arranging the  $m$  reacted groups on an  $N$ -functional monomer) [35]. The conversion at which the

percentage of unreacted multifunctional monomer,  $P_0'(x_c')$ , equals the percentage of unreacted styrene,  $P_0(x)$ , is the critical conversion,  $x_c'$  (Eq. 49):

$$P_0'(x_c') = P_0(x) \quad (49)$$

Substituting in Eq. 48, we have (Eq. 50):

$$(1 - x_c')^N = 1 - x \quad (50)$$

There is an analytical solution for the critical conversion for all multifunctional comonomers (Eq. 51):

$$x_c' = 1 - (1 - x)^{1/N} \quad (51)$$

For example, when the styrene conversion is 95% (5% unreacted styrene), which is typical of post-cured VE [1], the conversion at which 5% unreacted di-functional monomer remains is  $x_c' = 0.77$ . This shows that amount of unbound monomer is lower for di-functional monomers relative to styrene at the same conversion. However, di-functional monomers will increase diffusion limitations during cure and will increase the cross-link density. These factors tend to decrease the ultimate conversion of multifunctional monomers. Regardless, this analysis shows that there is a large potential for reducing emissions using multifunctional monomers, although we do not offer experimental proof. FTIR experiments will be run to determine the achievable conversion using di-functional comonomers. The resin and polymer properties of vinyl esters using mono-functional and di-functional comonomers are reported below.

### **3.2.4.2 Petroleum-Based Comonomers**

A number of petroleum comonomers were tested in place of styrene in VE resins (Figure 56). Cyclohexyl methacrylate (CHMA), isobornyl methacrylate (IBMA), and lauryl methacrylate (LM) were the mono-functional diluents tested. Lauryl methacrylate was not soluble in VE and thus was not tested further. The di-functional styrene replacements tested were 1,6-hexanediol diacrylate (HDDA) and 1,6-hexanediol dimethacrylate (HDDMA). These monomers were tested because of their low vapor pressures and viscosities (Table 19). The vapor pressures of these comonomers were determined as a function of temperature using the Antoine Equation. These results show that these replacement comonomers have considerably lower vapor pressures than styrene at all temperatures (Figure 57). Although these cost of these monomers are substantial (Table 19), VE resins using these comonomers would still be considerably less expensive than epoxies.

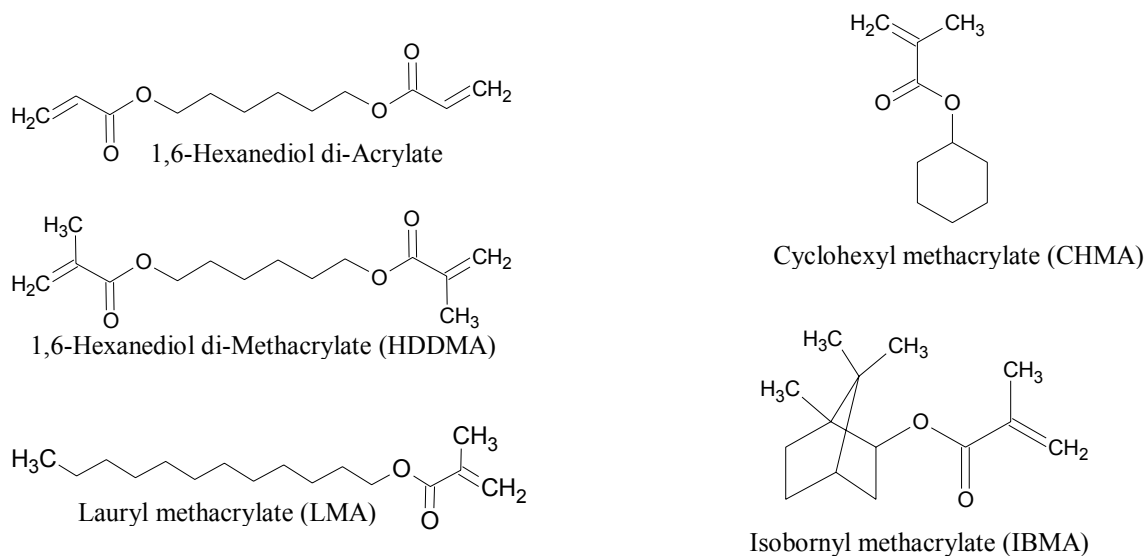


**Figure 56. The molecular structure of tested petroleum-derived styrene replacements for VE resins.**

**Table 19. The vapor pressure, viscosity, and cost of potential styrene replacements for VE resins.**

Comonomer	Vapor Pressure (mmHg)	Viscosity (cP)	Cost (\$/lb)
Styrene	6.594 @ 25°C	0.7 @ 30°C	0.40-0.80
Cyclohexyl methacrylate	0.994 @ 25°C	1.9 @ 20°C	3.55
Isobornyl methacrylate	0.020 @ 25°C 28.6 @ 142°C	8.5 @ 20°C	3.90
Hexanediol diacrylate	<0.01 @ 25°C	8 @ 20°C	2.58
Hexanediol dimethacrylate	0.02 @ 100°C	10 @ 20°C	2.97

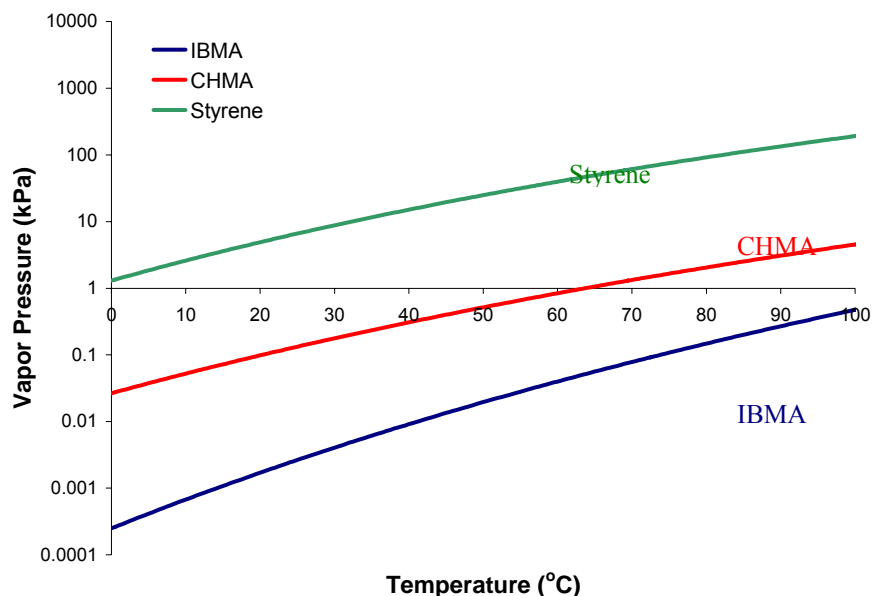


**Figure 57.** The vapor pressure of styrene, cyclohexyl methacrylate, and isobornyl methacrylate as a function of temperature as calculated with the Antoine Equation.

#### 3.2.4.2.1 Resin Viscosity and Gelation

The viscosities of VE resins using petroleum-derived styrene replacements were measured using a Brookfield digital viscometer. The resins contained 35 wt.% comonomer in VE 828. 1 mole of cumene hydroperoxide (in Trigonox) was used per 100 moles of vinyl groups and the CoNap mass used was  $\frac{1}{4}$  the mass of Trigonox. The viscosity was measured at 30°C. The viscosity as a function of gel time is shown in Figure 58. The VE/styrene system had the lowest initial viscosity (Table 20) and gelation occurred suddenly, as marked by the rapid increase in viscosity after the induction period. The isobornyl methacrylate had a high initial viscosity and it gelled fairly rapidly. The cyclohexyl methacrylate resin had a fairly low initial viscosity and it took longer to gel than styrene-based VE. This was expected because styrene-methacrylate polymerization occurs faster than methacrylate-methacrylate polymerization [36]. However, the polymerization kinetics of CHMA-VE polymerization have not been measured, as of yet. In addition, the diffusion rate of CHMA to growing radicals should be lower than that of styrene because CHMA is a larger molecule. The HDDMA and HDDA resins gelled very gradually over time, and the induction period was short. This was expected because both the VE and the comonomer are cross-linking agents.

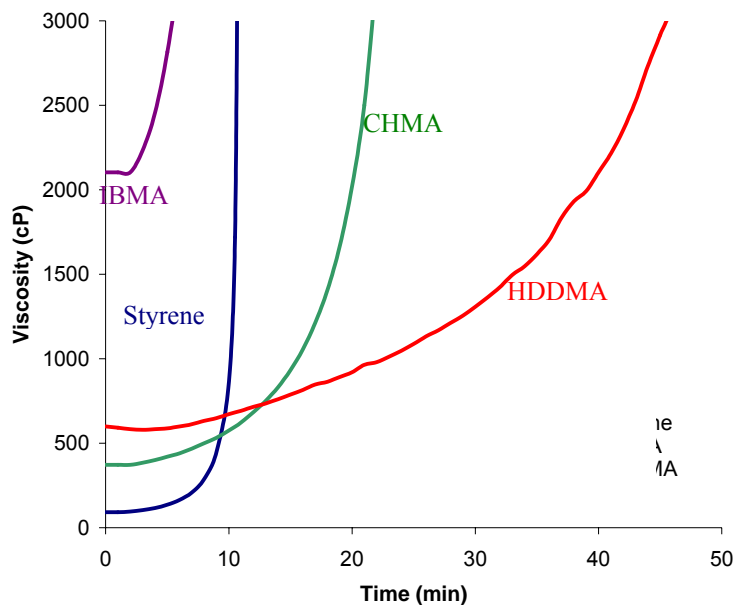
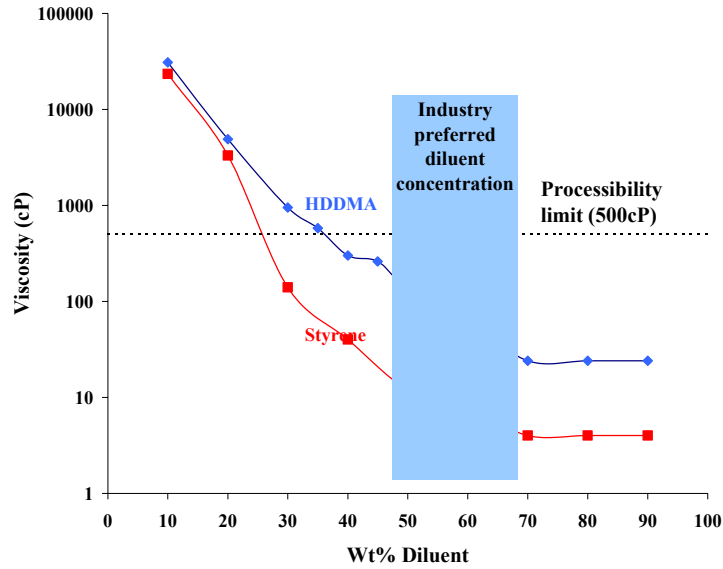


**Figure 58.** The viscosity of VE resins as a function of gel time and comonomer. VE/HDDA results are very similar to VE/HDDMA results and are omitted for clarity.

**Table 20.** Initial viscosity of VE 828 resins at 30°C using various comonomers.

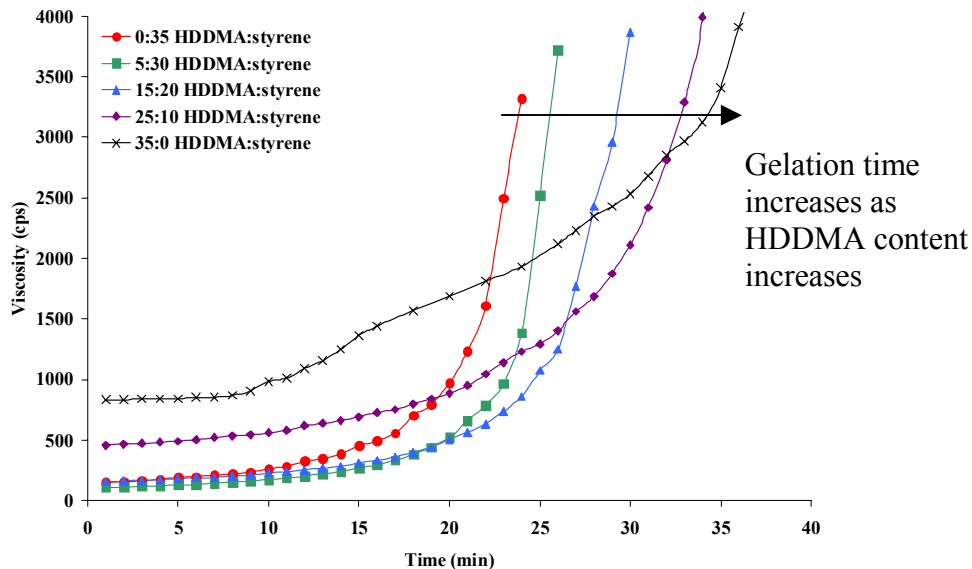
Comonomer	Viscosity @ 30°C (cP)
Styrene	56
Cyclohexyl methacrylate	364
Isobornyl methacrylate	2104
Hexanediol diacrylate	368
Hexanediol dimethacrylate	564

Figure 59 shows that the viscosity of VE/HDDMA resins decreased with HDDMA content similarly to VE/styrene resins. However, at all comonomer contents, the VE/HDDMA had a higher viscosity. These results also show that HDDMA contents of 40% or greater results in acceptable viscosities for liquid molding (< 500cP).



**Figure 59.** The viscosity of VE 828 resins as a function of styrene and HDDMA content at 30°C.

Figure 60 shows the viscosity of blends of VE, HDDMA, and styrene as a function of gel time. The initial viscosity increased as the HDDMA content increased. In addition, the viscosity increased without an induction period, but more gradually as the HDDMA content increased. This is expected because HDDMA is a cross-linking agent, not a reactive diluent. These polymers continuously branch during the course of polymerization causing the step-wise increase in the viscosity.



**Figure 60.** The viscosity as a function of gel time for VE/HDDMA/styrene blends at 30°C.

### 3.2.4.2.2 Resin Cure Kinetics

The cure kinetics of VE using CHMA as a reactive diluent were measured and compared to the cure kinetics of styrene based VE resins. Although the cure rate of CHMA-based resins was greater, the extent of cure was considerably lower. Figure 61 shows that the CHMA-based resins cured to a very low extent: ~60% before post-cure and 69% after post-cure versus styrene-based vinyl esters, which had an 85% extent of cure and a 95% extent after post-cure. Therefore, although CHMA may produce low emissions initially, there is a potential that CHMA-based vinyl ester polymers could produce significant VOC emissions during fielding, and large amounts of CHMA could leach out of the parts over time.

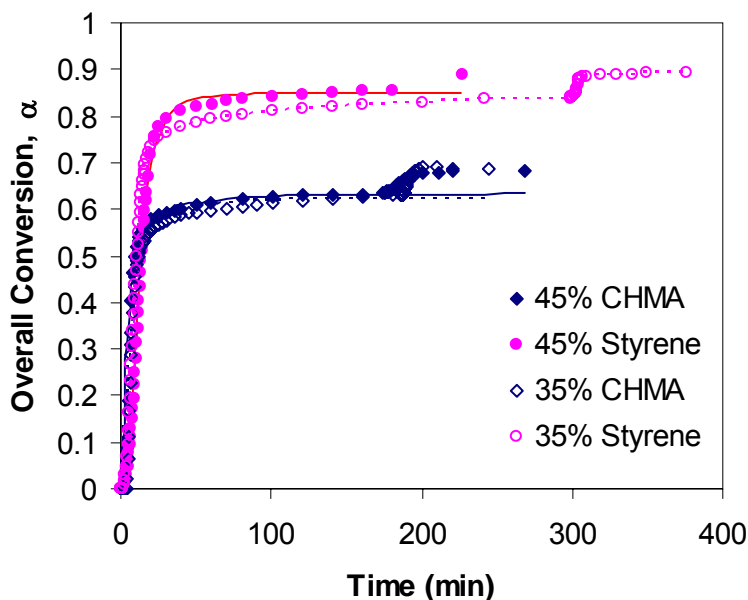


**Figure 61.** The overall conversion as a function of time for CHMA-based vinyl esters relative to styrene-based vinyl esters.

### 3.2.4.2.3 Polymer Properties

The DMA results for HDDMA show that the storage modulus decreased as HDDMA content increased for VE/HDDMA/styrene blends (Figure 62). In addition, the transition from glassy to rubbery behavior became less distinguished. Furthermore, VE/HDDMA sample did not retain its modulus as a function of temperature as well as the VE/styrene samples. The rubbery modulus increased as the HDDMA content increased because HDDMA is a cross-linker and it thus increased the cross-link density of the resulting polymer. The polymer transitions, shown by the loss modulus, became much less prominent as the HDDMA content increased (Figure 63). Furthermore, there were two peaks for VE/HDDMA/styrene blends, showing the resin mixture was inhomogeneous. It is hypothesized that the properties of VE/HDDMA polymers are lower than VE/styrene polymers because of low monomer conversion as a result of low conversions at gelation. Polymerization kinetics studies with FTIR need to be done to prove this hypothesis. Although the VE/HDDMA samples do not have ideal thermo-mechanical properties, resin mixtures with 10-20% have good polymer properties and acceptable resin viscosities. Therefore, resins with lower styrene contents can be synthesized by replacing some styrene monomer with

HDDMA. HDDA behaved similarly to HDDMA, but had inferior properties. For example, Figure 64 shows that the loss modulus peak of VE/HDDA was hardly visible.

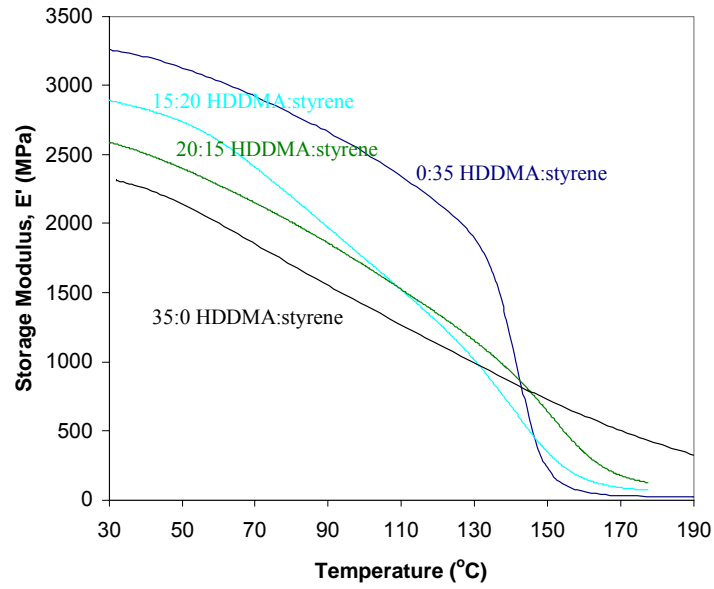


**Figure 62.** The storage modulus as a function of temperature for VE/HDDMA/styrene blends.

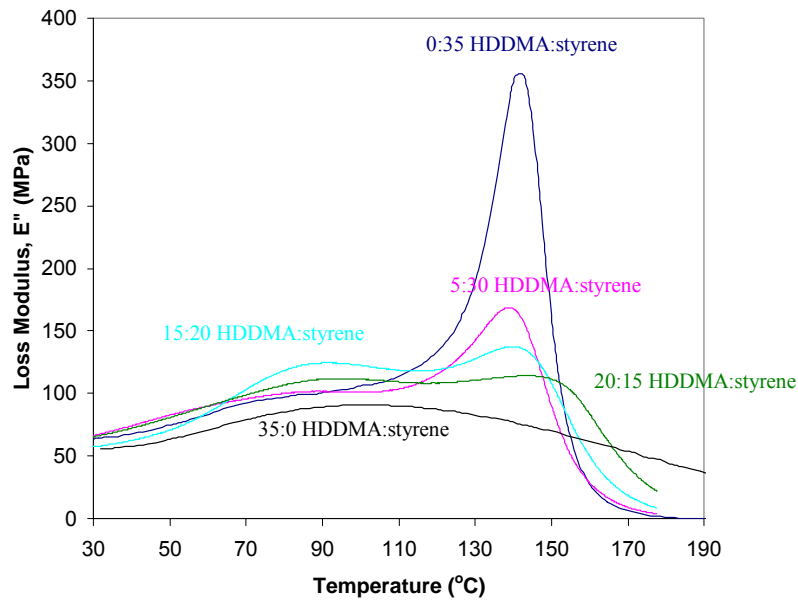


**Figure 63.** The loss modulus as a function of temperature for VE/HDDMA/styrene blends.

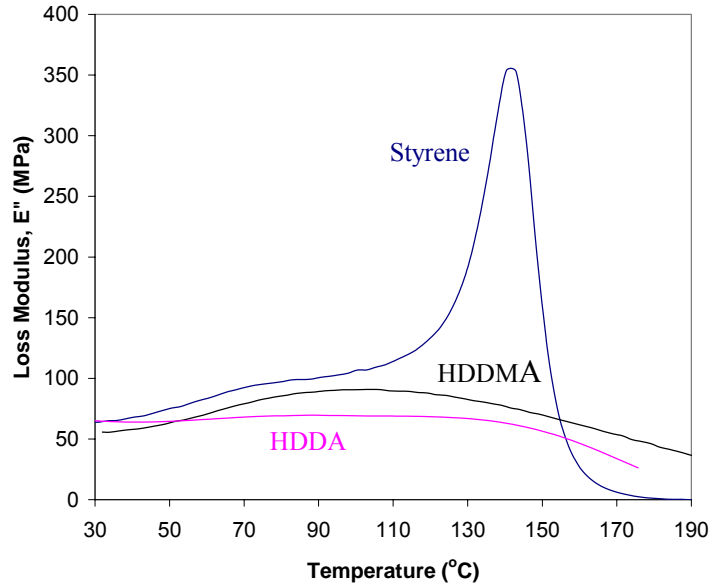


**Figure 64.** The loss modulus as a function of temperature for VE/HDDA relative to VE/HDDMA and VE/styrene.

The DMA properties of cyclohexyl methacrylate were similar to VE/styrene blends. The storage modulus was only slightly lower than VE/styrene in the glassy regime, and the glass transition was well pronounced. Figure 65 also shows that  $T_g$  of VE/CHMA was very similar to styrene-based resins. However, the glass transition was broader for CHMA-based resins probably due to a lower final monomer conversion in these resins. Polymerization kinetics work must be done to confirm this hypothesis. Regardless, these results show that CHMA is an excellent candidate for replacing styrene in VE resins.

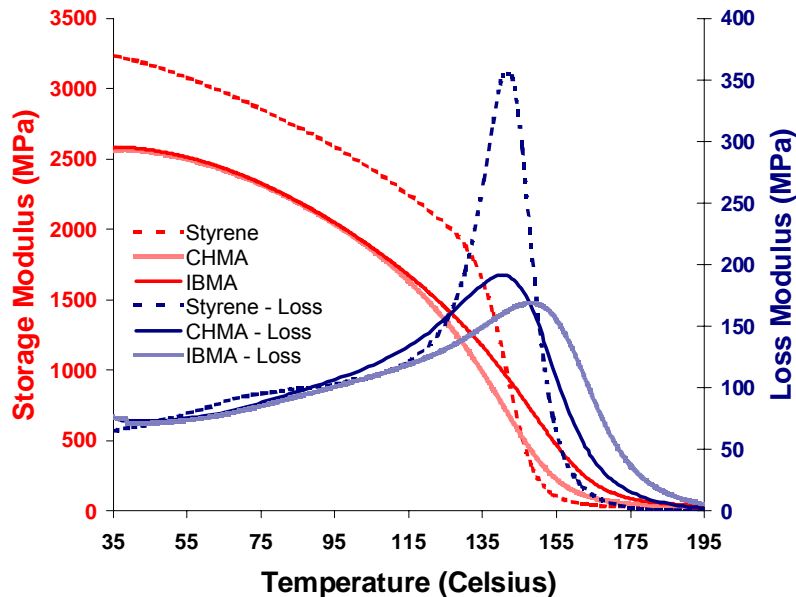


**Figure 65.** The DMA behavior of VE/CHMA and VE/IBMA resins relative to VE/styrene.

Isobornyl methacrylate has DMA properties that are very similar to VE/CHMA (Figure 65). Although  $T_g$  of IBMA resins are higher than that of CHMA resins, the viscosities of IBMA resins are an order of magnitude higher (Figure 58). IBMA would have to be blended with styrene to yield VE resins with acceptable viscosities for liquid molding. Therefore, IBMA can be used as a styrene replacement, but the slight improvements in polymer properties over CHMA resins are not worth the much lower processability of these resins relative to CHMA resins.

The fracture toughness of VE 828 using CHMA as a reactive diluent was measured and found to be similar to styrene based vinyl ester resins (Table 21). Although styrene based resins display better fracture toughness results for non-post-cured samples, CHMA samples have slightly better fracture toughness for post-cured samples. CHMA-based vinyl esters have been shown to have a low extent of cure. Therefore, the post-cured vinyl esters are heavily plasticized, resulting in higher fracture toughness than styrene-based vinyl esters. It seems likely that the low fracture toughness of non-post-cured CHMA-based resins is a result of a very fragile network due to the low extent of cure.

**Table 21. The fracture toughness of vinyl ester 828 resins using styrene and CHMA as reactive diluents.**

Comonomer	Post-cured	Fracture Toughness, $G_{IC}$ (J/m <sup>2</sup> )	
		35% Comonomer	45% Comonomer
Styrene	No	140	90
Styrene	Yes	80	70
CHMA	No	60	90
CHMA	Yes	130	100

#### 3.2.4.2.4 Petroleum-Based Comonomer Conclusions

Currently, cyclohexyl methacrylate appears to be the best styrene replacement for VE resins. This comonomer does not have to be blended with styrene to produce vinyl esters with good properties and acceptable resin viscosities. However, significant VOC emissions are possible during fielding of CHMA-based vinyl esters parts because of a low extent of cure of the CHMA monomers. Other comonomers, such as HDDMA and IBMA, can be used to reduce the styrene content in VE resins, but cannot be used to completely replace styrene because of poor polymer properties or unacceptable resin viscosities. Overall, petroleum-based monomers show good potential for replacing styrene in VE resins, but the cost of these comonomers are approximately 5 to 7 times that of styrene, making economics a strong deciding factor. For this reason, the use of fatty acid-based monomers as styrene replacements is attractive because of their low potential cost.

#### 3.2.4.3 Fatty Acid-Based Comonomers

##### 3.2.4.3.1 Synthetic Routes

A number of synthetic procedures have been established for making fatty acid-based monomers to be used as the reactive diluent in VE resins. Figure 66 lists the synthetic routes that have been established. In all of the synthetic routes, the starting materials are triglycerides (Structure 0),

fatty acids (Structure 1), fatty acid methyl esters (Structure 2), and cyclic fatty acids (Structure 5). Refined plant oils contain approximately 99% triglyceride molecules [37]. Industrially, fatty acids (FA) are produced from triglycerides by reaction with a strong acid, such as HCl [38, 39, 40]. Fatty acid methyl esters (FAME) are produced from a methanolysis reaction. In this reaction, methanol replaces the glycerol ester linkages under basic conditions [38-40]. Cyclized acids are produced by reacting polyunsaturated fatty acids of triglycerides at high temperatures under basic conditions [38-40].

In Route 1, fatty acids are reacted with an epoxy-methacrylate species, such as glycidyl methacrylate (GM). The carboxylic acid group of the fatty acid adds to the epoxide group on glycidyl methacrylate. The resulting species is a fairly long hydrocarbon (20-26 atoms in length depending on the fatty acid used) with a terminal unsaturation site that is capable of free radically polymerizing. The length of the fatty acid chain may affect the polymer properties. Therefore, the particular fatty acid used is of importance, and its effect on polymer properties has been studied and will be studied in more detail.

In Route 2, unsaturation sites on fatty acid methyl esters are first epoxidized, and then acrylated [41, 42]. The resulting monomer has an acrylate group, which is capable of free radically polymerizing, in the middle of the long hydrocarbon chain (20 atoms long). Ideally, this monomer will have no more and no less than a single acrylate group. For this to be the case, monounsaturated fatty acids need to be used. Pure mono-unsaturated acids are fairly expensive. Canola oil and olive oil are relatively inexpensive sources of mono-unsaturated acids, but they do have significant contents of saturated and polyunsaturated acids [37].

As discussed previously, di-functional monomers can be used to improve the properties of VE resins. Route 3 shows a way to produce di-functional monomers (Structure 3b) by combining the synthetic procedures of Routes 1 and 2.

Allyl alcohol is used to break up the triglycerides into allyl fatty acid monomers (Route 4, Structure 4) in a procedure that is very similar to the methanolysis reaction. These monomers have a primary unsaturation site that could potentially be used for free radical polymerization.

Routes 6-8 make use of the cyclized derivatives of triglycerides. In Route 6, a methyl ester of the cyclized species is formed via methanolysis (Structure 6a). The remaining unsaturation sites on the fatty acid are then epoxidized and acrylated to add free radical functionality to the fatty acid (Structure 6b). In Route 7, cyclized fatty acids are produced by acidolysis of cyclized triglycerides (Structure 7a). This species is then reacted with glycidyl methacrylate, in the same manner as Route 1), to attach vinyl functionality to the end of the cyclized fatty acid. Route 8 is just a combination of Routes 6 and 7, resulting in di-vinyl, cyclized fatty acid monomers (Structure 8b).

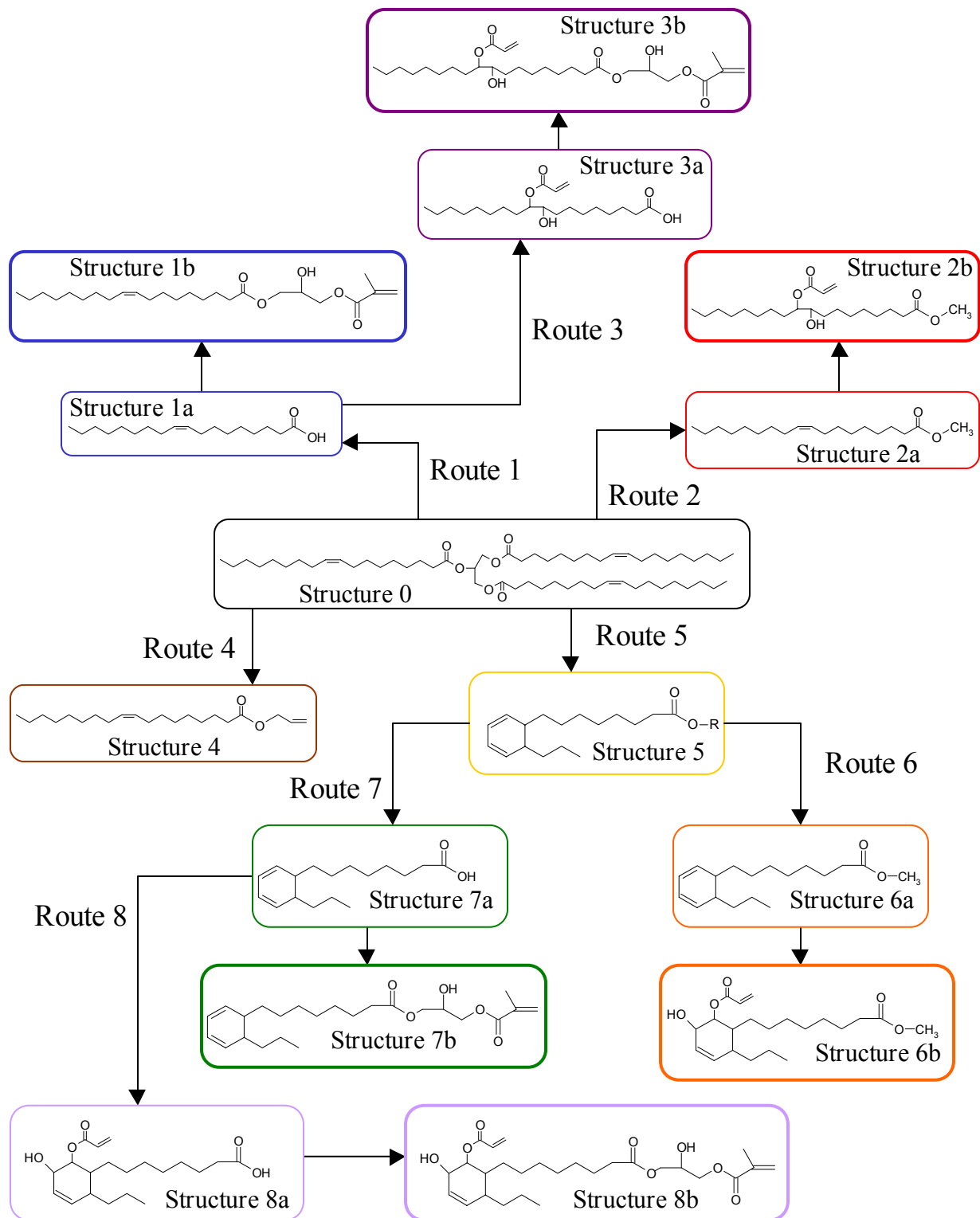
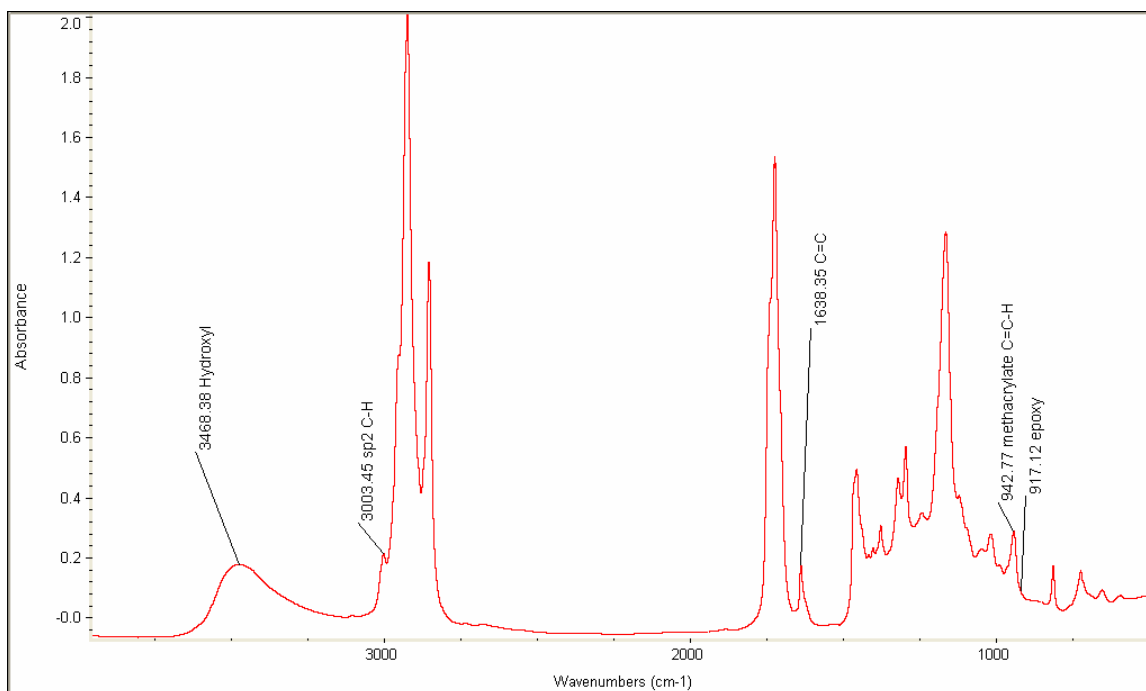


Figure 66. The proposed synthetic routes to produce fatty acid-based monomers [43].

### 3.2.4.3.2 Synthesis

#### *Glycidyl Methacrylate Modified Fatty Acid Monomers (MFA)*

Synthesis procedures for preparing the glycidyl methacrylate modified fatty acids (MFA) in Route 1 (Figure 66) were first established. Epoxides and fatty acids react at fairly low temperatures ( $< 100^{\circ}\text{C}$ ) with short reaction times if properly catalyzed. The AMC-2 (1-2 wt%) catalyst was used to catalyze this reaction. Near IR or mid IR (FTIR) can be used to determine the extent of reaction. The epoxide peaks at  $4530\text{ cm}^{-1}$  and  $917\text{ cm}^{-1}$  [15] were tracked during the reaction (Figure 67). Table 22 lists the reaction conditions tested and the corresponding extent of reaction and reaction time.



**Figure 67. The mid IR spectra of MOA (oleic acid) after reaction.**

The reaction between a stoichiometric amount of oleic acid (18 carbon atoms, 1 unsaturation site) and GM was catalyzed with 2 wt% AMC-2 catalyst and run at room temperature. The reaction went to ~90% completion after 3 days of reaction.

The reaction between a stoichiometric amount of oleic acid (OA) and GM was catalyzed with 0.5wt%, 1wt%, and 2wt% AMC-2 catalyst and run at  $70^{\circ}\text{C}$ . The reaction went to completion in 1.5 hrs when 2 wt% catalyst was used. The reaction went to completion after 2.5 hours when 1 wt% catalyst was used. When 0.5 wt% catalyst was used, the reaction took longer than 4 hours. In order to simultaneously minimize the catalyst concentration and reaction time, 1 wt% AMC-2 was found to be optimum for this reaction.

Work with acrylating epoxidized triglycerides showed that adding the acid in aliquots decreased the extent of etherification [7]. One-third the stoichiometric amount of OA was added to GM.

The reaction was run at 70°C and catalyzed with 2 wt% AMC-2. Gelation occurred after 1.5 hours of reaction, as a result of the etherification reaction. Therefore, adding OA in aliquots to the GM was found to be a poor method for producing the MFA monomer.

**Table 22. The reaction conditions tested to produce MFA and the resulting reaction times and extents of reaction.**

M:OA	AMC-2	Rxn Temperature	Rxn Time
1:1	0.5 wt %	70°C	> 4 hrs
1:1	1 wt %	70°C	2.5 hrs
1:1	2 wt %	RT	> 3 days
1:1	2 wt %	70°C	1.5 hrs
1:0.33	2 wt %	70°C	Gelled in 1.5 hrs

Three fatty acids were used to determine the effect of fatty acid structure on resin and polymer properties: lauric acid (Lau), stearic acid (SA), oleic acid, and linoleic acid (Lin). The molecular structure differences of these fatty acids are summarized in Table 23.

**Table 23. The molecular structure differences of the fatty acids used to prepare MFA monomers.**

Fatty Acid	Chain Length in Carbon Atoms	Unsaturation Sites
Butyric	4	0
Caproic (hexanoic)	6	0
Caprylic (octanoic)	8	0
Capric (decanoic)	10	0
Lauric	12	0
Myristic	14	0
Palmitic	16	0
Stearic	18	0
Oleic	18	1
Linoleic	18	2

#### *Acid Number*

Acid number titration was used during the course of the reaction to measure the amount of free (unreacted) acid in the VE system. Acid number tests were performed in accordance with ASTM D1980-87. Approximately 1 g of the VE reaction mixture was dissolved in 5 g of acetone. Three drops of 0.5 wt% phenolphthalein in 50% ethanol-water solution were added to the mixture to determine the neutralization point. The solution was then titrated with 0.5 N sodium hydroxide until the solution remained slightly pink in color for 30 seconds. An acid number (mg NaOH/g VE) of 10, corresponding to ~3% free acid, was the maximum allowable acid number. If the acid number was too high, the methacrylation reaction was allowed to continue until future acid numbers were below 10. Figure 68 shows typical acid number measurements during the synthesis of methacrylated lauric acid. The reaction is essentially done after only 2 hrs at 90°C.

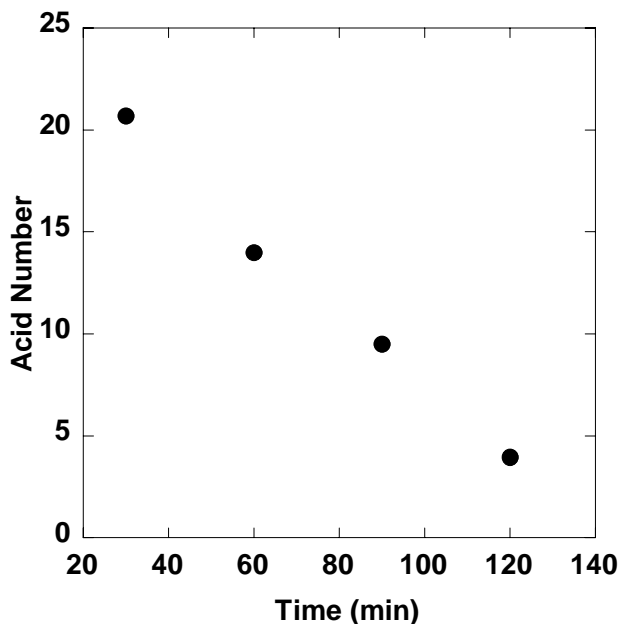


**Figure 68.** Acid number measurements during reaction at 90°C for the synthesis of Methacrylated Lauric Acid (MLau)

#### *Size Exclusion Chromatography*

Size exclusion chromatography was run on the pure acids and the methacrylated acids to ensure the completion of the reactions and that the reactions led to homogeneous products. A water's 515 solvent pump 515 GPC was used with PL gel (Polymer Laboratories Inc.) columns with fixed (50 Å) and mixed pore sizes. The columns were equilibrated and operated at 30°C using tetrahydrofuran as the elution solvent at a flow rate of 1 mL/minute. The column effluent was monitored by Waters 2487 dual UV absorbance detector operating at 270 nm and 254 nm wavelengths and a Waters 2410 refractive index detector. Samples were prepared by dissolving 2 mg of sample in 1 ml of THF. Since high molecular weight species diffuse more slowly into the packing, they elute first from the column, while lower molecular weight species elute later. Figure 69 shows SEC traces for the reactants and products during reaction and upon completion around 90 min. Glycidyl methacrylate has a retention time of 17.23 min and pure lauric acid has the retention time of 15.78 min. Methacrylated lauric acid has a retention time of 15.03 min. The traces show that there is no acid or glycidyl methacrylate left after 90 minutes. The results also show that there is considerable reaction upon mixing ( $t=0$ ). Figure 70 compares the SEC traces for lauric acid and its methacrylated counterpart. It is apparent that there are some higher molecular weight species in the 14-15 min retention time for lauric acid and that after the reaction the methacrylated lauric acid also exhibits a slight higher molecular weight shoulder (13.7-14.5 minutes retention time). Similar results were obtained for all of the synthesized fatty acids. Figure 71 is a compilation of the SEC traces for the series of MFAs synthesized in this work. As expected the higher molecular weight fatty acids exhibit shorter retention times. In all cases a single major peak is observed and no unreacted species are discernable.

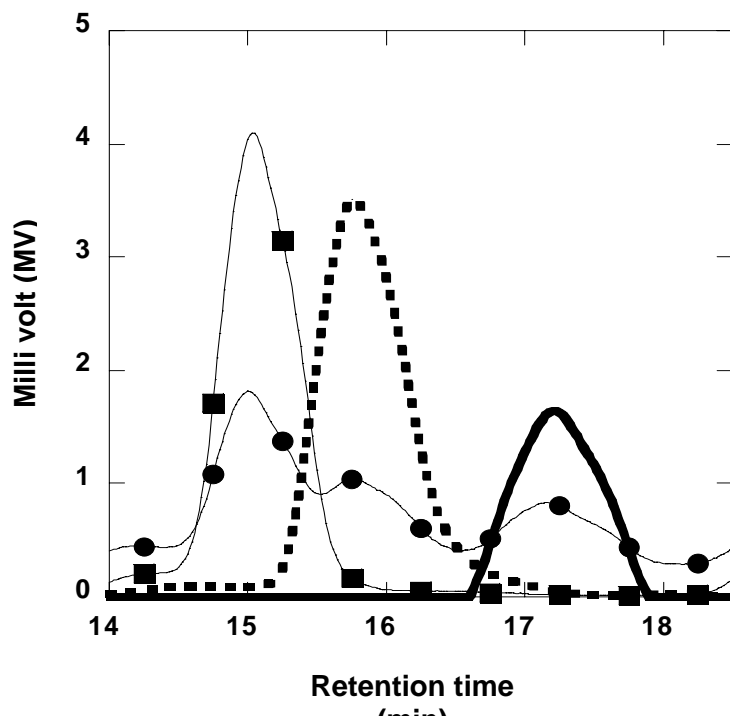


Figure 69. Reaction of Lauric Acid with Glycidyl Methacrylate to form MLau. Methacrylated lauric acid (MLau) (●) 0 min, (■) 90 min (—), Glycidyl methacrylate, ( - ) Pure lauric acid.

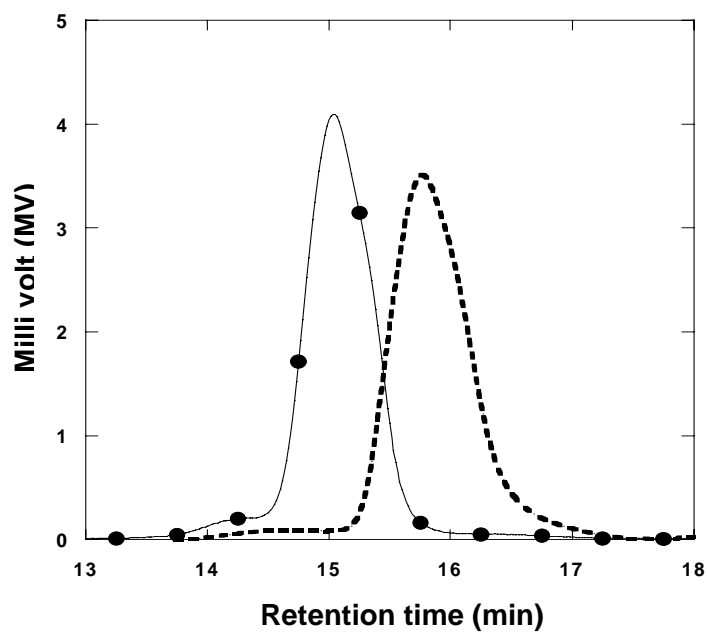
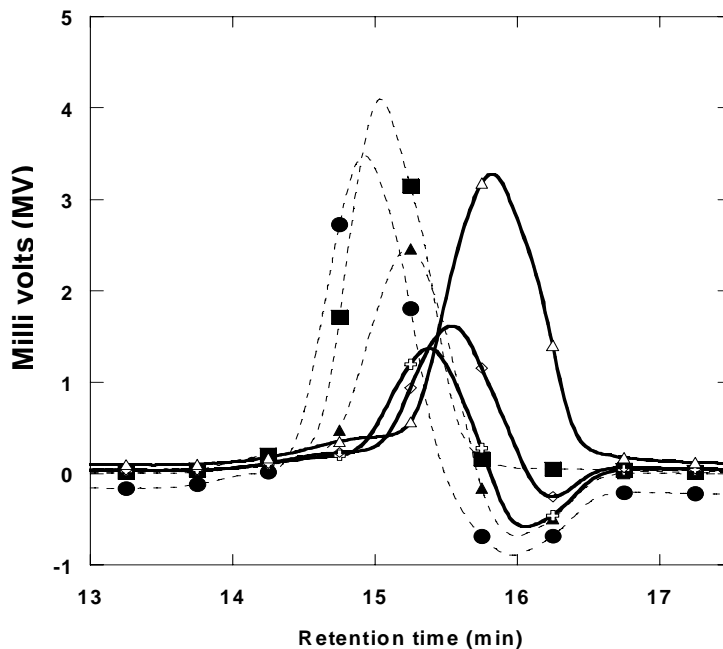


Figure 70. Shift of the peak of the ( - ) Pure lauric acid to (●) Methacrylated lauric acid.



**Figure 71.** The peak shift of the Methacrylated fatty acids (MFA) with increasing chain length of fatty acids, methacrylated Myristic acid (●), methacrylated lauric acid (■), methacrylated capric acid (▲), methacrylated caprylic acid (⊕), methacrylated caproic acid (◇), methacrylated butyric acid (△).

*Brominated Glycidyl Methacrylate Modified Fatty Acid Monomers (Di-BrMSA)*

In this study, a brominated fatty acid based monomer was synthesized and used as replacements for styrene in VE and UP formulations. For the synthesis of this monomer, oleic acid, which can be obtained from triglyceride oils, is brominated at RT to form di-bromo stearic acid and then reacted with glycidyl methacrylate to form 9-10 di-bromo stearyl glycidyl methacrylate (Di-Br) as shown in Figure 72. Since these resins are intended to be used in liquid molding processes and the Di-BrMSA exhibited a high viscosity, this monomer was used in the presence of styrene in VE and UP resins. The viscosities of the resins at changing Di-BrMSA content were determined and the modulus and  $T_g$  values of the resulting polymers were screened via DMA to determine the ideal formulations for each resin system. Similar analysis was performed, at similar oleic acid glycidyl methacrylate (MOA) contents, to determine the effect of the introduction of the Bromine groups onto the network. A novalac type VE resin was also used to further improve the  $T_g$ s of the resulting polymers.

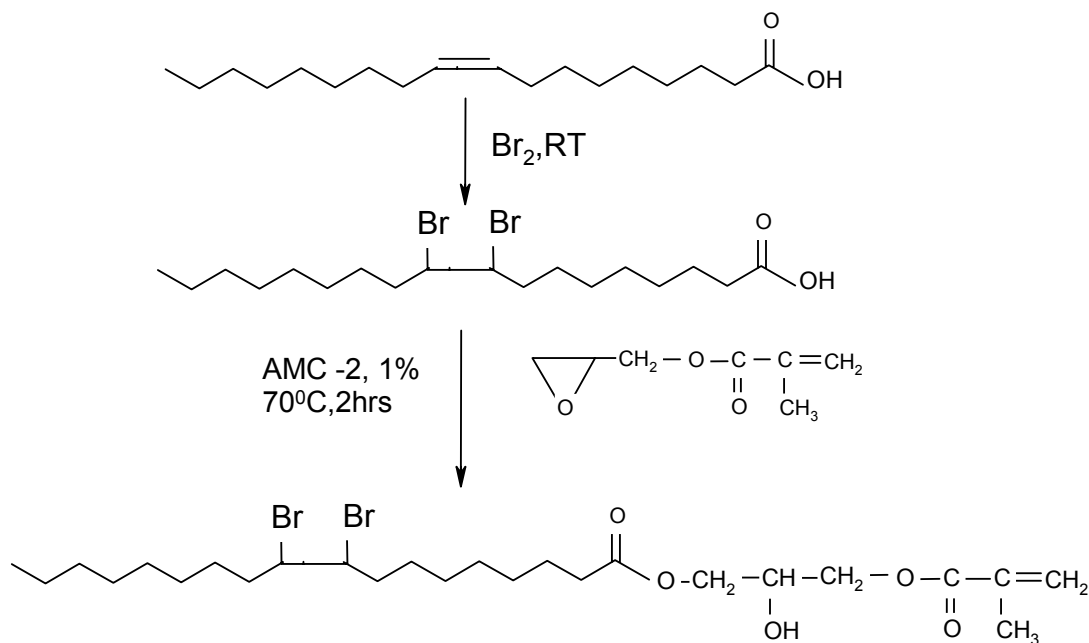
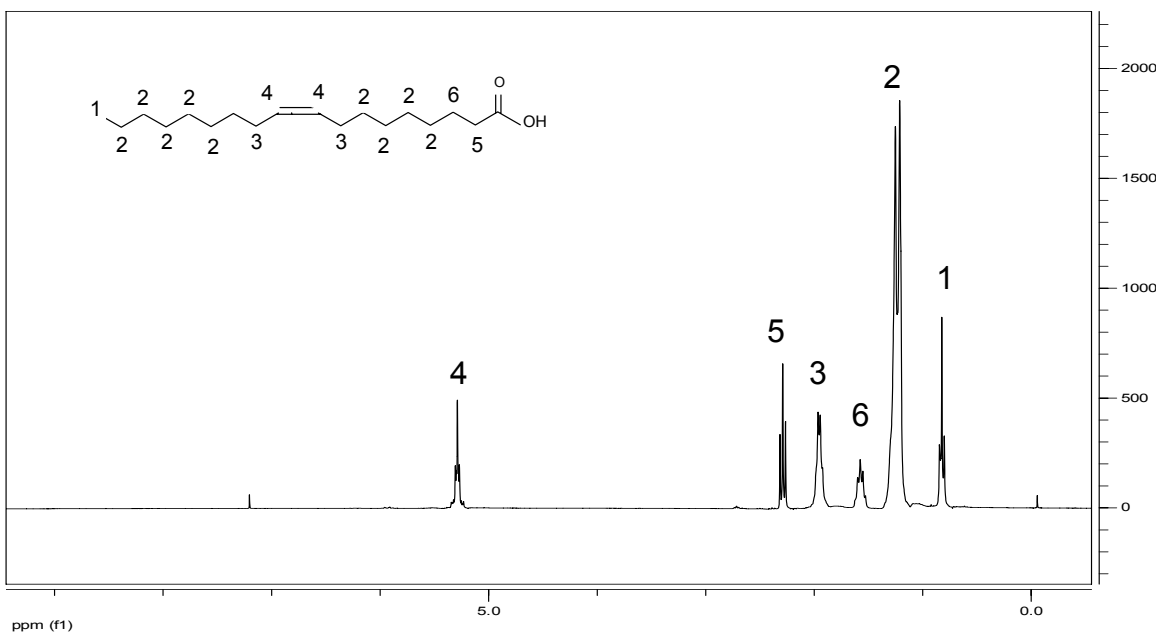
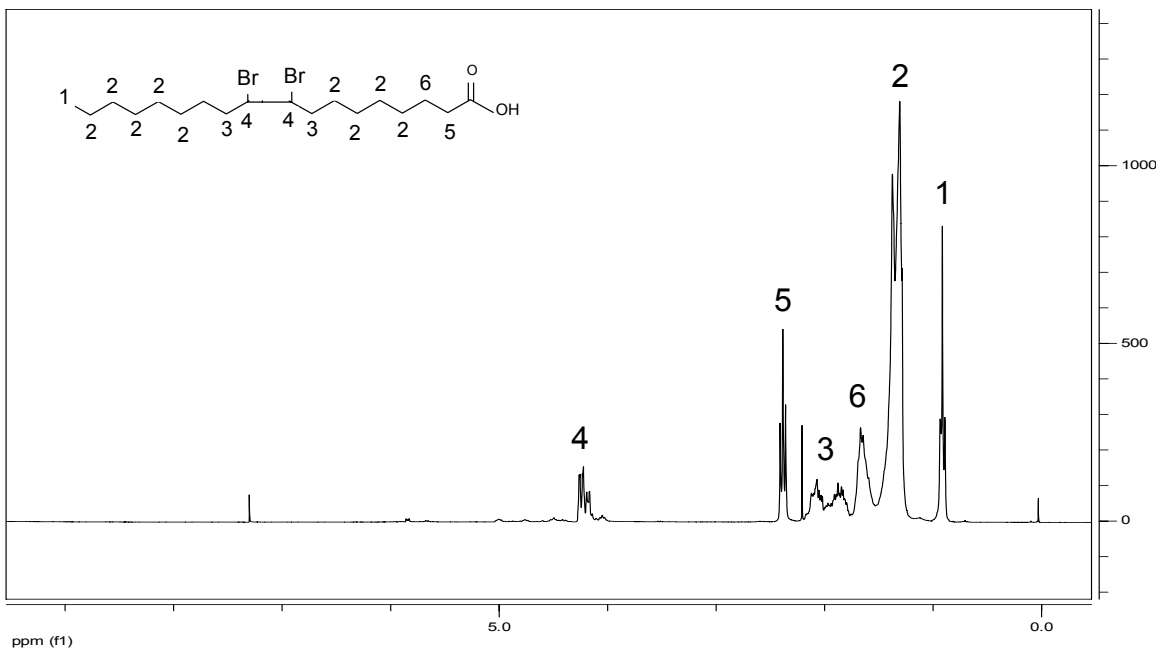


**Figure 72. The reaction scheme for the synthesis of 9-10 di-bromo stearic acid glycidyl methacrylate (Di-Br MSA) from oleic acid.**

The addition reaction of bromine ( $\text{Br}_2$ ) to unsaturation sites on fatty acids proceeds rapidly at room temperature. The red brown color of bromine disappears rapidly as long as the alkene is present in excess [44]. In this study, oleic acid is reacted with an equimolar ratio of  $\text{Br}_2$ . Bromine is added slowly in aliquots to prevent the excessive heating caused by the exothermic addition reaction. The red brown color of bromine instantly disappeared as bromine is added leading into a light orange colored solution. The solution was stirred at room temperature for an hour to ensure the completion of reaction. This solution was ether extracted to wash away any unreacted bromine. The  $^1\text{H-NMR}$  spectral analysis of the product indicated the complete reaction of the double bonds of oleic acid with  $\text{Br}_2$ . The  $^1\text{H-NMR}$  spectra of oleic acid and 9-10 di-bromo stearic acid with the peak assignments are shown in Figure 73 (a) and (b) respectively. The disappearance of the 5.35 ppm peaks that represent the vinyl protons of oleic acid and the appearance of the 4.10-4.50 ppm peaks that represent the methylene protons attached to Br confirms the complete conversion of oleic acid to 9-10 di-bromo stearic acid.



(a)



(b)

**Figure 73. The  $^1\text{H-NMR}$  spectra of (a) oleic acid  
(b) 9,10 di-bromo stearic acid(Di-BrSA).**

Bromine also reacts with saturated fatty acids in a substitution reaction to yield  $\alpha$ -halo acids, usually in presence of phosphorus as catalyst. This substitution reaction did not occur as a side reaction during the addition of bromine to oleic acid. The  $^1\text{H-NMR}$  analysis of the product indicates no decrease in the  $\alpha$  protons of oleic acid which show their peak at 2.35 ppm. The

C-Br stretching vibrations show a very weak peak at  $651\text{ cm}^{-1}$  in IR; however, this peak is complicated with other peaks in the fingerprint area and therefore not used to follow the reaction.

The 9-10 di-bromo stearic acid was reacted with an equimolar ratio of glycidyl methacrylate in the presence of 1wt% AMC-2 catalyst and 0.01 wt% hydroquinone for 2.5 hours at  $70^{\circ}\text{C}$  to yield 9-10 di-bromo stearyl glycidyl methacrylate (Di-BrMSA). The IR spectrum of the product showed the disappearance of the  $917\text{ cm}^{-1}$  epoxide peaks and also the replacement of the broad carboxylic acid band of oleic acid by the  $3468\text{ cm}^{-1}$  hydroxyl band, confirming the completion of the reaction. The  $^1\text{H-NMR}$  spectrum of this product is shown in Figure 74 with the peak assignments.

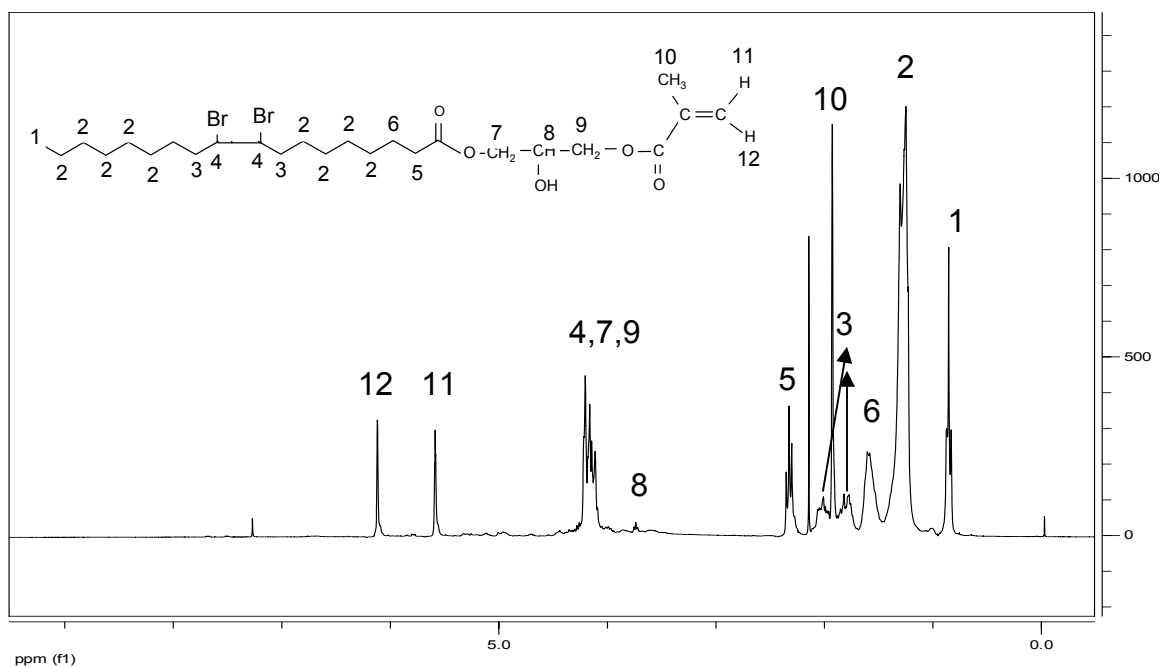


**Figure 74. The  $^1\text{H-NMR}$  spectrum of dibromo stearyl glycidyl methacrylate (Di-BrMSA)**

#### *Fatty Acid Methyl Esters (FAME)*

Fatty acid methyl esters (Structure 2a, Figure 66) are formed by the methanolysis of triglycerides. A genetically engineered high oleic soybean oil (DuPont Corporation, Wilmington, DE) and canola oil were used to make methyl esters. For both oils, 100g oil, 17.9 g methanol, and 20.6 g of 0.5 N KOH in methanol were mixed together. The reaction was run at  $60^{\circ}\text{C}$  for 1 day. The products were recovered using an ether extraction [41]. The reaction mixture was dissolved in approximately 150 ml diethyl ether and poured into a separatory funnel. Distilled water was added to remove the acid from the ether phase. The layers were allowed to separate, and the water layer was discarded. This step was repeated 4 times. The ether solution was washed with saturated aqueous sodium chloride to remove water from the ether phase and dried over anhydrous sodium sulfate. The ether was evaporated away at room temperature.  $^1\text{H-NMR}$  (250.13 MHz, spectral window of  $\pm 2000\text{ Hz}$ , 0.427 Hz/pt digital resolution, 16 scans at 293 K,  $90^{\circ}$  pulse width) with a Bruker (Billerica, MA) AC250

Spectrometer was used to determine if methanolysis was complete [39, 41]. In all cases, the methanolysis reaction was complete.

#### *Acrylated Methyl Esters (AME)*

Epoxidized samples were made by reacting the unsaturation sites of FAME with a mixture of formic acid and hydrogen peroxide [45]. The amount of formic acid used was one-third the oil mass. The amount of hydrogen peroxide used was twice the molar ratio needed to produce the completely epoxidized sample. This amount of hydrogen peroxide was used to drive the epoxidation to completion. The unsaturated methyl esters were added to an Erlenmeyer flask, which contained a magnetic stir bar. The appropriate mass of hydrogen peroxide was added, followed by the formic acid. The flask was stoppered and stirred vigorously. The reaction was run at room temperature, using a water bath for cooling. At the end of 16 hours reaction time, the samples were ether extracted to recover purified epoxidized oils. In the ether extraction, the samples were dissolved in diethyl ether and washed with aqueous sodium bicarbonate until the pH of the solution was slightly alkaline. The contents were allowed to phase separate, and the aqueous layer was discarded. Finally, the solution was washed with aqueous sodium chloride and dried over anhydrous sodium sulfate. The ether was evaporated at room temperature. The extent of epoxidation was measured using  $^1\text{H-NMR}$  [45]. The level of epoxidation of epoxidized HOSO and epoxidized canola methyl esters were 0.8 and 1.1 epoxides/FAME, respectively. Thus, the extent of epoxidation of HOSO methyl esters is low, considering we would like to have 1 functional group per FAME. This occurred because the level of unsaturation of HOSO is only 0.9 per FAME and epoxidation was not complete. Methyl esters of canola oil have 1.17 unsaturation sites on average. Therefore, the epoxidation of canola oil methyl esters was successful.

Acrylated samples (Structure 2b, Figure 66) were made by reacting the epoxide groups of epoxidized fatty acid methyl esters with acrylic acid [46]. The AMC-2 catalyst was used to reduce the extent of epoxy homopolymerization [4]. The AMC-2 was used in every sample at a concentration of 0.02 g/mL. A concentration of 0.0033 g/mL hydroquinone was used to inhibit free-radical polymerization. The reaction mixture was equilibrated at 70°C before adding acrylic acid to the mixture. The reaction was run at 70°C in a silicon oil bath on a hot plate while stirring vigorously.

The oils were acrylated by adding 1.1 moles of acrylic acid per epoxide group. The acrylic acid was added in aliquots during the course of the reaction to reduce the amount of epoxy homopolymerization [7]. The amount of 1/3 mole acrylic acid per mole of fatty acid methyl esters was added until the last aliquot, where the remaining acrylic acid was added to the mixture. Upon addition of the acrylic acid, the solution became a bright green color. This was due to the interaction of the acid with the chromium-based catalyst [4]. When the acid was consumed, as measured by pH paper, the reaction mixture became brown in color, and the next aliquot of acrylic acid was added. An aliquot of acrylic acid was added after 2 hours even if the reaction mixture was not brown. The reaction mixtures were removed from the heat 2 hours after the last acrylic acid aliquot was added. The acrylated oils were purified via ether extraction as described for the epoxidized oils. The level of acrylation in the product was measured using  $^1\text{H-NMR}$  [45]. The level of acrylation of HOSO methyl esters was 0.7 acrylates per FAME. This number is low because of the low level of epoxidation achieved. Therefore, some methyl

ester molecules have no functional groups and will act as plasticizers when polymerized with VE. The level of acrylation of acrylated canola oil methyl esters has not been established.

#### *Allyl Alcohol Modified Soybean Oil (AOH-SBO)*

Allyl alcohol was used to break apart the glycerol linkage of triglycerides to produce AOH-SBO (Structure 4, Figure 66). The reaction mixture contained 70g oil (soybean oil), 22 ml allyl alcohol, and 25.5 ml of a 0.5 N KOH/allyl alcohol solution. The contents were mixed and reacted at 60°C for 3 days. Afterwards, the reaction products were recovered using an ether extraction, as for the methanolysis reaction. The level of functionalization with allyl alcohol was measured using <sup>1</sup>H-NMR. The peaks at 5.9 ppm, 5.2 ppm, and 4.6 ppm represent the vinyl C-H, the vinyl C-H<sub>2</sub>, and the allylic methylene protons of the allyl group [46]. The areas of these peaks relative to the areas of the peaks representing the two protons alpha to the carbonyl and the three fatty acid methyl protons should be 1:2:2:2:3 at complete functionalization. Results have shown that the allyl alcoholysis reaction only proceeds to about 80% completion.

#### *3.2.4.3.3 Monomer Viscosity and the Effect of Fatty Acid Structure*

The viscosity of the fatty acid monomers and the reactants used to produce these monomers were measured using a Brookfield digital viscometer at 30°C or found through the literature [47, 48]. FAME and AOH-SBO had the lowest viscosity (Table 24) because they do not have functional groups that induce hydrogen bonding, whereas the GM-FA and AME have hydroxy-ester groups, which cause these monomers to have considerably higher viscosities. The viscosities of these monomers are higher than their starting materials (reactants) for this same reason. On the other hand, AOH-SBO and FAME have an even lower viscosity than triglycerides because of their considerably lower molecular weight. In addition, AOH-SBO and FAME have lower viscosities than fatty acids (Table 25) because fatty acids have highly polar carboxylic acid groups. The viscosities of GM-FA and AME are higher than their starting materials because of increasing molecular weight and polarity.

**Table 24. The viscosity of fatty acid-based monomers and precursors.**

Type	Chemical	Viscosity (cP)
Precursor	Canola-ME	8
Precursor	HOSO-ME	8
Monomer	AOH-SBO	10
Monomer	MLau	48
Monomer	MSA	N.A. (crystalline solid)
Monomer	MLin	56
Monomer	MOA	58
Monomer	AHOSO-ME	56
Monomer	Styrene	0.7

**Table 25. The viscosity of the starting materials/reactants for fatty acid monomers.**

Chemical	Viscosity (cP)
Methanol	< 1
Glycidyl methacrylate	~ 1
Allyl Alcohol	~ 1
Oleic Acid	24
Linoleic Acid	24
Lauric Acid	N.A. (Crystalline Solid)
Stearic Acid	N.A. (Crystalline Solid)
High Oleic Soybean Oil	52
Canola Oil	51
Soybean Oil	45

Table 26 shows the room temperature viscosities of Di-BrMSA monomer, its precursors and the oleic acid glycidyl methacrylate (MOA) analogue. As can be seen, the viscosity of Br-OA was considerably higher than that of oleic acid. The viscosity of the Di-BrMSA monomer shows a tremendous increase compared to the MOA monomer. This huge increase in the viscosity of the Di-BrMSA monomer is attributed mainly to the polar interactions brought to the MOA structure by the highly polar Br- functional groups and also to the considerable molecular weight increase caused by the addition of two Br atoms (+159.8g.). Additionally, the decrease in the level of unsaturation of fatty acids or triglycerides is expected to increase the viscosity since the unsaturation sites put kinks along the fatty acid chains and increase the intermolecular spacing.

**Table 26. The RT viscosities of Di-BrMSA and MOA monomers and their precursors.**

Precursor or Monomer	Viscosity at 25°C (cP)
Oleic Acid	24
GMA	1
Bromine	0.74
MOA	64
Di-BrOA	463
Di-BrMSA	834

The viscosity of the Di-BrMSA monomer was significantly higher than the viscosity of the common reactive diluents used in VE and UP resins. Thus, this monomer has to be used in the presence of the lower viscosity styrene or the MOA analogue to keep the resin viscosities in a processable range at room temperature. Table 27 shows the room temperature viscosities of Di-BrMSA monomer with MOA and styrene. As can be seen, blends of the Di-BrMSA with the MOA and styrene have viscosities suitable to be used as a reactive diluent.

**Table 27. The viscosities of Di-BrMSA monomer with MOA and styrene.**

Br-MSA (wt.%)	MOA (wt.%)	Styrene (wt.%)	Viscosity(cP)(25°C)
44.4	55.6	-	164±4
44.4	-	55.6	8±4
22.3	33.3	44.4	8±4

Alternatively, formulations containing Di-BrMSA monomer as the main comonomer can be used at higher temperatures to achieve a processable low viscosity. Figure 75 shows the viscosities of the Di-BrOA and Di-BrMSA as a function of temperature. As can be seen, the viscosities of both of the brominated structures decreased exponentially as the temperature increased from 25°C to 50°C. The decrease in viscosity with temperature reached a plateau after this point. The viscosity of the Di-BrMSA decreased to below 100 cP at temperatures above 60°C.

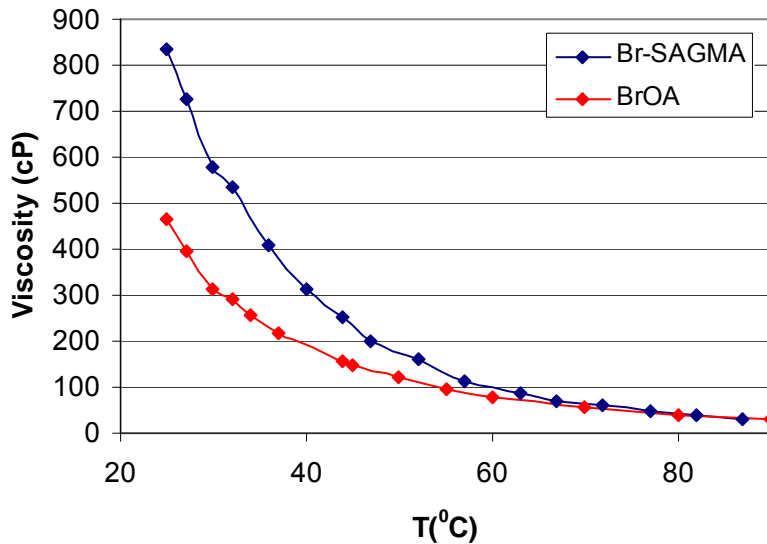


**Figure 75. The viscosities of the Di-BrOA and Di-BrMSA as a function of temperature.**

The viscosities of MFA monomers increased with chain length and as the level of unsaturation along the fatty acid backbone decreased. At 30°C, the viscosity was found to be a function of fatty acid chain length,  $l_f$  (Eq. 52):

$$\eta_{MFA} = 0.0111 * l_f^4 - 0.3857 * l_f^3 + 5.145 * l_f^2 - 29.684 * l_f + 92.351 \text{ [cP]} \quad (52)$$

The level of unsaturation affected the viscosity because these sites put kinks along the fatty acid chain that increase the intermolecular spacing [49], thereby reducing intermolecular interactions and the viscosity. An unsaturation site is the equivalent of having a fatty acid with 3.5 fewer carbon atoms according to Figure 76 (Eq. 53):

$$l_f(U) = l_f - 3.5 * U \quad (53)$$

where U is the level of unsaturation. Initially, the viscosities of polyunsaturated MFAs were similar to that of mono-unsaturated MFAs. However, the viscosities of polyunsaturated MFAs increase over time. Therefore, it was impossible to quantify the effect of two or more unsaturation sites on MFA viscosity, and Eq. 53 is only valid for  $U \leq 1$ .

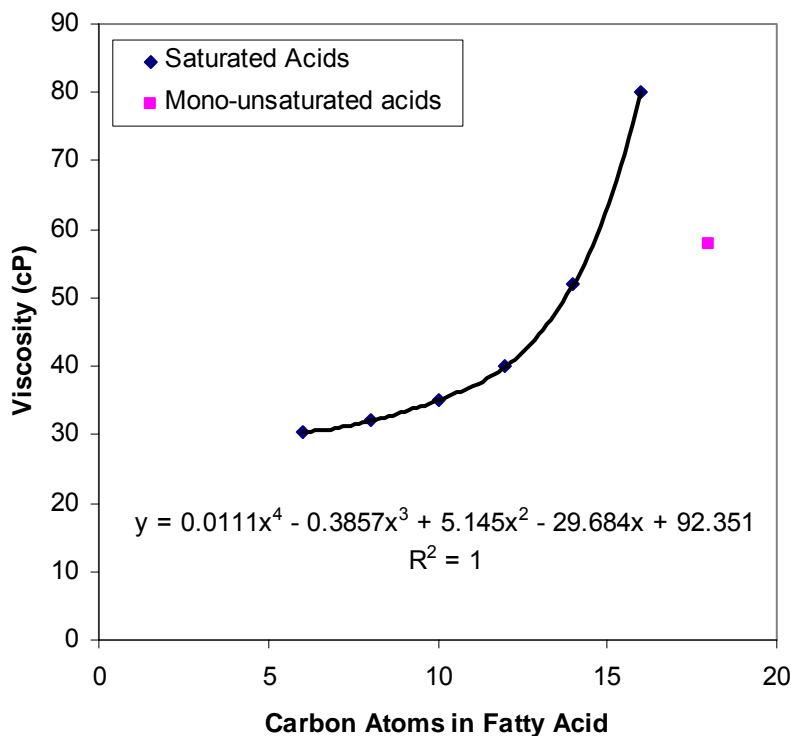


**Figure 76. Viscosity of MFA monomers as a function of fatty acid chain length.**

#### 3.2.4.3.4 Phase Separation and Cure of Mixtures of Fatty Acid Monomers and Vinyl Ester

##### *Introduction*

A number of fatty acid and triglyceride-based monomers were polymerized with vinyl ester. It was found that a number of such monomers phase separated with vinyl ester upon cure. Even more surprising was that phase separation and cure would occur upon the addition of only CoNap (i.e. no initiator) to the resin mixtures. The following describes the experiments that have been done and some conclusions that have been made.

##### *AOH-SBO – VE Resins*

The allyl alcohol modified soybean oil (AOH-SBO) is shown in Figure 66, Structure 4. The chemical is a fatty acid with an allyl group attached to the ester linkage. The molecule is aliphatic and non-polar in nature, with only a single ester group, no hydroxyl, epoxies or other such polar groups.

Vinyl ester 828 and AOH-SBO formed miscible solutions in the mass ratios of 1:1 and 2:1, respectively. Other mass ratios were not tested. The solution was stable with time with no phase separation. However, upon addition of CoNap, the sample cured at RT and micro-phase

separated. We use the term micro phase separation to mean that the resulting polymer was opaque, but no distinct layers of the immiscible components formed. The polymer, although fairly hard, was very brittle. When curing with trigonox, the polymer became harder and tougher, but it was still very brittle. The resin mixture was cured with trigonox at elevated temperature without using CoNap as an accelerator. The mixture again micro-phase separated, and formed a polymer that was very similar to the one formed at RT with the CoNap and trigonox. Resins were formed using 2 parts VE, 1 part AOH-SBO, and 1 part styrene. The resulting resins phase separated and cured in the same manner as the resins without styrene did.

To ensure that the AMC-2 catalyst used in synthesizing the VE from Epon and methacrylic acid was not causing this effect, vinyl ester 828 synthesized using the triphenyl antimony/triphenyl phosphine (SbPh<sub>3</sub>/ PPh<sub>3</sub>) catalysts were used [2]. This VE was mixed with the AOH-SBO monomer, and the same results were found as for the VE synthesized using the AMC-2 catalyst. However, it should be noted that cure occurred faster for VE that was prepared with the AMC-2 catalyst. This fact was also seen for the cure of VE with styrene, CoNap and trigonox; the VE prepared using AMC-2 cured 10 minutes faster than with the VE prepared using PPh<sub>3</sub>/SbPh<sub>3</sub>. Therefore, the AMC-2 catalyst is not the cause for the phase separation and premature curing, but it may accelerate the cure process.

A mixture of AOH-SBO and vinyl ester 828 was cured in the presence of CoNap at room temperature while monitoring with FTIR. The VE peak dropped relative to the internal reference as a function of reaction time, indicating VE cure (Figure 77). The allyl group appears at 929.6 cm<sup>-1</sup> and 989.2 cm<sup>-1</sup> [46] (Figure 77). The 929.6 cm<sup>-1</sup> peak is coincident with the vinyl group on VE. However, the 989.2 cm<sup>-1</sup> peak is clearly resolved over the course of reaction. The 989.2 cm<sup>-1</sup> peak height did not change relative to the internal reference, indicating that AOH-SBO did not cure with the VE.

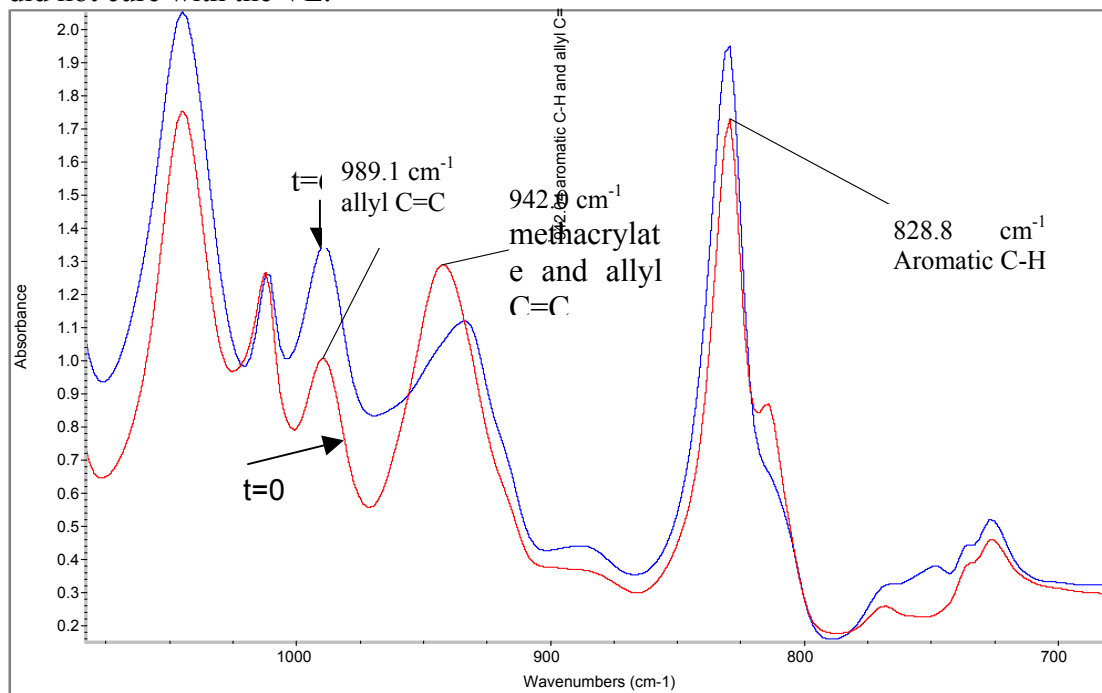


**Figure 77. The FTIR spectra of VE/AOH-SBO with CoNap at t =0 and t=6 days.**

DSC results showed that the  $T_g$  of the material was 135°C. However, when the sample was heated to 130°C, a layer of low viscosity liquid diffused to the surface. Upon returning the sample to RT, the liquid layer re-dissolved into the solid layer. We conclude that the  $T_g$  of 135°C is that of the plasticized cured VE, while the liquid is the unreacted AOH-SBO.

#### *Acrylated Soybean Oil – VE Mixture*

Acrylated soybean oil (Ebecryl 860), as seen in Figure 78, was mixed with AOH-SBO. The resin only cured at elevated temperatures (130°C) in the presence of trigonox alone or with the mixture of CoNap and trigonox. The components were miscible at all stages of cure. Unfortunately, the resulting polymers were very fragile rubbers. FTIR results show that the AOH-SBO monomers are not polymerizing. Even though the AOH-SBO did not cure, we believe that the polymer did not phase separate upon cure because of the chemical similarity of AOH-SBO to acrylated soybean oil.

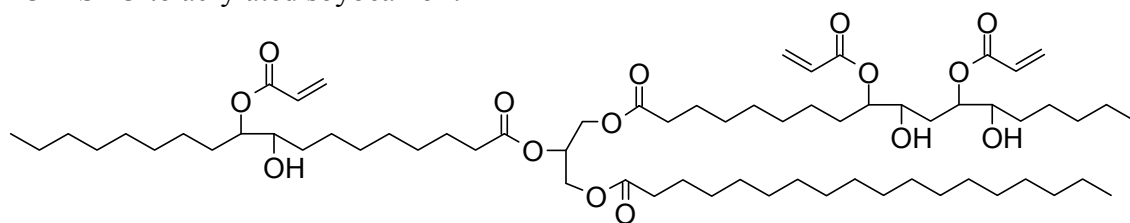


**Figure 78.** The molecular structure of acrylated soybean oil.

#### *Control Samples*

Just to rule out any simple explanations, a number of control samples were made. As was expected, VE did not cure in the presence of CoNap alone, but did cure in the presence of trigonox alone at elevated temperatures and cured at RT in the presence of both chemicals. AOH-SBO and allyl alcohol did not cure in the presence of CoNap and trigonox, even at elevated temperatures. Therefore, our conclusion that AOH-SBO does not polymerize in the presence of acrylated soybean oil or vinyl ester seems justified.

#### *FAME/SBO – VE Resins*

FAME (Figure 66, Structure 2a) were synthesized via a methanolysis reaction of high oleic soybean oil. The FAMEs were mixed with VE and were fully miscible. These resins cured at room temperature in the presence of CoNap alone. As in the case for the AOH-SBO/VE resins, the resulting polymers micro-phase separated. Furthermore, the apparent physical properties of these polymers were very similar to the AOH-SBO/VE polymers. The phase-separation behavior of these polymers was the same when the resin was cured at elevated temperature using trigonox or cured at RT using CoNap and trigonox. However, the samples cured with trigonox were harder and less brittle.

A mixture of vinyl ester and fatty acid methyl esters of high oleic soybean oil was made. 0.5 wt% CoNap was added to the resin mixture. The sample was monitored in mid IR as a function of time for 12 days at room temperature. Figure 79 shows that the methacrylic acid group of the VE decreased ( $945\text{ cm}^{-1}$ ) as a function of reaction time relative to the internal reference ( $830\text{ cm}^{-1}$ ), which represents the bending of the aromatic C-H. Therefore, vinyl ester cured in the presence of FAMEs. The extent of cure of VE as a function of time is shown in Figure 80. The

behavior does not seem to be autocatalytic; however, curing occurs so quickly that the initial cure kinetics was not observed with FTIR. In addition, the cure continues at least through twelve days, even though it appeared that the extent of cure was leveling off with reaction time after 300 minutes. The extent of cure even after 12 days was 75%, which is very high, especially considering the cure of vinyl ester with styrene at room temperature results in only 60% cure of VE. The unsaturation sites on the FAME ( $724\text{ cm}^{-1}$ ) did not react, as this peak height relative to the reference did not change over the course of the reaction.

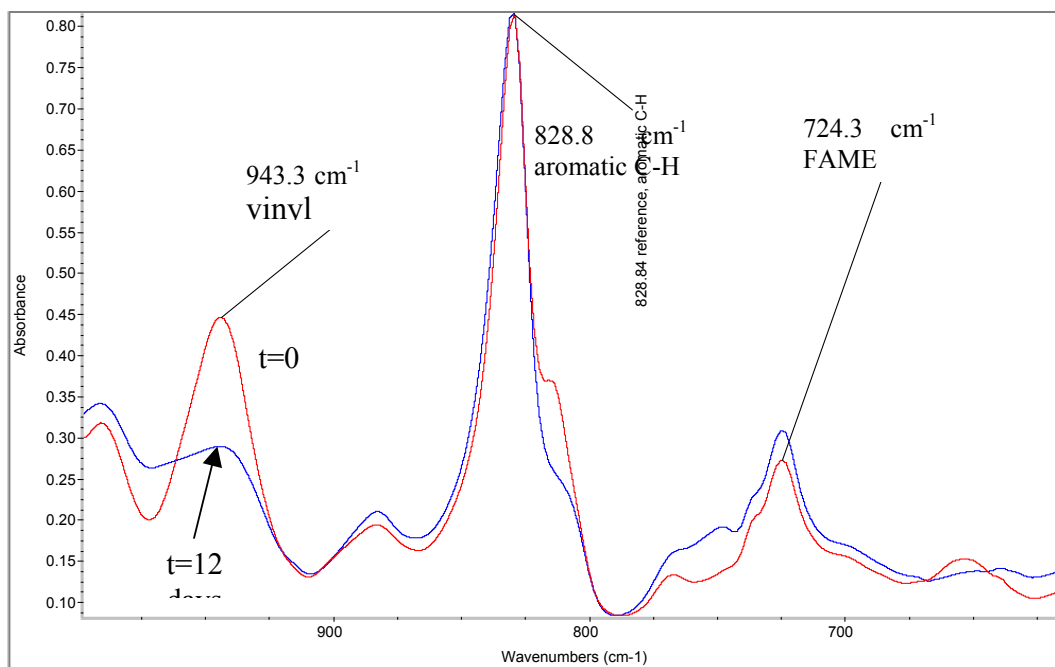


**Figure 79.** The FTIR spectra at t=0 and t=12 days for the induced cure of VE in the presence of FAME and CoNap.

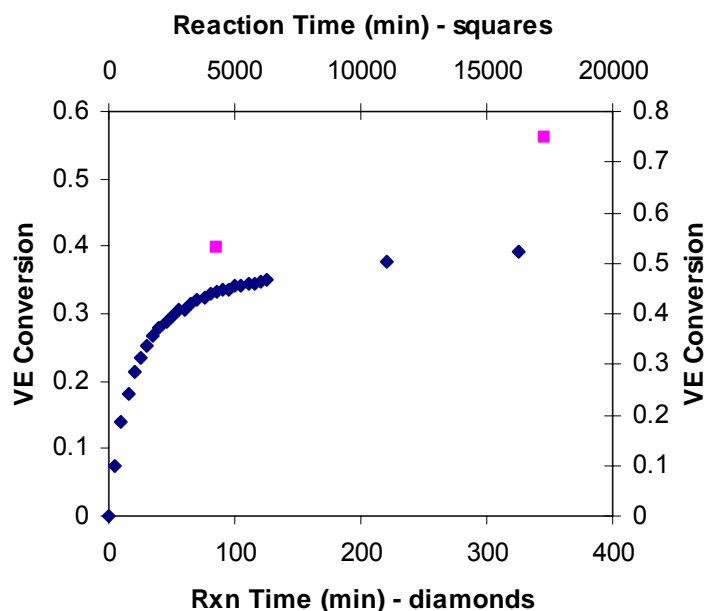


**Figure 80.** The extent of cure of VE as a function of time in the mixture of VE, FAME, and CoNap. There are two x-axes in order to show both the short-term VE cure and the long-term VE cure.

Soybean oil was mixed with VE monomer. Unfortunately, SBO and VE are not miscible. Therefore, the molecular weight difference of FAME and the soybean oil had a large impact on the solubility with VE. However, good mixing can produce a partially mixed resin. The addition of CoNap resulted in a cured, but phase separated polymer. The bottom layer was a hard solid, presumably VE, while the top layer was soft and grainy (probably a mixture of soybean oil and other non-polymerized components).

#### *Epoxidized oils – VE Resins*

The fatty acid methyl esters were epoxidized, as shown in Figure 81. These epoxidized oils (EHOSO-FAME) were mixed with VE. The components were fully miscible before cure. Upon addition of CoNap, the VE cured. However, the polymer was phase separated, where the top layer was a viscous liquid and the bottom layer was a hard solid (cured vinyl ester). The use of both trigonox and CoNap resulted in a single-phase polymer that was clear. When heated to temperatures of  $\sim 150^{\circ}\text{C}$ , a layer of liquid formed at the top of the polymer. This liquid was probably the EHOSO-FAME, indicating that it did not react into the polymer network. FTIR of this layer shows that the layer is epoxidized oil contaminated with other chemicals (VE, catalysts, etc.).

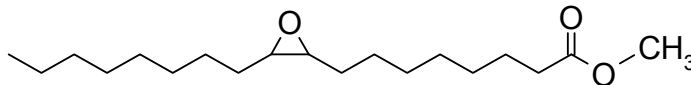


**Figure 81.** The molecular structure of epoxidized fatty acid methyl esters.

Epoxidized soybean oil (ESO) also induced cure of VE upon addition of CoNap. Two-phases were formed where the bottom layer was a hard polymer and the top was a soft and viscous liquid. However, when trigonox and CoNap were used, the resulting polymer was micro-phase

separated. The higher molecular weight of the ESO probably caused a larger driving force for phase separation during cure relative to the epoxidized FAMES.

FTIR experiments were performed to monitor the cure of VE/epoxidized FAME resins. The results show that the vinyl ester molecules cured, while the epoxidized FAMES did not polymerize (epoxy peak was constant with time).

The VE prepared using the triphenyl phosphine/triphenyl antimony catalyst was used instead of the VE prepared using the AMC-2 catalyst. No differences in the cure of epoxidized FAMES with VE was observed with the different catalyst systems. However, CoNap did not induce the cure of the VE-ESO when  $\text{PPh}_3/\text{SbPh}_3$  was present, while it did when the AMC-2 catalyst was present. The cause for this is unknown; except that it seems that the AMC-2 does accelerate the cure process, and could thus increase the likelihood of cure as well.

#### *AME – VE Resins*

CoNap was added to VE/AHOSO-ME resin in the amount of 1 wt%. The resulting resin did not cure. The resin also did not cure at elevated temperatures with or without the CoNap. Although both AHOSO-ME and FAMES are fatty acid derivatives, somehow the chemical make-up of AHOSO-ME does not induce cure of VE whereas cure is induced using FAMES, epoxidized FAMES, and AOH-SBO. A possible reason for this is that 2000 ppm hydroquinone inhibitor is added during the acrylation of EHOSO-ME (although some was removed during the ether extraction), which was not present in the other FA derivatives. However, the fact that the resin cured in a fairly short time (< 30 min) in the presence of CoNap and Trigonox indicates that the inhibitor content in this resin was low.

AME and VE cure in any proportion to form single-phase hard polymers upon addition of trigonox and CoNap (or trigonox alone if cured at elevated temperatures). On the other hand, AME does not cure in the presence of CoNap and trigonox, even at high temperatures.

#### *MFA – VE Resins*

A resin mixture containing MOA and VE was made containing 1 wt% CoNap. This mixture also did not cure at RT or 62°C even after 5 hrs of reaction. Somehow the chemical make-up of MOA does not induce cure of VE. A possible reason for this is again the presence of inhibitor in the glycidyl methacrylate (100 ppm MEHQ), which is not present in the other FA derivatives, but this does not seem likely.

GM-OA monomer alone cured in the presence of CoNap and trigonox at room temperature. The sample did not melt at temperatures as high as 130°C, indicating the sample was cross-linked. The unsaturation site on the backbone of MOA can result in chain transfer, which can cross-link the polymer. The sample was rubbery, and as expected, no  $T_g$  was visible in the DSC sweep from room temperature to 200°C. The extents of cure and cure kinetics have not been measured. In addition, MOA did not cure using 2 wt% IRGACURE with exposure to a UV lamp for 2 hours. MOA cured with 1 wt% trigonox at 130°C. However, samples of MOA with CoNap did not cure.

MFA and vinyl ester cure in any proportion to form a single-phase polymer in the presence of CoNap and Trigonox (or just trigonox if curing at elevated T). VE/MFA did not cure when only CoNap was added. VE/GM-FA cured using 2wt% IRGACURE with exposure to a UV lamp for 10 minutes. The material was nearly as stiff and tough as vinyl ester/styrene polymers. The extents of cure and reaction kinetics have not been measured.

#### *Effect of CoNap*

VE cured in the presence of FAMEs, AOH-SBO, or epoxidized FAMEs and CoNap. However, VE did not cure in the presence of CoNap at room temperature or 62°C even after 1 day of reaction. Furthermore, VE itself did not cure at 62°C even after 3 days of cure. FAMEs, epoxidized FAMEs, and AOH-SBO did not cure in the presence of CoNap after 1 day of reaction at room temperature. Although VE and FAMEs, Epoxidized FAMEs, or AOH-SBO (no CoNap) did not cure at room temperature, these samples did cure at 62°C. This shows that a free-radical reaction is occurring and the CoNap only accelerates the breakdown of the free-radical initiator.

#### *Free Radical Inhibitors*

Hydroquinone was added to mixtures of VE/AOH-SBO resins to try to prevent the premature curing of these resins. The resins contained 1 part AOH-SBO and 1.5 parts VE, and 0.5 wt% CoNap was added to the resin to decrease the cure time. Hydroquinone in the amounts of 259 ppm, 1275 ppm, and 17,000 ppm were added to the resin. Only the sample with 17,000 ppm hydroquinone did not cure, while the others cured within 10 minutes of the addition of CoNap. Because a free-radical inhibitor can inhibit the gelation of VE/FA resins, it appears that the curing process is free radical based. Unfortunately, a very large amount of free-radical inhibitor needs to be added to successfully prevent unwanted gelation (~10,000 ppm), which is ~100 times the amount that is typically added to monomeric resins.

#### *Phase Behavior Conclusions*

The phase behavior studies of VE/FA resins have led to a number of conclusions:

1. Even if the resin is miscible before cure, phase separation can occur because of one of two scenarios:
  - a. No polar character (epoxies, hydroxyl groups) in the resin.
  - b. Monomer molecular weight is too high (tendency for phase separation increases with molecular weight).
2. Phase separation does not occur if the monomers are similar in character (e.g. Ebecryl with the fatty acid based monomers), but this has no effect on the cure.
3. The AMC-2 catalyst accelerates the cure of VE resins.
4. The AMC-2 catalyst has little effect on the phase separation behavior and tendency to cure of the VE-fatty acid/triglyceride resins.
5. Vinyl ester cures in the presence of FAMEs with or without CoNap. CoNap acts only as a promoter for the reaction.
6. The unsaturation sites on fatty acid methyl esters and allyl groups on AOH-SBO do not participate in the premature cure of VE/AOH-SBO resins.
7. AHOSO-ME and MFA do not induce cure and phase separation of VE.

8. Free-radical inhibitors used in very large quantities can inhibit the gelation process of VE/FA resins. Therefore, the premature gelation process can be regarded as a free-radical process.
9. Because a very high amount of inhibitor must be used to prevent gelation, we conclude that there is a large quantity of the species that yields the free radicals.

Unfortunately, we have yet to determine why VE cures in the presence of these non-vinyl fatty acids and CoNap. Work will be done in the near future to elucidate this mechanism.

#### 3.2.4.3.5 Resin Viscosity and Gelation

The viscosities of fatty acid-based VE resins were measured at 30°C. CoNap and trigonox (45% cumene hydroperoxide) were used to cure the resins. 1 mole of cumene hydroperoxide was used per 100 moles of vinyl groups. The mass of CoNap was ¼ the mass of trigonox. The viscosity of the resins before cure is shown in Table 28. The viscosity of the GM-FA resins increased with chain length and decreased as level of unsaturation along the fatty acid backbone decreased. The level of unsaturation affected the viscosity because these sites put kinks along the fatty acid chain and increase the intermolecular spacing [14]. AHOSO-ME had a lower viscosity than GM-OA because it was not completely functionalized (some fatty acids did not have acrylate/hydroxyl groups on them) and it has a lower molecular weight. Figure 82 shows the gelation behavior of these resins. There was a significant induction period before gelation occurred, where the viscosity increased very rapidly, just as for vinyl ester/styrene resins.

**Table 28. The initial viscosity of fatty acid-based VE resins at 30°C.**

Comonomer	Viscosity (cP)	
	35% Comonomer	45% Comonomer
GM-Lau	1720 ± 4	792 ± 4
GM-Lin	2500 ± 4	1900 ± 4
GM-OA	2720 ± 4	2000 ± 4
AHOSO-ME	2000 ± 4	1300 ± 4

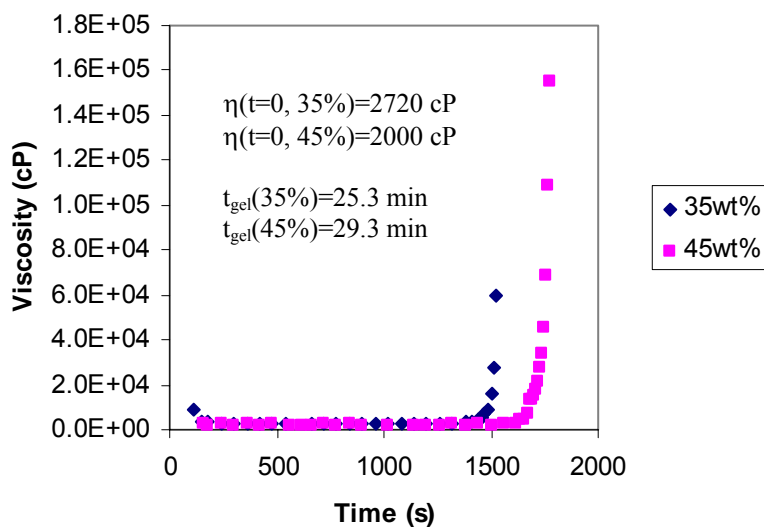


**Figure 82.** The viscosity of VE/GM-OA resins as a function of cure time.

Fatty acid chain length has a significant effect on the resin viscosity. The viscosity went through a minimum as a function of fatty acid chain length (Figure 83). At 35 wt% styrene, the minimum occurred at 6 carbon atoms, but increased to 8 carbon atoms for resins with 45 wt% styrene. These minima occurred as a result of two competing effects [13, 14]. For long fatty acids, fatty acid chain length/molecular weight effects dominate. Van der Waals interactions between these long fatty acids dominate the interactions between molecules. However, for short fatty acid chain lengths, the effect of the hydroxyl group (Figure 66), which induces hydrogen bonding, dominates the interactions between chains. As the chain length of the fatty acid increases, the effect of this hydroxyl group on the interactions decreases, allowing the molecular weight effect to dominate, causing the up-swing in viscosity.

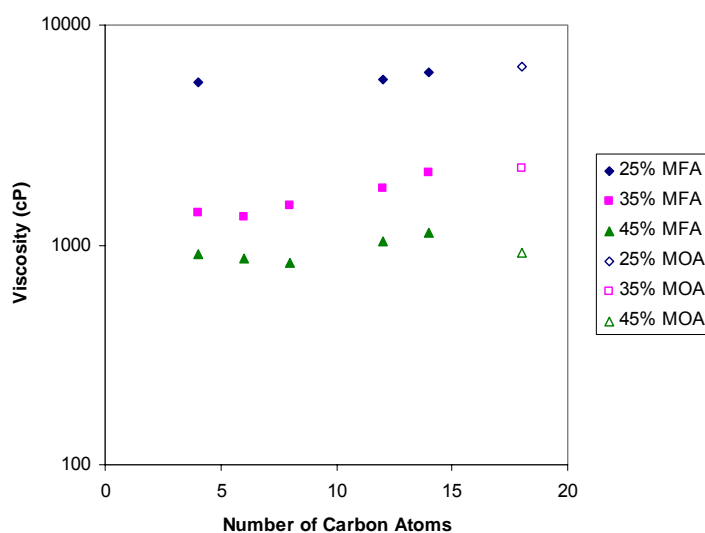


**Figure 83.** The viscosity of VE/MFA as a function of fatty acid chain length at 25°C.

The viscosities of the VE resins before cure are shown in Figure 83. The viscosities of FA-VE resins are considerably higher than that of VE/styrene resins (< 100 cP) because FA monomers have considerably higher viscosities than styrene. The viscosity went through a minimum at 6-8 carbon atoms as the fatty acid chain length increased. This occurred because two factors are affecting the resin viscosity. At short fatty acid chain lengths, polar interactions/hydrogen bonding, due to the MFA hydroxyl group, dominate. However, at longer fatty acid chain lengths, the concentration/effect of this hydroxyl group decreases and chain length effects dominate. Overall, it appears that fatty acids with chain lengths of 6-8 carbon atoms are ideal for producing low viscosity FA-VE resins. The presence of unsaturation sites along the fatty acid backbone decreased the resin viscosity (Figure 83), as they did for MFA monomers alone.

The effect of fatty acid content on VE viscosity was quantified. Figure 84 and Figure 85 show that the resin viscosity decreased exponentially with MFA content. Two functions were used to approximate the effect of MFA content on viscosity. The first was simply an exponential fit of the data (Figure 84), which does a good job of fitting the data, except at low MFA contents. A function similar to the VE/styrene viscosity model was also used (Figure 85). This function does an excellent job of fitting the data with the added benefit of taking into account the effect of vinyl ester molecular weight. Unfortunately, we are not able to prepare bimodal blends of vinyl ester monomers with MFA as the only comonomer, and therefore cannot verify the effect of bimodal molecular weight in this section. However, using blends of VE, MFA, and styrene, we will verify the form of this equation in a later section.

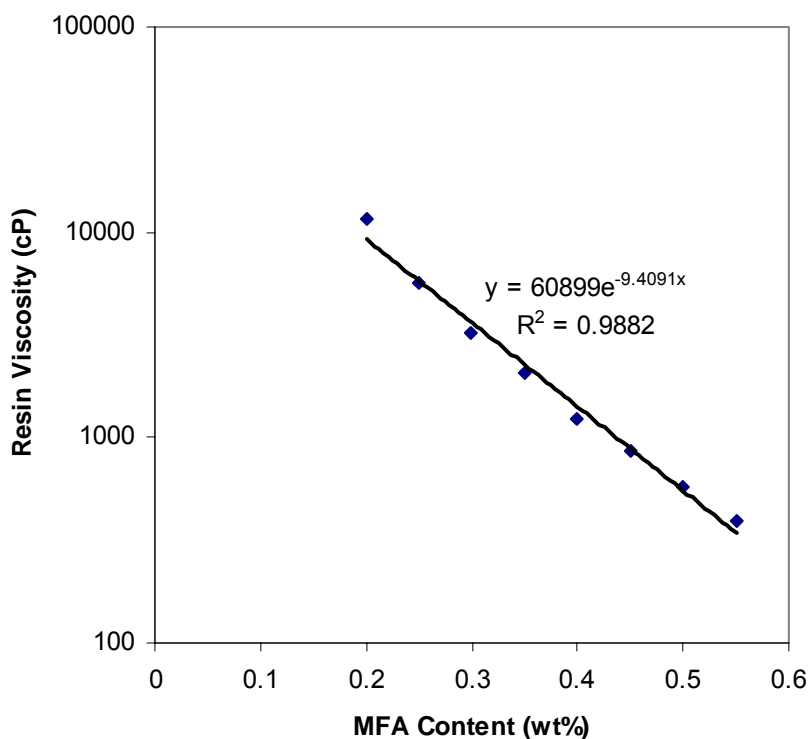


**Figure 84.** Viscosity of VE resin as a function of MFA content for MLau fatty acids, showing the exponential fit to the data.

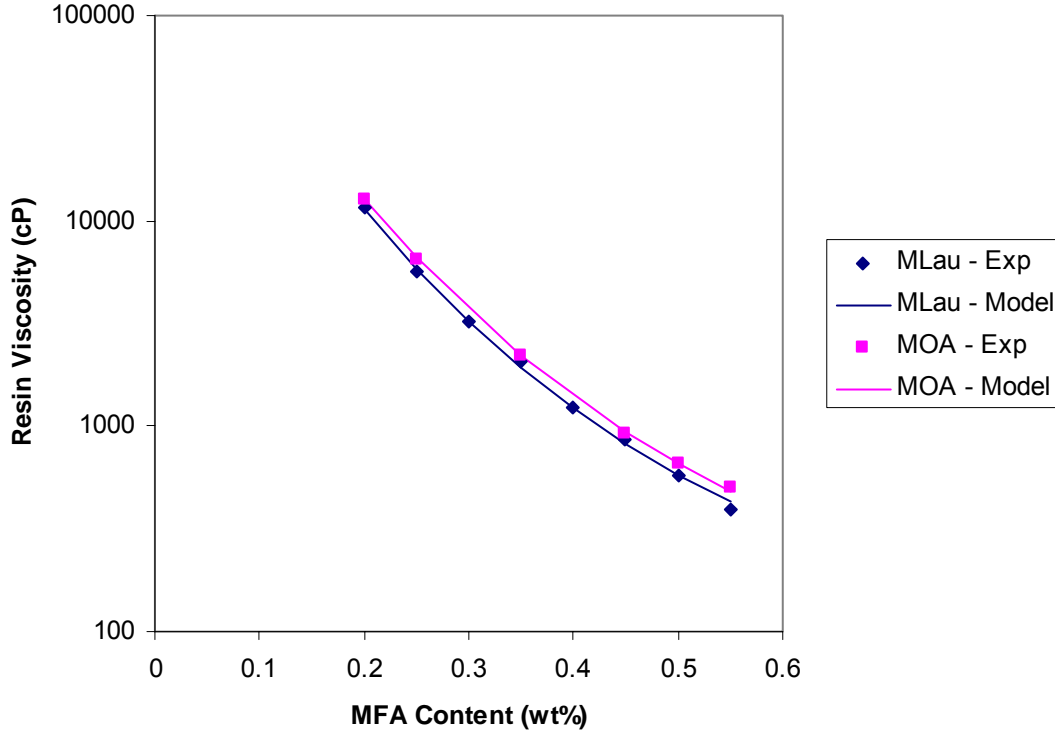


**Figure 85. Viscosity of VE resin as a function of MLau content, showing the exponential fit to the data.**

The best fit curves in Figure 85 have the form (Eq. 54):

$$\eta_{VE/MFA}(MFA, M_n) = \eta_{MFA}^* \cdot \text{Exp}\left[\frac{M_n}{M_e(MFA)}\right] \text{ [cP]} \quad (54)$$

where  $MFA$  is the weight fraction of MFA monomer and  $\eta_{MFA}^* = 50$  cP, which is the approximate viscosity for all MFA monomers at 30°C. As for styrene,  $M_e(MFA)$  was an exponential function of the MFA content (Eq. 55):

$$M_e(MFA) = 58.5 \cdot \text{Exp}[f(MFA)] \text{ [g/mol]} \quad (55)$$

$f(MFA)$  is an exact linear function of MFA viscosity (Figure 86) (Eq. 56):

$$f(\eta_{MFA}) = (2.9007 - 0.0063 \cdot \eta_{MFA}) \cdot MFA \quad (56)$$

Combining Eq. 53 and 56,  $f(MFA)$  can be related to the fatty acid chain length and unsaturation level (Eq. 57):

$$f(\eta_{MFA}) = [2.9007 - 0.0063 \cdot (0.0111 \cdot l_f^4 - 0.3857 \cdot l_f^3 + 5.145 \cdot l_f^2 - 29.684 \cdot l_f + 92.351)] \cdot MFA \quad (57)$$

Combining Eq. 54-56 gives the overall shows that the viscosity of bimodal blends was a predictable function of the  $M_n$  of the VE monomers and the styrene weight fraction (Eq. 58)

$$\eta_{VE/MFA}(MFA, l_f, U, M_n) = \eta_{MFA}^* \cdot \text{Exp}\left[\frac{M_n}{58.5 \cdot \text{Exp}((2.9007 - 0.0063 \cdot \eta_{MFA}) \cdot MFA)}\right] \text{ [cP]} \quad (58)$$

Therefore, the resin viscosity was proportional to the exponential of the inverse of the exponential of the MFA. This model is not likely to predict the up-turn in viscosity at short fatty acid chain lengths as seen in Figure 83. Overall, this empirical viscosity model does an excellent job of predicting the viscosity of VE/MFA resins as a function of MFA content and MFA type.

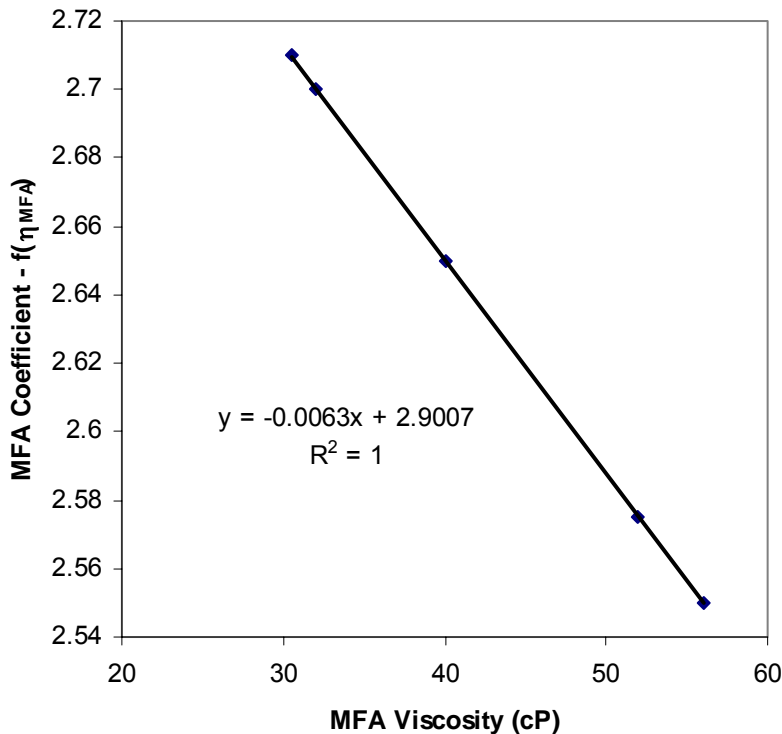


**Figure 86.** The MFA coefficient in Eq. 18 is a linear function of MFA viscosity.

#### 3.2.4.3.6 Effect of Temperature on Resin Viscosity

The viscosities of MFA-based vinyl esters follow an Arrhenius relationship. The activation energy for viscous flow and the pre-factors were calculated from the Arrhenius plots. The activation energy decreased linearly as a function of MFA content (Figure 87) as it did for styrene (Eq. 59):

$$E_{VE/MFA} = -114.1 * MFA + 114.6 \text{ [kJ]} \quad (59)$$

This indicates the sensitivity to temperature decreased as the MFA content increased. The three different monomers have very different viscosities alone and in VE resins. Therefore, it is expected that all fatty acid-based vinyl esters will have activation energies that fall along this line. The activation energy was higher for a given content of MFA monomer relative to styrene, because of a lower molar content of MFA monomers. Eq. 59 indicates that the activation energy is ~0 for MFA monomers alone, which is not correct. Therefore, we expect this curve to level out as the MFA content is increased above 55 wt%.

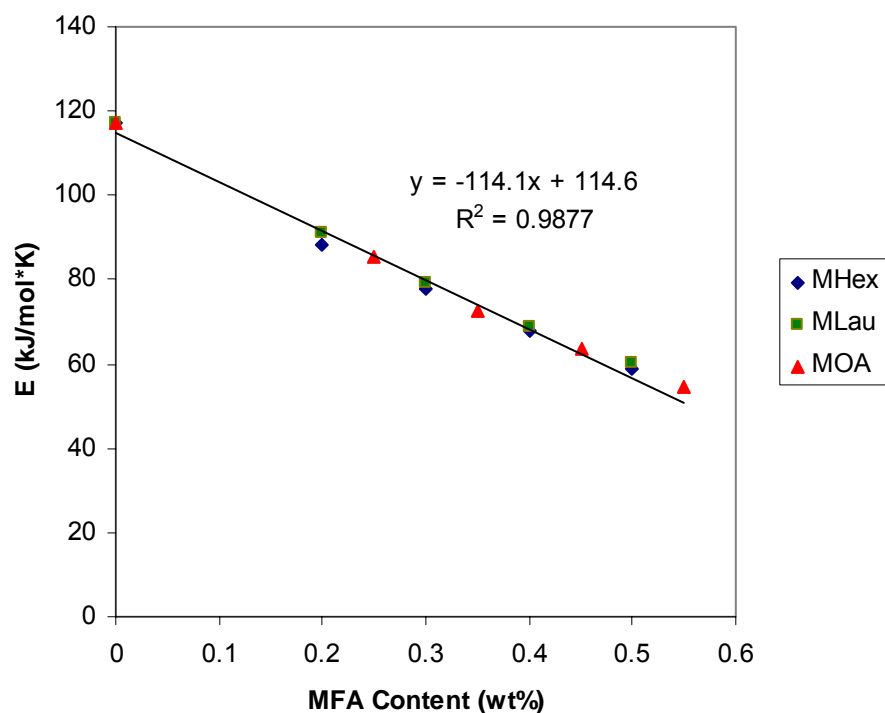


**Figure 87. The activation energy as a function of diluent content and fatty acid type.**

The pre-factor increased exponentially as a function of MFA content in the resin (Figure 88) (Eq. 60):

$$A_{VE/MFA} = 1.76 \cdot 10^{-18} \cdot \text{Exp}(34.7 \cdot MFA) \text{ [Pa*s]} \quad (60)$$

This factor was expected to increase because it is related to the frequency of interactions, which should increase given that high MFA contents produce resins with lower viscosities. For this same reason, the value of  $A$  is lower for VE/MFA resins relative to VE/styrene resins because of the lower molar concentration of MFA monomers used in this work.

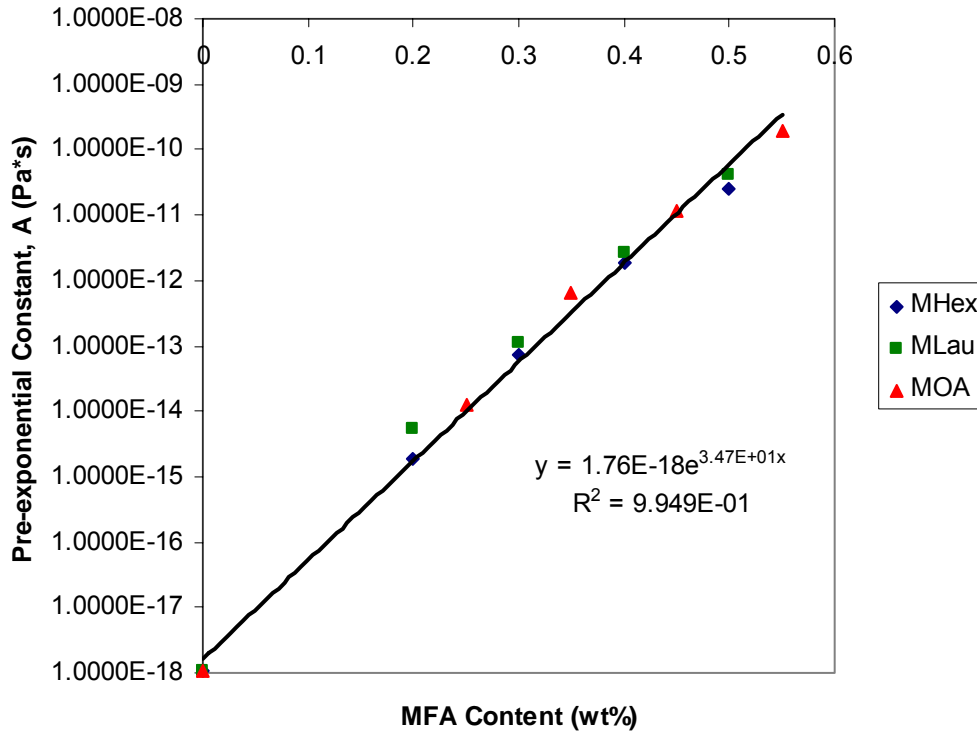


**Figure 88.** The pre-exponential constant as a function of diluent content and fatty acid type.

Combining Eq. 38, 59, and 60, we obtain the viscosity of VE/MFA as a function of temperature (Eq. 61):

$$\eta_{VE/MFA}(T) = 1.76 \cdot 10^{-18} \cdot \text{Exp}\left(\frac{-114100 \cdot MFA + 114600 + 34.7 \cdot S \cdot RT}{RT}\right) [\text{cP}] \quad (61)$$

### 3.2.4.3.7 Complete Viscosity Model for Fatty Acid-Based Vinyl Ester Resins

As for VE/Styrene resins, the viscosity model for VE/MFA resins was a simple combination of the effects of temperature (Eq. 59) and the effects of monomer content (Eq. 58), as well as monomer type (Eq. 62):

$$\eta_{VE/MFA}(MFA, T, l_f, U) = \eta_{MFA}^* \cdot \text{Exp}\left[\frac{M_n}{58.5 \cdot \text{Exp}((2.9011 - 0.0063 \cdot \eta_{MFA}) \cdot MFA)}\right] \quad (62)$$

$$\cdot \text{Exp}\left[\frac{-114100 \cdot MFA + 114600}{R} \left(\frac{1}{T_2} - \frac{1}{303K}\right)\right] [\text{cP}]$$

The model allows for calculation of the VE/MFA viscosity for any given temperature, VE molecular weight, MFA chain length, MFA unsaturation level, and MFA content. Figure 89 shows the operating window for VE/MFA resins as a function of temperature, fatty acid chain length and unsaturation level. Increasing temperature reduces the required MFA content, as was expected. Increasing the MFA chain length has little effect on the window until above chain

lengths of 12 carbon atoms. Above which, the required MFA content increased severely with chain length. Unsaturation sites decreased the required MFA content, as expected. Interestingly, Figure 89 shows that fatty acids of 8 carbon atoms minimize the required MFA content. Therefore, the viscosity model does predict the minimum in viscosity as a function of fatty acid chain length (Figure 83) at 6-8 carbon atoms.

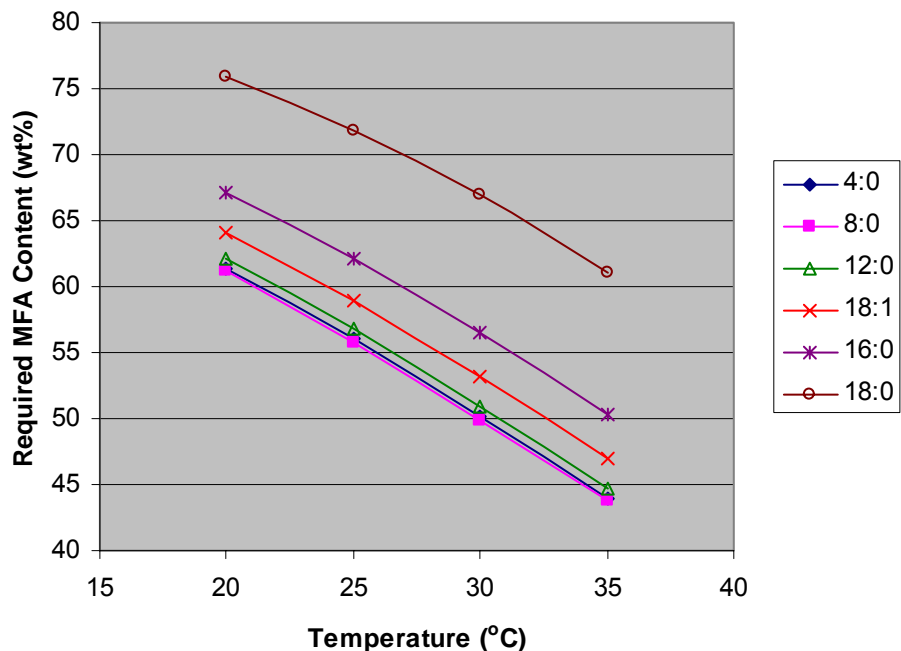


**Figure 89.** The minimum MFA content required to achieve VE resin viscosities below 500 cP as a function of temperature, fatty acid chain length, and unsaturation level. The operating window is any MFA content above the curve. Legend: [Carbon atoms:Unsaturation sites].

#### 3.2.4.3.8 Viscosity of Vinyl Ester Resins Using Both Fatty Acid Monomers and Styrene as Reactive Diluents

The viscosities of VE resins using MFA were fairly high. Only a small number of formulations achieve viscosities of 500 cP or lower at 30°C using less than 50 wt% MFA. To reduce the viscosity, blends of MFA and styrene were used as the reactive diluent in VE 828. The viscosity of VE/MFA/styrene was measured at 30°C and was found to decrease exponentially with styrene content for resins containing 55 wt% and 65 wt% VE 828 resin (Figure 90, shown for MHex-based resins). Styrene contents of ~10% or more reduced the viscosity of VE resins to the acceptable range (< 500 cP is required for most liquid molding processes [27, 28]). Only low styrene contents are necessary to reduce the viscosities of MFA/VE systems to acceptable processing conditions at 30°C.

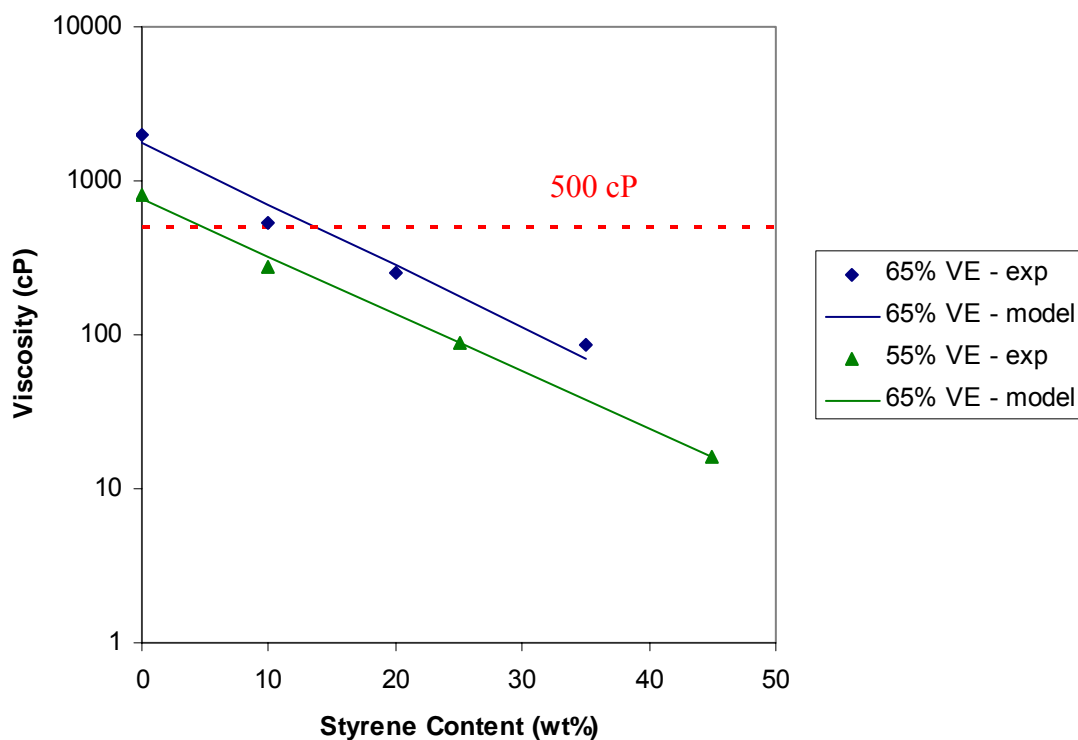


**Figure 90.** The viscosity of VE/MHex/styrene as a function of styrene content in the resin for resins containing 55 wt% and 65 wt% VE 828, along with model predictions.

The best fit curves in Figure 90 were derived from a logarithmic rule of mixtures [50] (Eq. 63):

$$\eta_{VE/MFA/Sty} = \exp[w_{S(D)} \cdot \ln(\eta_{VE/Sty}(D)) + w_{MFA(D)} \cdot \ln(\eta_{VE/MFA}(D))] \text{ [cP]} \quad (63)$$

where  $w_{S(D)}$  and  $w_{MFA(D)}$  are the styrene and MFA weight fractions, respectively, of the total diluent content,  $D$ , and  $\eta_{VE/Sty}(D)$  and  $\eta_{VE/MFA}(D)$  are the viscosities of VE/Styrene and VE/MFA, respectively, evaluated at the total diluent weight fraction. This logarithmic rule of mixtures does an excellent job of predicting VE/MFA/Styrene resin viscosity as a function of composition. On the other hand, a simple rule of mixtures does not accurately fit the data, nor does the Fox equation [30]. Furthermore, this model is able to accurately predict the effect of VE molecular weight (Figure 91) and temperature (Figure 92) on resin viscosity. Therefore, this overall viscosity model allows prediction of the viscosity of vinyl ester resins based on the vinyl ester molecular weight, styrene content, MFA chain length, MFA unsaturation level, MFA content, and temperature.

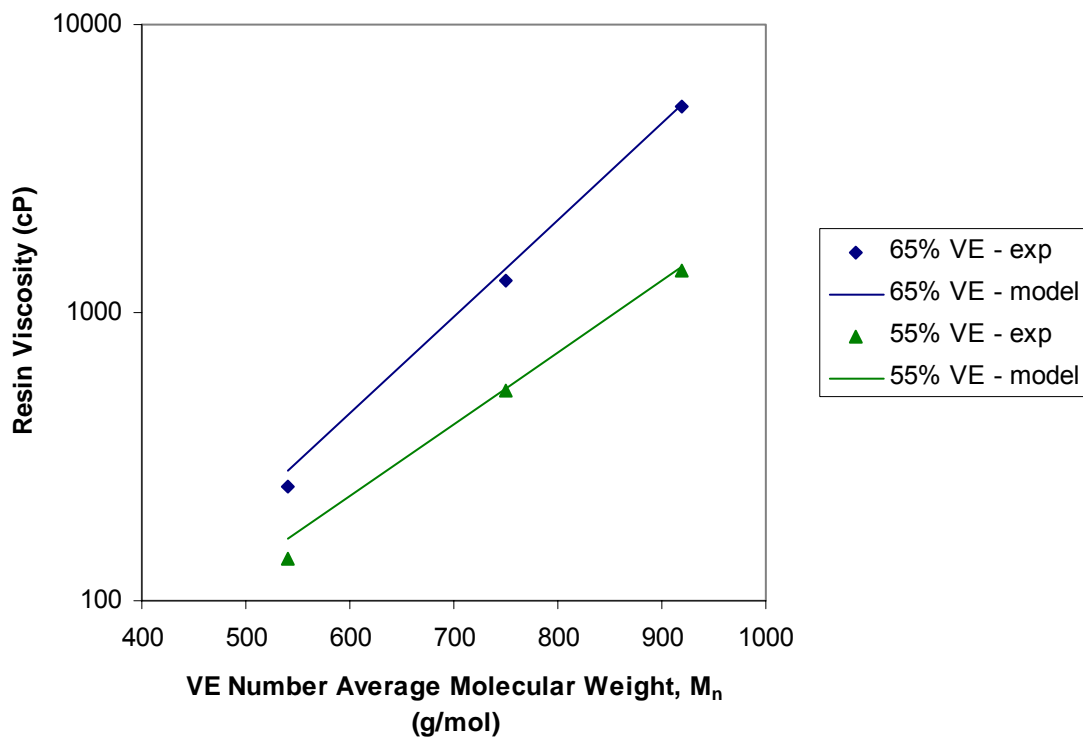


**Figure 91.** The experimental and model viscosities of VE/MHex/Styrene as a function of VE molecular weight and VE content for resins containing 20 wt% styrene.

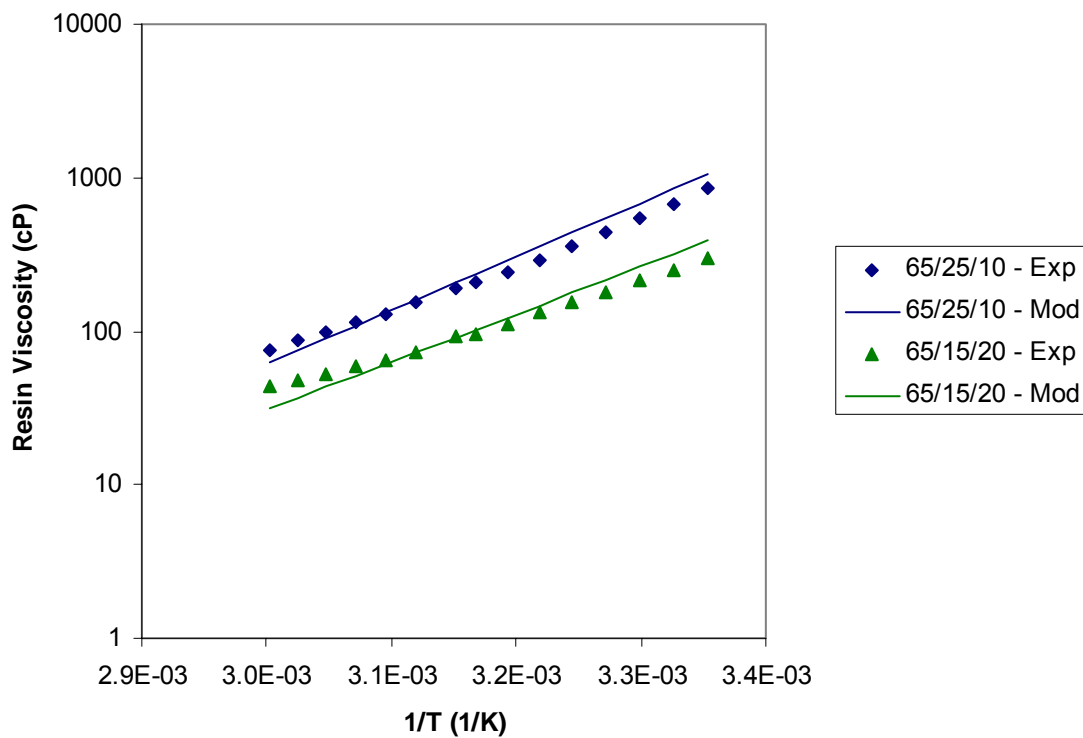


**Figure 92.** The experimental and model viscosities of VE/MLau/Styrene as a function of temperature.

Using this overall viscosity model, an operating window (i.e., viscosity below 500 cP) can be determined for a single variable while keeping the other variables constant. For instance, at 30°C, the required styrene content in VE/MFA/Styrene resins increases as the VE molecular weight increases (Figure 93). However, fatty acid chain length does not have a strong affect until effective fatty acid lengths of 14 are reached. Therefore, using lauric acid to make fatty acid-based VE resins will not result in significantly higher viscosities than hexanoic acid-based resins.

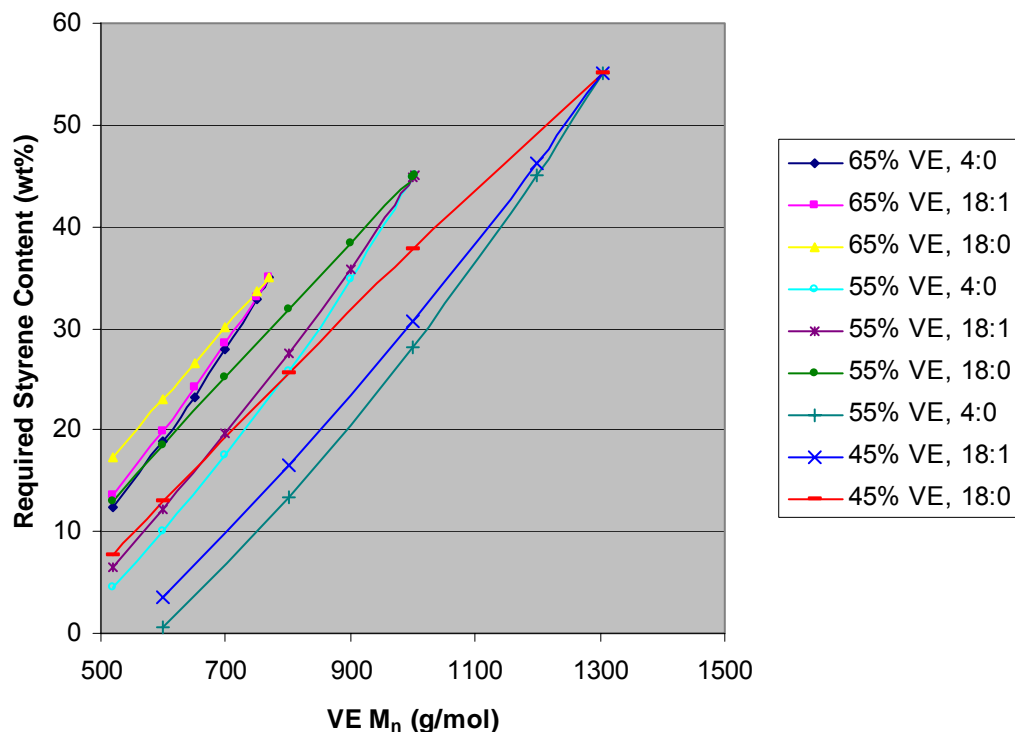


**Figure 93.** The minimum styrene content required to achieve VE resin viscosities below 500 cP as a function of fatty acid chain length, VE content, and VE molecular weight at 30°C. The operating window is any styrene content above the curve for any molecular weight along the curve. Legend: [Carbon atoms: Unsaturation sites].

### 3.2.4.3.9 Viscosity Conclusions

The viscosities of DGEBA-based vinyl ester resins are predictable functions of reactive diluent content, type, temperature, and vinyl ester molecular weight. The viscosity decreased exponentially with reactive diluent content. Therefore, changes in the diluent content have a larger effect on the resin viscosity at low diluent contents than they do at higher diluent contents. Two different types of reactive diluents affected the viscosity in the same manner, but not to the same extent. The viscosities of resins using both diluents were accurately predicted using a logarithmic rule of mixtures from the two-component viscosity functions. The viscosity increased exponentially and predictably as a function of the vinyl ester number average molecular weight. Increasing the temperature decreased the viscosity in an Arrhenius manner. The activation energy for viscous flow decreased linearly as the diluent content increased, but was unaffected by vinyl ester molecular weight, fatty acid chain length, and unsaturation level.

Overall, the resin viscosity can be modeled as simple functions of the resin temperature, vinyl ester molecular weight, styrene content, MFA content, MFA chain length, and MFA unsaturation level, which are all known quantities for a formulated resin.

#### 3.2.4.3.10 Cure Kinetics

For both homopolymerized MFA and VE/MFA resins, the cure rate decreased as the number of residual unsaturation sites on the fatty acid backbone increased (Figure 94). The effect is less pronounced for VE/MFA resins because of the lower concentration of MFA monomers (Figure 95). Furthermore, the ultimate conversion is decreased as a result of the presence of these residual unsaturation sites. The unsaturation sites on fatty acid backbones are similar to allyl groups. It has been shown that allyl groups do not free-radically polymerize. Instead, they absorb free-radicals, but do not propagate the radical, thereby reducing the cure rate of other free-radical monomers [51]. On the other hand, fatty acid chain length was not found to have any effect on VE cure kinetics. Therefore, methacrylated fatty acids based on lauric acid or stearic acid are ideal for achieving fast cure rates and high extents of cure, which should result in improved polymer properties.

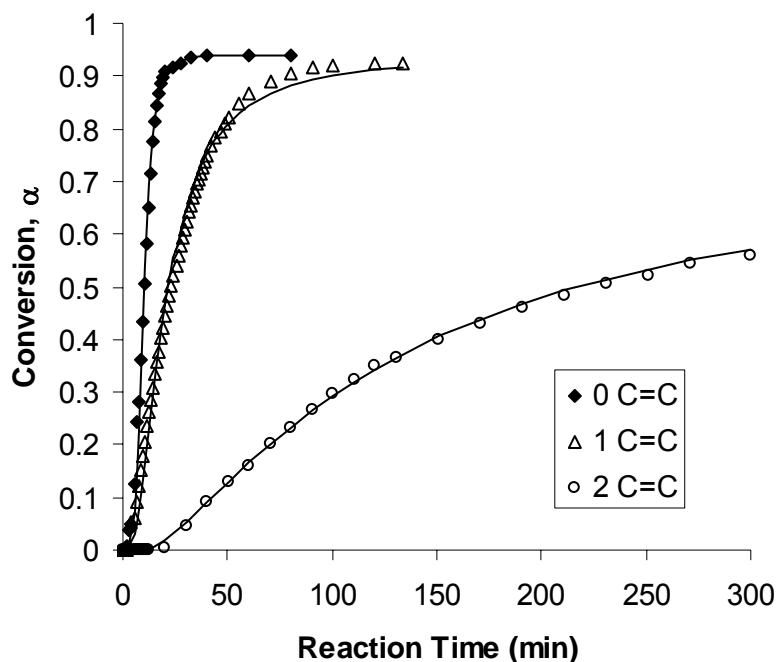


**Figure 94.** The conversion as a function of time for the homopolymerization at 90°C of MFA with 0, 1, and 2 residual unsaturation sites and their autocatalytic fit.

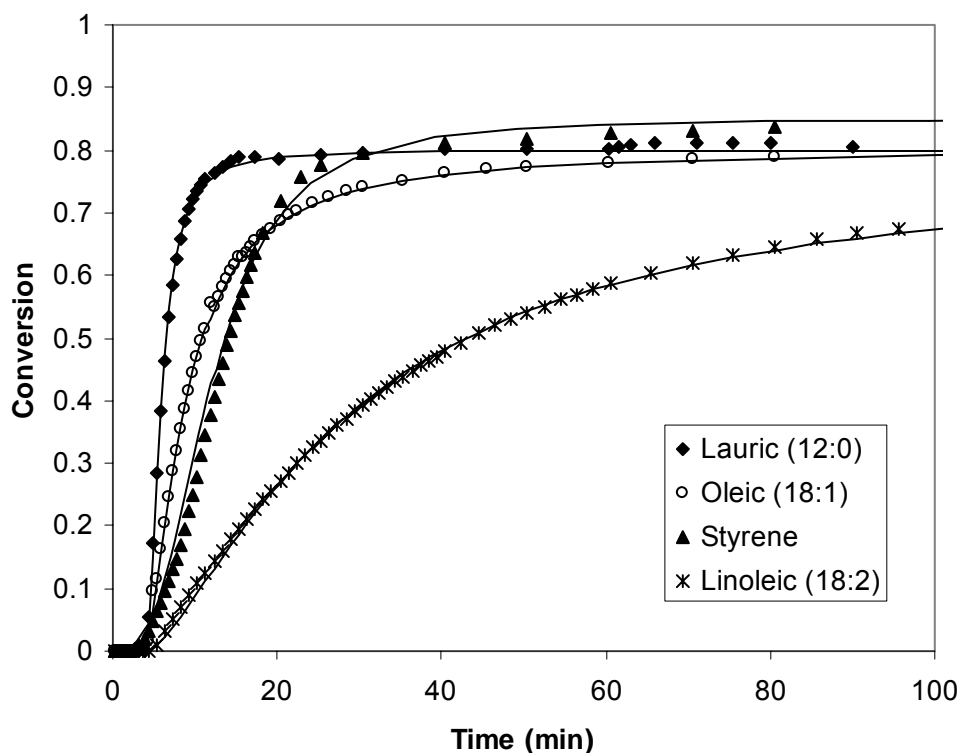


**Figure 95.** The overall conversion as a function of time for the cure of VE/MFA relative to VE/styrene and their autocatalytic fits using 45% reactive diluent. Samples were cured at 90°C and post-cured at 120°C once the cure reaction stopped.

The cure rate of all MFA resins, except linoleic acid based monomers, was higher than that of styrene-based resins (Figure 95). This effect is a result of the fact that VE/styrene blends vitrify at a much lower temperature than VE/MFA blends because of the greater amount of free volume introduced from the MFA. In addition, the VE/styrene cure rate could be decreased because of the presence of inhibitor in the styrene and styrene's aromatic nature. The overall conversion of VE/MFA resins was slightly lower than VE/styrene resins, due to the continuing polymerization of styrene even after VE polymerization is done because of styrene's high mobility (i.e. low molecular weight and compact size).

Using the acrylated vinyl esters, the conversion on the individual monomers was observed. It was found that the VE monomers of VE/MFA reacted to a high extent (85%), while the MFA only reacted to ~65% (Figure 96). This is in contrast to VE/styrene resins, where the VE only reacts to 75% while styrene reacts to >90% [1]. We hypothesize that VE monomers cure to a high extent in MFA resins because the long side groups of MFA allow for flexibility of the network and reduce diffusion limitations to growing radicals. MFA react to a low extent because of the inherent low reactivity of methacrylate groups relative to the vinyl group on styrene [1].

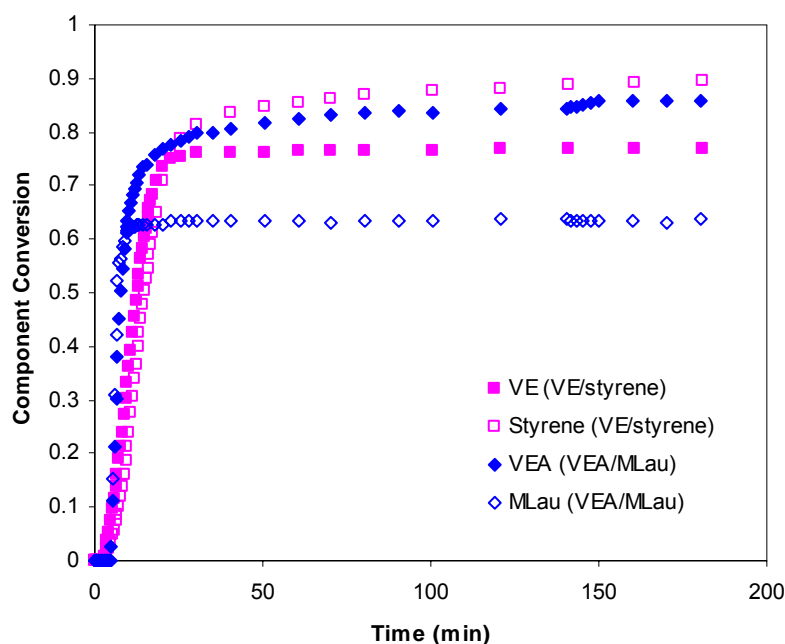


**Figure 96.** The individual cure kinetics of the components of VE/styrene and VE/MLau, each containing 45% reactive diluent.

#### 3.2.4.3.11 Polymer Properties

Thermo-mechanical properties of VE resins using fatty acid monomers were also measured using DMA. Polymers using MFA monomers produced hard and rigid polymers, similar to that of commercial VE polymers. Table 29 lists the properties of the VE/MFA polymers cured at room temperature and then post-cured with a 5°C/min temperature ramp from room temperature to 200°C. The moduli were greater than 1 GPa. DMA shows that  $T_g$  was less than 100°C for these polymers. Both  $T_g$  and the modulus increased as the fatty acid chain length decreased. This was expected because longer fatty acid chains increase the free volume of the polymer and increase the effective molecular weight between cross-links. The glassy modulus and  $T_g$  decreased as the level of unsaturation of the fatty acid chain increases. This is clearly visible for the MLin samples, which have considerably lower properties than the other MFA monomers. This is consistent with the fact that MLin monomers cure the slowest and to the lowest extent of the MFA tested.

The rubber moduli of the polymers were ~45 MPa, indicating the molecular weight between cross-links,  $M_c$ , was 200-300 g/mol. For fatty acids with chain lengths of 18 carbon atoms,  $M_c$  should be 280 g/mol and 300 g/mol for 35% and 45% MFA comonomer, respectively, which is in good agreement with our results.  $M_c$  decreased as the fatty acid chain length decreased, as expected (Table 29).

**Table 29. The properties of styrene and fatty acid based vinyl esters cured at room temperature and post-cured with a temperature ramp from room temperature to 200°C at 5°C/min.**

Comonomer	35% Comonomer			45% Comonomer		
	T <sub>g</sub> (°C)	E' @35°C (MPa)	M <sub>c</sub> (g/mol)	T <sub>g</sub> (°C)	E' @35°C (MPa)	M <sub>c</sub> (g/mol)
Styrene	147	2.9	328	142	2.6	642
MLau	79	2.0	211	71	1.5	304
MOA	76	1.6	240	75	1.1	373
MLin	72	1.6	290	69	1.0	400
AME	67	1.1	309	N.A.	N.A.	N.A.

Curing the resins at elevated temperature increased the polymer properties (Table 30). Comparing Table 29 and Table 30, it is obvious that both T<sub>g</sub> and the modulus increased while M<sub>c</sub> decreased as the cure temperature increased. These results were expected because elevated cure temperatures typically increase the extent of polymerization [1].

**Table 30. The properties of MFA-based vinyl esters cured at 90°C and then post-cured with a temperature ramp from room temperature to 200°C at 5°C/min.**

Comonomer	35% Comonomer			45% Comonomer		
	T <sub>g</sub> (°C)	E' @35°C (GPa)	M <sub>c</sub> (g/mol)	T <sub>g</sub> (°C)	E' @35°C (GPa)	M <sub>c</sub> (g/mol)
Styrene	150	3.0	297	145	2.7	432
MLau	94	1.9	213	77	1.6	321
MSA	93	1.65	206	84	1.2	299
MOA	90	1.7	164	76	1.3	275
MLin	79	1.6	218	69	1.2	335

The dynamic mechanical behavior of VE/MFA binary blends is given in Figure 99(a) and (b). Figure 99(a) shows the loss modulus plots for the series of fatty acids investigated, and Figure 99(b) contains the associated storage modulus traces. Generally a distinct, albeit broad transition, is observed for all materials with the butyric acid modified system exhibiting the sharpest transitions. The storage modulus of the VE/MFA blends was found to decrease significantly with increasing chain length of the MFA. The storage modulus for the butyric acid modified systems was close to 2.5 GPa at 50°C, a value comparable to styrene based systems, while the VE/MFA with the highest molecular weight fatty acid possessed a storage modulus value of 1 GPa at that temperature.

#### *Glass Transition Temperature Behavior*

Figure 97(a) and (b) contain the loss modulus and storage modulus traces, respectively, for the entire series of MFAs. It is clear that the T<sub>g</sub> of these systems was generally below room temperature. It is also clear that there were multiple loss modulus peaks and shoulders that are attributable to polymer glass transitions. Generally, however, for each material, there existed one major transition and a secondary one. We define the major transition as the one that resulted in the greatest drop in storage modulus – usually more than half of the starting value. The values

of these transition temperatures are given in Table 31. It is clear from these results that fatty acid molecular weight significantly influenced the  $T_g$  of the resulting polymers. Moreover, it is evident that for the range of molecular weights investigated, the major  $T_g$  passed through a minimum at a fatty acid chain length of about 10 carbon atoms.

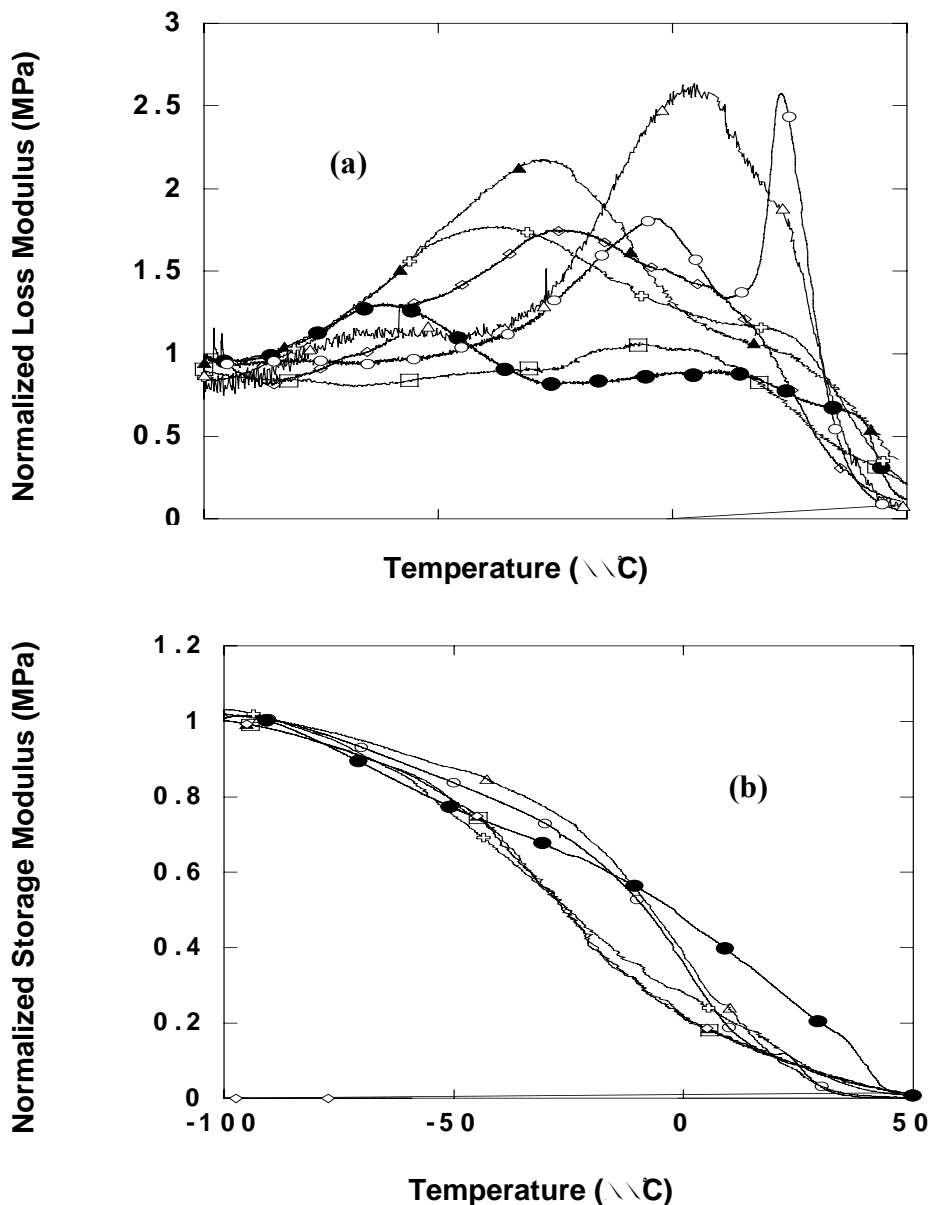


**Figure 97.** Normalized Loss (a) and storage modulus (b) behavior of Methacrylated Fatty Acids (MFA) as a function of fatty acid chain length. Methacrylated Palmitic acid (●), Methacrylated Myristic acid (□), Methacrylated Lauric acid (▲), Methacrylated Decanoic acid (◈), Methacrylated Octanoic acid (◇), Methacrylated Hexanoic acid(Δ), Methacrylated Butyric acid (O).

**Table 31. Glass transition temperature behavior ( $T_g$ ) of the Methacrylated Fatty Acids (MFA)**

Acid	Fatty acid chain length	Major Peak ' $T_g$ ' in K	Minor Peak ' $T_g$ ' in K
Butyric Acid	4	297	271
Caproic Acid	6	278	298
Caprylic Acid	8	240	277
Capric Acid	10	236	297
Lauric Acid	12	239	284
Myristic Acid	14	268	204
Palmitic Acid	16	287	213

This behavior can be seen more clearly in the plot of  $T_g$  versus MFA chain length given in Figure 98. Although the major transition went through a minimum, the minor transition monotonically decreased. Overall, the general transition of glassy to rubbery decreased as the fatty acid chain length increased, but to a larger degree at short fatty acid chain lengths. Two factors that can influence the rotational mobility of a polymer backbone are related to the presence of side groups. Bulky side groups are known to curtail rotational motions because of steric hindrance considerations. Specific interactions resulting from polar characteristics of the side groups can also limit rotational motion of the backbone segments by forming non covalent bonds. We suggest that the low chain length MFA expose the polar groups of the monomers which result in hydrogen bonding which limits polymer backbone motions (i.e. poly methacrylated butyric acid). As the chain length of the fatty acid increases, these polar groups are shielded and  $T_g$  decreases (i.e. poly methacrylated capric acid C=6). Higher side chain molecular weight (i.e., poly methacrylated palmitic acid C=12) potentially provides greater steric hindrance to backbone rotational motions thereby causing a lesser effect of fatty acid chain length on  $T_g$ .

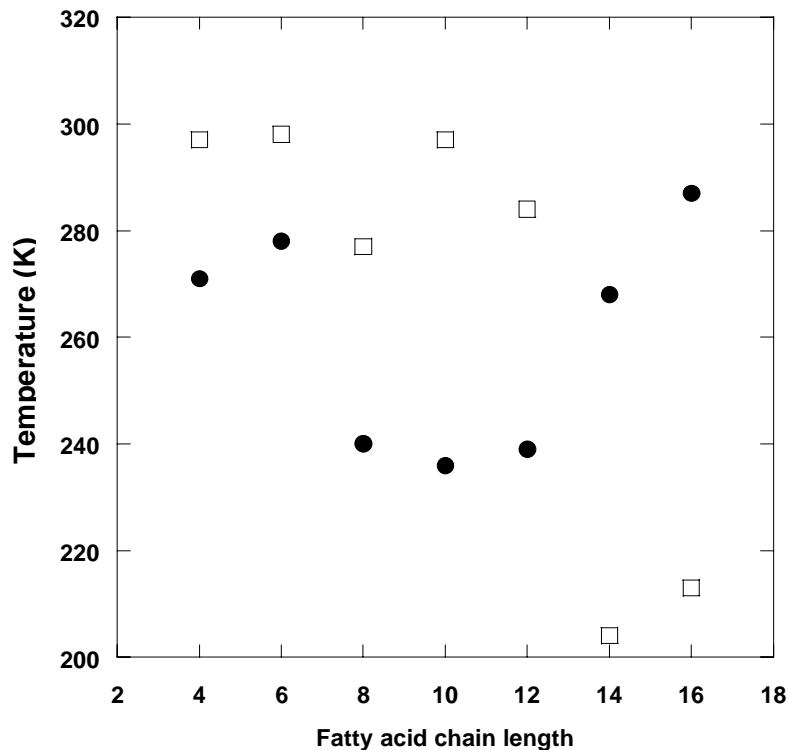


**Figure 98. Major (●) and Minor (□) Glass Transition Temperatures ( $T_g$ ) of the Methacrylated Fatty Acids (MFA)**

The  $T_g$  of the binary blends (VE/MFA) was taken to be the temperature corresponding to the maximum of loss modulus plots (Figure 99). The  $T_g$  versus fatty acid chain length is plotted according to the loss modulus maximum (Figure 100). The results show that  $T_g$  decreased with increasing fatty acid chain length. Furthermore, the effect is much stronger at short fatty acid chain lengths. This trend parallels the behavior observed for MFA homopolymers. The minimum in glass transition temperature suggests that as with the homopolymer, there are opposing mechanisms influencing the mobility of the polymer network. Two factors that can influence the mobility of a polymer network include cross-link density and the molecular mobility of the chains between cross-links. The characteristics that affect the latter have been discussed earlier and include the presence of (1) side groups known to curtail motions because of steric hindrance and (2) specific interactions resulting from polar characteristics of the side groups that also limit rotational motion of the backbone segments by forming non-covalent bonds. With regard to the former, while it can be argued that the molecular weight between cross-links remains the same, the chain length between cross-links (not including side chains) decreases. Yet, the side groups could act as plasticizing agents increasing molecular mobility and reducing  $T_g$ . We suggest that the combination of all of these effects results in the observed monotonic decrease in  $T_g$  with fatty acid chain length.

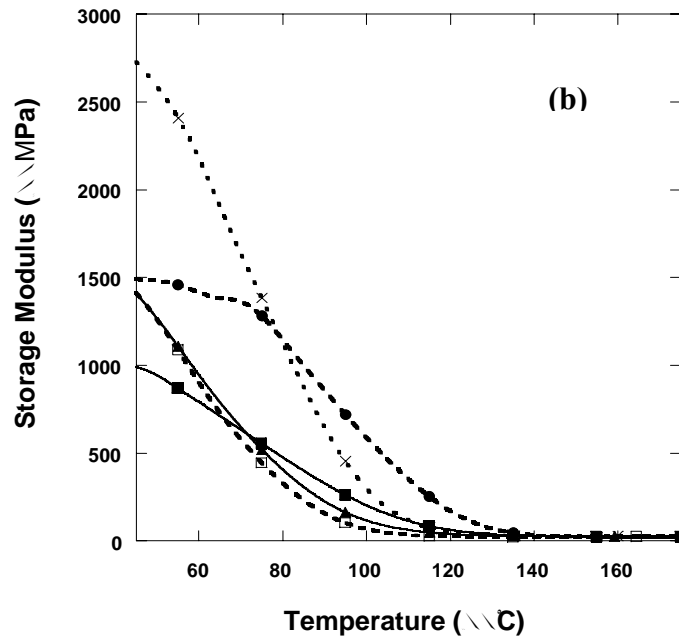
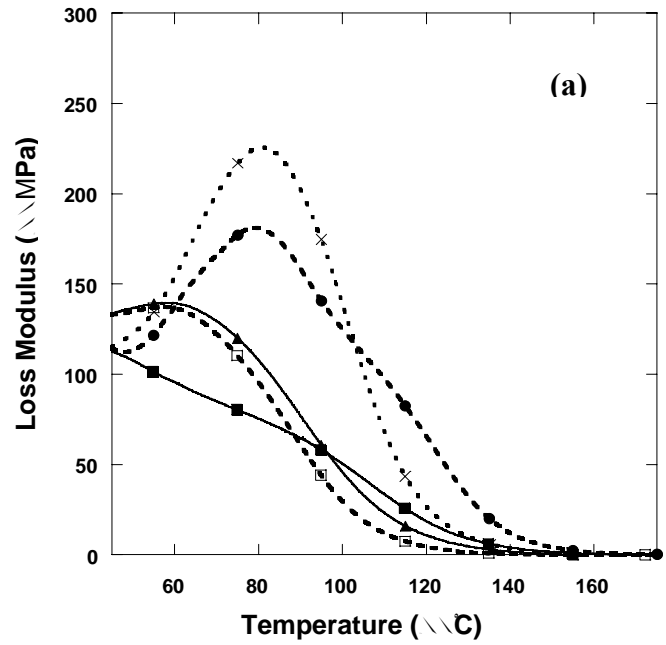
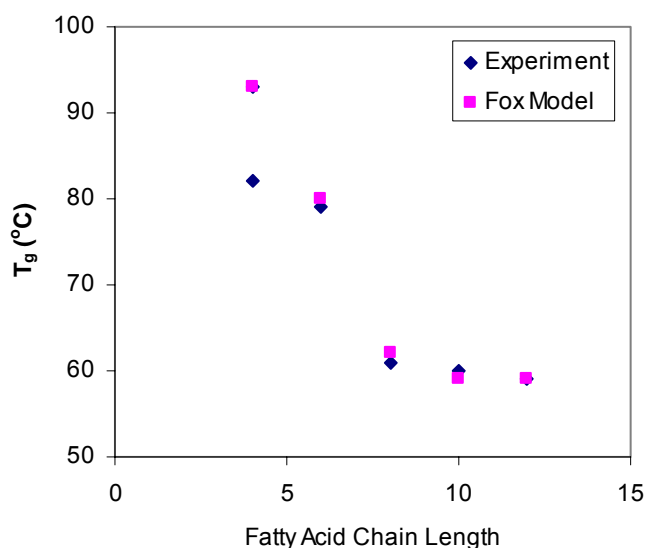


Figure 99. Loss (a) and Storage (b) modulus of 55 wt% VE with 45 wt% MFA. MBut (x), MHex (•), MOct (□), MLau (▲), MMyr(■)



**Figure 100. Glass transition temperature behavior changes with increasing chain length of VE samples with 45 wt% MFA as determined by experiment and as predicted by the Fox Model.**

A number of simple models exist to predict the  $T_g$  of polymer mixtures. The Fox equation [30] uses the mass fractions of the components,  $w_x$ , and the  $T_g$  of the pure components,  $T_{gx}$ , to calculate the glass transition temperature (Eq. 64):

$$T_g = \left( \frac{w_{VE}}{T_{gVE}} + \frac{w_{MLau}}{T_{gMLau}} + \frac{w_{Sty}}{T_{gSty}} \right)^{-1} \quad (64)$$

Figure 100 shows the predicted values of  $T_g$  based on the Fox equation rule of mixture  $T_g = 180^\circ\text{C}$  for vinyl ester (experimentally determined) and the  $T_g$  results for the homopolymers. The comparison between calculated and measured values shows fairly good agreement between the two sets of points.

### *Fracture Properties*

The fracture properties of fatty acid based vinyl esters depends on the structure of the fatty acid monomer. In all cases, methacrylated lauric acid-based resins had the best fracture properties, while methacrylated oleic and linolenic acid-based resins had the worst properties. For example, for resins with 35% reactive diluent, methacrylated lauric acid-based resins have a  $G_{IC}$  of  $148 \text{ J/m}^2 \pm 35 \text{ J/m}^2$ , while methacrylated oleic resins have a  $G_{IC}$  of  $110 \text{ J/m}^2 \pm 15 \text{ J/m}^2$ . Fracture theories show that fracture properties decrease as the content of defects in the polymer network increase [52]. Because of the lower extents of cure of VE resins using oleic and linoleic acid monomers, there is a greater concentration of defects, which cause the fracture properties to be low. The fracture properties of fatty acid VE resins were greater than that of styrene-based VE resins ( $G_{IC} = 85 \text{ J/m}^2 \pm 35 \text{ J/m}^2$ ). The reason for this has to do with the fact that vinyl ester monomers react to a fairly low extent (i.e. 70%) with styrene as the reactive diluent relative to when fatty acid monomers are used (i.e. 85%). Thus, there will be fewer defects, such as

dangling chain ends, in fatty acid resins. Furthermore, the larger content of free monomer in fatty acid resins will act as a plasticizer and toughen the polymer.

*Effect of Fatty Acid Type and Content*

Table 32 shows the viscosities and mechanical properties of all the VE/MFA/Styrene ternary blends prepared in this study. The properties of the commercial VE resin Derakane 411-350 are also listed for comparison. Overall, the flexural properties were low for every sample, including the Derakane 411-350 sample. It is likely there was an issue with the load cell or displacement measurement, which caused a systematic error in the flexural properties. Ignoring this systematic error, interesting trends are visible in the data. As can be seen at the same VE and styrene content, the flexural modulus decreased slightly and the flexural strength increased slightly with increasing fatty acid chain length of the MFA monomers. The decrease in the flexural modulus with increasing fatty acid chain length is expected since the plasticization effect of the fatty acids should increase with increasing carbon number of the fatty acids. The fracture toughness values of the ternary blends of VE with increasing chain length are shown in Figure 101. The fracture toughness was not significantly affected by fatty acid chain length. The  $T_g$ s of the polymers also decreased with fatty acid chain length due as can be seen in Table 32. The longer fatty acid chains increase free volume and reduce  $T_g$ .

**Table 32. The viscosities and mechanical properties of the VE/MFA/Styrene ternary blends**

Resins	Flexural Strength (MPa)	Flexural Modulus (GPa)	Viscosity (Cp)	$T_g$ ( $^{\circ}$ C)	Fracture Toughness ( $G_{IC}$ )( $J/m^2$ )
55%VE / 25%Mlau / 20%Sty	68.3±0.5	2.3±0.3	230	105.0	148±31
65%VE / 15%Mlau / 20%Sty	71.0±0.5	2.8±0.6	334	131.0	308±15
55%VE / 35%Mcap / 10%Sty	45.0±7.6	1.8±0.1	426	93.5	317±110
55%VE / 30%Mcap / 15%Sty	65.0±0.4	2.1±0.1	264	101.0	320±23
55%VE / 25%Mcap / 20%Sty	50.3±0.5	2.8±0.07	190	110.5	332±120
65%VE / 15%Mcap / 20%Sty	83.4±7.6	2.1±0.3	206	145.0	245±44
65%VE / 20%Mcap / 15%Sty	87.0±6.9	2.6±0.1	290	133.6	267±99
55%VE / 35%MBut / 10%Sty	36.0±0.6	2.8±0.4	468	103.5	129±27
55%VE / 30%MBut / 15%Sty	39.0±0.2	2.7±0.3	288	112.0	153±16
55%VE / 25%MBut / 20%Sty	41.0±14.5	2.8±0.1	172	122.0	207±18
55%VE / 25%MOct / 20%Sty	58.0±11.7	2.4±0.07	194	105.0	270±110
Derakane 411-350	71.7±15.2	2.6±0.2	360	120.0	262±88

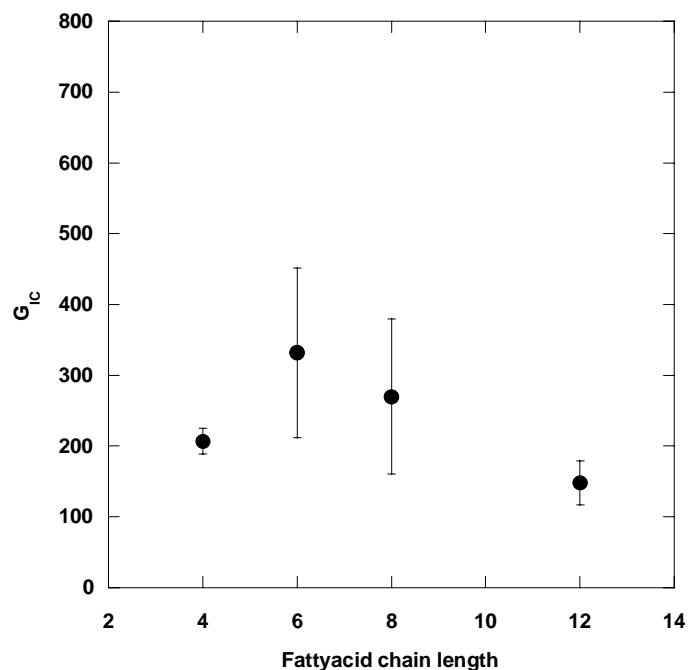


**Figure 101. The fracture toughness of the 55%VE/25% MFA/20% Styrene ternary blends at increasing fatty acid chain lengths.**

The flexural modulus and strength increased slightly or were not influenced significantly by increasing styrene content of the resins. However, fracture toughness went through a maximum with increasing styrene content (Figure 102). The replacement of the aliphatic fatty acid methacrylate comonomer with the aromatic rigid styrene monomer is expected to plasticize the polymer and thereby increase the toughness. The maximum in  $T_g$  occurred because of the high extent of cure that occurs in the ternary blends relative to the binary blends. The  $T_g$ s of these polymers also increased with increasing styrene content of the resins. This is expected because the  $T_g$  of polystyrene is considerably higher than  $T_g$  of any of the MFA homopolymers made in this work.

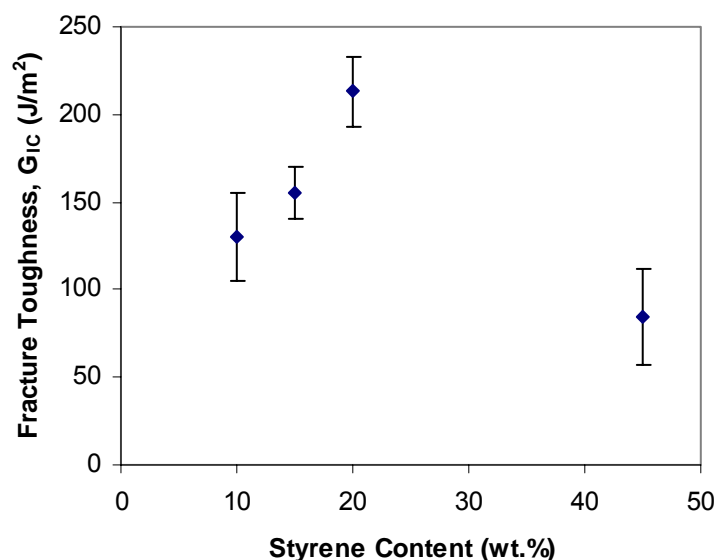


**Figure 102. The fracture toughness of VE/MBut/Styrene ternary blends containing 55% VE as a function of styrene content.**

As can be seen the overall properties of all the VE/MFA/Styrene blends are in a comparable range with those of the commercial VE resin Derakane 411-350. Among all the ternary blends, the VE/MLau/Styrene 65/15/20 and VE/MHex/Styrene 65/20/15 exhibit equal or improved mechanical properties compared to the commercial VE resin Derakane 411-350, with processable viscosities in liquid form. In addition these fatty acid based systems contain only 15-20 wt% styrene, decreasing the VOC emissions from these resins significantly. Thus, MLau and MHex based VE resins show a great potential to replace the current commercial VE resins.

#### 3.2.4.3.12 E-Beam of Fatty acid-Based Vinyl Esters

Electron beam (E-beam) cure has numerous advantages over thermal cure of composite structures [53]. E-beam is a fast curing technique, where typically the resin is irradiated for only a few minutes. Therefore, E-beam can substantially reduce VOC emissions can be substantial for a volatile resin. On the other hand, E-beam cure is ideally suited for a non-volatile resin, such as fatty acid-based vinyl ester resins.

Vinyl esters containing 35 wt.% and 45 wt.% MLau, MSA, and MOA were prepared. No initiator is required for E-beam cured. The resins were poured into 4 mm deep cylindrical molds with a 1.5 inch diameter. The resins were then E-beam irradiated with a dosage of 3.5 MRad followed by an immediate post-cure at 85°C.

The E-beam polymers were analyzed using near-FTIR to measure the extent of cure. The height of the vinyl peak (6160 cm<sup>-1</sup>) relative to the 5790 cm<sup>-1</sup> peak of the initial uncured resin compared to the E-beamed polymer was used to measure the conversion. Figure 103 shows that the extent of cures of all E-beam MFA resins are very high (>95%) relative to thermally cured resins

(~80%). In addition, post-cure was unnecessary because it did not increase the conversion significantly (Figure 104).

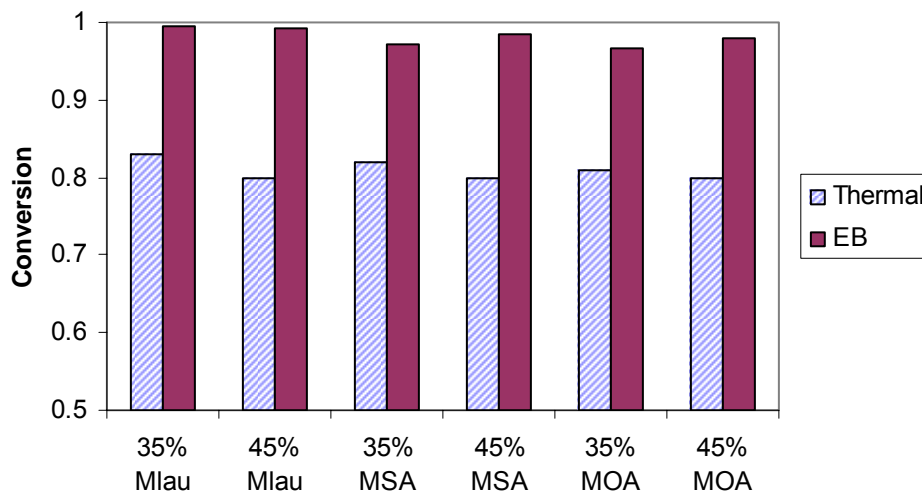


**Figure 103. The extent of cure of fatty acid-based vinyl esters, comparing thermal cure to E-beam.**

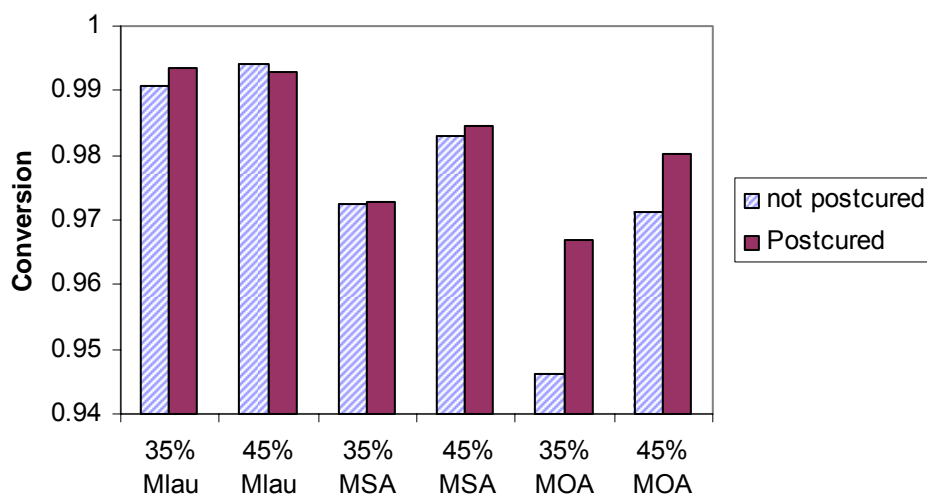


**Figure 104. The effect of post-cure on the conversion of E-beam cured VE/MFA polymers.**

The polymer properties were analyzed using DMA and compared to thermal cure results. First of all, the DMA properties were similar for multiple temperature sweeps because post-cure did not increase the conversion. Secondly, it is apparent that E-beam significantly improved the polymer properties (Figure 105) relative to thermal cure. The storage modulus increased from a maximum of 1.9 GPa to 2.2 GPa, which is a 16% increase. In addition,  $T_g$  increased from 90°C to 105°C. Furthermore, fatty acid monomer molecular structure has no significant effect on polymer properties as it did for thermal cure. Overall, E-beam cure produces polymers with superior thermo-mechanical properties relative to thermal cure because of improved monomer conversion. In the future, the E-beam dosage and other conditions will be adjusted to maximize

the performance of fatty acid-based VE resins. In addition, E-beam will be used to cure ternary blends of VE, MFA, and styrene in an effort to further improve properties and reduce VOC emissions.

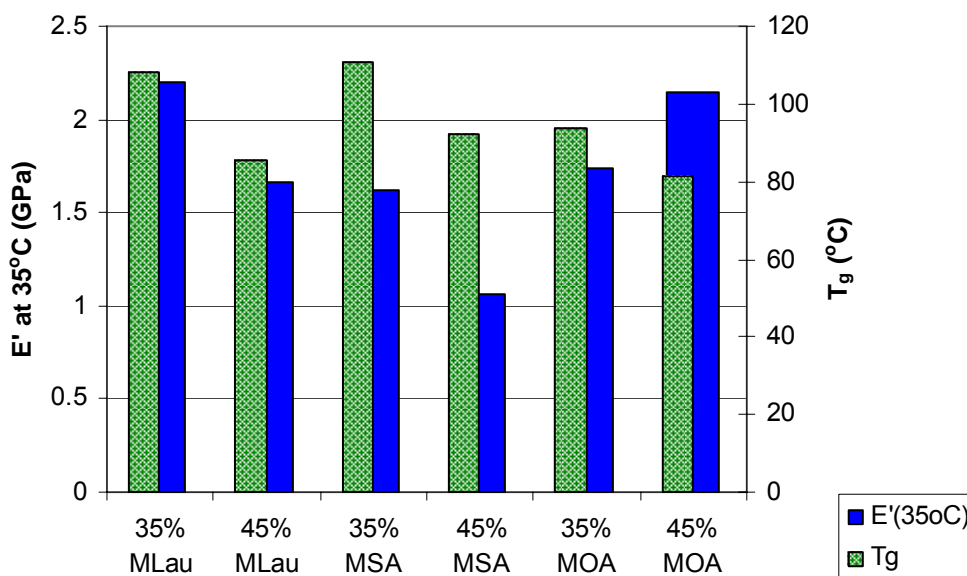


**Figure 105.** The storage modulus and T<sub>g</sub> of fatty acid-based vinyl esters cured thermally and via E-beam.

#### 3.2.4.3.13 VE/MFA/Styrene Blends

The properties of VE resins using MFA were fairly low and the viscosities were fairly high. To improve these properties, blends of MFA and styrene were used as the reactive diluent in VE 828.

#### Viscosity

The viscosity of VE/MFA/styrene was measured at 30°C and was found to decrease exponentially with styrene content for resins containing 55 wt% and 65 wt% VE 828 resin (Figure 106). Styrene contents of 10% or greater reduced the viscosity of VE resins to the acceptable range (< 500 cP). Therefore, only low styrene contents are necessary, from a viscosity view-point.

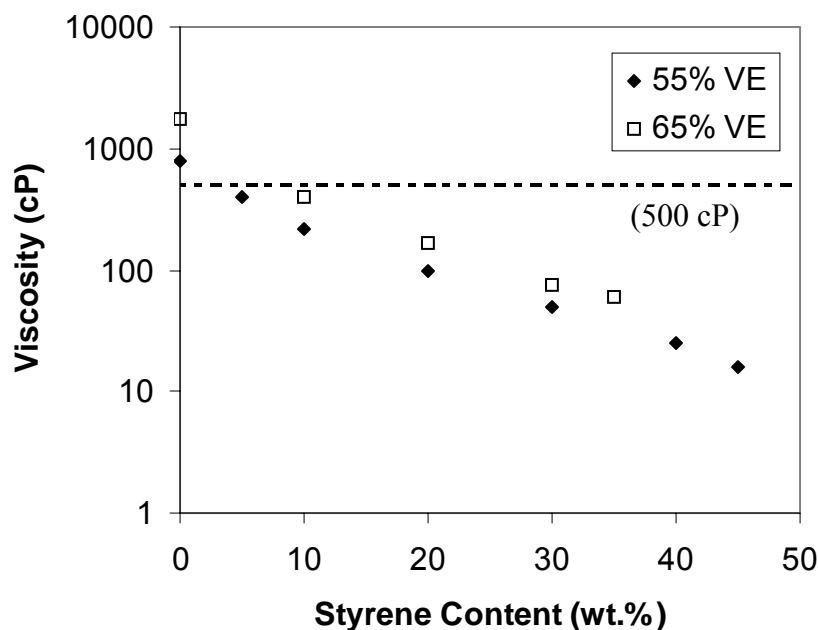


**Figure 106.** The viscosity of VE/MLau/styrene as a function of styrene content in the resin for resins containing 55 wt% and 65 wt% VE 828.

Viscosity experiments were conducted for VE/MFA/styrene at 24°C using a Brookfield viscometer as previously described. For this study, the weight fraction of VE was held constant at 55% and the ratio of MFA to styrene was varied for the remaining 45%. This was done for MFAs derived from butyric acid, caprylic acid, and lauric acid. The results are given in Figure 107. For all three MFAs, viscosity was found to decrease exponentially with increasing styrene content. At higher styrene content (>20%), the influence of fatty acid molecular weight was not significant. For styrene content less than 10%, the influence of fatty acid molecular weight on viscosity was more pronounced as higher molecular weight MFAs comport significantly higher values of viscosity. It is apparent that a great number of compositions fall below the 500 cPs desired value for liquid molding applications. From the data it is estimated that 12 wt% styrene is needed to obtain a 500 cps resin using methacrylated lauric acid while only 7% styrene is needed to obtain the same viscosity using methacrylated butyric acid. Thus from a viscosity point of view acceptable formulations with as little as 7 wt% styrene are possible.

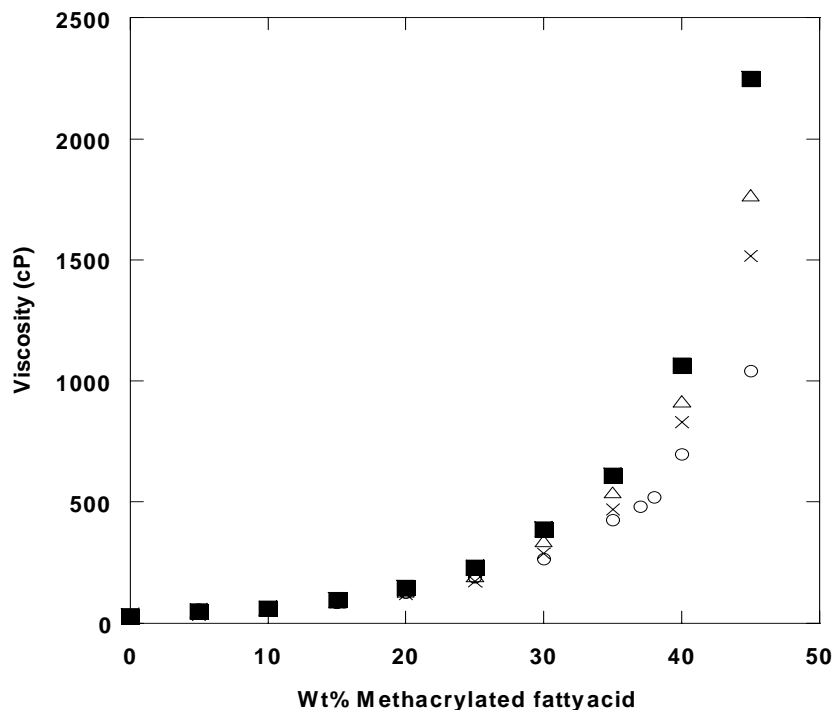


**Figure 107. Viscosity of methacrylated butyric acid (×), methacrylated caproic acid (○), methacrylated caprylic acid (Δ), methacrylated lauric acid (■) changes with increasing styrene content from 0 weight % to 45 weight % and 55 weight % vinyl ester monomer, at 24°C**

#### *Cure Kinetics*

Ternary blends of VE, MFA, and styrene have cure rates and extents of cure that are higher than both VE/MFA and VE/styrene alone (Figure 108). The lower  $T_g$  of the fatty acid zones allows for greater mobility of styrene in the polymer, enabling it to almost completely react into the polymer network, allowing for a high extent of cure. The greater cure rate for the ternary blend is a result of a lower vitrification temperature than VE/styrene along with higher monomer mobility than VE/MFA.

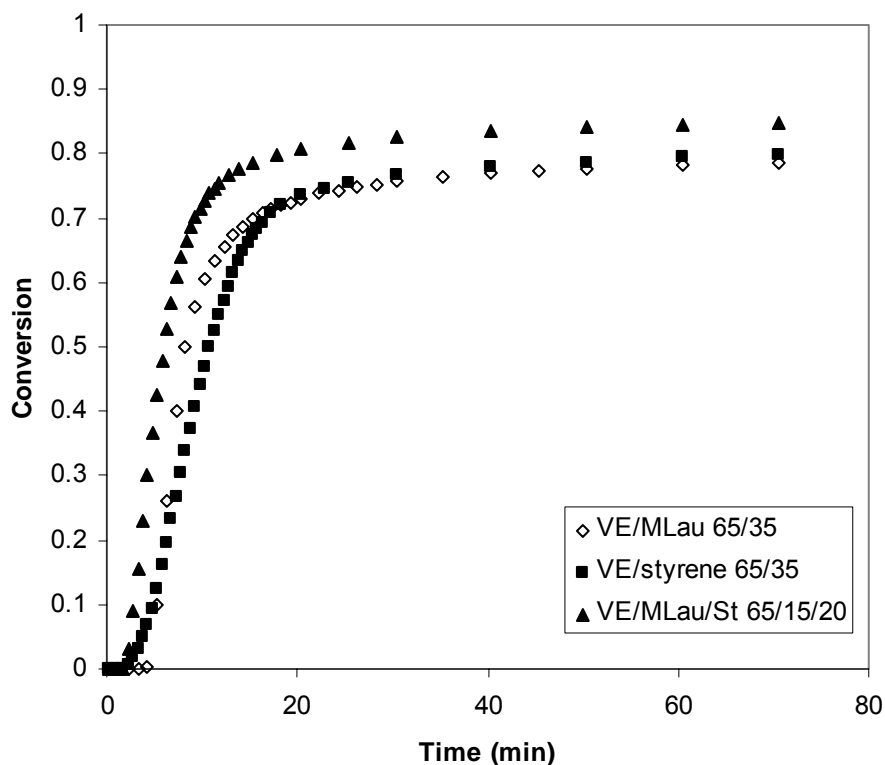


**Figure 108.** The conversion as a function of time for the cure of VE/MLau/Styrene 65/15/20 relative to VE/MLau 65/35 and VE/styrene 65/35. Samples were cured at 90°C.

*Dynamic Mechanical Properties*

The DMA character of these resins improved as the styrene content increased (Figure 109). Figure 110 and Figure 111 show that both the modulus and  $T_g$  improved with increasing styrene content. These results show that 15% styrene is sufficient to obtain an acceptable modulus and  $T_g$ . Furthermore, at this styrene content, the resin viscosity is well within the acceptable window. When DMA is run at 2°C/min ramp rates, the measured  $T_g$  values were at least 5°C lower than for a ramp rate of 5°C/min.

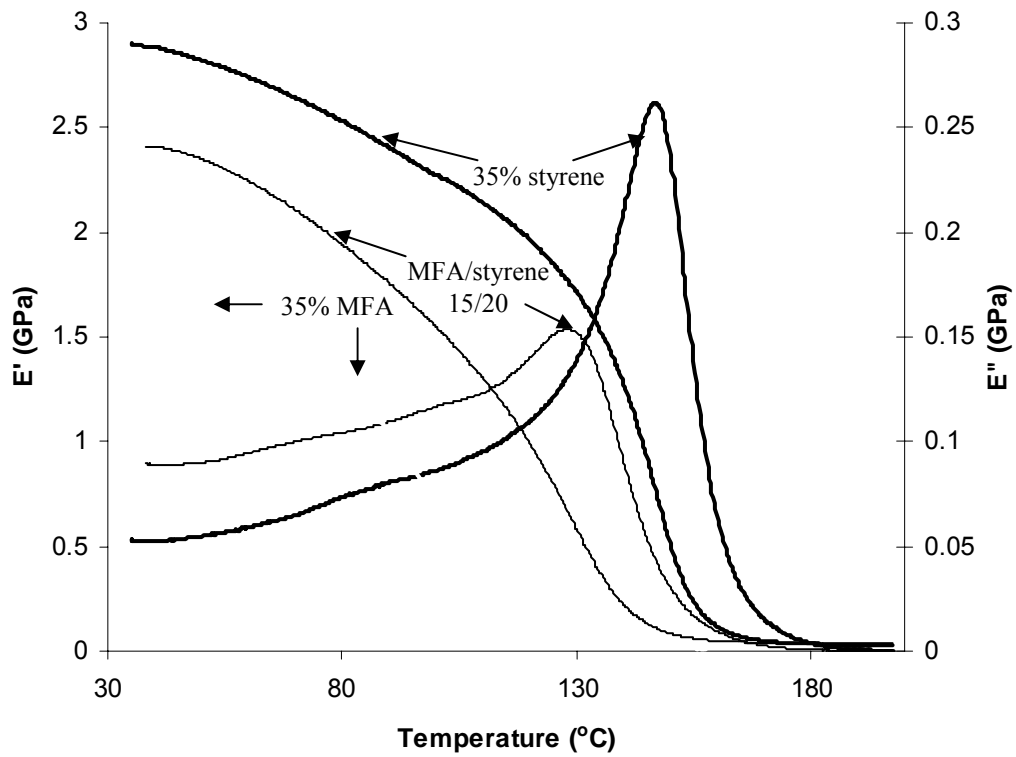


Figure 109. DMA behavior of VE/MOA/styrene with 65 wt% VE 828.

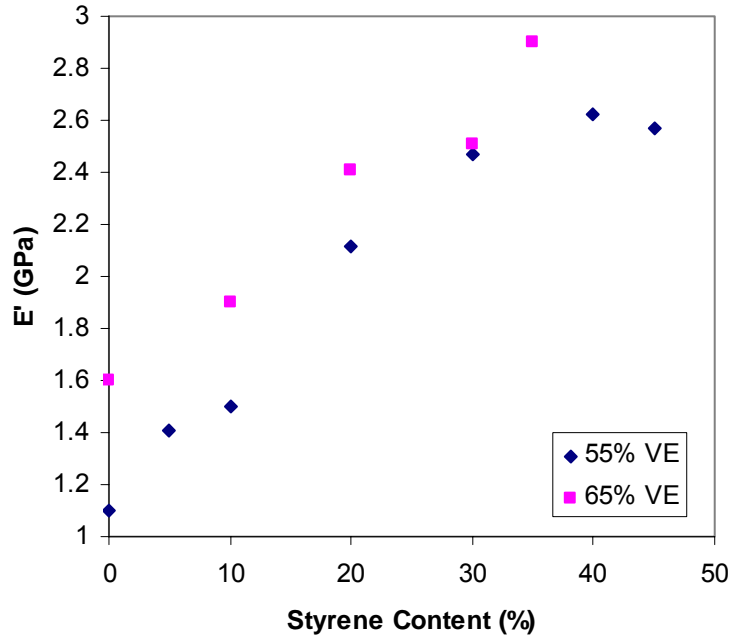
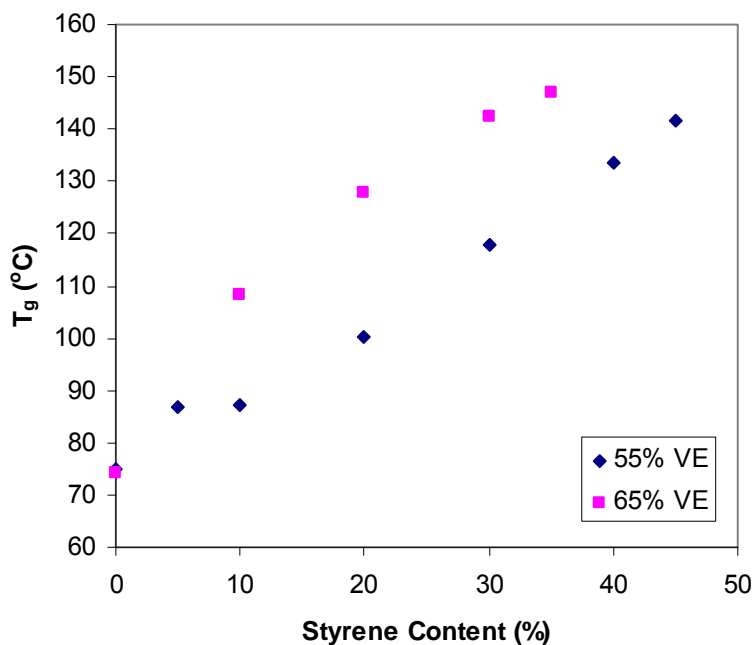


Figure 110. The storage modulus as a function of styrene content for VE/MOA/styrene blends.



**Figure 111.**  $T_g$  as a function of styrene content for VE/MOA/styrene blends.

Another interesting aspect of these polymers, which will be pursued more in the near future, is that VE/MFA/styrene blends cured in open molds with a perfectly hard finish. There was no uncured layer that typically forms due to oxygen inhibition. A possible reason for this is that the high hydrocarbon content of the resin formed a waxy layer at the surface. However, unlike waxes, these hydrocarbons were functionalized enabling them to react into the polymer network. This indicates that hydrocarbon monomers may segregate to the surface and could potentially reduce styrene emissions. Further work must be done to validate this hypothesis. Regardless, these materials do not need to be polished to form a good and useable surface. The financial, production, and environmental implications of this result are enormous and warrant further investigation.

To determine if  $T_g$  of these blends of VE, MFA, and styrene can be predicted using the Fox equation,  $T_g$  of the pure components were measured.  $T_g$  of pure styrene is well known to be 100°C. Pure VE 828 was cured using 0.5 wt% trigonox and found to have a  $T_g$  of 180°C. Pure MLau was also polymerized and found to have a  $T_g$  of -30°C. Resins with various contents of VE, MLau, and styrene were prepared and cured, and their  $T_g$ s were measured using DMA. Figure 112 shows that the experimentally measured  $T_g$  at 2°C/min ramp rates very closely matched the predictions from the Fox equation. Therefore, the Fox equation can be used to predict  $T_g$  of these binary and ternary blends of monomers. Furthermore, because  $T_g$  of MLau is so low, the Fox equation shows that improved overall  $T_g$  can be best achieved by increasing  $T_g$  of the fatty acid component. A simple way to do this would be to use shorter chain fatty acids, such as hexanoic acid instead of lauric acid.

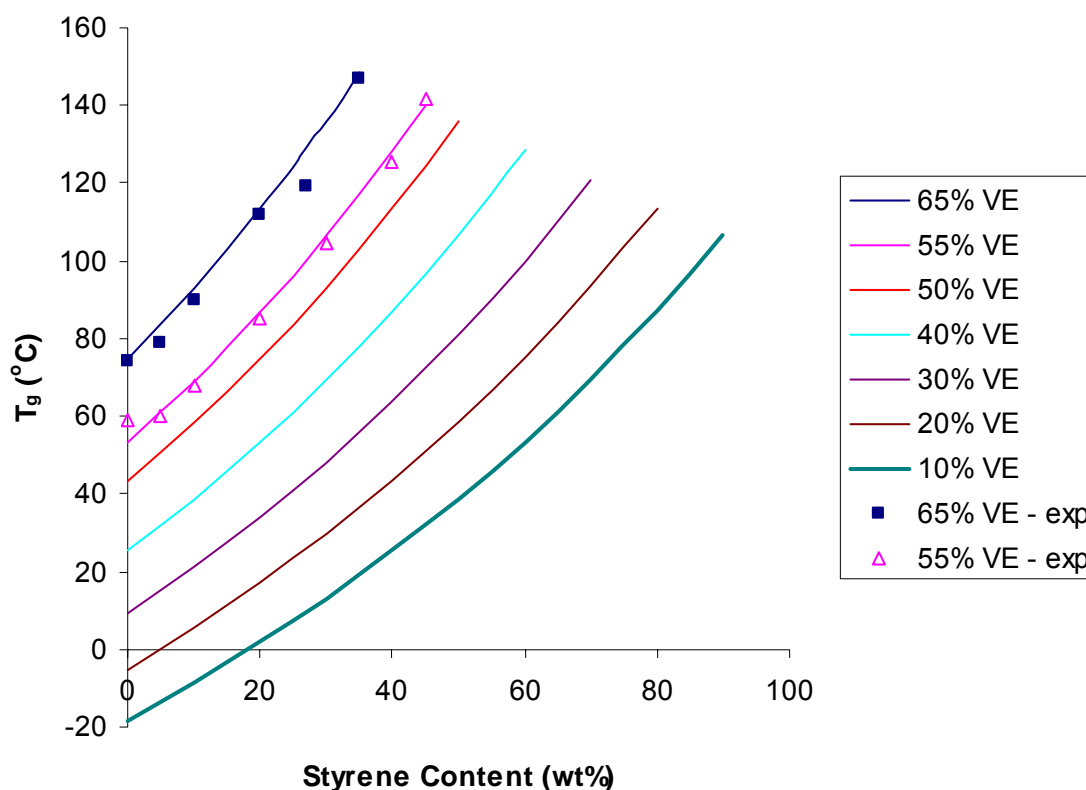


**Figure 112.** The Fox equation can be used to predict  $T_g$  of blends of VE, MLau, and styrene.

Figure 113 and Figure 114 contain the loss modulus traces respectively for the entire series of ternary blends made using methacrylated butyric acid and methacrylated lauric acid. In this series, vinyl ester content was fixed at 55 wt.% and the ratio of MFA to styrene was varied. The room temperature moduli of all of these materials were close to 3.0 GPa. This value is representative also of commercial vinyl ester resins. The loss modulus behavior of the methacrylated butyric acid system is interesting in that only one peak was evident when styrene and methacrylated butyric acid were not mixed (i.e., 45 wt.% styrene and 45 wt.% methacrylated butyric acid) or when low concentrations of styrene are used. However, when the weight fractions of methacrylated butyric acid and styrene were more closely matched, two peaks were observed, suggesting the formation of distinct domains with micron scale dimensions.

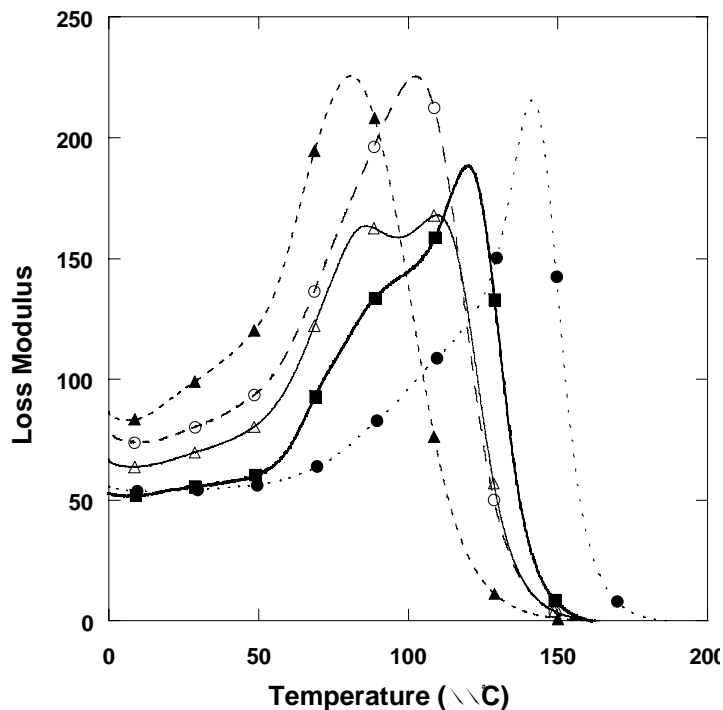


**Figure 113.** Loss modulus (MPa) behavior of 55 weight% VE and 45 weight% of methacrylated butyric acid and styrene combination. 45 wt% MBut (▲), 35 wt% MBut & 10 wt% Styrene (○), 30 wt% MBut 15 wt% Styrene (Δ), 25 wt% MBut & 20 wt% Styrene (■), 45 wt% Styrene (●).

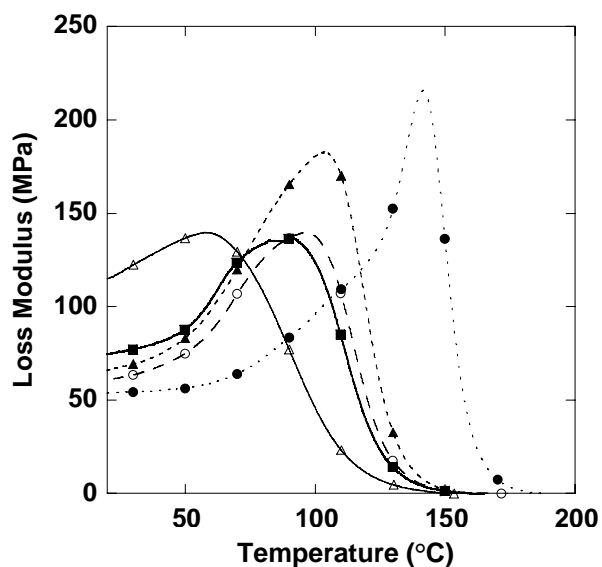


**Figure 114.** Loss modulus (MPa) behavior of 55 weight% VE and 45 weight% of methacrylated lauric acid and styrene combination. 45 wt% MLau (Δ), 35 wt% MLau & 10 wt% Styrene (■), 30 wt% MLau 15 wt% Styrene (○), 25 wt% MLau & 20 wt% Styrene (▲), 45 wt% Styrene (●).

Figure 114 shows the loss modulus traces for the entire series of ternary blends made using methacrylated lauric acid. The impact of increasing MFA content in these systems was more pronounced as shown by a very significant drop in modulus with increasing methacrylated lauric acid content. On the other hand, the loss modulus curves for the entire set of compositions exhibited only one peak. The breadth of this peak decreased with increasing styrene content. Overall, this behavior suggests that methacrylated lauric acid was more compatible with styrene during polymerization compared to methacrylated butyric acid.

Figure 115 shows the loss modulus behavior of methacrylated caproic acid for the entire series of ternary blends. Again, the loss modulus curves for the entire set of compositions exhibited only one peak, suggesting that no phase separation occurred in this system.

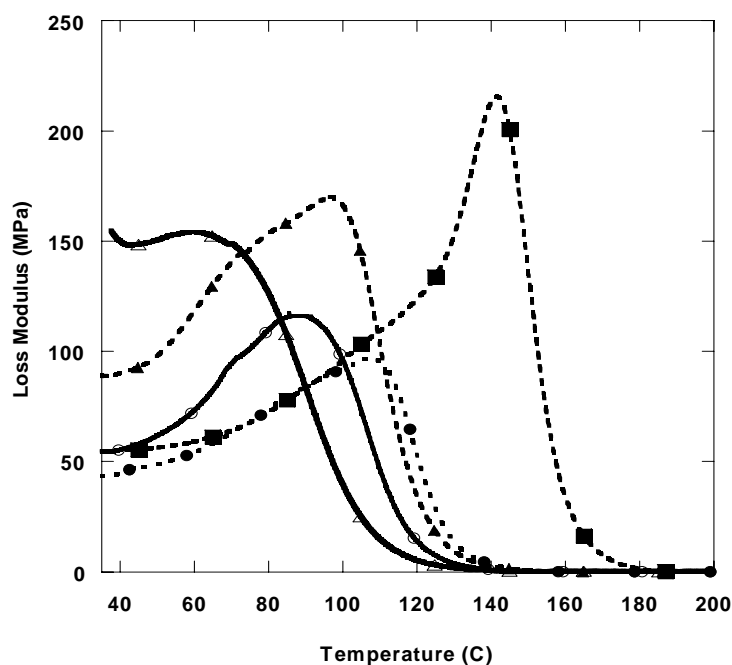


**Figure 115. Loss modulus (MPa) behavior of 55 weight% VE and 45 weight% of methacrylated caproic acid and styrene combination. 45 wt% MHex ( $\Delta$ ), 35 wt% MHex & 10 wt% Styrene ( $\blacktriangle$ ), 30 wt% MHex 15 wt% Styrene ( $\circ$ ), 25 wt% MHex & 20 wt% Styrene ( $\bullet$ ), 45 wt% Styrene ( $\blacksquare$ )**

By defining  $T_g$  as the temperature at which the loss modulus passes through a maximum, and for the cases where multiple peaks existed selecting the one associated with the greatest drop in storage modulus, plots of  $T_g$  versus composition for ternary blend systems were obtained. Figure 116 shows these plots for VE/MFA/Styrene ternary blends produced with four MFAs: methacrylated butyric acid C=4, methacrylated caproic acid C=6, methacrylated octanoic acid C=8, and methacrylated lauric acid C=12. Clearly systems based on butyric acid possessed significantly higher  $T_g$ . Interestingly, a series of experiments conducted using methacrylated octanoic acid was run, which possessed a significantly lower molecular weight than lauric acid but whose corresponding homopolymer had the same  $T_g$  as that of methacrylated lauric acid. As a consequence the  $T_g$  values for polymers prepared from ternary blends based on methacrylated lauric acid were virtually identical to those prepared with methacrylated octanoic acid.

Methacrylated caproic acid ternary blends systems  $T_g$  was higher than MLau and MOct but lower than MBut ternary blends system, but did not have the odd behavior of two loss modulus peaks like MBut ternary blends.

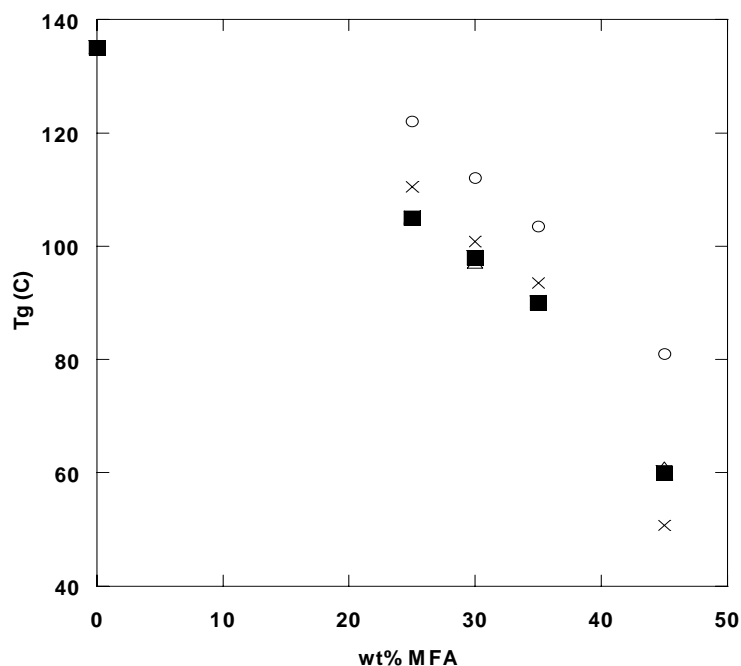


**Figure 116.** Glass transition temperature ( $T_g$ ) of 55 weight% vinyl ester and 45 weight% of acids with styrene. MBut ternary blends (○), MHex ternary blends (×), MOct ternary blends (Δ), MLau ternary blends (■).

#### *Flexural Properties*

The flexural properties of fatty acid-based vinyl esters increased with styrene content (Figure 117). The modulus increased because styrene is more rigid in nature than the fatty acid monomers. The strain and flexural strength increased because the connectivity of the network (degree of cure) increased as styrene was introduced into the network. Although the degree of cure of ternary blends were found to be higher than that of VE/styrene, the flexural strength and max strain may be increasing due to changes in morphology and phase separation behavior.

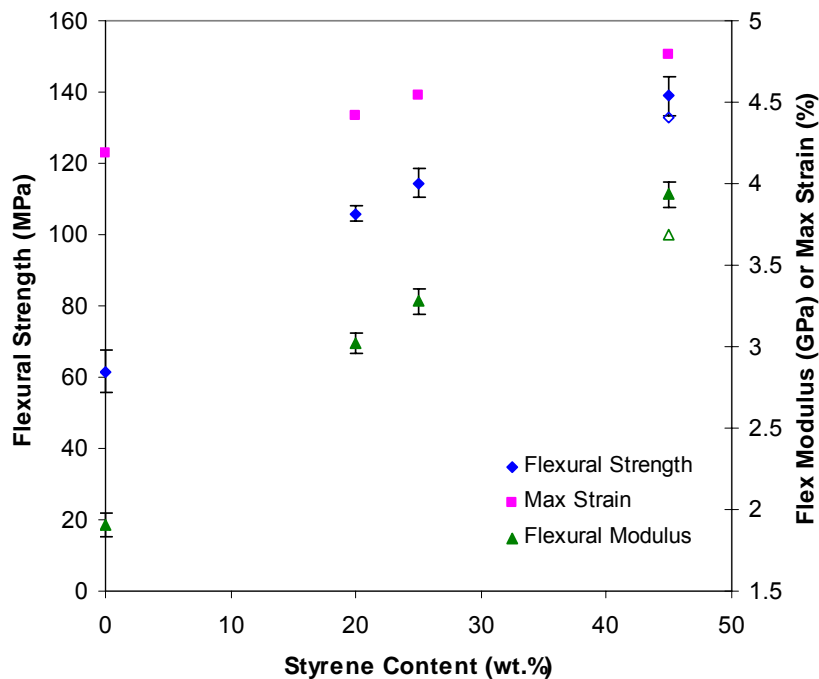


**Figure 117.** The flexural properties as a function of styrene content for resins containing 55% VE and using MLau and styrene as the reactive diluent. The open points show the results for Derakane 411-350.

Ternary blends of VE, styrene, and fatty acid monomers produce polymers with better fracture properties than their binary counterparts, as shown in Figure 118. This occurs because of a combination of fewer defects and high modulus. The fatty acids allow for high vinyl ester monomer conversion, while the styrene causes a high overall conversion, resulting in a lower content of dangling chain ends relative to the binary blends. Fracture theories, such as vector percolation, show that fracture properties increase with increasing modulus if the connectivity of the polymer is unaffected [52]. As shown previously, increasing the styrene content increases the rigidity of the ternary blends, therefore causing an increase the fracture properties.

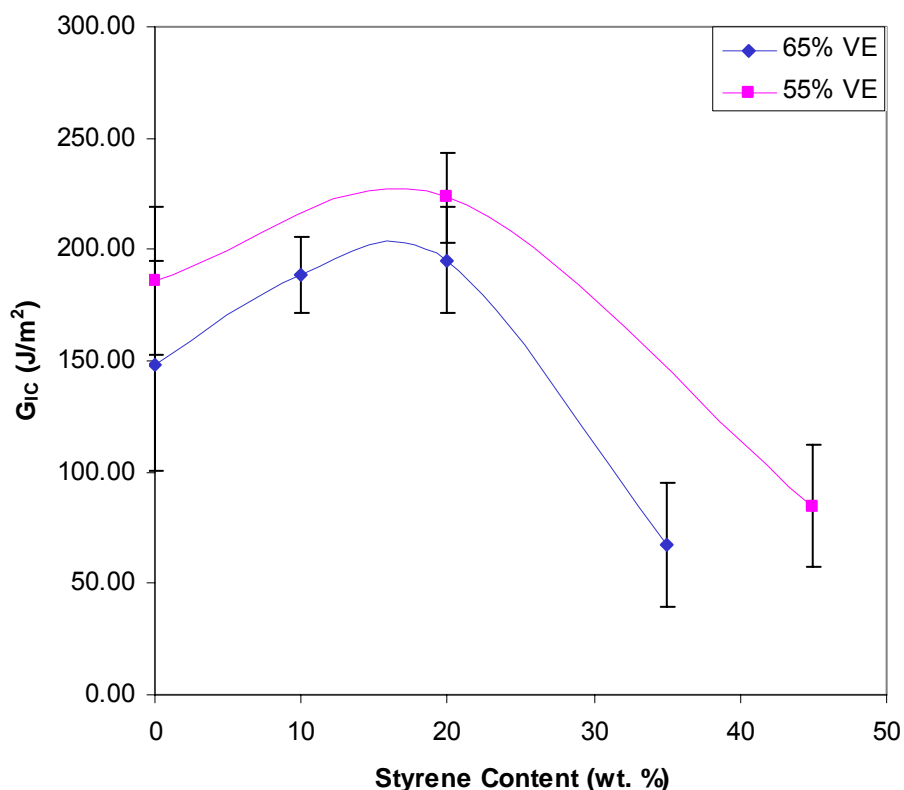


**Figure 118.**  $G_{IC}$  of VE/MLau/styrene as a function of styrene content in the resin for resins containing 55 wt% and 65 wt% VE 828.

#### 3.2.4.3.14 VE 828 MOA- Br-MSA Styrene Polymer Properties

The VE resins containing Di-Br-MSA polymers were cured at room temperature in the presence of 1.5 wt.% Trigonox 239A and 0.375 wt.% Cobalt naphthanate. The resins containing 35 wt.% Di-Br-MSA did not cure completely in 24 hrs at room temperature. This was attributed to the presence of hydroquinone used in the preparation of the Di-Br-MSA and to the presence of bromine functional groups which may further inhibit the polymerization. Thus, this resin was post-cured at 120°C for two hours and 160°C for two hours. No phase separation was observed in any of the formulations. The polymers obtained had a green color caused by the AMC-2 catalyst used in the methacrylation reaction. The polymers containing the Di-Br-MSA and the blends of Di-Br-MSA with MOA had a distinct brown-green color caused by the presence of Bromine.

Dynamic mechanical analysis was used to determine the thermo-mechanical properties of the polymers. Table 33 lists the storage modulus values  $E'(30^\circ\text{C})$  and the glass transition temperatures ( $T_g$ s) as determined by the peak in the loss modulus and tan delta curves for the post-cured samples (DMA 2<sup>nd</sup> run). For samples which did not have a distinct peak in the loss modulus curve, the peak in the Tan delta curve was taken as  $T_g$ . The post-cured samples exhibited significantly higher modulus and  $T_g$  values than the room temperature cured samples. As can be seen in Table 33, the 35 wt.% Di-Br-MSA polymer exhibited the lowest modulus and

$T_g$  values. The 45 wt.% Di-Br-MSA polymer exhibited significantly higher modulus and  $T_g$  values than that of the 35 wt.% Br-MSA polymer which can be attributed to incomplete solubilization of the VE in the Br-MSA monomer at this concentration. At 45 wt.% comonomer content, Br-MSA and the MOA VE 828 polymers had similar  $T_g$  and modulus values. The modulus and  $T_g$  of the polymers decreased as styrene was replaced with the Di-BrMSA comonomer. This result is expected because the replacement of the rigid aromatic structure of styrene by the flexible long alkyl chains of the fatty acid based monomers has a plasticizing effect that reduces both the modulus and  $T_g$  of the network [54]. However, as can be seen in Table 33, the red highlighted formulations containing mixtures of the Br-MSA monomer with styrene and the MOA monomer exhibited room temperature modulus values higher than 2 GPa and  $T_g$  values higher than 100°C, with processable viscosities at room temperature, as shown in Table 32. Commercial fire resistant VE resin formulations containing brominated DGEBA (Figure 119) generally contain around 5-10 wt.% Bromine based on total resin weight for 35-45 wt.% styrene contents.

**Table 33. The storage modulus values  $E'(30^\circ\text{C})$  and the  $T_g$ s of the post cured VE 828 resins.**

Br-MSA wt.%	MOA wt.%	Styrene wt.%	VE828 wt.%	$E'(30^\circ\text{C})$ wt.%	$T_g(^\circ\text{C})$ ( $E''$ max)	$T_g(^\circ\text{C})$ (Tan delta max)
20	25	0	55	1.02	-	100.1
<b>20</b>	<b>0</b>	<b>25</b>	<b>55</b>	<b>2.73</b>	<b>104.3</b>	<b>121.5</b>
10	15	20	55	2.11	96	117.26
<b>10</b>	<b>10</b>	<b>15</b>	<b>65</b>	<b>2.32</b>	<b>108.5</b>	<b>129.3</b>
<b>15</b>	<b>0</b>	<b>20</b>	<b>65</b>	<b>2.40</b>	<b>114</b>	<b>132.1</b>
20	0	15	65	2.53	99.3	123.3
35	0	0	65	0.53	-	82.2
0	35	0	65	1.72	-	126.1
0	0	35	65	3.18	144	153.3
45	0	0	55	1.30	-	111
0	45	0	55	1.34	-	112.6
0	0	45	55	2.42	140.7	151.7

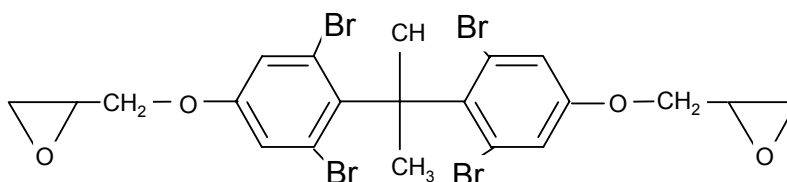


**Figure 119. The chemical structure of ortho-tetra bromo-diglycidyl ether of Bisphenol A (DGEBA).**

The resins containing 20wt% Di-Br-MSA, which contain about 5.5 wt.% Bromine based on total resin weight, show promise as an alternative to commercially available brominated vinyl ester resins. This resin with 5.5 wt.% Bromine content, had a viscosity that was in the processable range and polymer properties that were comparable to those of standard VE resins. This formulation is as a promising alternative to present fire resistant VE resins. The Bromine content of resins with lower Br-MSA content can be increased by using partially brominated VE 828 in the formulation. Further mechanical property analysis and fire tests (e.g. cone calorimetry and oxygen index) to determine the fire resistance potential of the resins with, ideal formulations would need to be performed to fully evaluate these formulations as alternatives to commercially brominated systems.

#### *3.2.4.3.15 Morphology of Fatty Acid-Based Vinyl Esters*

DMA and FTIR cure kinetics results indicate that the morphology of fatty acid-based vinyl esters is significantly different from that of styrene-based vinyl esters. In addition, the morphology of the polymers depends on the type of fatty acid used and the type of vinyl ester monomers used. This section aims to explain why these differences occur and how they impact polymer performance.

#### *Dynamic Mechanical Analysis*

Peaks in the loss modulus of a homogeneous material represent the glass transition temperature,  $\beta$  transitions,  $\gamma$  transition, in order of decreasing temperature. Non-homogeneous samples can have multiple transitions of all three types. Being that  $\beta$  and  $\gamma$  transitions typically occur at temperature far below room temperature, any transitions that occur at room temperature and above represent glass transitions of the entire material of phase separated domains. Figure 120 shows that the glass transitions for MLin and MLau-based vinyl esters are considerably broader and less defined than styrene-based vinyl ester. The maximum in the loss modulus occurs at higher temperatures for the styrene sample because of its higher  $T_g$ . More interestingly, there are two glass transitions for all ternary blends of VE, MLin, and styrene, while most VE, MLau, styrene resins do not have two glass transitions (Figure 121). In fact, other fatty acids tested, such as methacrylated hexanoic acid, MSA, and MOA behave similarly to MLau. The loss modulus peak for the VE/MLau/Styrene occurred at a slightly lower temperature than one of the VE/MLin/Styrene peaks, but at a higher temperature than the other VE/MLin/Styrene peak.

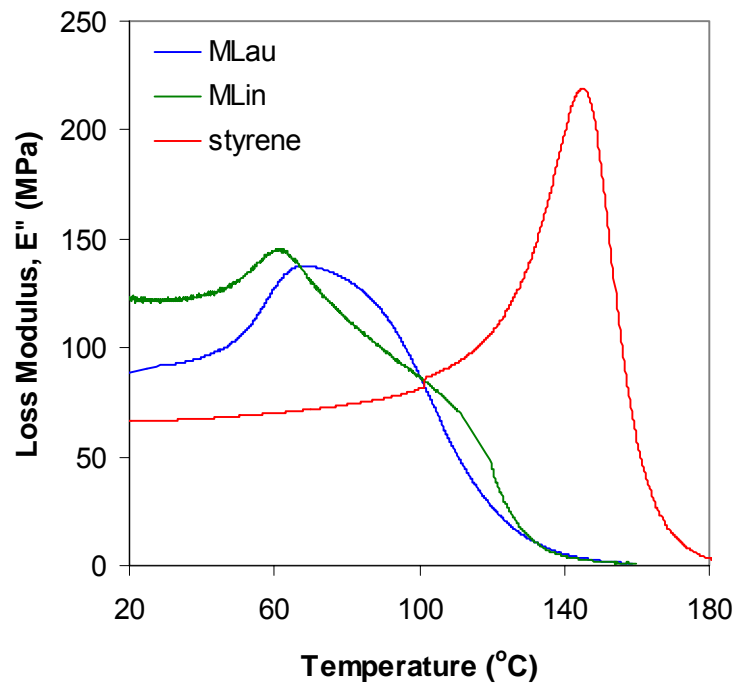


**Figure 120.** The loss modulus as a function of temperature for MLau, MLin, and styrene based vinyl esters using 35% reactive diluent.

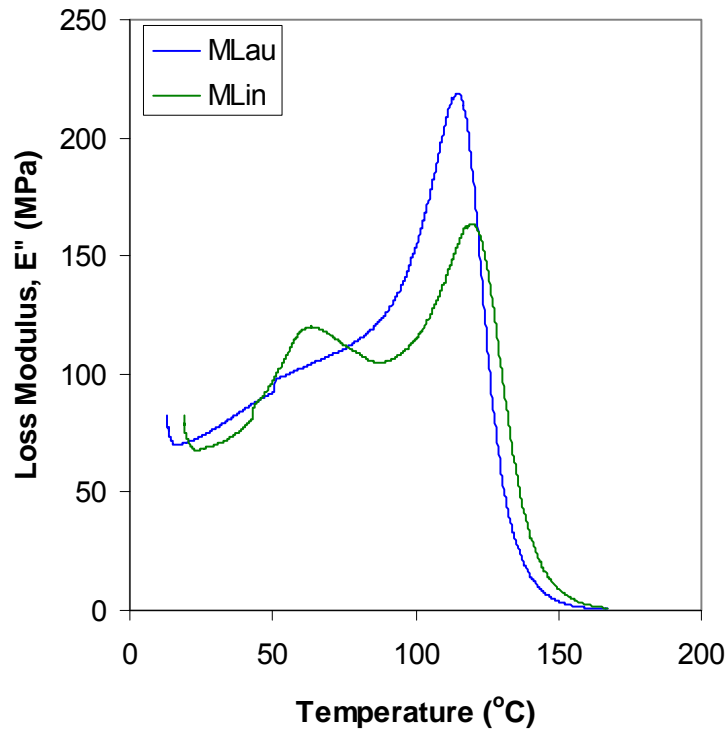


**Figure 121.** The loss modulus as a function of temperature for ternary blends of VE/MLau/Styrene and VE/MLin/Styrene with weight ratios of 65/15/20.

When VEA is used to replace VE monomer, the glass transition of blends with MLau and MLau/Styrene become more narrow (Figure 122). In some cases, there is visible phase separation in VE polymers, while the glass transition is sharp for the same VEA blend (Figure 123). When two phase regions are not observed in VE polymers, there is likely to be a peak shoulder at  $\sim 65^{\circ}\text{C}$ . The  $T_g$  for the VEA polymer is considerably lower than that of the VE polymer because acrylates are less stiff than methacrylates, and usually have a lower  $T_g$ . Lastly, the cross-link densities of these polymers were calculated using rubber elasticity theory. The results show that the molecular weight between cross-links was lower for VE/MLau polymers relative to VEA/MLau, and both were lower than that of VE/styrene (Figure 124). Therefore, these results indicate that VE resins are more cross-linked than VEA resins and fatty acid-based vinyl esters are more cross-linked than styrene-based resins. The fact that  $M_c$  is higher for VEA polymers means that the level of cross-linking in these polymers is lower than in their VE counterparts. This could occur for three reasons: (i) the vinyl ester cured to a higher extent in VE polymers, (ii) the reactive diluents cured to a lower extent in VE polymers, (iii) combination of i and ii. Overall, the DMA results show that there are large morphological differences between VE and VEA polymers and MLin and other fatty acid-based resins.

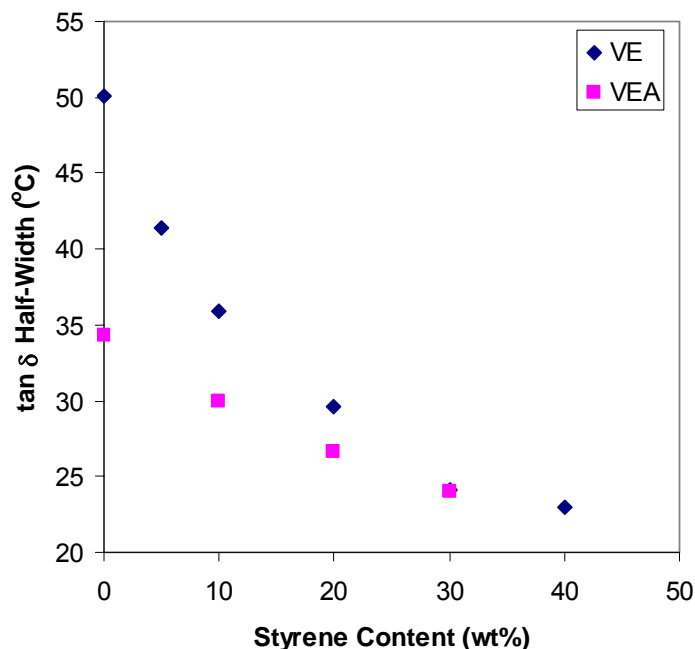


**Figure 122.** The width of the  $\tan \delta$  peak at half-height for VE and VEA resins using 45% reactive diluent (MLau and styrene) as a function of styrene content.

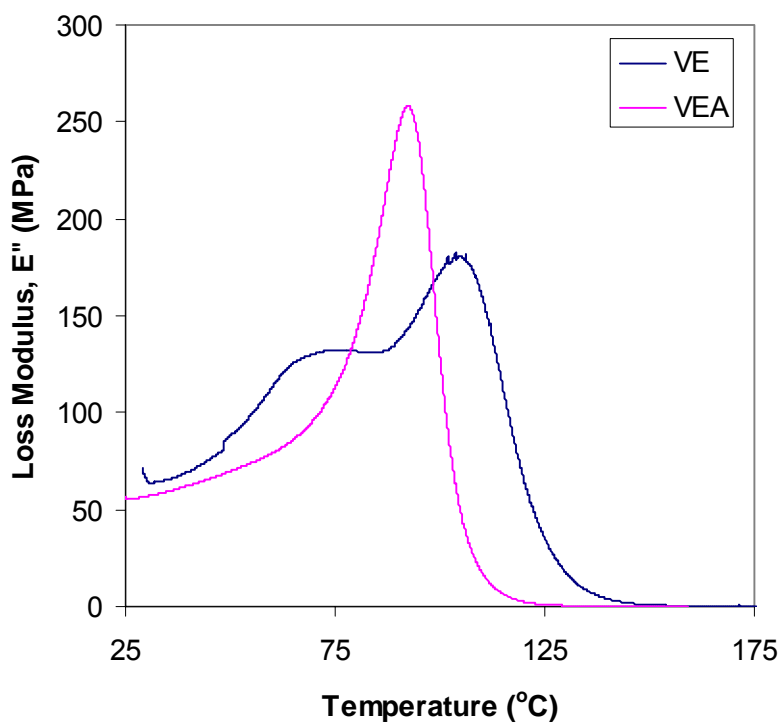


**Figure 123.** The loss modulus as a function temperature for VE/MLau/Sty and VEA 55/15/30.

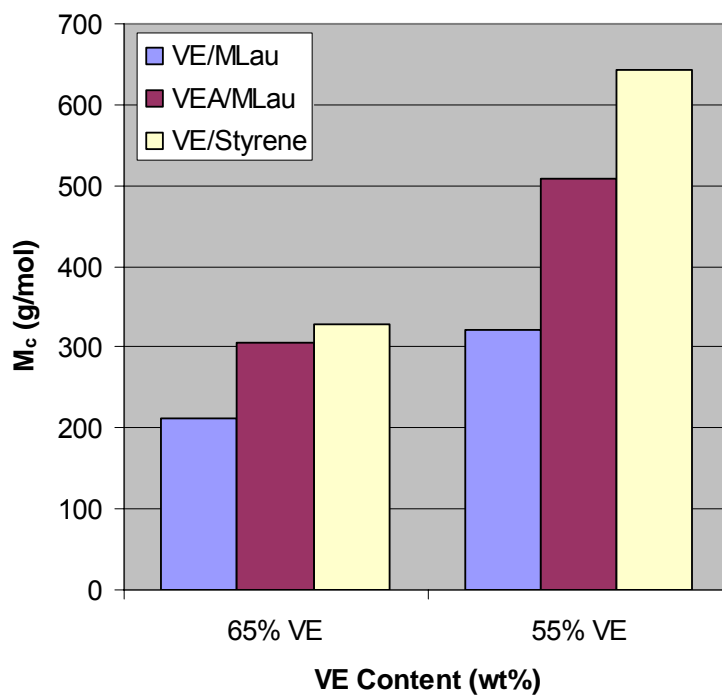


**Figure 124.** The molecular weight between cross-links for VE/MLau, VEA/MLau, and VE/styrene polymers.

### FTIR Cure Kinetics

The cure kinetics of VE/MLin vs. the other fatty acid monomers have already been reported (Figure 94 and Figure 95). MLin resins cure slower and to a lower extent of cure because of chain transfer to the allyl groups.

The cure kinetics of VE vs. VEA resins is more difficult to analyze because the vinyl groups of MFA and VE monomers are coincident. However, an in-depth analysis of the results can show some difference between the cure of these resins. Figure 125 shows that the overall cure of VE/MFA is similar to that of VEA/MFA. However, the overall cure of VEA/MFA/styrene (Figure 126) was higher than that of VE/MLau/Styrene (Figure 127). Specifically, it appears that the cure of VEA/MLau is higher than that for VE/MLau in the ternary blends. As expected, the molecular weights between cross-links of VEA ternary blends were slightly lower (~260 g/mol) relative to VE ternary blends (~300 g/mol) because of the higher extent of cure of VEA resins.

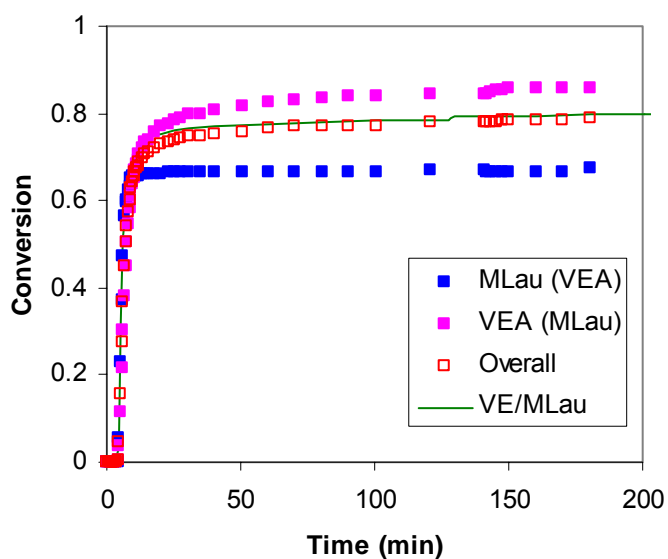


**Figure 125.** The overall conversion of VE/MLau is similar to that of VEA/MLau for resins containing 45 wt% MLau.

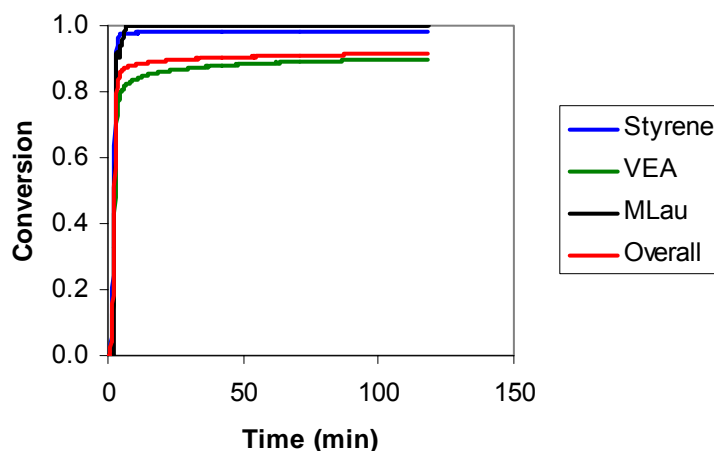


**Figure 126.** The component and overall cure of VEA/MFA/Styrene 65/15/20.

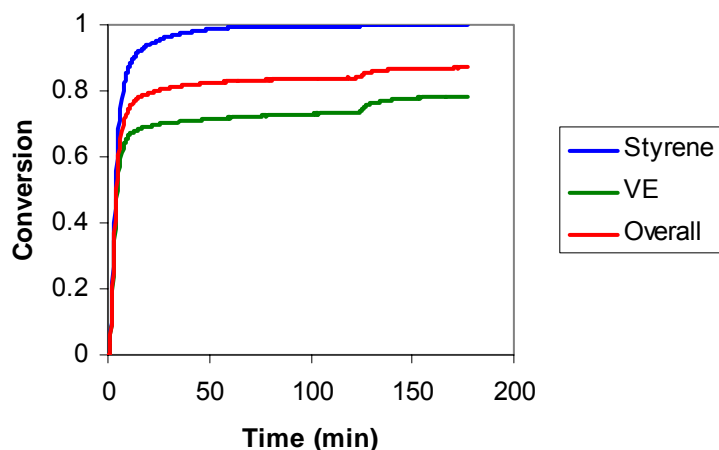


**Figure 127. Component and overall cure of VE/MFA/Styrene 65/15/20.**

The reactivity ratios were calculated by monitoring the copolymerization of VEA and MFA monomers. Reactivity ratio results show a major difference between MLin resins and other MFA resins (Table 34). All reactivity ratios were greater than 1, indicating a preference to homopolymerize. The MFA reactivity ratio was considerably higher than the vinyl ester reactivity ratio, indicating that MFA will initially cure faster than the vinyl ester. Furthermore, both reactivity ratios are higher in the MLin polymer.

**Table 34. The reactivity ratios of the binary blends of vinyl ester, MFA, and styrene measured at 90°C.**

$r_{VE}$	$r_{VEA}$	$r_{MLau, MOA, MSA}$	$r_{MLin}$	$r_{Styrene}$
~1		~1		
>1			>1	
0.3				0.3
	1.7	4		
	2.6		7.7	
	0.5			0.7
		1.3		0.5

The reactivity ratios of vinyl ester are higher in VEA resins than they are in VE resins. In addition, the reactive diluent reactivity ratios are much higher in VEA than in VE resins. Therefore, there appears to be a greater likelihood of alternating copolymerization in VE resins and VEA resins should be more “blocky” in nature.

### *Morphology*

Optical microscopy was used to examine the macro scale morphology of the fracture surfaces of the vinyl ester polymers prepared in this work. Most optical images were similar to Figure 128. Essentially, the images were relatively smooth, with low amounts of shear markings, as visible from the diagonal markings along the sample. Figure 129 shows the optical micrograph typical

of vinyl ester resins containing MLin. The images clearly show the rough morphology as a result of the phase separation that occurred in these samples.

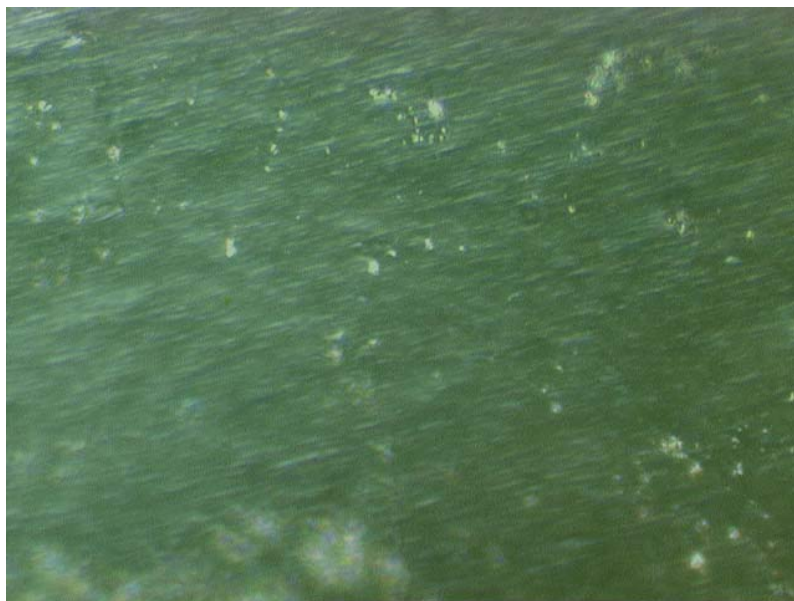


**Figure 128. Optical image of VEA/MLau 65/35 at 50x magnification.**

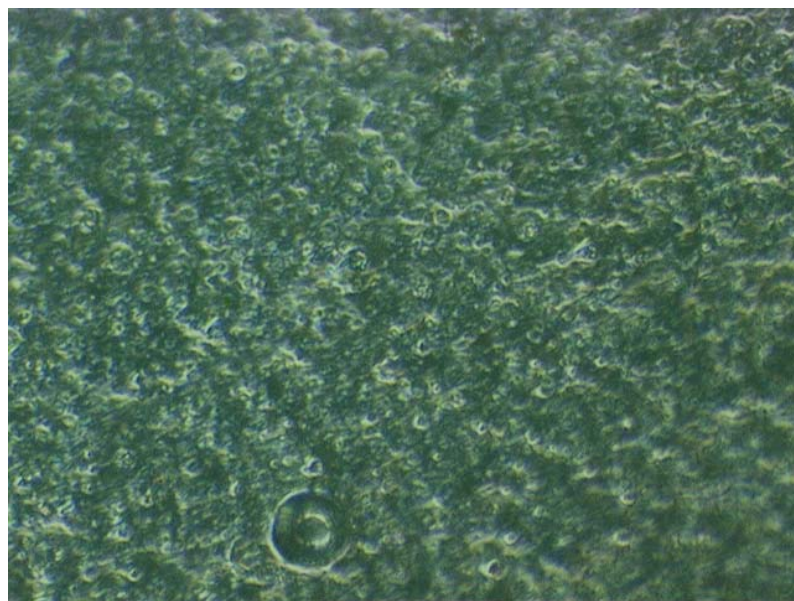


**Figure 129. Optical image of VEA/MLin 65/35 at 50x magnification.**

According to the DMA results, phase separation occurs in MLin vinyl esters, but does not in other MFA resins. MLin monomers have the two unsaturation sites, more than the other MFA monomers tested. MLin monomers are initially soluble in vinyl ester resin, just as other MFA monomers. Only during cure does phase separation occur in the VE/MLin polymers.

Mlin resins cured the slowest and to the lowest extent because of chain transfer to allyl groups. It is likely that these chain transfer events results in different initial morphologies than other MFA resins. Specifically, all chain transfer events would occur in-conjunction with a Mlin molecule. Therefore, there should be a high concentration of Mlin monomers in this phase separated zone. Figure 121 shows that a phase region has a  $T_g$  65°C, far lower than the  $T_g$  of VE/MLau/Sty 65/15/20 of 116°C, which supports this theory. In addition, the main glass transition for the Mlin materials (120°C) was slightly higher than its MLau counterpart indicating a slightly lower Mlin concentration in that phase. The  $T_g$  of pure Mlin was found to be -40°C. Using the Fox equation, we can predict that composition of the phase regions in Figure 121. Assuming the low  $T_g$  region has an elevated Mlin content and a low content of styrene, which is likely according to the reactivity ratios, the compositions of the phase regions in Mlin were calculated (Table 35). The Mlin composition has the least variability in each phase region. The Mlin and styrene compositions vary strongly from the high  $T_g$  region to the lower  $T_g$  region, while the VE composition was similar.

**Table 35. The composition of the phase regions in VE/Mlin/Styrene 65/15/20.**

Phase	Component	Composition
Low $T_g$	VE	51-64
Low $T_g$	MLau	31-36
Low $T_g$	Styrene	0-19
High $T_g$	VE	40-65
High $T_g$	MLau	3-11
High $T_g$	Styrene	24-57

The reactivity ratios were higher in Mlin resins relative to other MFA resins because phase separation reduced the contact between the Mlin-rich phase (low  $T_g$ ) and the Mlin-poor phase (high  $T_g$ ). Because the same phase separation occurred in VE/Mlin polymers, we would expect both their reactivity ratios to be greater than 1. These results explain why Mlin resins behave so differently relative to other fatty acid-based vinyl esters. In addition, these results support the compositions calculated for the phase regions of VE/Mlin resins (Table 35).

The VE/MFA resins should have visible microgel regions because the ratios of the component reactivity ratios are similar in VE/MFA relative to VE/styrene. It is likely that the microgels are slightly larger in VE/MFA resins because of the higher value of the VE reactivity ratio in VE/MFA resins. This indicates a lower likelihood for alternation and a higher probability of forming regions of high cross-link density. On the other hand, the microgels found in VEA/MFA should be very small because of the low value of the VE reactivity ratios relative to the MFA reactivity ratios.

The overall extent of cure was similar for VEA/MFA and VE/MFA. Because the cross-link density of VE/MFA was higher than that of VEA/MFA (Figure 124), it is likely that the vinyl ester reacts to a lesser extent and the MFA reacts to a greater extent in VEA resins. This hypothesis is supported by the reactivity ratios, which indicate that the reactive diluent reacts faster relative to vinyl ester in VEA resins. The overall extent of cure in VEA ternary blends was higher than that in VE blends (Figure 126 and Figure 127). Again based on the reactivity

ratios, it is likely that the extent of cure of VE is higher than that of MFA in ternary blends of VE resins.

The glass transition width is smaller for VEA resins relative to VE resins. This occurred for a few reasons. The glass transition typically broadens as the cross-link density increases [9]. In addition, the higher content of unreacted MFA in VE resins broadens the glass transition. For ternary blends, the lower overall extent of cure in VE ternary blends broadens the glass transition. This broadening of the glass transition in VE polymers can result in phase separation if there is enough unreacted monomer.

The morphology of ternary blends of vinyl ester, MFA, and styrene depends on the vinyl ester used. The reactivity ratios show that the order of reactivity in methacrylated and acrylated vinyl esters is MFA>VE>styrene and MFA>Styrene>VEA, respectively. These results indicate that the microgels should be small for both ternary blends, but considerably smaller in VEA resins. The smaller microgels in VEA resins should be less likely to phase separate from the rest of the matrix, thus narrowing the glass transition in VEA resins.

#### 3.2.4.3.16 Improvements to Low VOC Fatty Acid Resins

The results thus far show that low VOC fatty acid-based vinyl esters have good properties, but their flexural modulus and strength are significantly lower than that of commercial VE resins. We have tested a few methods of improving the flexural properties (Table 36). Divinyl benzene (DVB) was used to replace some of the styrene in the resin. VEA was used instead of the methacrylated VE. Lastly, methacrylated hexanoic (MHex) acid was used instead of the methacrylated lauric acid.

**Table 36. Flexural properties of modified resins relative to DVB resins.**

<b>Formulation</b>	<b>Flexural Strength (MPa)</b>	<b>Strain at Failure (in/in)</b>	<b>Flexural Modulus (GPa)</b>
VE/MLau/Sty 65/15/20	125 ± 12	0.038 ± 0.008	3.69 ± 0.10
VE/MLau/Sty/DVB 65/15/17/3	111 ± 8	0.034 ± 0.004	3.54 ± 0.08
VEA/MLau/Sty 65/15/20	119 ± 3	0.048 ± 0.006	3.39 ± 0.10
VE/MHex/Sty 65/15/20	133 ± 7	0.039 ± 0.004	3.86 ± 0.10
VE/MHex/MLau/Sty 65/7.5/7.5/20	138 ± 11	0.041 ± 0.006	3.72 ± 0.34

Divinyl benzene is a low molecular weight cross-linking agent. Its aromatic nature should increase the rigidity of most polymer networks. The divinyl benzene we used was provided by Dow, and is 67% pure. The other 33% is a mixture of ethyl vinyl benzene and styrene, which are reactive diluents. We used resin formulations of VE/MLau/Sty/DVB of 65/15/17/3 to see the effect of DVB on flexural properties. Flexural samples were made and tested as previously described. Table 36 shows that the flexural strength and modulus of DVB-based resins were lower than that of the standard low VOC fatty-acid formulation. Previous work with DVB has shown that once one of the vinyl groups polymerizes, the reactivity of the other group drops significantly [55]. This would reduce the amount the DVB would increase the modulus, but

would not explain a reduction in the modulus. Therefore, it is possible that the DVB has an effect on the morphology, possibly increasing the size of the fatty acid zones, causing a reduction in the modulus. The flexural strength decreased because the modulus decreased and the strain at failure decreased slightly. Certainly, DVB is less compliant than the fatty acids, and should reduce the maximum strain.

Results have shown that fatty acid resins using VEA have different morphologies than VE resins. It is possible that the greater homogeneity in VEA polymers should improve the modulus of the polymers. However, acrylate groups are less rigid than methacrylate groups, and this effect seems to have dominated. However, the flexural strength was not reduced significantly because VEA polymers were more elastic in nature (i.e. failed at higher strains).

Shorter fatty acids increase the modulus and  $T_g$  of fatty acid-based vinyl esters. Therefore, we were not surprised to see an improvement in the flexural properties. The MHex gives much better flexural properties than MLau polymers at low styrene contents (Figure 130 and Figure 131). This effect of MFA type was reduced as the styrene content increased. This was likely due to dilution of the MFA as well as the high cross-head speed used in this particular set of tests.

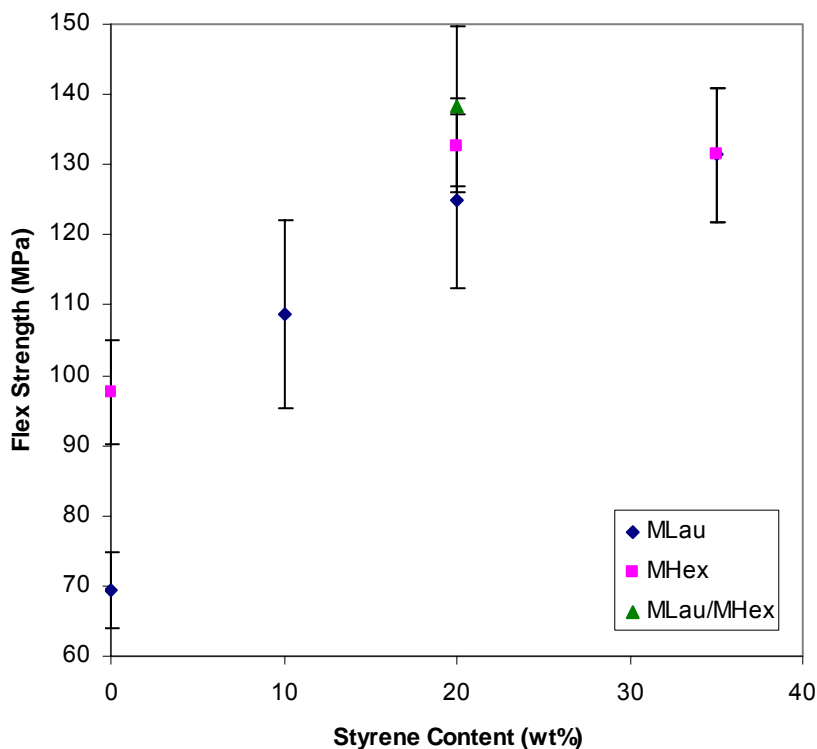


**Figure 130.** The flexural strength as a function of styrene content for MHex and MLau-based resins.

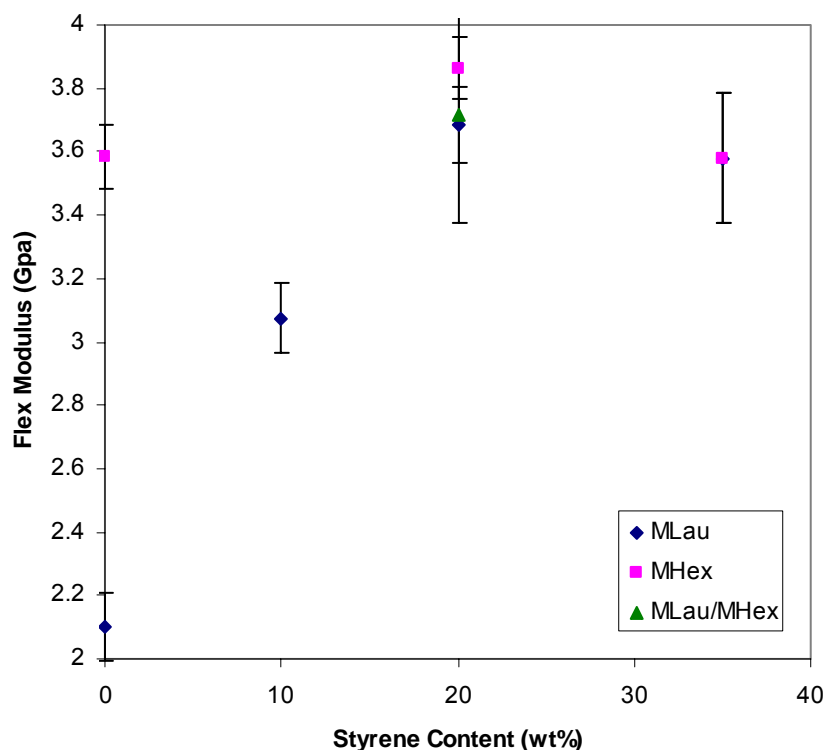


**Figure 131. The flexural modulus as a function of styrene content for MHex and MLau-based resins.**

#### 3.2.4.3.17 VE/MFA/Petroleum Monomer/Styrene Blends

Further reductions in styrene content would be useful in meeting EPA regulations. One way of doing this is to replace more of the styrene in fatty acid-based VE with lower volatility petroleum monomers. Therefore, the purpose of our research is to test different resin formulations using fatty acid monomers and other low volatility petroleum monomers hoping to obtain a formulation with a viscosity under 500 cP, a high modulus, and a high  $T_g$  with low styrene content.

#### Procedure

The mono-functional petroleum monomers that were used were methoxy PEG 350 methacrylate (CD550), ethoxy (4) nonyl phenol methacrylate (CD612), and CHMA from Aldrich. The di-functional petroleum monomers used were PEG 600 dimethacrylate (SR252), PEG 200 diacrylate (SR259), 1,6-hexanediol dimethacrylate (SR239), and ethox. (10) bis A dimethacrylate (SR480). First, the CN151 must be heated for 10 minutes at 70 degrees Celsius for easy pouring. After heating CN-151, 9-11 grams should be carefully poured into a 20 mL scintillation vial. Based on this vinyl ester content, the amounts of other monomers were calculated according to their particular formulation. If a di-functional monomer was used, it was added after the vinyl ester. After the di-functional monomer was added, the MLau was poured into the vial. If a mono-functional monomer was used, MLau was added to the vial after the vinyl ester monomer followed by the mono-functional monomer. The styrene was added last because of its high volatility. After all of the solutions were added to the vial, it had to be heated

at 70°C for ten minutes and then stirred to get all viscous components into solution. The clarity of the solution was noted, especially if the monomers did not dissolve in each other. Approximately half of the resin sample was saved for the viscosity measurements. To the other half of the resin sample, 0.375wt% CoNap was added, followed by 1.5wt% trigonox. The resin sample was then stirred and poured into a mold to cure. After the resin cured, it was sliced into approximately 3 millimeter wide samples for dynamic mechanical analysis.

The rheological character of the resins was measured using a TA Instruments AR 2000 Rheometer. The geometry used for all the samples was the 40 mL parallel steel plates. The gap distances for all samples were set to 1000 microns. A constant temperature was used for all samples, which was 20°C. A shear rate of 1 to 100 inverse seconds was used in increments of 3 points per decade on a logarithmic scale in a steady state experiment. The TA data analysis program was used to analyze the results from the rheometer.

The 3mm wide strips of resin were sanded into flat rectangular samples. After measuring the width and thickness, the samples were then placed in the clamps of the DMA. The length of each sample was measured after it was clamped tight in the machine. All of these dimensions were recorded in the Thermal Advantage computer program along with the formulation and name of each sample. The sample was run isothermally for five minutes with a ramp rate two degrees per minute to 200°C from room temperature, with 15 micron amplitude and a frequency of one hertz. Each sample was run two times under these conditions. The first run post-cured the samples. The second run was used to post-cure the sample. The Universal Analysis program was then used to analyze the data from the DMA. The  $T_g$  was the temperature at which the peak in the loss modulus occurred, and the modulus was recorded as the value of the storage modulus at 35°C.

### *Results and Discussion*

Figure 132 shows the effect of resin formulation on the viscosity for resins composed with 65% CN151 and different percentages of mono-functional petroleum monomers and styrene. For example, it appears that the original ternary compound with 10% styrene had a viscosity of 1337 cP. Using the same components but with 20% styrene and less MLau had a lower viscosity (516 cP). Therefore, increasing the amount of styrene decreased the viscosity.

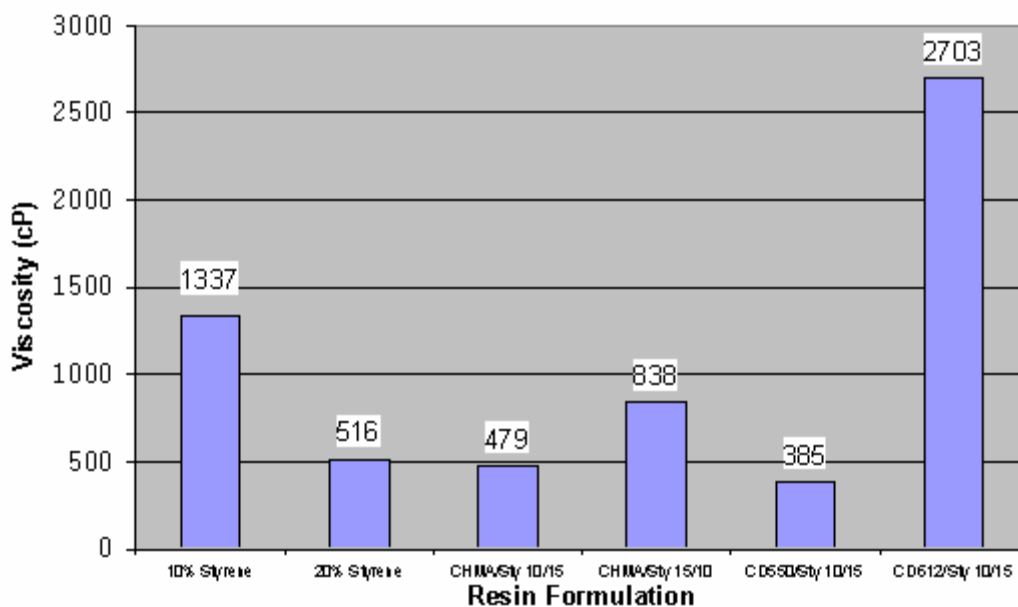


**Figure 132. Viscosity as a function of mono-functional resin formulation for resins with 65% CN151.**

The resin viscosity is required to be below 500 cP in order to easily process the resin [14]. The samples CHMA/Sty 15/10, CD612/Sty 10/15, and CD 612/Sty 15/15 were not good candidates for resin formulations since their viscosities were above 500 cP (Table 37 and Table 38). From the results, we can infer that CD612 is more viscous than styrene, which is true according to Table 38.

**Table 37. Viscosity of resin formulations containing mono-functional petroleum monomers.**

Petroleum Monomer	%VE (CN151) wt%	Petroleum Monomer wt%	MLau Wt%	Styrene wt%	Viscosity (cP)
CD550	65	10	10	15	385
CD612	65	10	10	15	2703
CHMA	65	10	15	10	838
CHMA	65	10	10	15	479
CD550	55	15	15	15	342
CD612	55	15	15	15	1795
CHMA	55	15	15	15	167

**Table 38. The viscosity of mono-functional monomers [www.sartomer.com].**

Monofunctional Monomer	Monomer Label	Viscosity (cP)
Methoxy PEG 350 methacrylate	CD550	19
Ethoxy (4) Nonyl phenol methacrylate	CD612	79
Cyclohexyl methacrylate	CHMA	364
Styrene	Styrene	0.7
MLau	MLau	70

Figure 133 shows the viscosity results for resins with 55% CN151 and di-functional monomers with 20% styrene, compared to the original ternary resin with no di-functional petroleum monomers added. When comparing the original ternary resin with the di-functional monomer samples, the ternary resin had a higher viscosity than the resins containing di-functional monomers while maintaining the same amount of styrene (Table 39 and Table 40). Therefore, the addition of di-functional monomers decreased the viscosity of the resins because the di-functional monomers were less viscous than the CN151 they replaced.

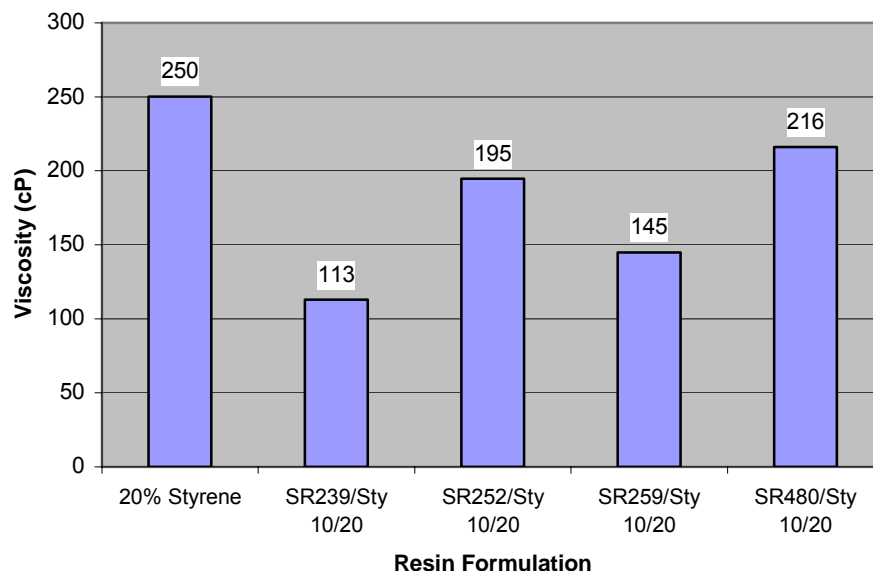


**Figure 133. Viscosity as a function of di-functional resin formulation for resins with 55% CN151.**

**Table 39. Viscosity of resin formulations containing di-functional petroleum monomers.**

Petroleum Monomer	%VE (CN151) wt%	Petroleum Mon wt%	MLau Wt%	Styrene wt%	Viscosity (cP)
SR 252	55	10	15	20	195
SR 259	55	10	15	20	145
SR 239	55	10	15	20	113
SR 480	55	10	15	20	216
SR 252	45	20	15	20	98
SR 259	45	20	15	20	68
SR 239	45	20	15	20	71
SR 480	45	20	15	20	131

**Table 40. Viscosity of di-functional monomers [www.sartomer.com].**

Di-functional monomer	Petroleum monomer Label	Viscosity (cP)
PEG 600 Dimethacrylate	SR252	67
PEG 200 Diacrylate	SR259	25
1,6-Hexanediol dimethacrylate	SR239	8
Ethox. (10) Bis A dimethacrylate	SR480	410
Vinyl Ester	CN-151	150000

The ternary formulations of VE, MLau, and styrene with 65% CN151 and 20% styrene had a viscosity of 516cP and the resin with 55% CN151 and 20 wt.% styrene had a viscosity of only 250 cP (Figure 132 and Figure 133). Therefore, for constant styrene content, decreasing the amount of CN151 sharply decreased the resin viscosity. This is expected because CN151 had a very high viscosity (Table 40). The formulations using the low VOC petroleum monomers displayed similar behavior.

The results show that mono-functional and di-functional petroleum monomers reduced the viscosity of vinyl esters. These monomers also reduce the VOC and HAP content of the resins. Therefore, based on the viscosity results, the addition of these low VOC monomers is advantageous.

Typical dynamic mechanical analysis plots are shown in Figure 134. The storage modulus decreased with temperature. The loss modulus went through a maximum as a function of temperature. Figure 134 shows that the CHMA sample had a higher modulus and  $T_g$  than the CD 550 sample. The modulus at 35°C (MPa) and  $T_g$  from the DMA results were plotted as a function of resin formulation. The goal was to find the sample with a high  $E'$  at 35°C in MPa (high modulus), denoting higher stiffness, and a high  $T_g$ , meaning it can be used at higher operating temperatures [16].

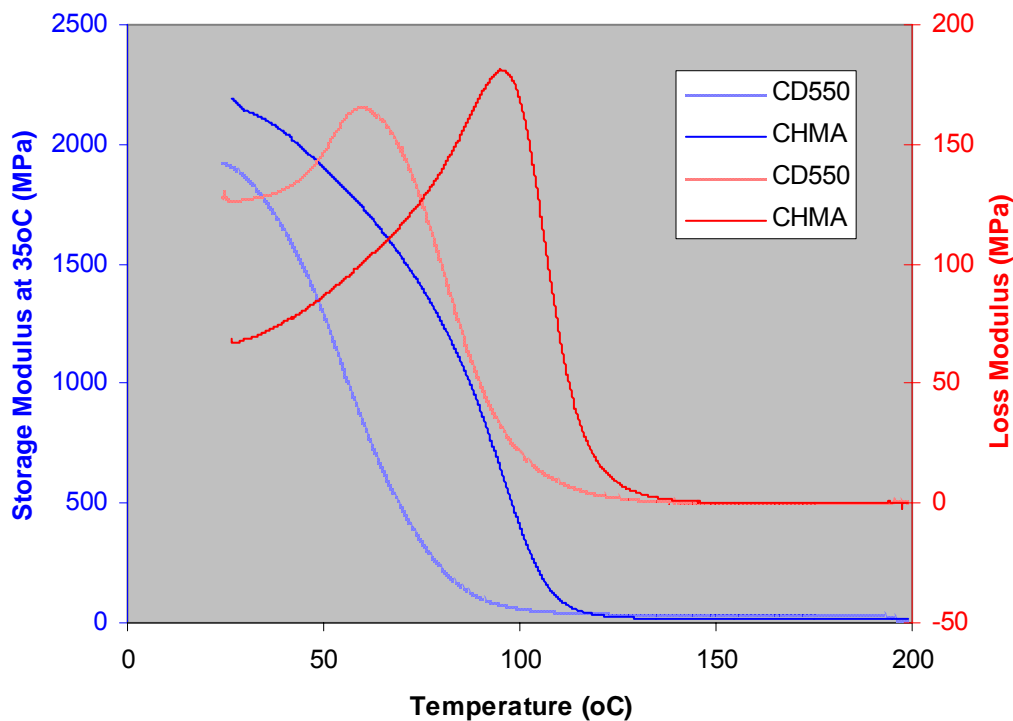


**Figure 134. The storage modulus and loss modulus as a function of temperature for VE/MLau/Styrene/CHMA 55/15/15/15 and VE/MLau/Styrene/CD550.**

It was first noted that the moduli of the post-cured samples were typically slightly higher than that of the non-post-cured samples. Figure 135 of mono-functional petroleum monomers shows that the CHMA had a high modulus. Figure 136 shows that the CD612 and CHMA had a high  $T_g$ . CHMA is a better candidate than CD612 because the formulations containing CHMA had a higher modulus. This fact also indicates that CD612 is a less rigid molecule than CHMA.

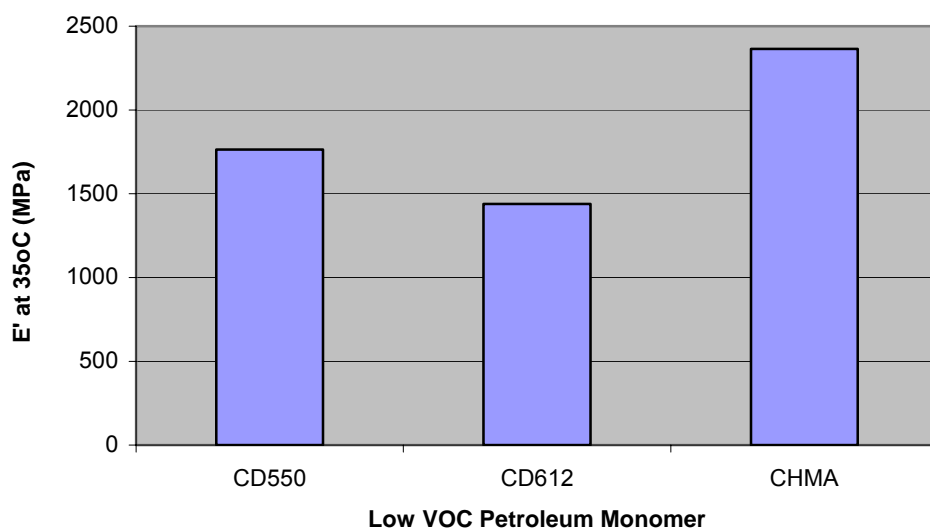


**Figure 135. Storage modulus as a function of mono-functional monomers for resins with 55% CN151, 15% MLau, 10% low VOC petroleum monomer, and 15% Styrene.**

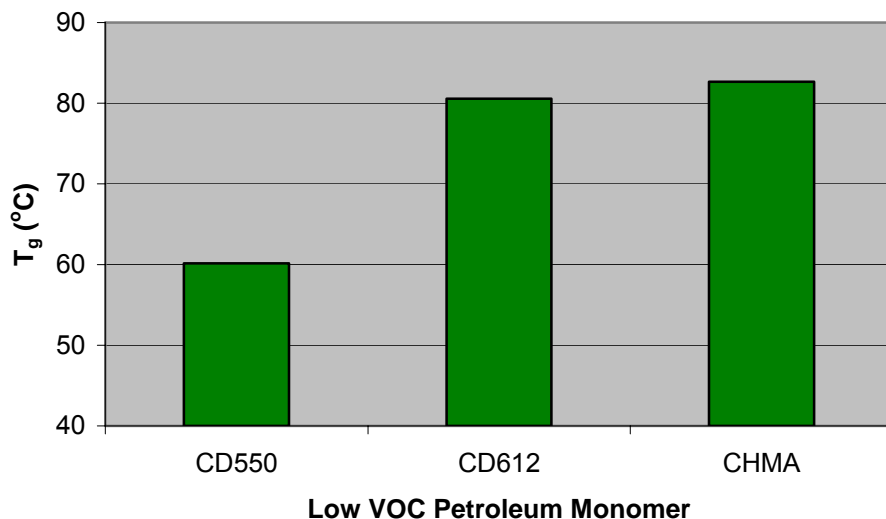


**Figure 136. T<sub>g</sub> as a function of low VOC mono-functional monomers for resins with 55% CN151, 15% MLau, 10% low VOC petroleum monomer, and 15% Styrene.**

Figure 137 and Figure 138 show that resins using the di-functional monomer SR239 had the highest modulus by far and the highest T<sub>g</sub>. SR239 (10% Petroleum) had a higher modulus by 6,000 MPa than SR252 and SR259, and its T<sub>g</sub> was 15°C higher. SR239 (20% Petroleum) has a higher modulus and higher T<sub>g</sub> by 25°C than SR252 and SR480 (Table 41 and Table 42). Therefore, SR239 is the best di-functional monomer because it is the stiffest di-functional monomer and can be used at the highest operating temperatures. When comparing the previous figures to Figure 137 and Figure 138, both using 55% CN151, it is apparent that the di-functional monomers had a higher T<sub>g</sub> and higher modulus than the mono-functional monomers.

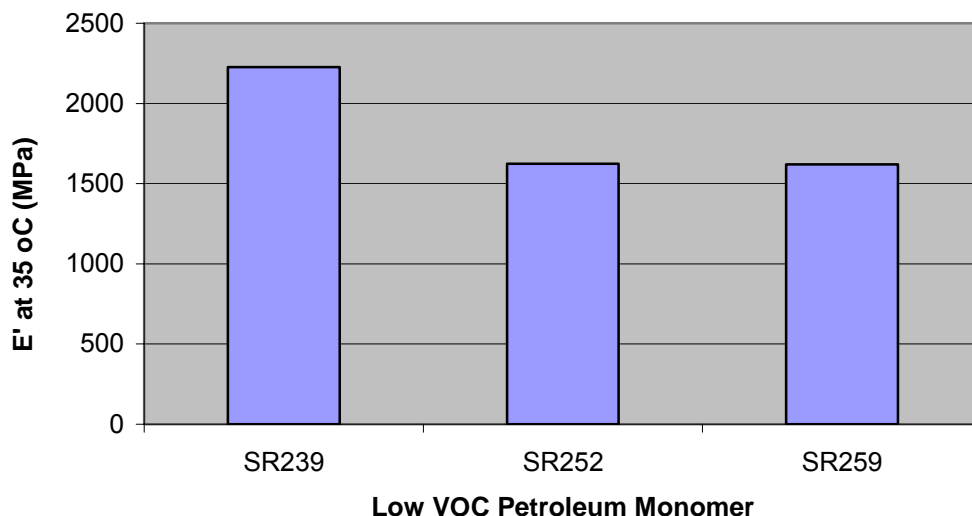


**Figure 137. Modulus as a function of low VOC di-functional monomer for resins containing 55% CN151, 15% MLau, 10% low VOC petroleum monomer, and 20% styrene.**

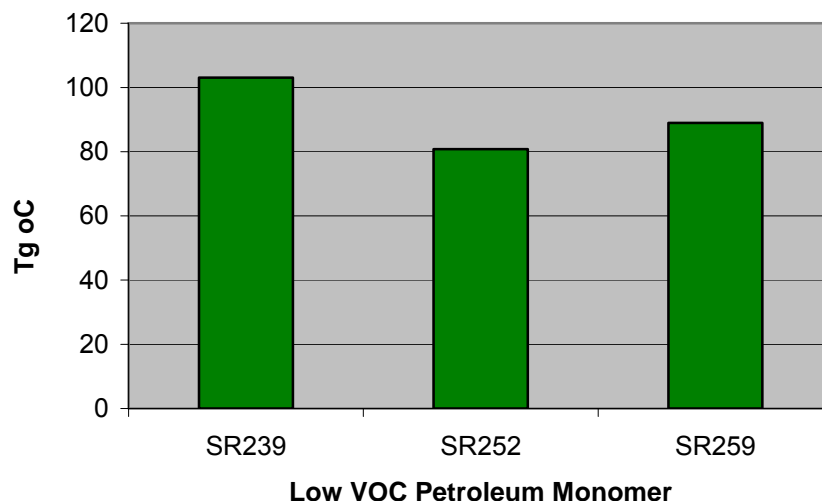


**Figure 138.** T<sub>g</sub> as a function of resin formulation for of low VOC di-functional monomers containing 55% CN151, 15% MLau, 10% low VOC petroleum monomer, and 20% styrene.

**Table 41.** DMA properties of mono-functional low VOC petroleum monomer formulations.

Petroleum Monomer	CN151 Content	MLAU Content	Petroleum Content	Styrene Content	E(35°C)	T <sub>g</sub>	M <sub>c</sub> (g/mol)
CD550	55	15	15	15	1764	60	1082
CD612	55	15	15	15	1440	81	620
CHMA	55	15	15	15	2365	83	414
CD550,15%Sty	65	10	10	15	2037	85	60
CD612,15%Sty	65	10	10	15	1558	75	691
CHMA,15%Sty	65	10	10	15	1794	103	528
CHMA,10%Sty	65	15	10	10	2399	95	467

**Table 42.** DMA properties of di-functional low VOC petroleum monomer formulations.

Petroleum Monomer	CN151 Content	MLAU Content	Petroleum Content	Styrene Content	E(35°C)	T <sub>g</sub>	M <sub>c</sub> (g/mol)
SR239	55	15	10	20	2226	103	285
SR252	55	15	10	20	1624	81	495
SR259	55	15	10	20	1620	89	347
SR239	45	15	20	20	1832	102	254
SR252	45	15	20	20	1427	70	337
SR480	45	15	20	20	1629	79	383

Comparing Table 41 and Table 42, di-functional monomers had higher modulus and T<sub>g</sub> overall. Reviewing all of the data, it was found that the di-functional monomers produced resins with lower viscosities, higher modulus, and higher T<sub>g</sub> than the mono-functional monomers. Because

CN151/Mlau/SR239/Sty 55/15/10/20 had the lowest viscosity of 113 cP, the highest modulus at 2226 MP and the highest  $T_g$  with 103°C, SR239 was the best petroleum monomer to replace styrene content without being an HAP or VOC.

### *Conclusions*

The di-functional petroleum monomers show better promise in the formulation of resins compared to mono-functional petroleum monomers. Every formulation using the di-functional petroleum monomer had viscosities significantly less than 500 cP, a higher modulus and higher  $T_g$  than mono-functional monomers. The combination of the di-functional petroleum monomer and styrene is more environmentally safe than styrene alone because it decreases the amount of styrene (VOC and HAP) while maintaining similar properties compared to the original ternary formulation. SR239 in particular was the best monomer for styrene replacement because its sample had the lowest viscosity, highest modulus, and highest  $T_g$ . CHMA was the best mono-functional monomer with a fair viscosity, high modulus and high  $T_g$ . Because of its extremely high viscosity, CD612 was a poor substitute for resin formulation even though it had an average modulus and  $T_g$ . Therefore, it is possible to use petroleum monomers like SR239 and CHMA in addition to fatty acid based monomers in resin formulations to replace styrene while maintaining characteristics like low viscosity, high modulus, and high  $T_g$ .

#### *3.2.4.3.18 Cyclized Fatty Acids*

No work has been done with making cyclized fatty acid-based (Structures 5-8, Figure 66) monomers as of yet. This work will begin in 2003.

#### *3.2.4.3.19 Di-Functional Fatty Acid Monomers*

Di-vinyl monomers have not been prepared from fatty acids. Figure 66 shows that the synthetic routes are similar to the chemical routes already explored. Therefore, we should be able to prepare di-functional monomers shortly.

#### **3.2.4.4 VOC Emissions from Fatty Acid-Based Resins**

Experiments with the macro-TGA have shown that fatty acid monomers do not produce VOC emissions. Figure 139 shows that some slight mass loss occurs followed by mass gain for MFA monomers. The initial mass loss may represent the loss of some very small percentage of volatiles, while the mass gain indicates the adsorption/absorption of water or some other component of air.

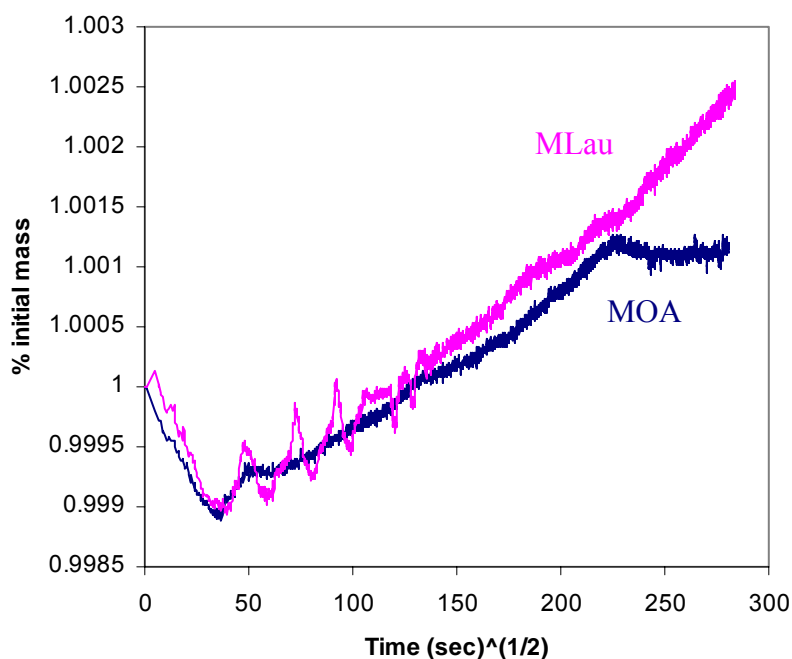


**Figure 139.** The percentage mass change as a function of time for MFA monomers.

VE blends were prepared using the MFA monomers, and were measured in the macro-TGA to gauge their influence on VOC loss. The general shape of the VOC loss curve approximated that of the other systems that have been evaluated; e.g. a brief period of latency before a linear region of loss, followed by a plateau (Figure 140). The tremendous benefit of these materials, though, remains the reduction in total VOC content of the system. The MFA monomers were essentially non-volatile over the temperature range studied, and brought the VOC content down by 60-80% compared to our baseline system or commercial resins, such as Derakane 411-C50. The systems maintained low viscosity while simultaneously decreasing VOC out-gassing. Figure 140 shows the total mass-loss of the FAME-VE-styrene blends. Note that the baseline 1:1 styrene-VE system exhibits almost 45% mass loss (or 90% of volatiles) at  $300 \text{ s}^{1/2}$ . The samples containing FAME styrene replacements still lose the majority of their VOC content, but the amount of styrene incorporated into the formulation is reduced by 60-80%. The resultant change in mass loss is shown by the difference in plateau regions at extended times in Figure 140. The fatty acid chain length and number of unsaturation sites on the backbone had no significant effect on the emissions characteristics of these monomers or vinyl ester resins.

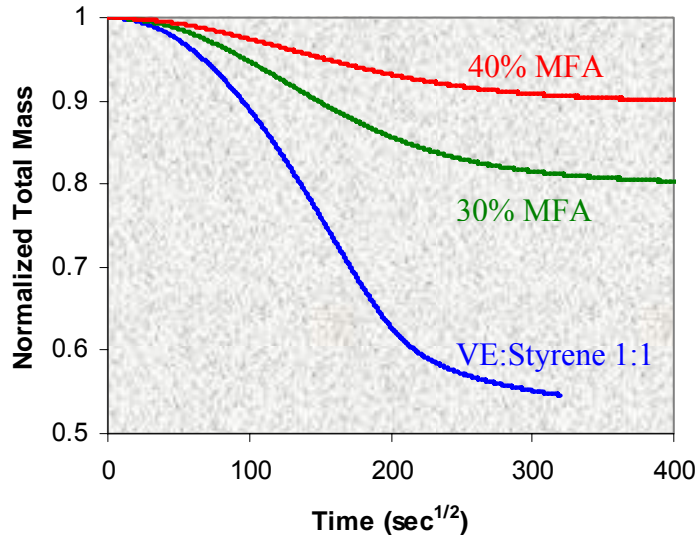


**Figure 140.** The normalized mass loss as a function of time for vinyl esters containing 50 wt% vinyl ester monomers and 50 wt% reactive diluent.

### 3.2.4.5 Kinetic Modeling of Fatty Acid Methacrylation Using Glycidyl Methacrylate

To prepare MFA monomers on a large scale, a fundamental understanding of the reaction kinetics is necessary. This section details the methods used to determine the reaction kinetics, the results, and the implications.

#### 3.2.4.5.1 *Experimental*

Three materials were used in the synthesis of MFA, the fatty acid, the methacrylate functional addend, and the catalyst. The fatty acid used was Lau (Aldrich, 99.5%), the methacrylate used was GM (Aldrich, 97%) and the catalyst was AMC-2.

The MFA reaction is schematically shown in Figure 141. The carboxylic acid end group on of the fatty acid undergoes an addition reaction with an epoxy group on GM to form the MFA. The kinetics of this reaction were investigated by reacting GM and Lau in stoichiometric proportions while varying catalyst (AMC-2) concentration (1%, 0.5%, 0.25% and 0.1% by weight) and temperature (60°C, 70°C, 80°C, and 90°C). Special care was taken in working with lauric acid. Since it is a solid at room temperature it was measured and then melted in the oven before adding the GM and AMC-2.

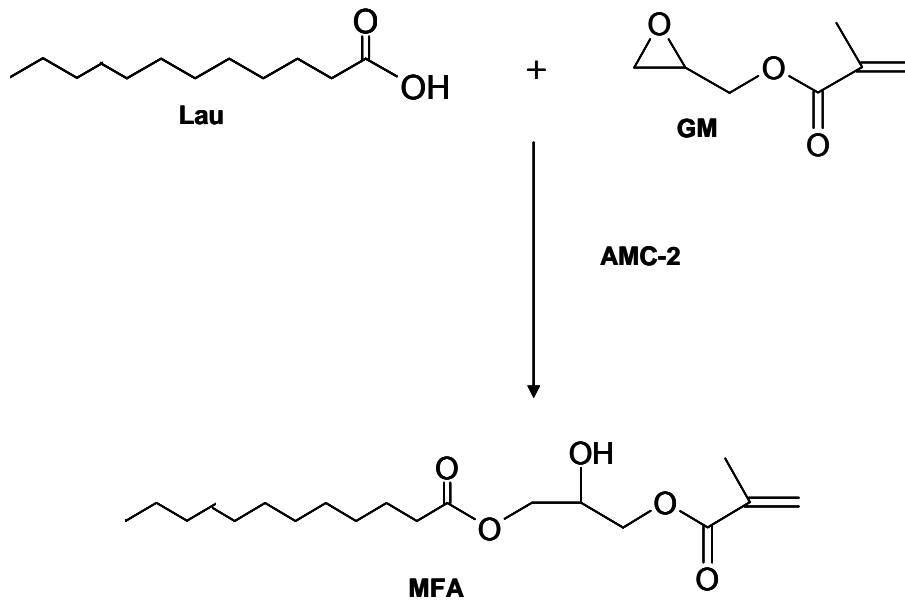


**Figure 141. Methacrylated fatty acid synthesized from lauric acid and glycidyl methacrylate with AMC-2 catalyst.**

The reaction kinetics was monitored using Near IR Fourier Transform Infrared Spectroscopy (FTIR) (Thermo Nicolet Nexus 670 FTIR) between 4000 and 8000  $\text{cm}^{-1}$ . Experiments were conducted in transmission mode, taking 32 scans per spectrum with a resolution of 8  $\text{cm}^{-1}$ . Characteristic epoxy group peaks analyzed for the reaction were at wave numbers of 6071  $\text{cm}^{-1}$  and 4531  $\text{cm}^{-1}$ .

The following procedure was used for preparing the samples. 10g of Lau was measured into a scintillation vial and maintained at 60°C to melt the Lau powder. After the Lau melted, GM was added in stoichiometric proportions to the Lau melt and placed back in the oven at 60°C to keep the sample in its liquid state. AMC-2 was then added to the GM/Lau mixture, mixed thoroughly and injected into glass NIR sample tubes before being completely sealed. Sampling was done at 4 minute intervals except at 90°C where sampling was conducted every 2 minutes due to the faster reaction rates.

The resulting spectra were analyzed by measuring the peak height of the epoxy at either 6071  $\text{cm}^{-1}$  or 4531  $\text{cm}^{-1}$ . The change in peak height was directly related to the concentration of the epoxy group using Beer's law since the sample thickness remained constant throughout the reaction.

#### 3.2.4.5.2 Results and Discussion

The change in epoxy peak height is equal to the change in concentration of the epoxy group through out the reaction as a function of time. This is necessary for evaluating the parameters needed in developing a kinetic model of the reaction as a function of catalyst concentration and temperature. The general rate expression for this reaction is, given by Eq. 65:

$$\frac{d[E]}{dt} = k[A]^\alpha [E]^\beta [C]^\delta \quad (65)$$

where [A], [E] and [C] are the concentration of the fatty acid, epoxy group (on GM), and the catalyst, respectively,  $\alpha$ ,  $\beta$ ,  $\delta$  are the individual orders of the reaction, and  $k$  is the rate constant. The goal of this analysis is to determine the orders  $\alpha$  and  $\beta$  of the two reactants and to determine  $\delta$  for the catalyst and  $k$  as a function of temperature in order to develop a comprehensive kinetic model. Two modifications can be made that simplify Eq. 65. The reactants A and E are mixed in stoichiometric proportions so the overall concentration can be reduced to  $[E]^{\alpha+\beta}$ . Furthermore for each catalyst concentration investigated we can lump  $[C]^\delta$  with  $k$  to form a new constant  $k'$ . The resulting equation is (Eq. 66).

$$\frac{d[E]}{dt} = k'[E]^{\alpha+\beta} \quad (66)$$

Moreover,

$$\ln\left(\frac{d[E]}{dt}\right) = \ln(k') + (\alpha + \beta) \ln([E]) \quad (67)$$

So that a plot of  $\ln\left(\frac{d[E]}{dt}\right)$  versus  $[E]$  will yield a straight line with a slope of  $(\alpha + \beta)$  and an intercept of  $\ln(k')$ . Figure 142 shows representative plots for data collected at 80°C and a number of catalyst concentrations.

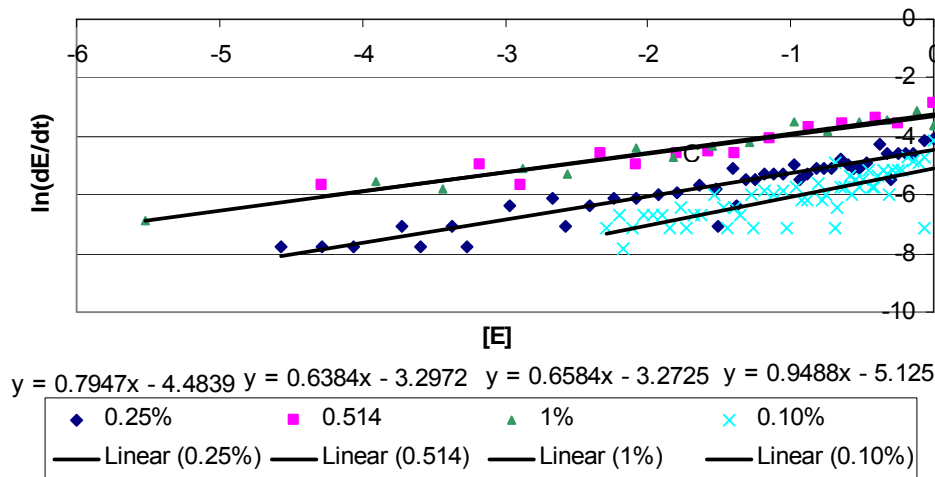


**Figure 142. Representative plots of  $\ln(dE/dt)$  vs.  $[E]$  for experiments conducted at 80°C for four catalyst concentrations.**

The slope of each data set is approximately the same but the intercept changes due to changes in concentration and the  $k$  value which changes as a function of temperature. By averaging the slope of each line an average value for  $(\alpha + \beta)$  obtained was 0.79. Additionally,  $\delta$  and  $k$  and  $k'$  are related by (Eq. 68):

$$\ln(k') = \ln(k) + \delta \ln([C]) \quad (68)$$

A plot of  $\ln(k')$  versus  $\ln([C])$  should yield a line with a slope equal to  $\delta$  and an intercept of  $\ln(k)$ . Figure 143 shows these plots for the four temperature conditions investigated.

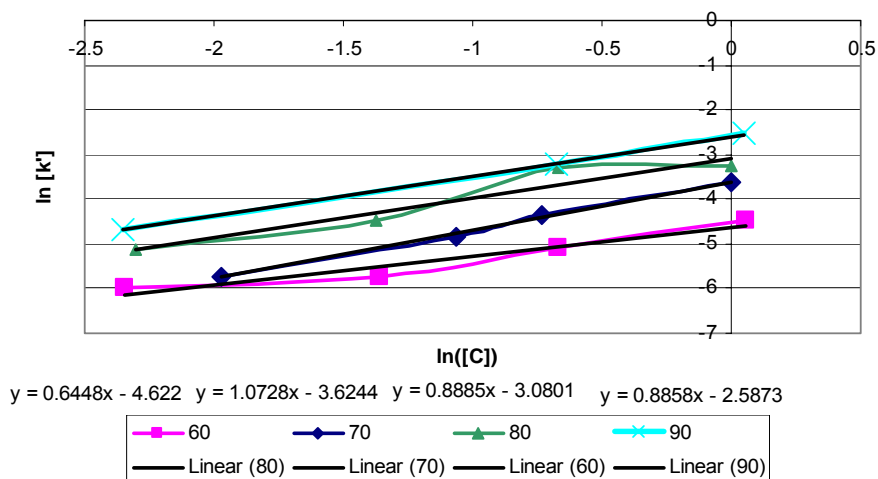


**Figure 143. Plot of  $\ln[k']$  versus  $\ln[C]$  for the four temperatures investigated.**

From Figure 143, and by averaging,  $\delta$  was determined to be 0.88, and the reaction rate constant determined for each temperature and catalyst concentration was used to determine the Arrhenius parameter,  $A_0$  and activation energy,  $E_a$  in equations 69 and 70:

$$k = A_0 e^{\left(\frac{E_a}{RT}\right)} \quad (69)$$

$$\ln(k) = \ln(A_0) + \frac{E_a}{RT} \quad (70)$$

Figure 144 is an Arrhenius plot for  $k$ . From this figure the slope of the line,  $E_a/R$ , was found to be -7657 K, corresponding to an activation energy of 63 kJ/mol and the intercept,  $\ln(A_0)$ , was found to be 18.6 resulting in  $A_0$  equal to  $1.16 \times 10^8$ .

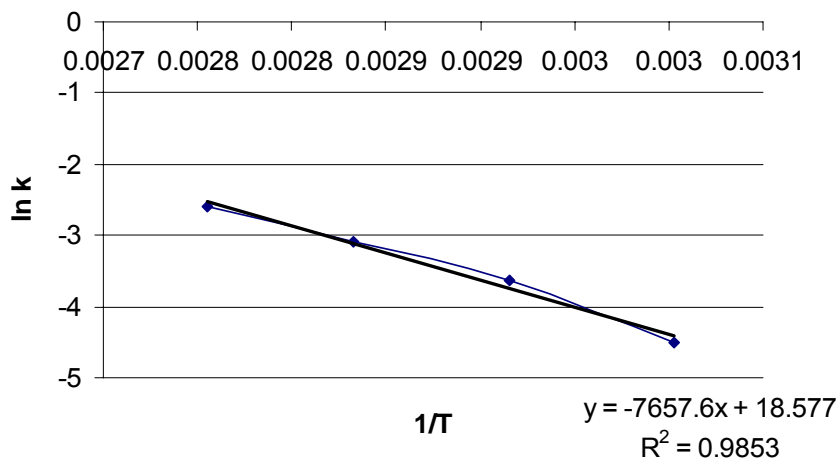


**Figure 144. Plot of  $\ln(k)$  versus  $1/T$  used to determine  $E_a$  and  $A_0$**

A complete rate expression takes the following form (Eq. 71):

$$\frac{d[E]}{dt} = 1.16 \times 10^8 e^{\left(\frac{-7,657}{T}\right)} [E]^{0.79} [C]^{0.88} \quad (71)$$

Integrating Eq. 71 yields the following relationship (Eq. 72):

$$[E]^{0.21} - 4.76 = 1.16 \times 10^8 e^{\left(\frac{-7,657}{T}\right)} [C]^{0.88} t \quad (72)$$

Equation 72 can then be solved for [E] as a function of time and plotted alongside the experimental data as shown for representative temperatures of 60°C and 80°C in Figure 145 and Figure 146, respectively. The results indicate that the model fits the data well.

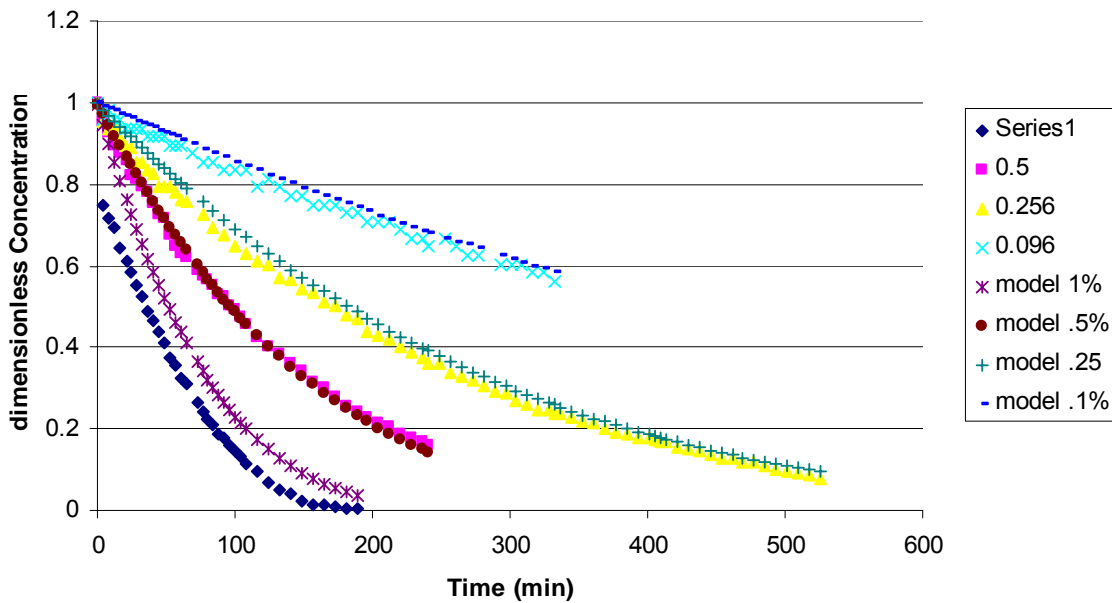


**Figure 145.** Plot showing a change in concentration [E] as a function of time for both model and experimental data at varying [C] for data obtained at 60°C.

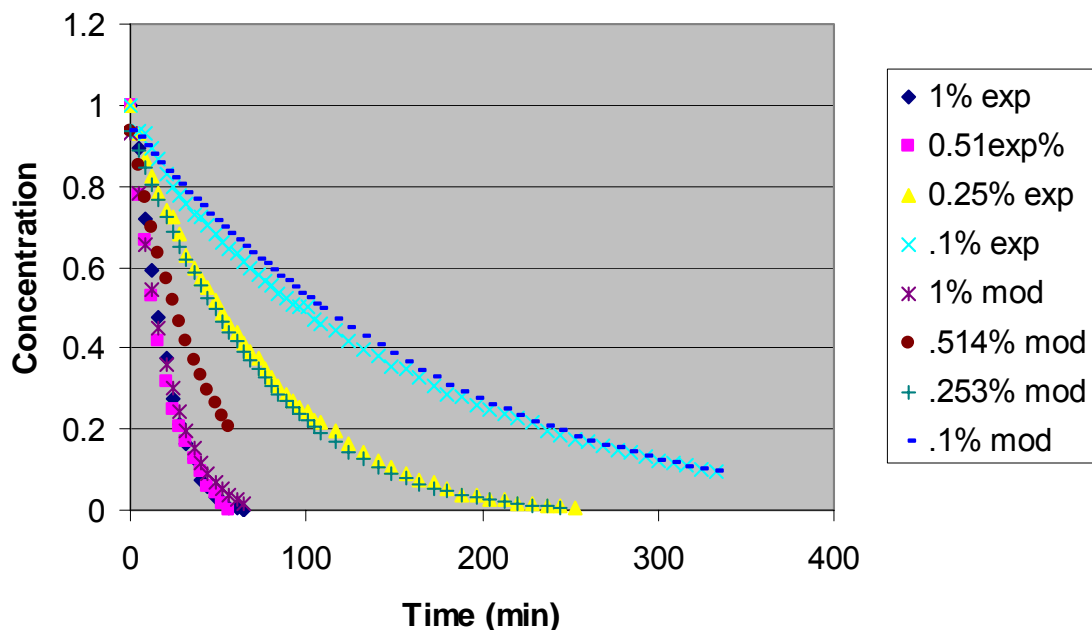


**Figure 146.** Plot showing a change in concentration [E] as a function of time for both model and experimental data at varying [C] for data obtained at 80°C.

#### 3.2.4.5.3 Conclusions

Through the use of IR spectroscopy, the FA methacrylation reaction was monitored. By varying the catalyst concentration and reaction temperature, a kinetic model was developed to fit experimental data. This model was found to be a good predictive tool for the range of conditions investigated. It will therefore be possible to predict reaction times over a range of conditions. This is an important contribution to future reactor design for industrial production of the MFA.

### 3.2.4.6 Scale-Up of MFA Production

#### 3.2.4.6.1 Introduction

Until recently, MFA monomers have only been produced in batches of 500 mL at the largest. For these monomers to be actual replacements for styrene in VE and UPE resins, these monomers must be produced in large quantities. This work describes the procedures used to scale up the reaction to 20 L in size. From there, scale-up to larger batches can be accomplished.

#### 3.2.4.6.2 Experimental Procedure

Lauric acid and glycidyl methacrylate (GM) react in stoichiometric quantities to form a single product, MLau. Lauric acid (Twin Rivers) was a solid block inside a 5 gallon bucket. We removed the lauric acid from the bucket by chopping it up into a fine powder using a garden spade and shoveling the reactant out into a three liter beaker. Once the beaker was full, it was weighed. The contents were added to the 20 L reactor by lifting the top section of the reactor and pouring the lauric acid into the reactor. The beaker was re-weighed to determine the amount

of lauric acid added to the reactor. This procedure was repeated until approximately 5800 g of lauric acid had been added to the reactor.

The AMC-2 catalyst was used to catalyze the reaction. The catalyst concentration used was 0.5 wt% of the entire reaction contents. The mass of the reaction contents was calculated based on the amount of lauric acid in the reactor and the amount of GM that should be added to the reactor to have a 1:1 molar ratio of the two reactants. The AMC-2 was then added to the reactor through a port at the top. It is important not to mix the AMC-2 into the GM directly, as the AMC-2 will induce reaction of the GM.

Because of the hazardous nature of GM, care was taken to avoid exposure to the chemical, which is also a reason why this chemical was added last. Inside a hood, a hand pump was used to extract GM from its 5 gallon can, into a ~800 ml bottle. The bottle was capped and weighed. The contents were then carefully poured into the top of the reactor. The bottle was then capped and re-weighed to determine the amount of GM charged to the reactor. This procedure was continued until a stoichiometric quantity of GM was added.

Temperature was measured in the reactor at three different locations. One thermocouple was placed into the reaction mixture. This thermocouple was only used to monitor the reaction temperature, and was not used to control the temperature. Two thermocouples were placed on the outside of the reactor. One was placed in the middle of the heating jacket that heated the side walls of the reactor. The other thermocouple was placed at the meeting point of the heating jacket and the heating mantle at the reactor base. These thermocouples were used to control the temperatures of the heating jacket and the bottom heating mantle, respectively. The set point temperature on the outside of the reactor was set to 70°C to reduce the likelihood of a temperature spike.

Once all of the GM was added, the reactor was sealed. Water was immediately flowed through the condenser to reduce evaporative losses of GM. Unfortunately, because of the quantity of solid lauric acid in the reactor, it was initially very difficult to lower the impeller blade and cooling coils completely into the reactor. Therefore, the reactor was heated using the heating jacket. Shortly thereafter, we were able to completely lower the impeller and cooling coils. The impeller was then used to mix the reaction contents at a low speed (~35 rpm). As the reaction contents became more and more dissolved, the mixing speed was increased, up to as high as 200 rpm.

The heating jacket was allowed to heat for 2 hours. Because the base heating mantle was not used, the temperature did not exceed 45°C during the course of the afternoon. After 2 hours, the heating was stopped to prevent any overnight problems. The water to the condenser was stopped 30 minutes later to prevent overnight flooding. It should be noted that the reaction mixture contained at least 30% by volume undissolved chunks of lauric acid when I left for the night. However, the next morning, the reaction contents were homogeneous and the reaction temperature was approximately 42°C. This indicates that the reaction temperature probably went at least as high as 50°C overnight, and reaction occurred overnight.

Acid number tests were performed in accordance with ASTM D1980-87. FTIR spectra comprised of 16 scans with a resolution of 4  $\text{cm}^{-1}$  from 4000-400  $\text{cm}^{-1}$  were taken every 30 seconds during the course of the reaction. A 600 MHz Bruker (16 scans at 293 K, 90° pulse width) was used to run  $^1\text{H}$ -NMR of the MLau samples. The viscosity of the samples were also measured with a TA Instruments AR2000 rheometer using 40 mm parallel plates in a steady state flow experiment with a rotation rates ranging from 0.1  $\text{s}^{-1}$  to 10  $\text{s}^{-1}$ .

#### 3.2.4.6.3 Results/Discussion

FTIR, NMR, and acid number tests were indicated that the reaction had gone to completion. Viscometry was also run on the sample to ensure that the product was acceptable. Previous MLau samples had viscosities of  $\sim 60$  cP using a Brookfield digital viscometer in Couette geometry at 30°C. The results showed that the viscosities of both the final MLau sample and previously prepared MLau samples made on a smaller scale were 70 cP. Therefore, it is likely that the quality of both MLau batches were similar.

#### 3.2.4.6.4 Conclusions

Scale up of the MLau to 20 L scale was successful. We also found that:

- FTIR, NMR, acid number, and viscosity tests indicate that the product were of similar or better quality than previously made smaller scale MLau products.
- A reaction temperature of  $\sim 50^\circ\text{C}$  was found to work very well for this reaction.
- 0.5 wt% AMC-2 catalyst did a good job of catalyzing the reaction and preventing epoxy homopolymerization.

### 3.2.4.7 Unsaturated Polyester Resins

#### 3.2.4.7.1 Introduction

The purpose of this study was to evaluate the compatibility of the MOA and the Di-Br-MSA monomers in Viapal UPE resins and determine the liquid resin and polymer properties of the Viapal-Br-SAGAMA-MOA resins for potential applications. In order to prepare binary and ternary blends of the UP resin with the fatty acid based monomers and styrene, a commercially available unsaturated polyester without styrene was used. The viscosities of these binary and ternary blends with 65-55 wt.% UPE compositions were determined. DMA was performed on these resins to determine the effect of fatty acid based comonomer content and bromination on the modulus and  $T_g$  of the network.

#### 3.2.4.7.2 Resin Formulation

The UPE used in this study was VIAPAL 570G (Surface Specialties UCB), which is a low reactivity general purpose unsaturated polyester based on phthalic anhydride, ethylene glycol, and maleic anhydride. The VIAPAL 570G was a colorless solid in the form of granules with a melting range of 80-90°C. The Viapal 570G resin is designed to be used as anti-corrosive paint for metals, concrete and other substrates. This specific UPE resin was used in this study, since it

was commercially available without styrene. The MOA and the Di -BrMSA monomers were prepared as described in previous sections.

The UPE-styrene solutions at 35-45 wt.% styrene concentrations were prepared by magnetic agitation of the UPE in styrene at room temperature. For the ternary blends of the UPE–styrene and the fatty acid based monomers with 45 wt.% comonomer content, the mixtures were heated at around 80°C and mixed. For the preparation of the blends containing 35 wt.% comonomer, the UPE which is in the form of granules was powdered before use with a mortar and pestle. The blends were heated to 90°C and mixed. The viscosities of all the resins were measured using a Brookfield digital viscometer as previously described. For the resins with 45 wt.% fatty acid monomer or 35 wt.% styrene content, the viscosities were measured using spindle #21 at 5 rpm. For all the other resins containing 35 wt.% fatty acid monomer, the viscosities were measured using spindle #27 at 5 rpm.

### 3.2.4.7.3 Liquid Resin Properties

The binary and ternary blends of the Viopal 570G with styrene and the fatty acid based monomers, prepared in this study are listed in Table 43. The solutions of the UPE in styrene were colorless and clear liquids. The solution of the UPE in MOA with 45 wt.% MOA content was a milky green colored paste at room temperature with a viscosity of 47200 cP at 50°C. The MOA monomer had a much higher viscosity than styrene. The viscosity of this solution decreased drastically with increasing temperatures as shown in Figure 147. The UPE was insoluble in the Br-MSA comonomer in the 35-60 wt.% Br-MSA concentration range. The mixtures were heated to temperatures as high as 110°C which resulted in partial gelation.

**Table 43. The viscosities of the Viopal 575G, MOA, Br-MSA, styrene blends.**

Br-MSA Wt.%	MOA wt.%	Styrene Wt.%	Viopal 575 G Wt.%	Viscosity (cP) (25°C)
-	-	45	55	300(±40)
-	45	-	55	47200(±400) (50PP <sup>OPP</sup> C)
-	<b>10</b>	<b>35</b>	<b>55</b>	<b>760(±80)</b>
-	20	25	55	3200(±80)
-	30	15	55	4280(±80)
<b>10</b>	-	<b>35</b>	<b>55</b>	<b>880(±80)</b>
20	-	25	55	4040(±80)
30	-	15	55	25400(±80)
-	-	35	65	3240(±80)
-	10	25	65	9400(±400)
-	15	20	65	19200(±400)
-	20	15	65	29200(±400)
10	-	25	65	11400(±400)
15	-	20	65	45200(±400)
20	-	15	65	20000(±400) (50PP <sup>OPP</sup> C)

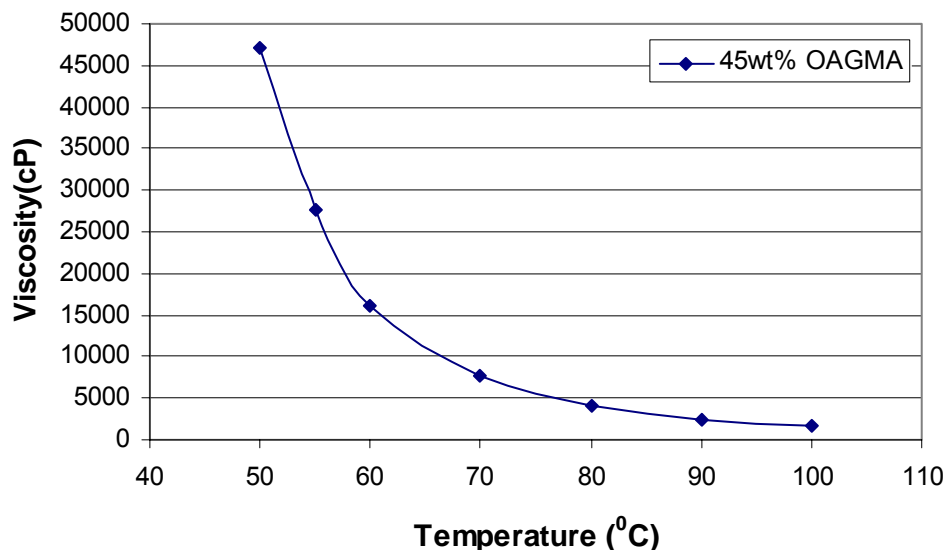


**Figure 147. The viscosity of the of the 45 wt.% MOA-55 wt.% UP resin as a function of temperature.**

At 45 wt.% comonomer content, all the ternary blends of the UPE with styrene and MOA or Br-MSA listed in Table 43, except the resin with 30wt% Br-MSA, were clear green-colored liquids. At 35 wt.% comonomer content, ternary blends containing less than 20 wt.% styrene, and therefore more than 15 wt.% of the oleic acid based monomer, were cloudy. Blends with 20 wt.% styrene and higher styrene contents were clear. The viscosities of all the UPE solutions with 35-45 wt.% comonomer content, are listed in Table 43. For the resins containing 45 wt.% MOA and 20 wt.% Br-MSA-15 wt.% styrene which are solid at room temperature, the 50°C viscosities are listed. Figure 147 and Figure 148 show the change of viscosity with increasing temperature for the 45 wt.% MOA and the 20 wt.% and 30 wt.% Br-MSA resins respectively. As can be seen for both of the MOA and the Br-MSA-styrene resins, the viscosity decreased exponentially with increasing temperature. The viscosities of all the three resins are in a processable range at temperatures above 90°C.

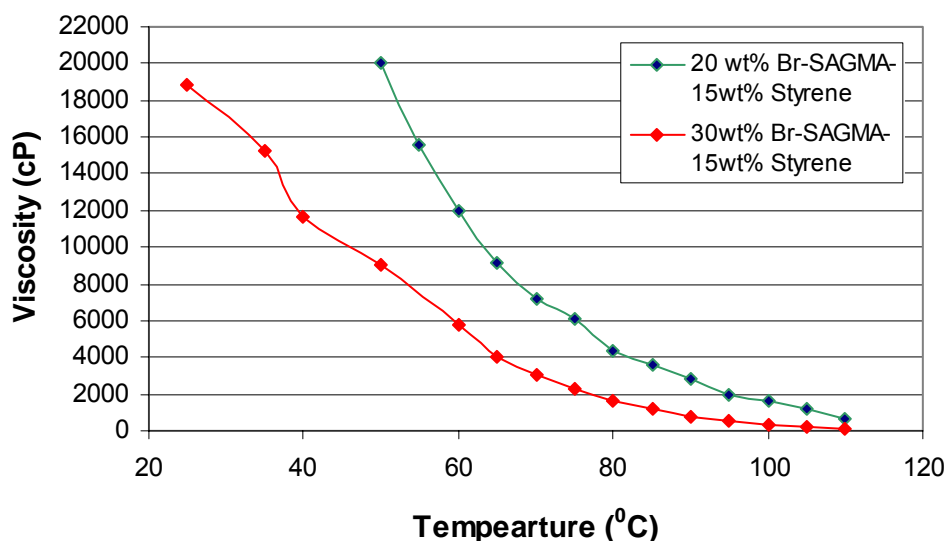


**Figure 148.** The viscosity of the of the 20 wt.% Br-MSA-15wt% Styrene-55wt% UPE resin and the 30 wt.% Br-MSA-15wt% Styrene-55wt% UP Eas a function of temperature.

A quick examination of the table clearly shows the expected trends. The viscosity of the resins decreased with increasing styrene content of the resin. At the same concentrations, the resins containing MOA comonomer had lower viscosities than the resins containing Br-MSA comonomer. These trends are expected because the viscosities of the comonomers increased considerably in the following order:

$$\text{Styrene}(0.7 \text{ cP}) < \text{MOA}(64 \text{ cP}) < \text{Br-MSA}(834 \text{ cP}) \quad (25^\circ\text{C})$$

These results show that the comonomer content needs to be at least 45 wt.% and the styrene content must be at least around 35 wt.% to have viscosities suitable for a liquid molding process with these MOA and Br-MSA monomers and the VIAPAL 570G UPE. However, as mentioned earlier, lower viscosities can be achieved at higher temperatures and with lower MW UPE resins. These high viscosity VIAPAL 570 G resins, on the other hand, may have potential applications as fire resistant coatings.

#### 3.2.4.7.4 Polymer Properties

##### *Experimental*

The compositions of the Viapal 570G polymers prepared in this work are as listed in Table 43. For the cure of the resins with 45 wt.% total comonomer content, Methyl-ethyl-ketone peroxide (MEKP)-Cobalt-naphthanate initiator-catalyst system was used. The MEKP obtained from Aldrich Chemical Company was 45% solution in plasticizers. The initiator (MEKP, 45% soln.) concentration was 2% of the total resin weight and the catalyst (Co-Nap, 6% soln.) was 0.3% of the total resin weight. The resins containing 45 wt.% comonomer, with the exception of the resin with 45 wt.% MOA, were all cured at room temperature with a gel time of 30 minutes or less. For the resins containing 35 wt.% comonomer, and the resin with 45 wt.% MOA, a high temperature cure cycle was employed to avoid air bubbles formed because of the high viscosity of these resins at room temperature. These resins were cured at 90°C for two hours in the

presence of 2 wt.% of the MEKP, post-cured at 120°C for 1 hr and 150°C for 1 hr. Dynamic mechanical analysis was used to determine the thermo-mechanical properties of the polymers using a temperature ramp to 200°C at 2°C/min. Two temperature ramps were performed for each sample. The results of the second test were taken as the properties of the post-cured samples.

### *Results and Discussion*

The cured Viapal resins containing MOA, Br-MSA, and styrene as the comonomers exhibited different physical appearance, depending on the comonomer identity and concentration. The Viapal-styrene polymers were colorless and clear. The Viapal MOA and Br-MSA polymers were green colored. However the 10 and 15 wt.% Br-MSA (25 wt.% and 20 wt.% styrene, respectively) polymers exhibited a distinctive yellow color. Additionally, the resins containing MOA and styrene at 45 wt.% total comonomer concentration, which were cured at room temperature, changed their color from green to orange at the end of the first temperature ramp from room temperature to 200°C during DMA. This color change was less noticeable for the resins containing MOA and styrene at 35 wt.% total comonomer concentration. The resins containing Br-MSA did not exhibit any color change during post-cure.

The  $E'$  and  $T_g$  values of the post-cured Viapal UPE resins at 45 wt.% total comonomer concentration are listed in Table 44. A quick examination of the table clearly shows that both the storage modulus and  $T_g$  values of the resins decreased as the fatty acid comonomer content of the resins increased. This result is expected because the aromatic structure of styrene brings more rigidity to these systems compared to the fatty acid based monomers, which have long flexible alkyl chains as pendant groups. The resins containing Br-MSA instead of MOA exhibited increased  $T_g$  values and slightly higher modulus values at the same fatty acid comonomer content. The resins containing MOA as the fatty acid monomer exhibited two peaks in their tan delta curves at 20 wt.% and 30 wt.%, as shown in Figure 149. The 10 wt.% MOA polymer exhibited only one peak. Figure 149 indicates that the Viapal-MOA-styrene polymers exhibited phase separation at 20 wt.% and higher MOA concentrations. The lower  $T_g$  peak should represent an MOA rich phase and the higher  $T_g$  peak should represent a styrene rich phase since the replacement of styrene with the fatty acid based monomers decreased the  $T_g$  of these systems as discussed above. Figure 150 (a) and (b) show that the Viapal-Br-MSA-Styrene polymers did not show phase separation at 20 wt.% and 30 wt.% Br-MSA concentrations. The phase separation observed for the MOA-Viapal resins at higher MOA contents can be attributed to the non-polar structure of the alkyl chains in this monomer which should make it less compatible with the comparatively more polar UPE backbone. The use of shorter MFA monomers could make this system more compatible because of their increased polar nature. At the same time, shorter fatty acids will also reduce resin viscosity and improve polymer properties. The presence of the polar bromine groups on the fatty acid chains should make the Br-MSA monomer more compatible with the UPE system, as shown in Figure 150. The increased  $T_g$  values of the Viapal Br-MSA polymers as compared to the Viapal-MOA polymers at the same fatty acid comonomer content, in the same way, may be attributed to the introduction of the polar bromine groups to the network which should increase the polar interactions between the fatty acid chains. The phase separation observed for the MOA polymers may also result in decreased  $T_g$  and modulus values for these polymers as compared to the Br-MSA polymers.

**Table 44. E',E'' and T<sub>g</sub> values of the post cured Viapal UPE resins at 45 wt.% total comonomer concentration.**

Br-MSA wt.%	MOA wt.%	Styrene wt.%	VIAPAL 570G wt.%	E' (30°C) (GPa)	T <sub>g</sub> (°C) (E'' max)	T <sub>g</sub> (°C) (Tan delta max)
-	-	45	55	3.1	92	107
-	45	-	55	0.19	48	-
-	10	35	55	3.0	71	93
-	20	25	55	2.2	53	65 96
-	30	15	55	0.96	-	50 92
10	-	35	55	3.0	75	92
20	-	25	55	2.3	59	80
30	-	15	55	1.5	45	65

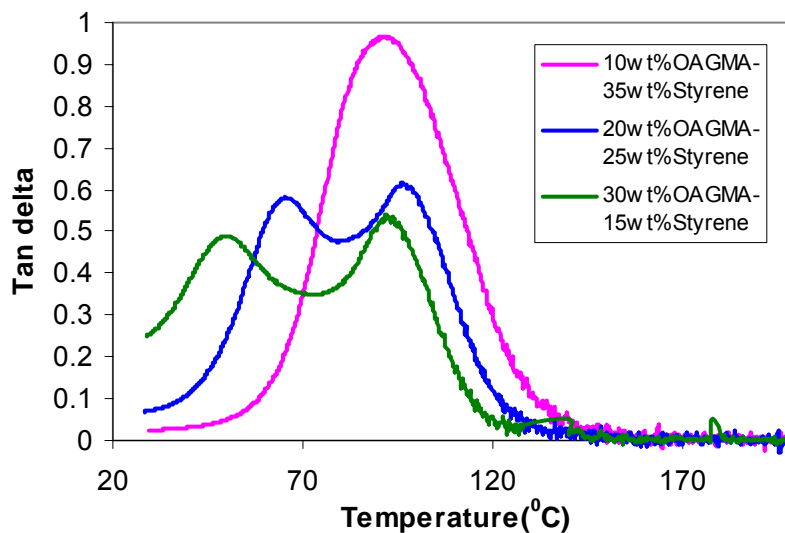
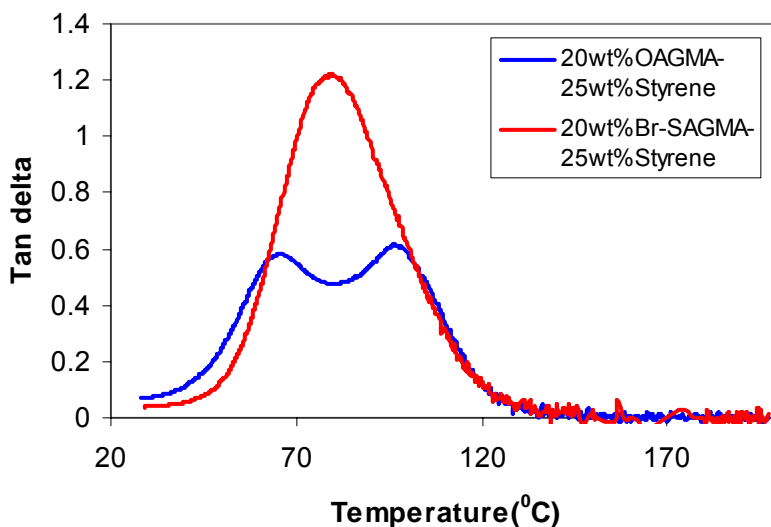
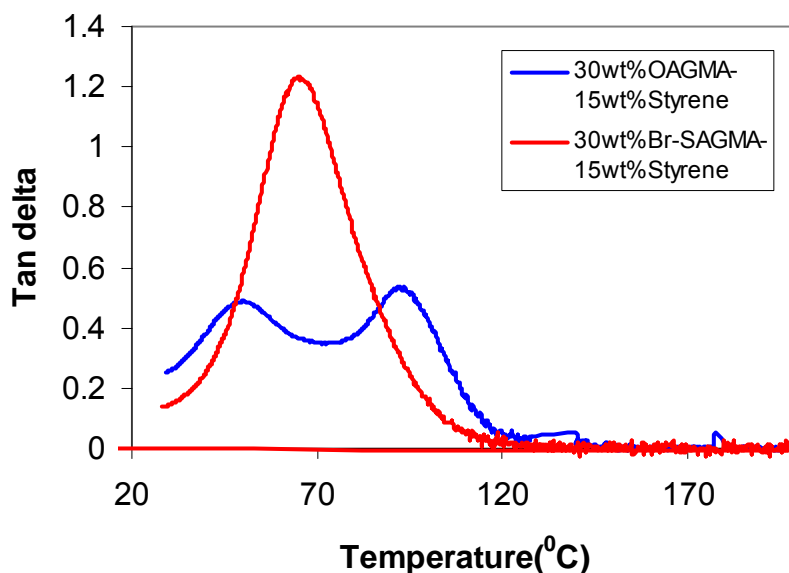


**Figure 149. The tan delta curves of Viapal-MOA-Styrene polymers at 10-30 wt.% MOA content. (45 wt.% total comonomer content)**



(a)



(b)

**Figure 150. The tan delta curves of Viapal-MOA-Styrene and Viapal-Br-MSA-Styrene Polymers at (a) 20 wt.% and (b) 30 wt.% fatty acid comonomer content.**

The  $E'$  and  $T_g$  values of the high temperature cured Viapal UPE resins at 35 wt.% total comonomer concentration are listed in Table 45. The properties of the post-cured resins are listed in Table 46. A comparison of the two tables shows that, although the samples were cured at 90°C and post-cured at 120°C and 150°C for 1 hour, the temperature ramp to 200°C during the second DMA run caused a considerable increase in the modulus and  $T_g$  of the polymers. As expected, both the modulus and  $T_g$  values decreased with increasing fatty acid comonomer content. The resins with Br-MSA monomer exhibited higher  $T_g$  values than the polymers with the MOA monomer at the same concentrations, although the modulus values did not have a clear

difference. The MOA polymers similarly exhibited two peaks in their tan delta curves as observed for the samples with 45 wt.% total comonomer content. Figure 151 shows the tan delta curves for the polymers with 10-20 wt.% MOA content. As can be seen, phase separation starts at 15 wt.% MOA content, where a second peak becomes apparent in the tan delta curve. The Br-SAGAMA polymer, on the other hand, exhibited one peak in the same composition (Figure 152). Higher concentrations of Br-MSA polymers were not prepared because of processing difficulties.

**Table 45. E',E'' and T<sub>g</sub> values of the high temperature cured Viopal UPE resins at 35 wt.% total comonomer concentration.**

Br-MSA Wt%	MOA wt%	Styrene wt%	E' (30°C) (GPa)	T <sub>g</sub> (°C) (E'' max)	T <sub>g</sub> (°C) (Tan delta max)
-	-	35	2.797	91.07	107.17
-	10	25	2.571	71.34	86.08
-	15	20	2.237	62.07	76.63
-	20	15	1.803	49.48	65.89
10	-	25	2.492	74.81	99.0
15	-	20	2.256	66.75	80.51

**Table 46. E',E'' and T<sub>g</sub> values of the post-cured Viopal UPE resins (2<sup>nd</sup> run DMA) at 35 wt.% total comonomer concentration.**

Br-MSA Wt%	MOA wt%	Styrene wt%	E' (30°C) (GPa)	T <sub>g</sub> (°C) (E'' max)	T <sub>g</sub> (°C) (Tan delta max)
-	-	35	3.424	99.63	113.54
-	10	25	2.976	75.02	92.43
-	15	20	2.643	67.16	81.34
-	20	15	2.122	53.57	68.6
10	-	25	2.909	79.1	92.8
15	-	20	2.926	68.46	94.43
					85.93

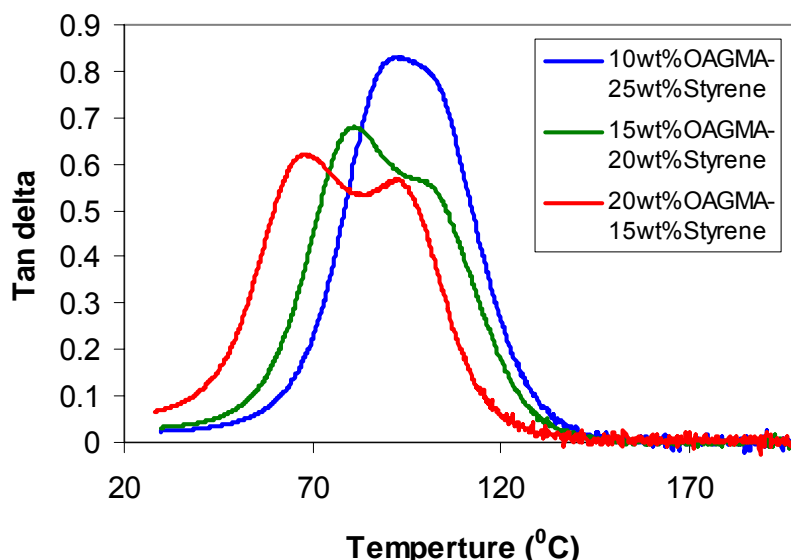


**Figure 151.** The tan delta curves of Viopal-MOA-Styrene polymers at 10-20 wt.% MOA content. (35 wt.% total comonomer content)

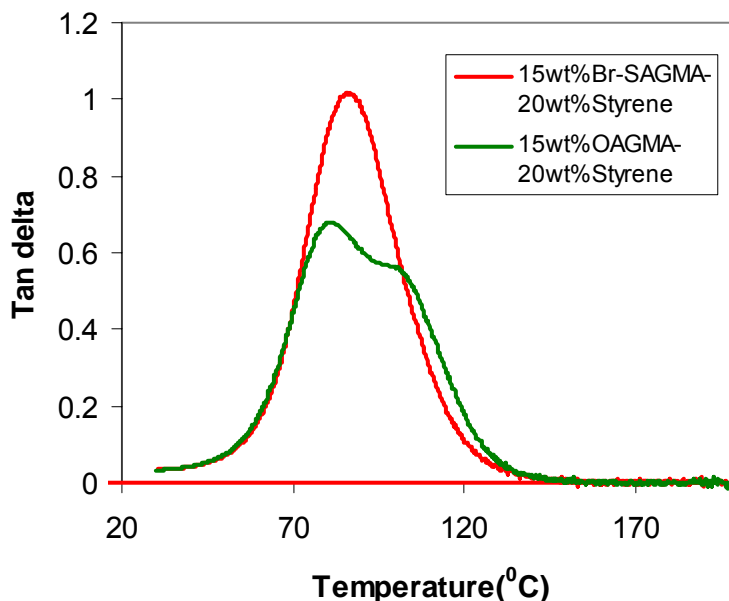


**Figure 152.** The tan delta curves of Viopal-MOA-Styrene and Viopal-Br-MSA-Styrene Polymers at 15 wt.% fatty acid comonomer content.

#### 3.2.4.7.5 Conclusions

The Viopal 570G - MOA and Br-MSA resins exhibited high room temperature viscosities thereby limiting their use in processes like vacuum assisted resin transfer molding (VARTM). The  $T_g$  values of these polymers were also all lower than 100°C, showing that these polymers are not suitable for transport or structural applications. However the Viopal 570G-Br-MSA polymers may have potential uses in fire resistant coating applications (where low viscosity is not a stringent requirement). Further investigation should be performed with lower viscosity and

higher  $T_g$ . UPE resins to explore the potential of the use of the fatty acid based monomers in these resin systems for structural applications.

### **3.2.4.8 Novalac Type Vinyl Ester (VE 160) - MOA-Br-MSA – Styrene Liquid Resin and Polymer Properties**

#### *3.2.4.8.1 Introduction*

The MOA and the Br-MSA comonomers decreased the glass transition temperature ( $T_g$ ) and modulus of the Bisphenol A type VE resins (VE 828) when used as replacements for styrene. In an effort to increase the  $T_g$  and the modulus of these systems, VE 160 which is a Bisphenol F type Novalac resin, was used instead of VE 828. VE 160 was prepared via methacrylation of Epon 160 which is a Bisphenol F/ Epichlorohydrin type epoxy resin, as shown in Figure 153. Epon 160 is an epoxy novalac resin with an average functionality of 2.5 ( $n=0.5$ ). It has an epoxy equivalent weight of 174 g/mol as determined by the ASTM standard ASTM D1652. The VE 160 also has an average functionality of 2.5 (Figure 153) as opposed to 2 for the VE 828. Thus the replacement of the VE 828 with VE 160 should increase the cross-link density and therefore the  $T_g$  and the modulus of the resulting polymers. In this study, similar to the previous work on the VE 828 and UPE resins, first the viscosities of the VE 160-MOA-Br-MSA-styrene blends were determined. DMA analysis on these polymers was then performed to determine the effect of both the type and content of the fatty acid comonomer on the  $T_g$  and modulus values of the network. Ideal formulations involving the fatty acid based monomers for the VE 160 polymers were then determined according to these results. Previous work has shown that the VE 828-methacrylated butyric acid (MBut) and VE 828-methacrylated caproic acid (MHex) polymers have the optimum properties among all the VE 828 polymers prepared using fatty acid based comonomers with different carbon lengths. Thus, VE 160 polymers with MBut and MHex comonomers were also prepared. Finally, a comparison of the properties of the VE 160 polymers with the VE 828 polymers at similar comonomer contents was made.

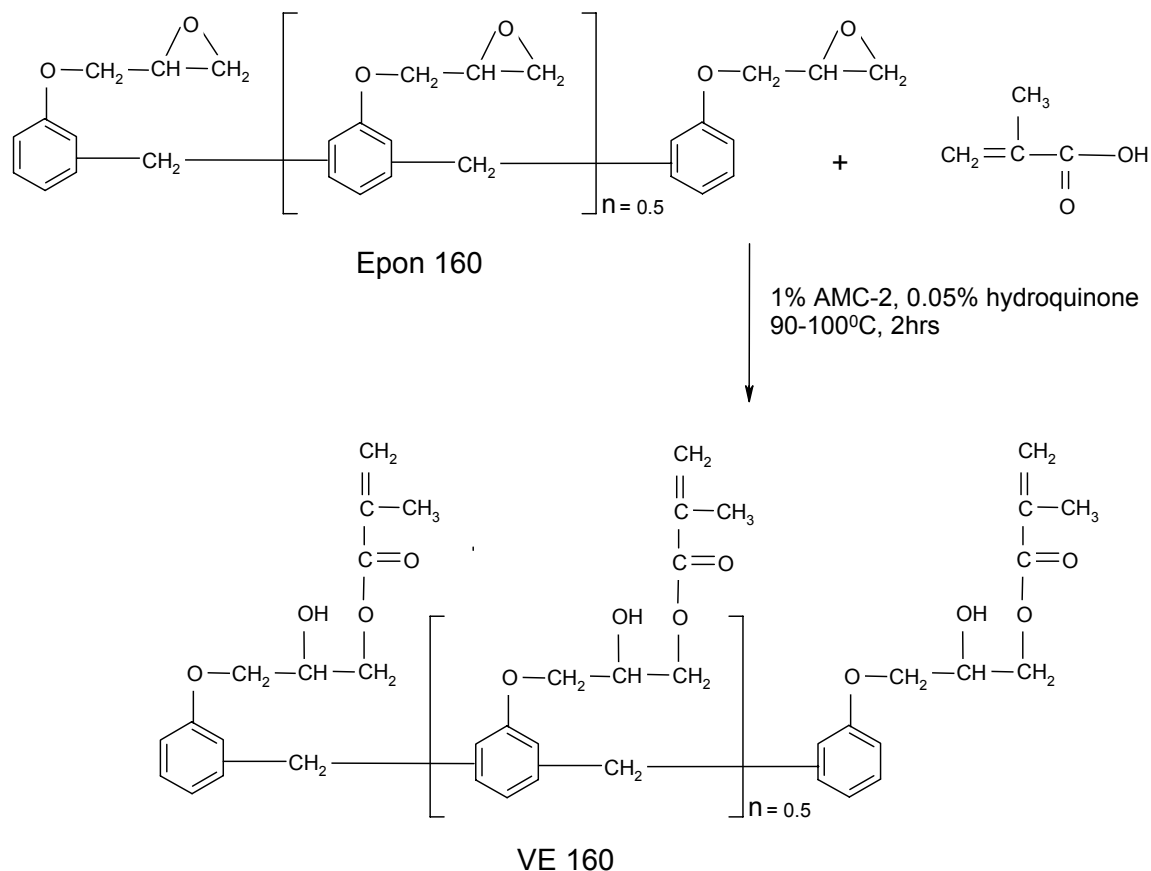


**Figure 153. The synthesis of VE 160 from Epon 160 and methacrylic acid.**

#### 3.2.4.8.2 VE 160 - MOA-Br-MSA – Experimental

For the preparation of VE 160 resin, 200g Epon 160 resin was reacted with 1.01 times the stoichiometric amount of methacrylic acid (99.84g) necessary to convert all the epoxies to methacrylates. The reaction was run in the presence of 1 wt.% AMC-2 catalyst and 0.05 wt.% hydroquinone for 2 hours at 90°C. At the end of this time, the Mid IR spectrum of the product showed no epoxy peak at 917 cm<sup>-1</sup> confirming the conversion of all the epoxy functional groups to methacrylates. The acid number of the VE 160 product was 4 as determined in accordance with the ASTM standard ASTM D1980-87, showing that little unreacted methacrylic acid remained.

For the preparation of the VE 160-MOA-Br-MSA-styrene blends, the VE 160 was first heated to 60-70°C, and then the comonomers were added and mixed at room temperature with magnetic stirring for about two hours. The weight compositions of all the solutions prepared are listed in Table 47. The VE 160 was soluble in both MOA and Br-MSA comonomers. The viscosities of all the blends were measured using a Brookfield Digital viscometer at 25°C. Additionally, for the 35 wt.% and 45 wt.% Br-MSA and MOA resins, the solution viscosities were measured at increasing temperatures. For all the blends except for the 35 wt.% Br-MSA solution, the viscosities were measured using spindle type #21 at a speed of 20 or 50 rpm, to record the most

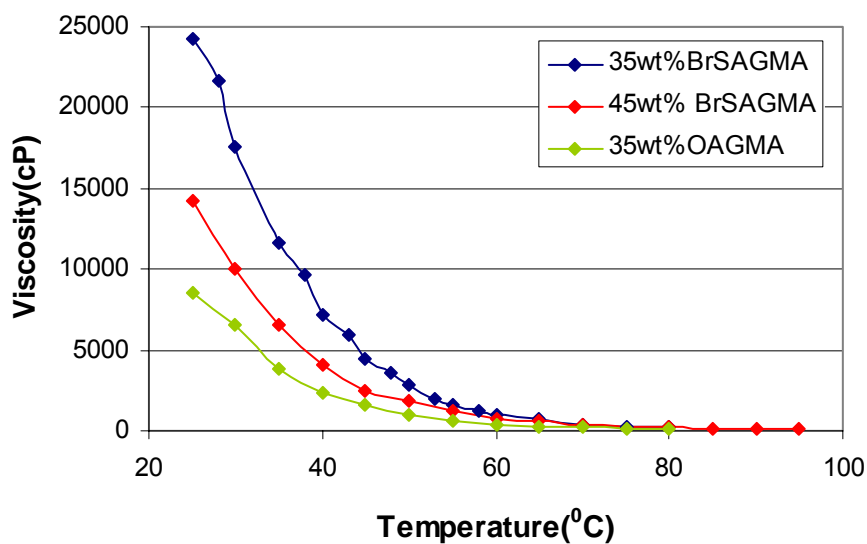
stable reading. For the 35 wt.% Br-MSA solution, the viscosity was determined using spindle type #27, at a speed of 20 rpm.

**Table 47. The viscosities of the Epon 160, MOA, Br-MSA, styrene blends.**

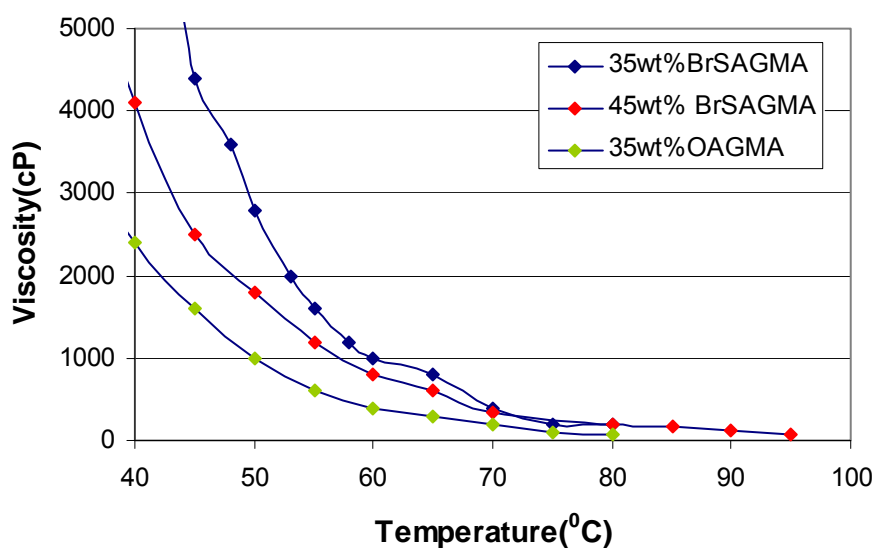
MOA wt.%	Br-MSA wt.%	Styrene wt.%	Epon 160 wt.%	Viscosity (cP) (25°C)
-	-	45	55	48(±8)
45	-	-	55	2544((±8)
-	45	-	55	17340(±20)
10	-	35	55	64(±8)
20	-	25	55	128(±8)
30	-	15	55	368(±8)
-	10	35	55	68(±8) 50 RPM
-	20	25	55	224(±8)
-	30	15	55	840(±20)
-	-	35	65	100(±8)
35	-	-	65	7800((±20)
-	35	-	65	24400(20 rpm #27)
10	-	25	65	344(±8)
15	-	20	65	480(±8)
20	-	15	65	750((±20)
-	10	25	65	340(±20)
-	15	20	65	620((±20)
-	20	15	65	1480((±20)

### 3.2.4.8.3 VE 160 - MOA-Br-MSA – Liquid Resin Properties

Table 47 lists the room temperature viscosities of the VE 160 resins. As can be seen, the viscosities of all the mixtures increased with increasing MOA and Br-MSA comonomer content, as expected. The viscosities of the 35 wt.% and 45 wt.% MOA and Br-MSA comonomers were too high at room temperature to be used in a liquid molding process. However as shown in Figure 154(a), the viscosities of these mixtures decreased exponentially with increasing temperatures. Figure 154(b) shows that the VE 160- MOA systems reached a processable viscosity (<1000 cP) at temperatures above 50°C, and the VE 160-Br-MSA systems reached a processable viscosity (<1000 cP) at temperatures above 60°C. The ternary blends containing styrene and MOA or styrene and Br-MSA all have viscosities that are suitable to be used in a liquid molding process at both 35 wt.% and 45 wt.% total comonomer concentrations, with the exception of the blend with 20 wt.% Br-MSA and 15 wt.% styrene. Thus, the VE 160-MOA-Br-MSA-styrene resin systems show a great potential, in terms of processability in liquid molding processes.



(a)



(b)

**Figure 154. (a) The change in the viscosity of VE 160-MOA and VE 160-Br-MSA resins with increasing temperature (b) magnified in the 0-5000 cP viscosity range.**

#### 3.2.4.8.4 VE 160 – Polymer Properties

##### *Experimental*

The VE 160 and comonomer content of the polymers prepared in this study are as listed in Table 47. The VE 160 resins using styrene or MOA as the reactive diluent were cured in the presence of 1.5 wt.% Trigonox and 0.8 wt.% CoNap. The VE 160 resins using Br-MSA as the reactive content were cured in the presence of 2.5 wt.% Trigonox and 0.8 wt.% CoNap. All the other VE

160 and VE 828 resin formulations were cured in the presence of 3 wt.% Trigonox and 0.8 wt.% CoNap.

### *Results and Discussion*

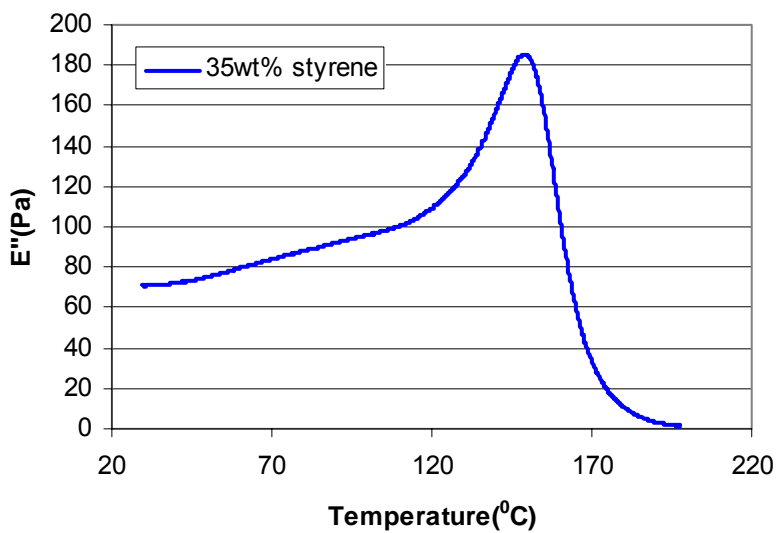
All the resins cured at room temperature changed color at the end of the first temperature ramp from room temperature to 200°C during DMA analysis, showing that the cure was incomplete at room temperature. The  $E'(30^\circ\text{C})$  and  $T_g$  values of the post cured VE 160 resins are listed in Table 48. Because the 35 wt.% and 45 wt.% MOA and Br-MSA polymers did not show a peak in the loss modulus curves, the tan delta maxima are listed in tables as well in order to compare the  $T_g$ s of these polymers. As can be seen in Figure 155(a), although the sample with 35 wt.% styrene exhibited a sharp peak in the loss modulus curve, a clear maximum cannot be observed in the loss modulus curves of the MOA and Br-MSA polymers (Figure 155b). A quick examination of Table 48 clearly shows that both the storage modulus and  $T_g$  values of the resins decreased as the fatty acid comonomer content of the resins increased, as previously observed for the VE 828 and UPE resins. However, all the red highlighted formulations in Table 48 have storage modulus values higher than 2 GPa and  $T_g$  values higher than 100°C, with processable viscosities at room temperature. For a comparison of the properties of the polymers with the same MOA and Br-MSA content, a clear trend was not observed. Although the polymer with the 45 wt.% MOA had a  $T_g$  5°C higher than that of the 45 wt.% Br-MSA polymer, the 35 wt.% Br-MSA polymer has a 3°C higher  $T_g$  than the corresponding MOA polymer. A number of effects should be considered in terms of the comparison of the glass transition temperatures of the VE polymers with the MOA and Br-MSA comonomers. The introduction of the polar bromine groups into the network by the Br-MSA comonomers could have an increasing effect on the  $T_g$  as compared to the MOA polymers, due to polar interactions between the fatty acid chains. However,  $T_g$  is typically not associated with intermolecular interactions. On the other hand, the bromine groups increase the molecular weight between cross-links thereby decreasing the cross-link density of the network as will be discussed in the next section, which have a decreasing effect on the  $T_g$  as compared to that of the MOA polymers.

**Table 48. The modulus E'(30°C) and the temperatures of E'' maximum and the tan delta maximum of the post-cured VE 160 resins.**

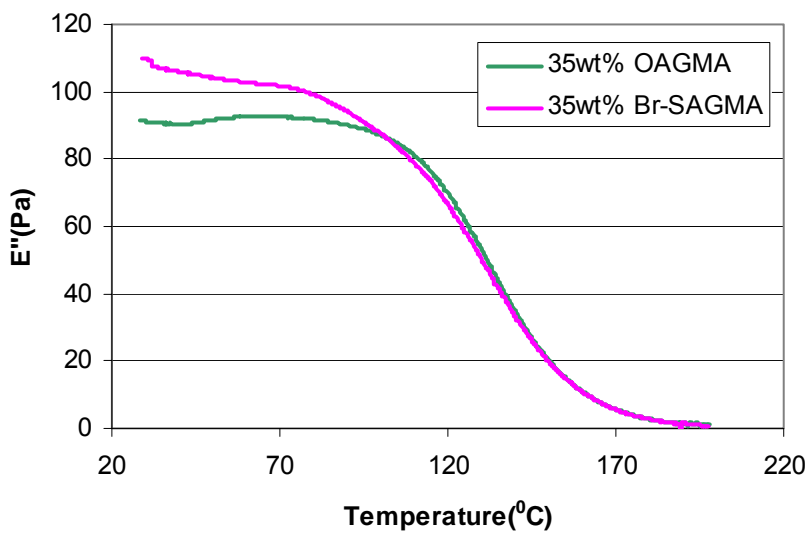
MOA wt.%	Br-MSA wt.%	Styrene wt.%	VE 160 wt.%	E' (GPa) (30°C)	E''max (°C)	Tan delta max (°C)
-	-	45	55	2.40	150	160
45	-	-	55	1.185	63.8	120.9
-	45	-	55	1.162	-	115.4
10	-	35	55	2.124	93.12	135.9
20	-	25	55	2.124	112.9	135.4
30	-	15	55	1.782	86	130.9
-	10	35	55	2.39	128.3	146.0
-	20	25	55	2.17	110.1	135.6
-	30	15	55	1.85	84.2	128.5
-	-	35	65	2.81	149.4	161.2
35	-	-	65	1.60	-	135.6
-	35	-	65	1.66	-	138.7
10	-	25	65	2.88	131.7	153.0
15	-	20	65	2.43	114.7	145.7
20	-	15	65	2.11	110.1	147
-	10	25	65	2.70	131.4	149.2
-	15	20	65	2.51	120.6	145.8
-	20	15	65	2.36	116.8	140.8

#### 3.2.4.8.5 Comparison of VE 160 and VE 828 Polymer Properties

Figure 156(a) and (b) show a comparison of the T<sub>g</sub>s (Tan delta max) and the 30°C storage modulus values of the VE 160 and VE 828 polymers at the same MOA, Br-MSA, and styrene concentrations. A comparison of the T<sub>g</sub>s and the 30°C storage modulus values of the VE 828 and VE 160 polymers prepared from butyric acid glycidyl methacrylate and hexanoic acid glycidyl methacrylates is also shown in Figure 157 (a) and (b), respectively. As can be seen, the VE 160 polymers exhibited about 5-30°C higher T<sub>g</sub> values than those of the VE 828 polymers at the same comonomer concentrations. On the other hand, the modulus values are generally slightly lower for the VE 160 formulations relative to the corresponding VE 828 formulations. The VE 160 polymers exhibited higher moduli than the VE 828 polymers for the 35 wt.% MBut and 35-45 wt.% MHex copolymers. It is significant to note that T<sub>g</sub> values as high as 121°C and 103°C (E''max) can be obtained with 35 wt.% MBut and MHex VE 160 polymers, respectively, in the absence of styrene.

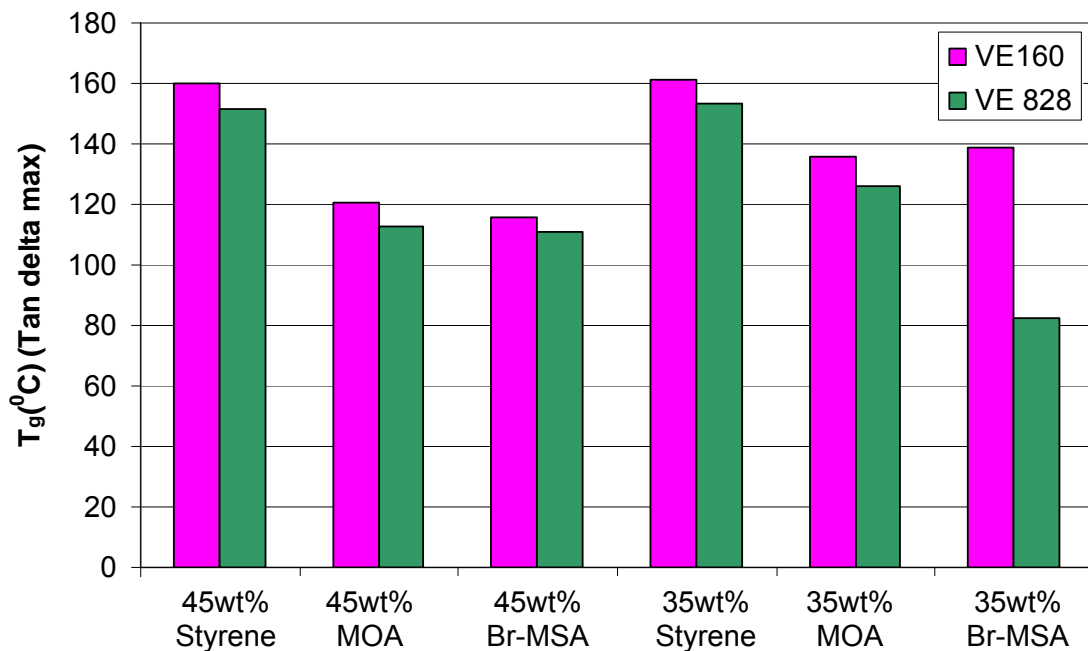


(a)

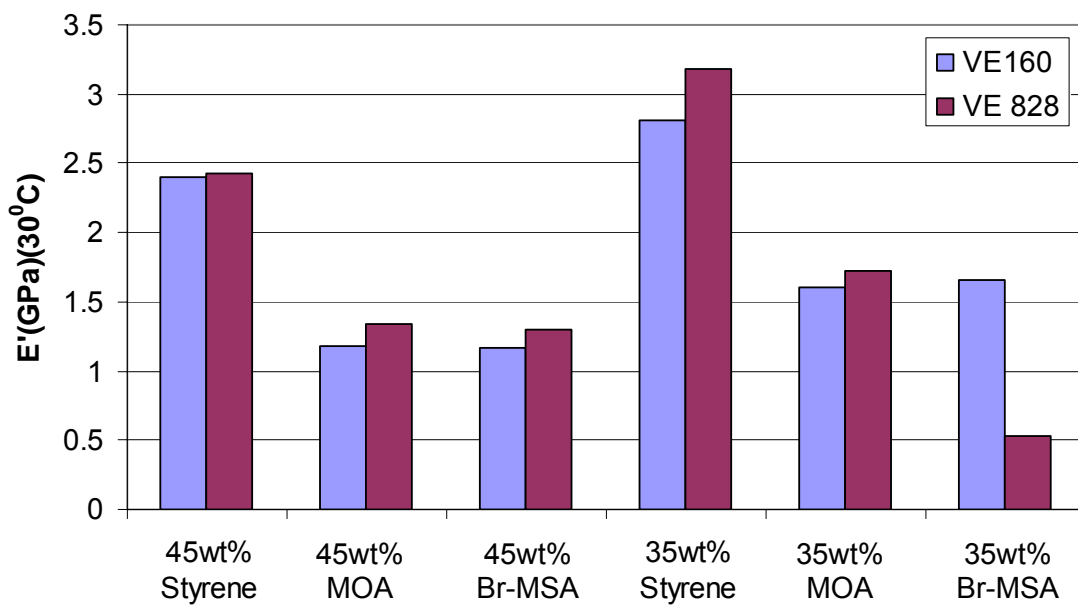


(b)

**Figure 155. The loss modulus curves of the (a) 35 wt.% styrene (b) 35 wt.% MOA and Br-MSA-VE 160 polymers.**

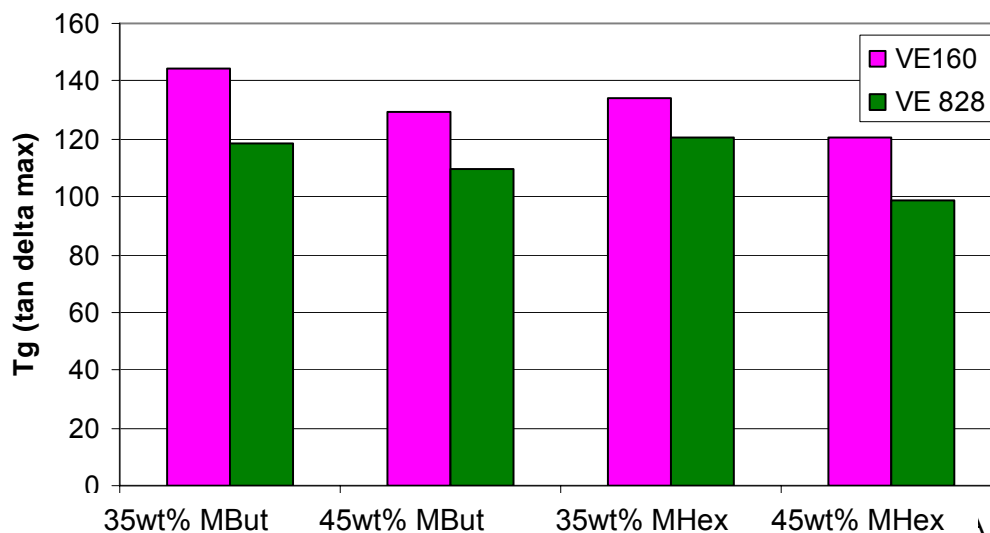


(a)

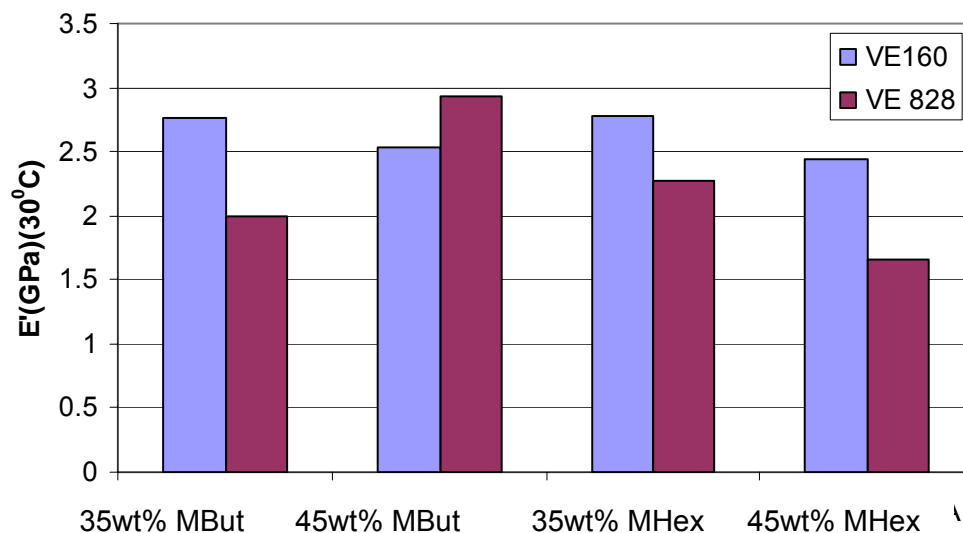


(b)

**Figure 156. Comparison of (a) the T<sub>g</sub>s (tan delta max) and (b) E' (30°C) of the post-cured VE 160 and VE 828 resins containing MOA, Br-MSA, and Styrene as reactive diluents.**



(a)



(b)

**Figure 157. Comparison of (a) the  $T_g$ s (tan delta max) and (b)  $E'(30^\circ\text{C})$  of the post-cured MBut, MHex-VE 160 and VE 828 resins.**

Table 49 shows the crosslink densities ( $\nu$ ) and the effective molecular weights ( $M_c$ ) of the VE 828 and VE 160 polymers as calculated from the DMA data using the modulus values in the rubbery plateau region and rubber elasticity. As expected, the cross-link densities of the VE 160 polymers were considerably higher than the VE 828 polymers for corresponding formulations. Apart from the 45 wt.% comonomer VE 160 polymers, the MOA polymers seemed to exhibit higher cross-link densities than the styrene polymers. This result was expected because the fatty acid monomers react to a lower extent and the VE monomers react to a higher extent in these resins, causing a higher crosslink density. Additionally for the same resin at the same

comonomer concentration, the Br-MSA polymers exhibited the lowest cross-link densities. This occurred because the bromine groups add extra molecular weight between cross-links.

**Table 49. The cross-link densities and the effective molecular weight values,  $M_c$ , of the post-cured VE 160 and VE 828 resins.**

MOA wt.%	Br-MSA wt.%	Styrene wt.%	VE 160 wt.%	$v$ (mol/m <sup>3</sup> )	$M_c$ (g/mol)
-	-	45	55	4056	253
45	-	-	55	3700	297
-	45	-	55	2631	445
-	-	35	65	5349	203
35	-	-	65	6217	182
-	35	-	65	4440	271
MOA wt.%	Br-MSA wt.%	Styrene wt.%	VE 828 wt.%	$v$ (#/m <sup>3</sup> )	$M_c$ (g/mol)
-	-	45	55	2405	426
45	-	-	55	3277	336
-	45	-	55	2592	453
-	-	35	65	3528	
35	-	-	65	4945	225
-	35	-	65	546	2173

The slight decrease in the modulus of the VE 160 polymers as compared to the modulus of the VE 828 polymers is probably due to a chemical structure effect. While the increased cross-link density is expected to increase both the  $T_g$  and the room temp modulus values, the effect of the chemical structure may dominate the cross-link density effect for the modulus. In this case, the neopentyl center of the Bisphenol A backbone of the VE 828 polymer may be responsible for increased modulus values. The moduli of UPE polymers are considerably increased when neopentyl glycol is used as the polyol instead of ethylene glycol in the formulations [56]. The considerable increase in modulus and  $T_g$  values of the VE 160 polymer at 35 wt.% Br-MSA content as compared to the VE 828 polymer, on the other hand, should be as a result of the incomplete solubility of the VE 828 in the Br-SAGAMA monomer at this concentration.

### 3.2.4.8.6 Conclusions

The ternary blends of VE 160 with styrene and the MOA or Br-MSA monomers all exhibited processable room temperature viscosities. The room temperature modulus values were higher than 2 GPa and the  $T_g$ s were higher than 100°C for a majority of these resins. The VE 160 polymers exhibited 5-30°C higher  $T_g$  values than the VE 828 polymers at the same comonomer concentrations with generally a slight decrease in modulus. At 35 wt.% MBut content, the VE 160 polymer exhibited a  $T_g$  of 121°C ( $E''$  max) and  $E'$  of 2.8 GPa values that are very close to commercial VE formulations. For the Br-MSA polymers, VE 160/Br-MSA/Sty 55/10/35, 55/20/25, 65/10/25, and 65/15/20 exhibited processable viscosities in the liquid form,  $T_g$ s above 100°C and modulus values higher than 2 GPa when fully cured. Thus, VE 160 resins show great potential to be used in the presence of fatty acid based monomers in commercial formulations. Mechanical properties, such as flexural strength and fracture toughness of these resins, should be

determined in future work. Also, the VE 160 was chosen in this study for its low viscosity for corresponding functionality. In order to achieve further improvements in the  $T_g$  and also to increase the modulus of the polymers as compared to those of the VE 828 polymers, other Novalac type resins with higher functionalities (e.g., Epon 161,164) can also be used.

### 3.2.4.9 Fatty Acid Monomer Conclusions

Fatty acid monomers are excellent alternatives to styrene for use in VE resins. These monomers are the only known low VOC alternative to styrene with a similar cost. Although VE/fatty acid resins have resin viscosities and polymer properties inferior to VE/styrene, there are ways to obtain improved resin properties. E-beam cure has been shown to significantly improve the properties of VE/fatty acid resins. Furthermore, the use of saturated, short-chain fatty acids reduces the resin viscosity and improves the polymer properties. In addition, ternary blends of VE, fatty acid monomers, and styrene have viscosities below 500 cP, good thermo-mechanical properties, and superior fracture properties relative to VE/styrene. We have selected a few resin formulations that so far have exhibited excellent performance (Table 50). In all cases, MLau is used as the fatty acid monomer because of its superior properties. These resin formulations will be used to make and test composites more rigorously next year.

**Table 50. VE formulations using fatty acid monomers and styrene with optimum polymer properties.**

VE/MLau/St	Viscosity (cP)	$T_g$ ( $^{\circ}$ C)*	Modulus (GPa)*	$G_{IC}$ (J/m <sup>2</sup> )
65/15/20	170	>128	>2.4	195
65/25/10	400	108	1.9	189
55/20/25	~80	>110	>2.3	N.A.
55/25/20	100	>100	>2.1	224

\* The numbers listed are for VE/MOA/styrene resins. The properties of VE/MLau/styrene are expected to exceed that of MOA based resins.

It is important to note that the VE used cannot be CN151 alone in these formulations. After extensive composite trials and testing, it is now clear that CN-151 does not completely cure and is very sensitive to oxygen inhibition. As a result, the properties of CN-151-based resins are lower than that of Derakane formulations and VE 828 resins with similar formulations. Furthermore, we expect that the properties of CN-151-based composites would be even poorer because air trapped in the fibers will affect fiber-matrix adhesion, thereby significantly reducing the composite performance.

We have had initial success with using Derakane 441-400 as our base resin and diluting the resin with MFA and additional vinyl ester monomer (CN-151 or monodisperse VE 828). To make the low VOC resin formulation VE/MLau/Sty 65/15/20, 100 g Derakane 441-400, 40.25 g VE (CN-151), and 24.75 g MLau are mixed together. Initial trials show a much lower sensitivity to oxygen. In fact, samples cured in air only had a slightly tacky surface, unlike CN-151 resins which had a wet surface, full of unreacted monomer.

### 3.2.5 Low VOC Composites

#### 3.2.5.1 Exploratory Composite Work

##### 3.2.5.1.1 *Resin Formulation*

A source of vinyl ester resin was required because composites require large amounts of resin. With the facilities at ARL or Drexel, it is difficult to prepare large quantities of the VE monomers with controlled molecular weight distributions (monodisperse or bimodal). Sartomer produces CN-151, which is a low molecular weight DGEBA-based vinyl ester. This VE monomer was looked at because it was the only commercially available vinyl ester containing no reactive diluents available in large amounts. We characterized the properties of this resin to determine if it was an appropriate replacement for the VE 828 monomers we normally prepare ourselves.

Viscosity is an important parameter as far as practical application is concerned as it determines the ease of handling. The Brookfield digital viscometer was used at 25°C to compare the viscosities of CN-151 and VE 828 resins. These results clearly show that the viscosity values were in a comparable range and hence increased the candidacy of CN-151 (Table 51).

**Table 51. Viscosity measurements (using spindle 21 and a speed of 50 RPM) for ternary blends.**

VE-MLau-styrene blends (in wt%)	Viscosity (in cP)	
	VE 828	CN-151
65-15-20	432	504
65-25-10	1464	1520
55-25-20	232	232

DMA showed that  $T_g$  of CN-151 resins were approximately 5°C lower than that of VE 828 resins. The modulus was unaffected. SEC showed nearly identical chromatographs for both resins. Epoxy titration showed that there is an insignificant amount of unreacted epoxide groups in CN-151 resin and VE 828. Lastly, NMR showed that the molecular weight of CN-151 ( $n=0.16$ , MW = 560 g/mol) was slightly higher than that of VE 828 ( $n=0.10$ , MW = 540 g/mol). Therefore, it seemed that CN-151 was a good replacement for VE 828.

The reactive diluent used in this work was the methacrylated lauric acid, because of the high availability of lauric acid and relatively good polymer properties. The CN-151 was used exclusively as the vinyl ester monomer because of its commercial availability. A number of composites were fabricated using a single low VOC resin formulation of CN-151/MLau/Sty 65/15/20. Some composites were also formulated with CN-151/MLau/Sty 65/25/10 and 55/25/20.

##### 3.2.5.1.2 *Composite Fabrication*

All of the composites in this work were fabricated using vacuum assisted resin transfer molding (VARTM). The lay-up of the composite is the same for all samples (Figure 158). A layer of

double sided tacky tape is applied to a clean flat surface. Three coats of Freekote were applied to the surface within the tacky tape to prevent the composite from sticking to the surface. The fabric (E-glass, carbon fibers, etc) were then placed inside the tacky tape borders. A layer of peel ply was placed on top of the fibers and a layer of distribution media (plastic net) was placed on top of the peel ply. The peel ply prevents the distribution media and other components of the VARTM process from sticking to the composite. The distribution media allows resin to quickly flow on top of the fibers. Plastic inlet and outlet tubes were attached to the tacky tape. A plastic sheet was then applied to the tacky tape. The vacuum line (outlet) was opened until the VARTM chamber was completely evacuated. The feed line was finally opened, allowing the resin to flow into the mold where it could cure to form a composite part. Figure 159 shows actual photographs of the VARTM process. Figure 160 shows what the composite parts look like after removing the parts from the VARTM mold.

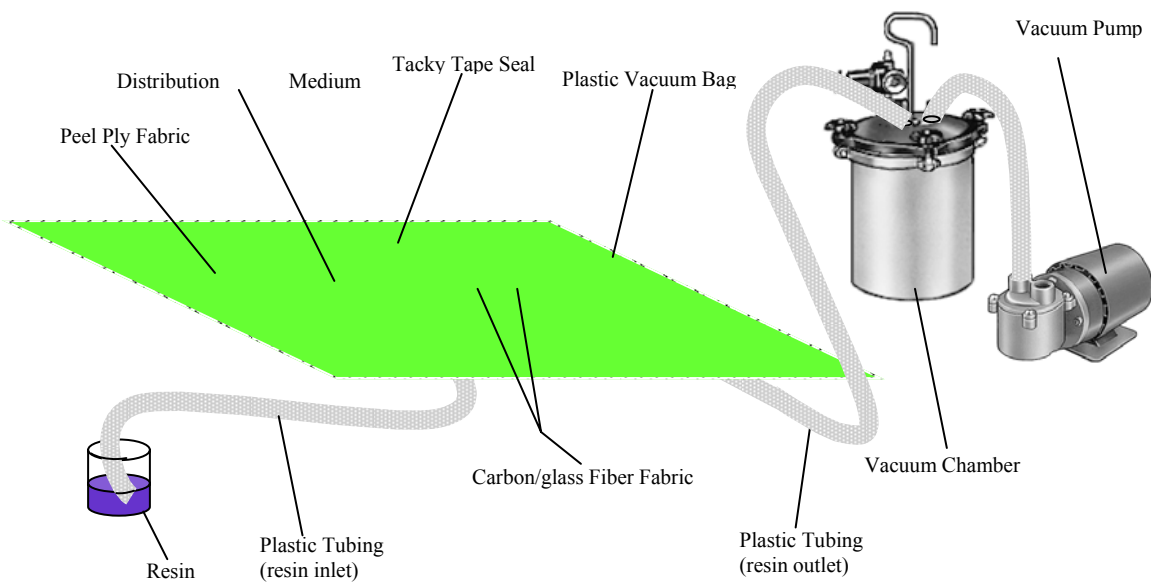


**Figure 158. Schematic representation of the VARTM process used to fabricate composites in this work.**

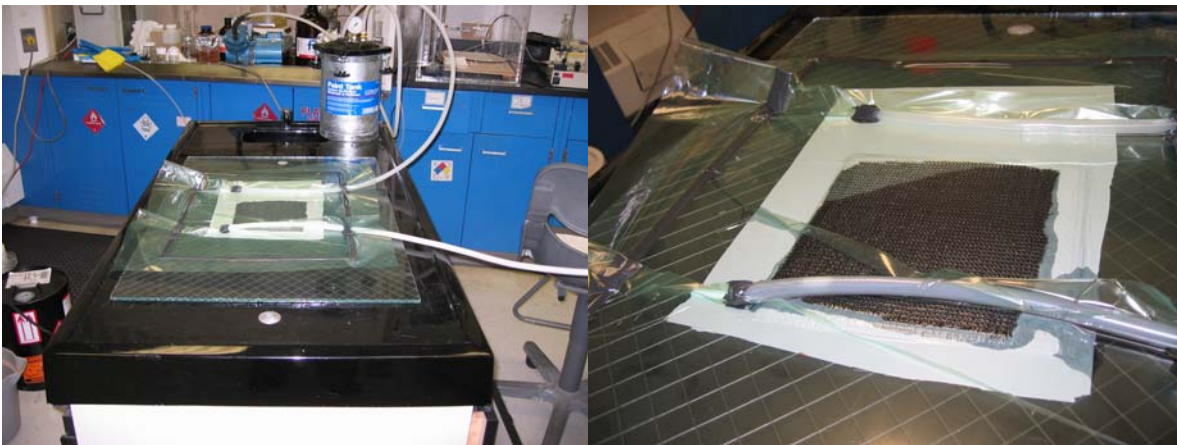


**Figure 159. Photographs of the VARTM process.**

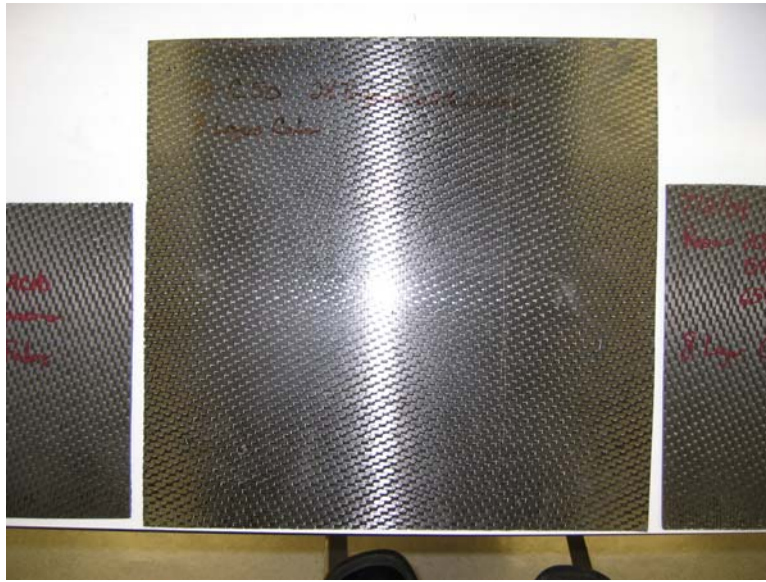


**Figure 160. Photograph of the composites produced from VARTM.**

A number of composites were fabricated using the CN-151/MLau/Styrene 65/15/20 resin. Hydroquinone in the amount of 200 ppm was used to prevent pre-mature gelation. Initially, 16 oz. epoxy-sized E-glass was used as the reinforcement. Samples were made with 4 plies of fabric resulting in thicknesses of 0.1 in and with dimensions of 4 ft x 1 ft and 2.5 ft x 1 ft. Also, samples were made using 4 plies of S2 fabric, again resulting in thicknesses of 0.1 in. The sample dimensions were 3 ft x 1 ft. As a comparison, composites were fabricated using standard S2 fabric and high-sized S2 ballistic fabric. Lastly, 9 oz. universally sized E-glass fabric was used as the reinforcement. 20 plies of fabric were used to give a part thickness of 0.25 in. The composite dimensions were 20 in x 15 in. The low VOC resin was used as well as Derakane 411-350 to make composite panels using these universally sized fibers. All composites were molded on either glass table tops of epoxy table tops.

The vacuum was partly compromised during the first few composite trials using the standard E-glass. The reason for this was that the tacky tape did not stick well to the epoxy table surface. When using a glass table top, the vacuum was maintained during VARTM. To prevent losing vacuum when molding on an epoxy surface, we decided to use two rows of tacky tape. The inner mold contains the fibers and the resin. The outer mold was also evacuated, but contains only breather cloth to allow vacuum to be applied within the entire outer mold area. To reduce the number of failed composite trials, two rows of tacky tape were used on all surfaces to help maintain vacuum.

When vacuum was compromised, the panels had a tacky finish and smelled of styrene. Post-cure could reduce, but not eliminate the tackiness and styrene smell. This occurred because of oxygen inhibition. On the other hand, when vacuum was maintained, the panels had a good finish and did not smell of styrene at all. This is in contrast to commercial resins that will smell of styrene for years after fabrication. However, these samples were very easy to break because the resin had not penetrated the fiber toes. This occurred because the E-glass did not have sizing

compatible with the vinyl ester resin. The resin flowed through the entire length of the mold within 20 minutes.

The S2 glass composites were prepared. These composites had good finishes and did not smell like styrene. Unfortunately, these samples were also very easy to break because the resin had not penetrated the fiber toes. The qualitative properties and appearance was similar whether the standard S2 or high-sized S2 ballistic fabric was used. Again the resin flowed through the entire length of the mold within 20 minutes.

The universally sized E-glass composites produced excellent panels with the low VOC resin and the Derakane 411-350. The surface finish was good and there was no styrene smell. The resin completely wetted out the toes of the fabric, and produced parts with very high strength. As an added benefit of the low VOC resin, the part was translucent, as opposed to the opaque Derakane composites. Apparently, the indices of refraction of the resin and fiber are closer for the low VOC resin. This could be useful for various applications, such as transparent armor. As before, the resin took less than 20 minutes to fill the entire length of the mold.

Therefore, the universally sized fibers must be used with the low VOC vinyl ester as well as Derakane vinyl esters to produce good parts. The low VOC resins produced composites with good surface finishes that do not smell of styrene. Lastly, two rows of tacky tape in the VARTM setup help maintain vacuum.

### **3.2.5.2 Gel Times**

It is imperative to know the time required for gelation before composite structures can be prepared. This is especially important for the Navy, which requires gel times as long as 4 hours to infuse large scale ship structures. Using the CN-151/MLau/Styrene 65/15/20 formulation, the gel time was varied using different cure temperatures, inhibitor, initiator, and catalyst contents.

Hydroquinone was used as the inhibitor in the amount ranging from 100 to 200 ppm. CoNap was used as the catalyst with contents ranging from 0.05 wt% to 0.5 wt% of the total resin mass. Trigonox was used as the initiator in the amount of 1 wt% or 1.5 wt% of the resin mass. Ten grams of resin were placed in 30 mL scintillation vials. The temperatures used were maintained at 22°C, 27°C or 32°C in a heated shaker table. The time required for a sample to visibly gel (no longer flow) after the initiator was mixed into the resin was the gel time.

Figure 161 shows that the gel time can be extended from as short as a few minutes to as long as 7 hours. Therefore, large scale structures can be fabricated using these resins. The gel times decreased as the cure temperature, CoNap content, and Trigonox content increased, and increased as the inhibitor content increased. The gel time was most dependant on the CoNap content, and secondly on the cure temperature.

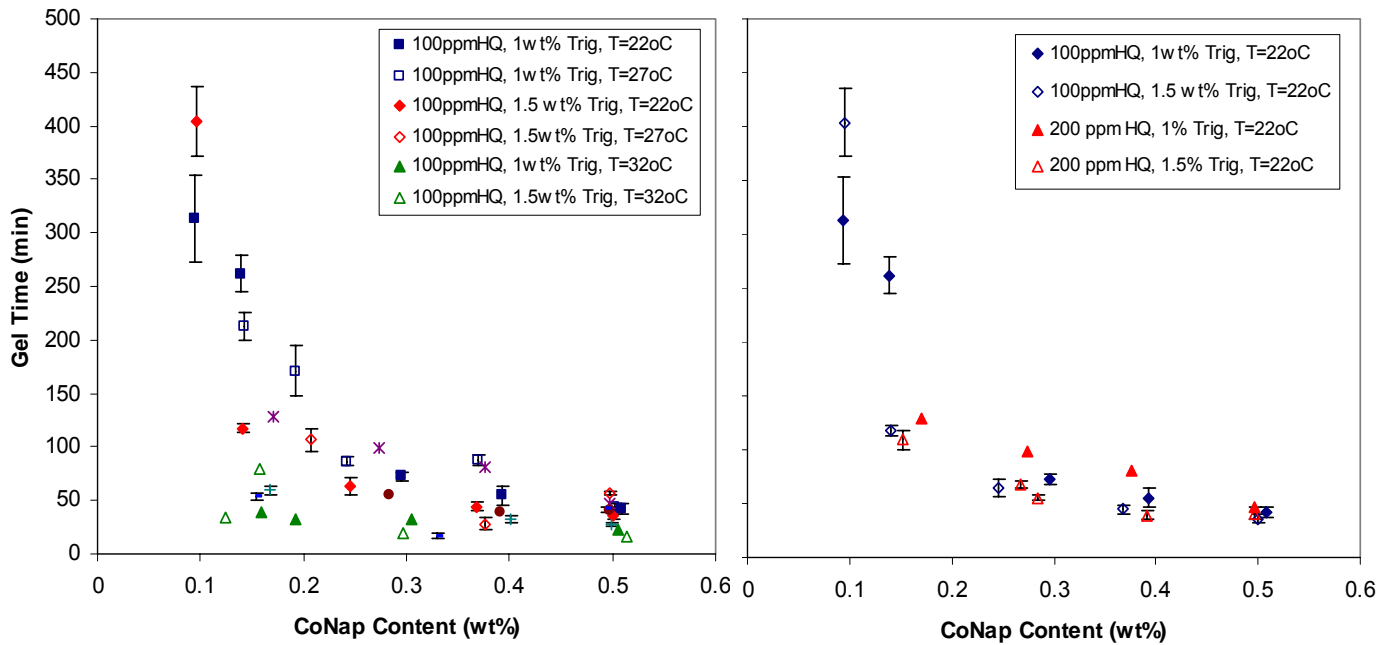


**Figure 161. The gel time for CN-151/MLau/Sty 65/15/20 as a function of cure temperature, inhibitor, initiator, and catalyst contents.**

The gel times for other resin formulations were tested as well (Table 52). The samples were prepared and allowed to cure at room temperature. These results again show the large effect of CoNap content.

**Table 52. Gel time as a function of resin, CoNap content, and trigonox content at room temperature.**

Resin	CoNap (wt.%)	Trigonox (wt.%)	Gel Time (minutes)
Der. 441-400	0.05	1	82
Der. 441	0.075	1	40
Der. 441	0.1	1	31
Der. 441	0.2	1	18
Der. 441	0.3	1	12
Der. 441	0.4	1	10
VE 828/1007f 62/38 +33% Sty	0.5	2	32
VE 828/1007f 72/28 +33% Sty	0.4	1	79
VE 828/1007f 72/28 +33% Sty	0.5	2	35

### 3.2.5.3 Composite Testing

#### 3.2.5.3.1 Glass Fiber Composites – Preparation and Testing

Testing has been performed to obtain mechanical properties of E-glass fiber PMCs using various FA-VE and BM-VE formulations. These low VOC PMCs were compared to the PMCs using commercial vinyl ester resins: Dow Derakane 411-350 (45% styrene) and Dow Derakane 441-400 (33% styrene). The glass fibers used in the composite were 9 oz. and 24oz. E-glass 7500 series vinyl ester-sized fibers with I-627 finish from BFG Industries, Inc. VARTM was used to manufacture 12.5 in. x 12.5 in. panels to be used for testing. Panels were cured at room temperature using 0.1 wt.% CoNap and 1 wt.% Trigonox. All panels were post-cured for 4 hours at 120°C. Testing was done on these composites to evaluate flexural properties, short beam shear strength, and glass transition temperature. The samples were cut to the appropriate dimensions using a table saw.

In order to evaluate flexural properties, a 3-point bending test following ASTM D790-92 guidelines was performed. The dimensions used for the testing was a depth range of approximately 0.125-0.150 inches, a width of 1 inch, and a L/d ratio of 32 to 1 as recommended by ASTM. The crosshead rate used was 0.33 in/min.

The interlaminar strength of each composite system was tested following ASTM D2344-84. Each specimen was subjected to a three-point bend, where the crosshead was lowered at a rate of 0.05 in/min. until interlaminar failure occurs. Each specimen was 1/8 in. thick, dictating that the span of these tests was 1/2 in. and the width was 1/4 in. Ten samples were tested for each composite.

DMA was used to evaluate the loss and storage moduli as a function of temperature from 30°C to 200°C and the  $T_g$  of each composite investigated. Temperature scans with a frequency of oscillation of 1 Hz and amplitude of 15  $\mu\text{m}$  were performed at a rate of 2°C/min. Typical sample dimensions in the DMA were 18 mm in length, 10 mm in width, and 3.2 mm in thickness. The  $T_g$  was taken as the temperature corresponding to the peak of the loss modulus curve.

The fiber fractions of the composites,  $V_f$ , were measured using Eq. 73:

$$V_f = \frac{d}{n_{plies} * \rho_f^a / \rho_f} \quad (73)$$

where  $d$  is the sample thickness,  $n_{plies}$  is the number of plies of fiber,  $\rho_f$  is the fiber density, and  $\rho_f^a$  is the aerial density of the fiber plies. For glass fabric, the aerial density is  $\rho_f^a = 2550 \text{ kg/m}^3$ . The aerial density is usually supplied by the manufacturer, but can be experimentally determined by dividing the mass of a ply by its area. Experiment and manufacturer numbers agreed within 2%. The aerial density was 9.6 oz/yd<sup>2</sup> for the 9 oz fibers and 23.1 oz/yd<sup>2</sup> for the 24 oz fibers. The fiber fractions for all of the composites made were similar for the same weight fiber:  $0.346 \pm 0.013$  for the 9 oz fibers and  $0.524 \pm 0.02$  for the 24 oz fibers (Table 53).

**Table 53. Fiber fraction of the E-glass composites.**

Resin	Fiber Fraction, 9 oz fiber composites	Fiber Fraction, 24 oz fiber composites
411-350	0.352	0.526
441-400	0.346	0.525
VE/MLau/Sty 65/15/20	0.331	0.55
VE/MLau/Sty 65/20/15	0.331	0.493
VE/MLau/Sty 55/25/20	0.333	0.526
VE 828/1007F 72/28 + 33% sty	0.352	0.515
VE 828/1007F 72/28 + 30% sty	0.360	0.495
VE 828/1007F 62/38 + 33% sty	0.361	N.A.

3.2.5.3.2 Glass Fiber Composites – Results

The flexural strength and modulus of the 9 oz fiber reinforced composites were normalized to 0.36 fiber fraction to normalize the effects of fiber fraction. The results clearly show that the FA-VE and BM-VE composites had significantly higher modulus (Figure 162) and strength (Figure 163). These results indicate that the low VOC resins transfer fiber load better than the Derakane resins. This result was not completely expected, considering the modulus and strength of the neat resins were similar (BM-VE) or lower (FA-VE) than that of the commercial resins. In addition, the inter-laminar shear strengths of the low VOC composites were similar or better than that of the commercial resins (Figure 164). A possible explanation for all of this can be found in the cure profiles. The components of FA-VE and BM-VE resins cure at a much more uniform rate than commercial resins. Therefore, it is possible that the fiber sizing is reacting more effectively with the polymer matrix, allowing for better load transfer.

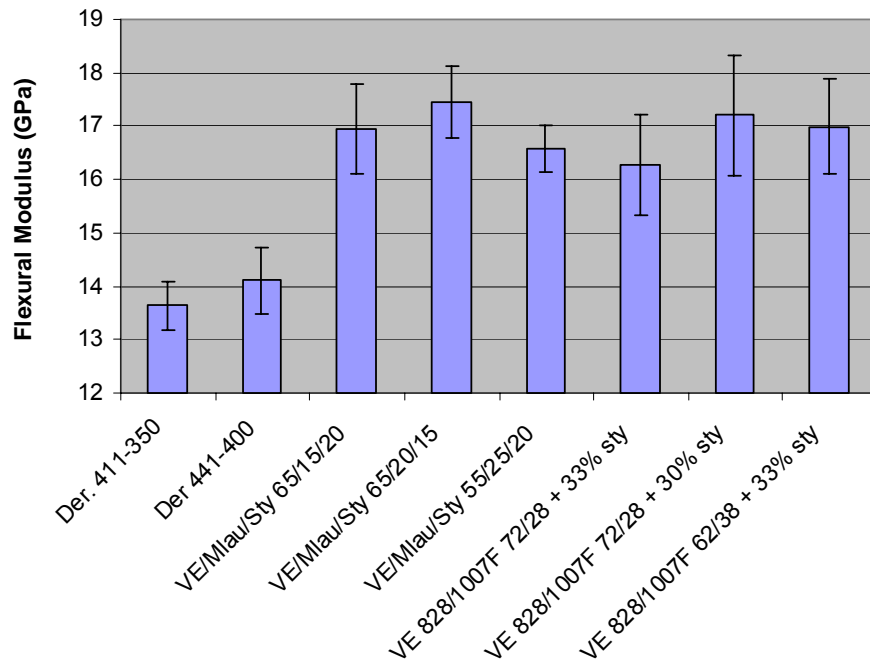


**Figure 162. Flexural modulus for commercial resins and low VOC formulations using 9 oz glass fiber reinforcement.**

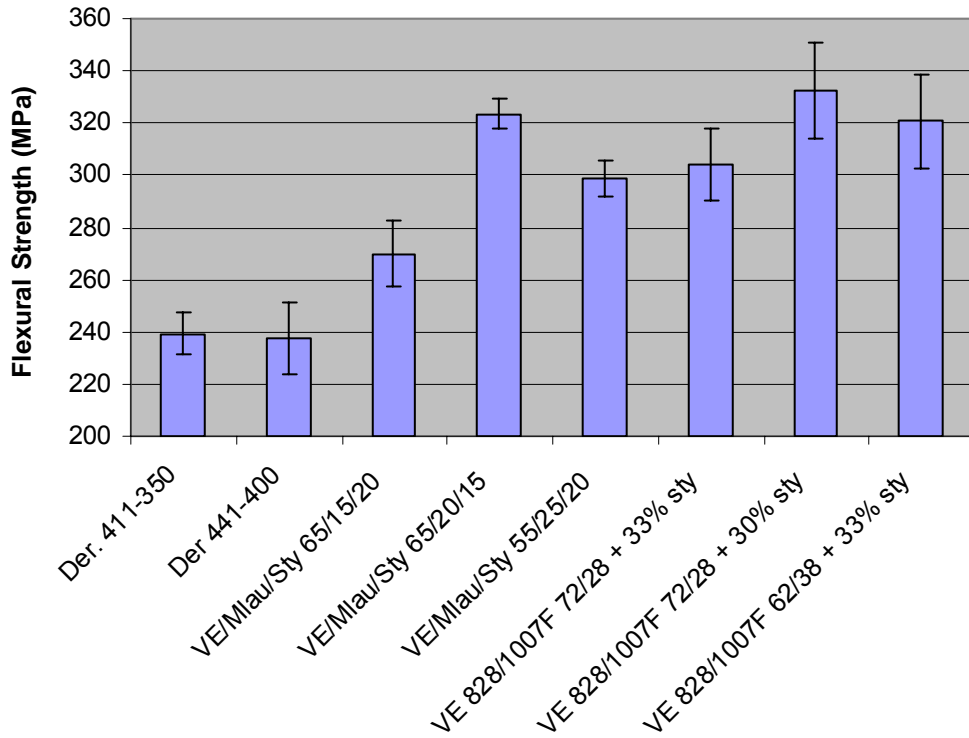


**Figure 163. Flexural strength for commercial resins and low VOC formulations using 9 oz glass fiber reinforcement.**

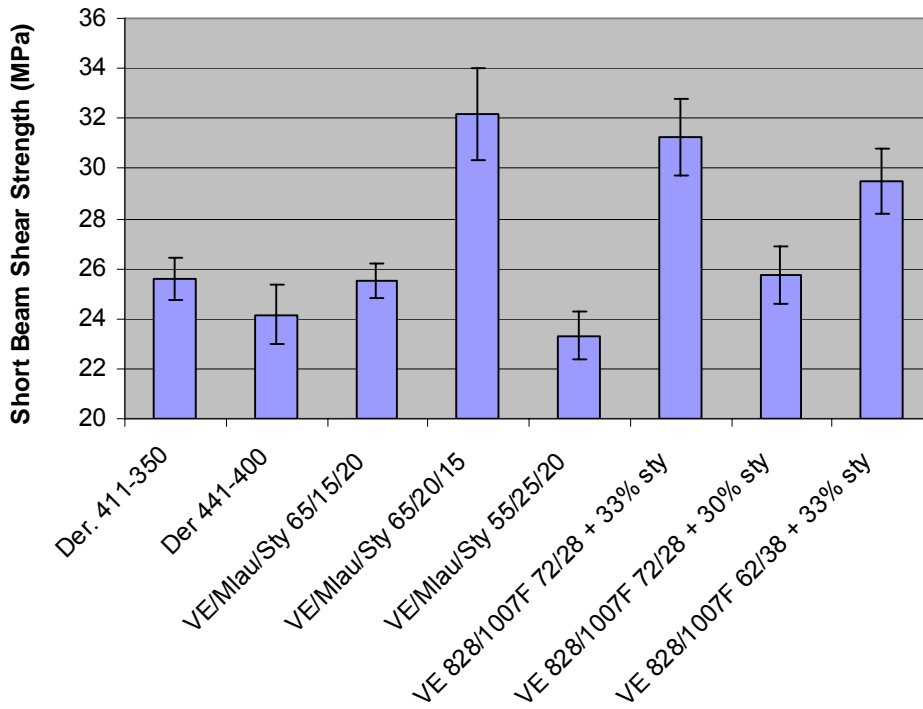


**Figure 164. Short beam shear strength for commercial resins and low VOC formulations using 9 oz glass fiber reinforcement.**

The dynamic mechanical results of the composites were analogous to that of the neat resins. The fatty acid resins had the lowest  $T_g$  values while the bimodal resins had similar  $T_g$  values relative to commercial resins. Modulus values at room temperature were similar, as this property is fiber dominated.

The 24 oz fiber composites behaved very differently than the 9 oz fibers. The commercial resins, yielded composites with better properties than the low VOC resins. However, the reason for this was due to poor fiber wetting. For all of the samples, the interior fibers were not completely wetted by the resin. In fact, the center of the part looked quite dry. This effect was more pronounced with the low VOC resins, likely because of their slightly higher viscosity.

#### *3.2.5.3.3 Carbon Fiber Composites – Preparation*

Composites containing three resin compositions were investigated in this work. Two of the composites contained resins of varying diluent content and composition with a vinyl ester monomer, CN151, supplied by Sartomer. Composite 1 was comprised of 20 wt.% styrene, 25 wt.% MLau, and 55 wt.% vinyl ester monomer. Composite 2 was comprised of 20 wt.% styrene, 15 wt.% MLau, and 65 wt.% vinyl ester monomer. The other composite studied contained a commercially available vinyl ester resin, Derakane 411-C50 (Dow Chemical), and was used as a comparison to our synthesized resin systems.

The composites studied in this work were fabricated using vacuum assisted resin transfer molding (VARTM). The composite reinforcing fibers consisted of G'-sized AS4 carbon fibers with a 5-harness satin weave and 12k tow. Eight layers of 12" x 12" were compressed under vacuum as the resin was drawn into the composite, resulting in composites of roughly 1/8" thickness. During fabrication, vacuum was applied to the system until 30 minutes after resin gelation. After cure, the composite was removed from the glass tool and post-cured at 150°C for one hour.

#### *3.2.5.3.4 Carbon Fiber Composites – Results*

The DMA results showed that the modulus and  $T_g$  of the Derakane 411-C50 composite were slightly better than that of the low VOC fatty acid-based composites (Figure 165 and Table 54). This was expected because  $T_g$  and modulus of the low VOC resins were lower than that of Derakane 411-C50. The short beam shear results of the composites were also better for the Derakane samples. This is likely to be caused by two factors. First, short beam shear was likely reduced because of the lower modulus and strength of the low VOC resins relative to the commercial resin. As a result, the resin will yield and fail sooner for the low VOC composites, thereby reducing the interlaminar strength. Secondly, the molecular weight of MLau is approximately tripled that of styrene. As a result, the low VOC resin formulations used have a much lower concentration of polymerizable groups in the resin. Therefore, there will be less fiber-matrix bonding for the low VOC resins. However, because the carbon fibers we used do not have vinyl ester sizing (there are no commercial carbon fibers with vinyl ester sizing), we doubt that the low concentration of polymerizable groups was affecting this particular set of composites results.

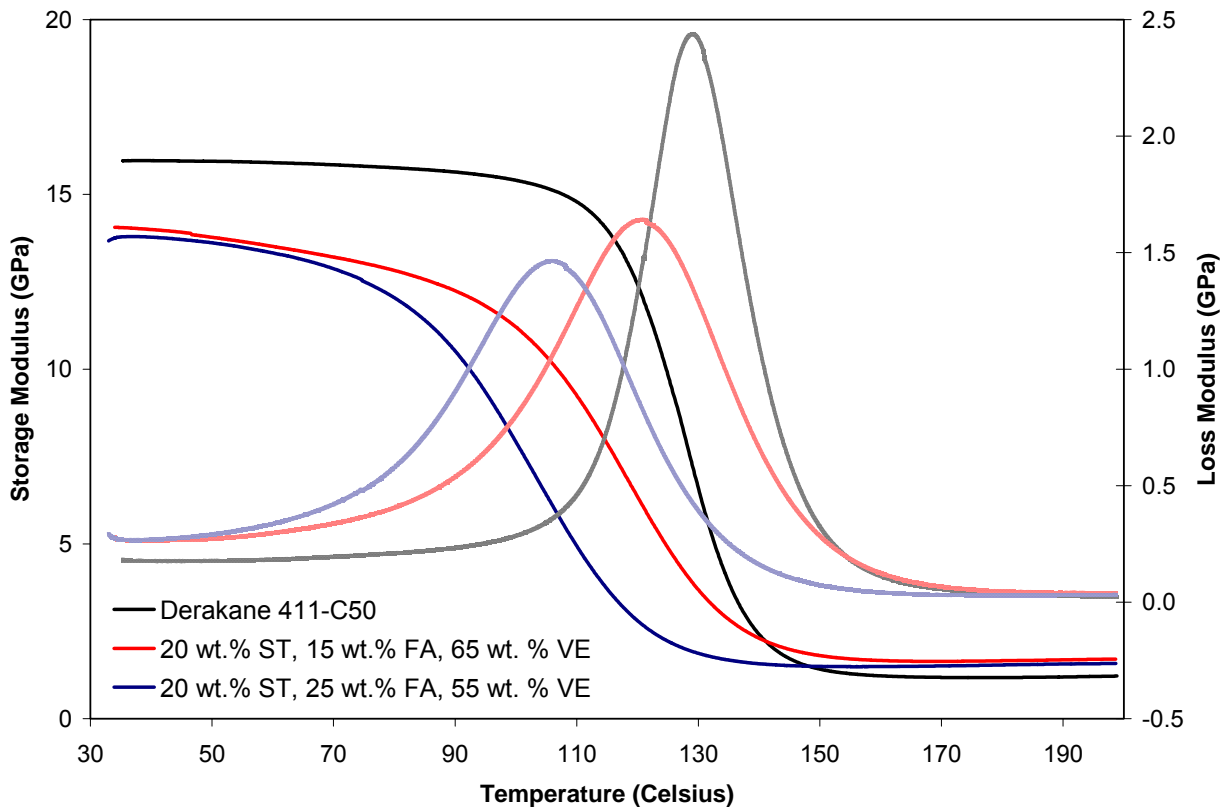


**Figure 165. DMA scans of composites with G'-sized AS4 carbon composites with low VOC resins and Derakane 411-C50.**

**Table 54. The composite properties of composites with G'-sized AS4 carbon composites with low VOC resins and Derakane 411-C50.**

Composite Resin	T <sub>g</sub> (°C)	E' at 35°C (GPa)	Interlaminar Strength (kpsi)
411-C50 (VE + 45% styrene)	129.0	15.96	6.95 ± 0.12
VE/MLau/Sty 65/15/20	120.8	14.05	4.02 ± 0.12
VE/MLau/Sty 55/25/20	106.0	13.78	3.99 ± 0.15

### 3.2.5.3.5 Effect of MFA Type and Chain Length on Composite Properties

Results have shown that MFA chain length, type, and content have an effect on resin and polymer properties. Therefore, we would expect these parameters to also have an effect on composite properties. Glass fiber composites were prepared using various types and amounts of fatty acid monomers to determine ideal formulations. E-glass 7500 series vinyl ester-sized fibers with I-627 finish from BFG Industries, Inc. was used as reinforcement. The resin used was cured with 1 wt.% Trigonox and 0.1 wt.% CoNap. VARTM was used to manufacture 1 ft x 1 ft panels for testing.

Table 55 shows the mechanical properties of the composites prepared E-glass reinforced VE/MFA/Styrene ternary blends. In general, the composite properties were superior for the low VOC fatty acid-based resins relative to the commercial resins. Overall the composite prepared using VE/MHex/Styrene 65/15/20 ternary blends and the light glass fiber mats (Table 55) exhibited significantly improved flexural modulus, strength and  $T_g$  values with a slight decrease in short beam strength (within the error range) compared to those of the composites prepared using the commercial Derakane resin. These results indicate that VE/MFA/Styrene ternary blends, with styrene contents as low as 20 wt% and therefore significantly decreased VOC emissions can successfully be used instead of commercial VE resins to prepare glass fiber composites.

**Table 55. The mechanical properties of the composites prepared using VE/MFA/Styrene ternary blends and the 9 oz glass fiber mats.**

Composites	Flexural Strength (MPa)	Flexural Modulus (GPa)	$V_f$	$T_g$ (°C)	Short Beam Shear Strength (MPa)
55%VE / 25%MLau / 20%Sty	294±10	12.8±0.28	0.35	112	26.2±2.6
65%VE / 15%MLau / 20%Sty	215±22	12.3±0.40	0.35	126	22.4±1.7
55%VE / 35%MHex / 10%Sty	314±29	12.7±0.9	0.35	101	29.7±2.0
55%VE / 30%MHex / 15%Sty	294±10	12.8±0.30	0.35	111	22.6±3.9
55%VE / 25%MHex / 20%Sty	265±19	12.4±0.40	0.35	113	26.7±3.2
65%VE / 15%MHex / 20%Sty	369±10	13.9±0.07	0.35	139	28.9±2.8
65%VE / 20%MHex / 15%Sty	308±10	13.0±0.1	0.35	125	25.3±3.7
Derakane 411-350	265±32	12.5±0.2	0.35	117	30.8±1.0

As can be seen the overall properties of all the VE/MFA/Styrene blends are in a comparable range with those of the commercial VE resin Derakane 411-350. Among all the ternary blends, the VE/MLau/Styrene 65/15/20 and VE/MHex/Styrene 65/20/15 exhibited improved mechanical properties compared to the commercial VE resin Derakane 411-350, with processable viscosities in liquid form. In addition these fatty acid based systems contain only 15 to 20 wt% styrene, decreasing the VOC emission from these resins significantly. Thus the MLau and MHex based VE resins, presented in this study, show a great potential to replace the current commercial VE resins.

### **3.2.5.4 Composite Truck Hood**

A composite hood for an M35-A3 truck (Figure 166) was prepared using a low VOC, fatty acid-based vinyl ester resin. Except as noted, this truck hood was prepared using methods identical to those developed for the composite truck hood run by the Center for Composite Materials at the University of Delaware. This work demonstrates that large composite structures can be successfully fabricated using the low VOC resins developed in this work.



**Figure 166. Commercial hood fabricated by Sioux Manufacturing Corp. mounted on M35-A3 truck**

Electronic drawings were provided to us by the CCM to allow us to cut the fiberglass to specification. Because the fiberglass rolls are not long enough, each ply contains a seam. The location of the seam moved closer to the front of the part as the plies went from the bottom to the top of the part. Typically, 4 plies of 24 oz woven roving are used to make the bulk of the part. Ply “A” is the bottom ply while ply “D” is the top ply as placed on the tool.

For our part, 9 oz woven roving, universally sized, E-glass fibers from Northern Fiberglass Industries were used as the fiber reinforcement. Experimental measurements showed that 8 plies of the 9 oz fibers should give us the correct part thickness. Because the hood is about 7ft long and 6 ft wide and our roll of E-glass was only ~ 3 ft wide, we had to introduce yet another seam to the fiberglass plies. The large section of the drawings was made by placing two fiberglass plies next to each other with an overlap of 1 inch. The fiber-cutter was then allowed to cut the fibers to the specifications. Two fabric layers were cut of samples A-D. The two plies of the same letter had their additional seam (i.e. the one added because of the shortness of the roll) located in a slightly different place by zeroing the fiber cutter a few inches from the previous ply. The originally planned seam incorporated in the drawings was located in the same place.

16 “St-1,” 8 “R-1,” and 16 “S-1” stiffeners were also cut to specifications (Figure 167). The St-1 stiffeners are used to cover and attach the PVC foam stiffeners to the bulk of the hood. The R-1 stiffeners are used to reinforce the back of the hood. The S-1 side stiffeners are used to thicken the edges of the part.

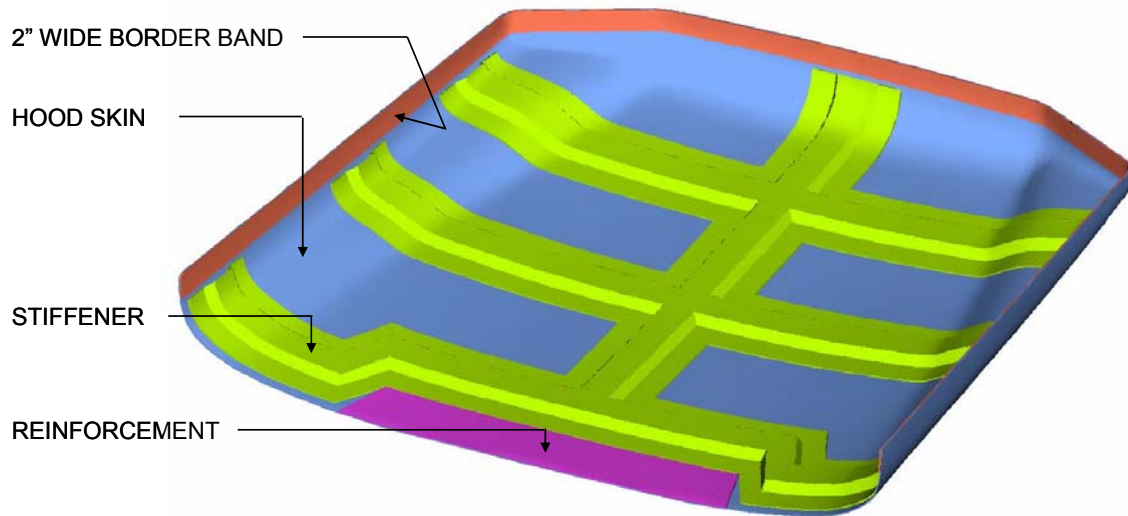


**Figure 167. Bottom view of the hood with the stiffeners.**

#### 3.2.5.4.1 Fiber Lay-Up

The tool (Figure 168) was cleaned with acetone. Tacky tape was placed along the edges of the mold. Two layers of tacky tape were used to reduce the chance of a leak. A vacuum line was setup in between the two rows of tacky tape along with breather fabric that spans the entire perimeter. Figure 169 shows these aspects of the mold. Numerous tacky tape pieces were placed along the perimeter to account for the extra slack in the bag. The mold was coated with three layers of Freekote. After the last coat had been applied, the Freekote was allowed to dry for 40 minutes.



**Figure 168. The tool used for fabricating the composite hood.**

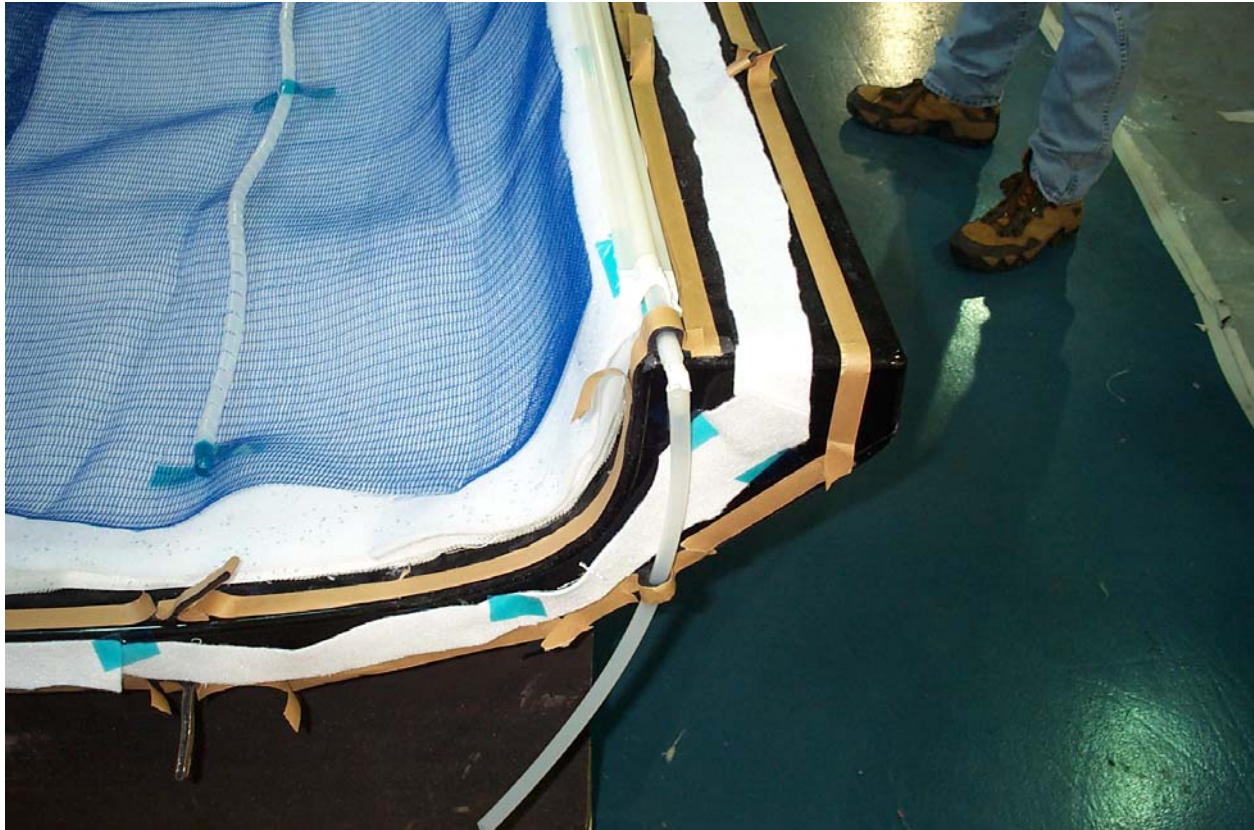


**Figure 169. Photograph showing the two rows of tacky tape, the breather cloth, and the method with which the inlet and outlet lines enter the inner mold area.**

F-77 spray adhesive was applied lightly to the tool surface to prevent the first fiber glass layer from slipping. Ply A was placed carefully on the tool. The next ply A was then placed down, followed by the two “B” plies , “C” plies, and “D” plies, respectively. Occasionally, F-77 was used to keep the fabric from collapsing at the curved upward edges of the tool.

PVC foam was used to make the stiffeners. A groove was cut into each stiffener ~1 cm deep every two inches to allow resin to flow underneath the stiffeners. At places of high curvature, the grooves were cut ~ 2 cm deep every inch to allow the foam to conform to the tool contours. The three sets of stiffeners perpendicular to the axis of the truck were placed down first (Figure 167 and Figure 170). The stiffeners were run up to about 3 inches from the side edges of the tool. The back-most stiffener was not placed in a simple line. In both directions from the middle of the part, the stiffener extended ~18.5 inches. A 45° cut was made in the stiffener on each end. The corresponding piece ran another two inches across the hood and 2 inches towards the back of the hood. Another 45° was cut on each end of the stiffeners, and the stiffeners were then extended straight out towards the sides of the hood and up the curved surface. The backmost part of this stiffener was placed 9 inches from the back of the tool surface. The middle stiffener and front-most stiffener were placed 24.5” and 39.8”, respectively, from the 9 inch mark. The lone stiffener parallel to the truck axis was then pieced together to run most of the length of the hood. The foam was attached to the fabric with F-77 adhesive.

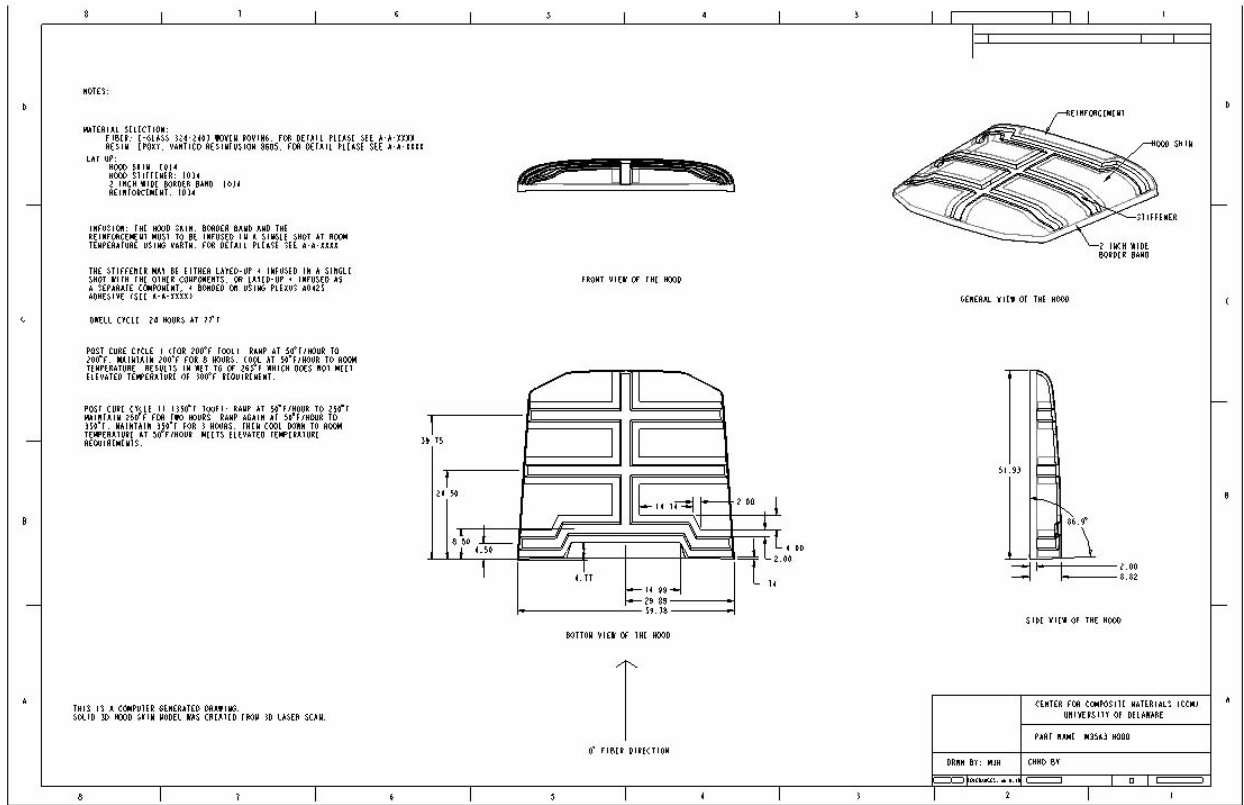


**Figure 170. The schematics of the composite hood.**

The St-1 stiffeners were placed over the foam stiffeners to permanently attach the stiffeners to the hood structure. Each ply was laid down one at a time and interleaved with intersecting plies. Much effort was spent making these plies fit to the contours of the hood and the foam stiffeners. Gaps between the plies and the foam would result in zones of resin accumulation that were not desired. Small slits were made in the fabric to allow the fabric to follow the hood contour. F-77 spray was used to keep the fabric tucked next to the foam. Three plies were placed down the parallel beam, while two plies were placed on the three perpendicular beams. Small patches of fabric were placed at the intersection of the fabric.

The R-1 stiffener was placed right behind the backmost perpendicular beam to strengthen the structure. 4 plies of this fabric were used and were interleaved with the three plies along the parallel foam stiffener.

Five S-1 stiffeners were stacked on top of each other vertically offset by ~ 0.5 in. Each layer was sprayed with F-77 to keep it in place. The fabric was then cut down the central axis to make two identical side stiffeners that increase in thickness from bottom to top. These stiffeners were applied to the top edges of the mold overlapping with the hood fabric so that the edges gradually increase in thickness as you move up to the edge of the tool. At least three such stiffeners were placed along the sides while at least four were placed in the front of the part.

Two large strips of white peel ply were placed over the structure. Breather cloth was placed over the peel ply and up onto the ledge on the sides and front of the part. Two large strips of

distribution media were placed up to 1 inch from the top of the mold to increase the fill rate of the part.

An omega channel was used as the resin inlet and placed down the parallel foam stiffener. Helical tubing was placed at the end of the omega channel and attached to a standard tube that would feed into the resin bucket. Also, an inlet port was placed in the center of the omega channel as a secondary inlet. Furthermore, one strip of helical tubing was placed halfway between the center and the edge on each side of the center feed. These would be used as additional feed lines if the part was filling too slowly (however, these ports were unnecessary as the part filled in ~30 minutes). The vacuum was applied using two omega channels on the two sides of the tool. The breather cloth was placed under the vacuum channel to pull vacuum through the fibers of the hood. Figure 171 shows the three inlets and the two vacuum lines.

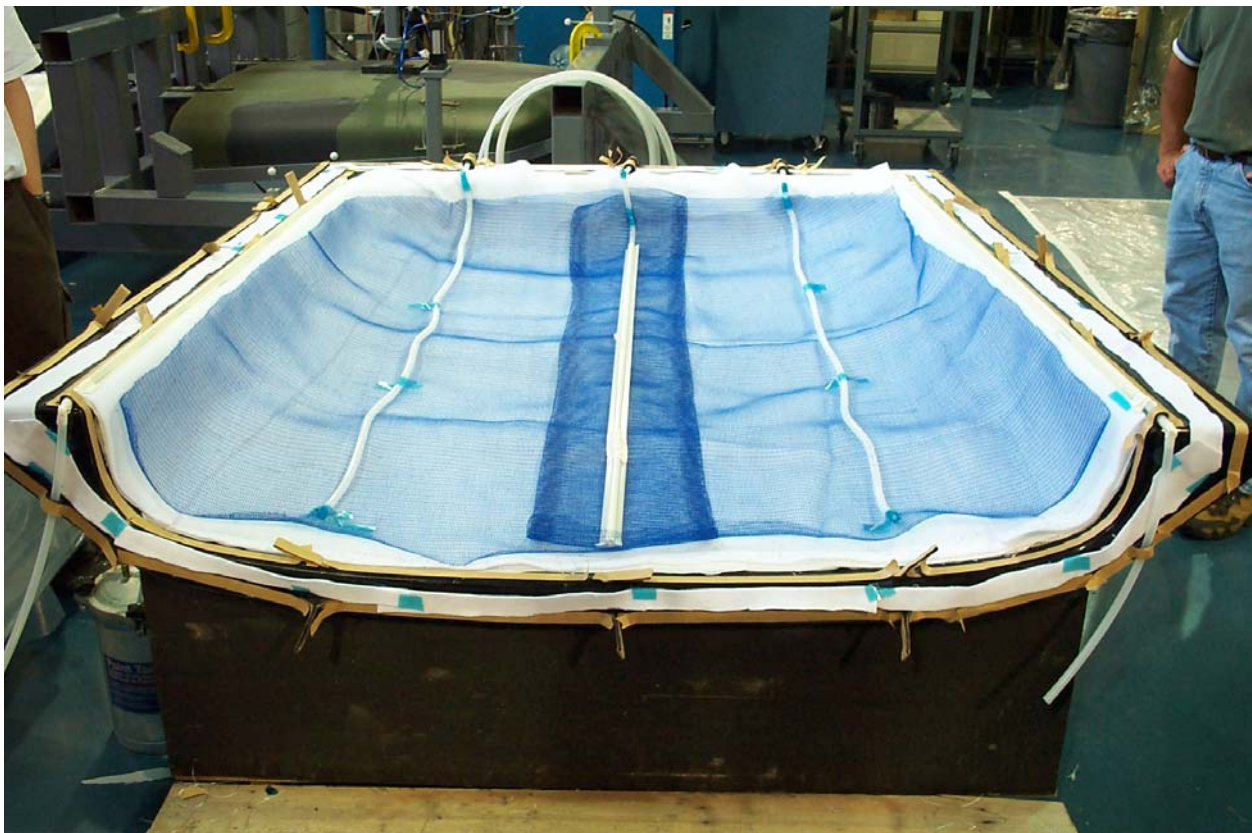


**Figure 171: The composite hood lay-up showing the three inlet lines and two vacuum lines.**

The inner section was bagged first and vacuum was applied. A small hole was poked into the bag at the middle inlet port. The port was pulled through the vacuum bag and was attached to a flexible piece of tygon tubing. The other end of the tygon tubing was connected to the standard vacuum tubing into the resin bucket. Both junctures were sealed with tacky tape. The bag surrounding the port was also sealed with tack tape to prevent a bag leak at the inlet port. No leaks were found and the part maintained vacuum when the valve to the pump was turned off. The outer section was bagged and checked for leaks. One leak was found and repaired. The

system was then allowed to sit under vacuum over night. In the morning, the part was still under full vacuum and no leaks developed. Figure 172 shows the mold after bagging.



**Figure 172. Photograph of the mold after bagging.**

#### *3.2.5.4.2 Resin Infusion*

The resin used was the low VOC FA-VE resin comprised of CN-151/MLau/Styrene in the weight ratios of 65/15/20. 3.8 gallons of resin were initially prepared for injection. 150 ppm HQ were added and 0.14 wt% CoNap was added and mixed well. 1 wt% Trigonox was added and mixed.

The resin was injected into both ports in the center omega channel. The resin flow was uniform except at the foam stiffeners, where the flow race-tracked at about double the speed of the resin at other parts. This indicates that there were still gaps in between the fibers and foam stiffeners despite our efforts. Figure 173 shows how the resin infused through the part.

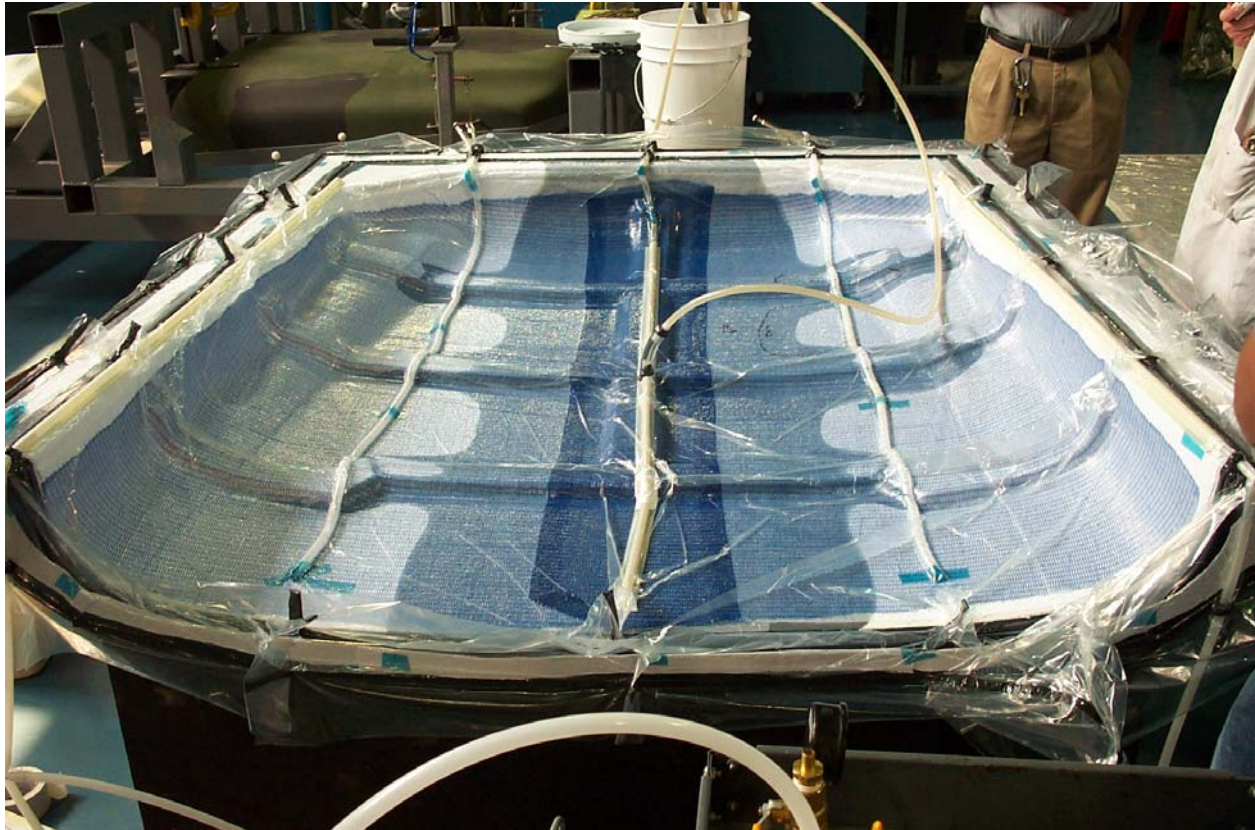


**Figure 173. The resin infused fairly uniformly except that it race-tracked at the foam stiffeners.**

In approximately 15 minutes, it was obvious that more resin was required. Another gallon of resin was initiated and added to the injection bucket. Unfortunately, the ~5 gallons of resin used was not enough to fill the part. Presumably, the breather cloth absorbed much of this resin making the estimate of 3 gallons far too low. Although most of the part was filled when we clamped off the injection port (<30 minutes after injection), the flow was still stopped. However, in the process some air was gulped into the part. It only required another 10 minutes to completely wet out the part even though no more resin was being added. Over the next 15 minutes, quite a bit of resin was sucked into the vacuum bucket. We decided that this loss of resin was probably going to be detrimental to the part. Therefore, we decided to push the resin outside into the summer heat (~90°F + substantial radiative heating). After another 10 minutes or so (75 minutes since injection), the exotherm from the resin could be felt and the system gelled completely within 5 minutes.

#### *3.2.5.4.3 Demolding*

The cured part easily lifted from the tool surface. The part was trimmed to match the required hood dimensions. The final part was good (Figure 174). There were a small amount of air bubbles/voids in the part. This probably occurred because air was gulped into the part and we could not continuously feed resin until gelation. Near the foam stiffeners, there were small pools of uncured resin. This probably occurred because the resin pooled in this region and air may

have also accumulated there causing free-radical inhibition. When you hit the part, it did not “clang” the way a good composite part does. Also, the part has a slight styrene smell to it because of the uncured regions. On the other hand, the resin cured completely and there was no more styrene smell after a post-cure for 4 hours at 180°F.



**Figure 174. The completed low VOC composite hood.**

The truck hood was painted using a low VOC water-dispersible chemical agent resistant coating (CARC) (MIL-DTL-64159) that was formulated in SERDP PP-1056 and developed in ESTCP 200024. Prior to painting, the hood was sanded down to make the entire surface level, with no bumps or voids. A primer was then applied. Lastly, two coats of the low VOC water-dispersible polyurethane CARC were applied to the surface. The part looks excellent after painting (Figure 175). These results show that not only does this work address current DoD environmental needs, but it can take advantage of prior environmental solutions to have a synergistic positive environmental impact on the military.



**Figure 175. Photograph of the inside of the low VOC truck hood after painting with the low VOC CARC.**

#### *3.2.5.4.4 M35-A3 Truck Hood Conclusions*

There were a number of things that can be improved in the production of the composite hood. First of all, to maintain consistency with what has been done at the CCM, a wide spool of 24 oz. woven roving (universally sized) will be used exclusively in the next lay-up. Secondly, we will consider not using the breather cloth over the entire part. This will decrease the amount of resin required to make the part. Also, ~ 10 gallons of resin should be brought to the manufacturing site to eliminate the chance of running out of resin before the part is cured. Future work is necessary to validate that this low VOC technology can be used to replace current systems. To do this, a Derakane 411-350 hood must be prepared for comparison with the low VOC hood. Also, the hoods will need to be tested on the hood testing fixture at the CCM to ensure that it meets Army specifications. Tests should be run to make sure that the F-77 adhesive spray does not affect our resin more than a typical resin. Overall, although not a complete success, we have demonstrated that this low VOC resin can be used to make a large composite structure by means of vacuum infusion. We are confident that additional low VOC truck hood could be fabricated with excellent quality. Therefore, this low VOC resin will work as well as commercial resins in fabricating large structures.

#### **3.2.5.5 Navy Composite Fabrication**

The Naval Surface Warfare Center (NSWC), Carderock Division agreed to test the low VOC resins developed at ARL for trials to make structures for DD(X). Initial processing trials were performed on three panels made using 24 oz E-glass woven roving. The panels were 1 ft x 1 ft, 2 ft x 2ft, and 3 ft x 3 ft. The first two panels consisted of 6 plies of E-glass with a warps parallel orientation. The 3 x 3ft. panel consisted of 12 plies of the E-glass with a panel thickness of 0.25 in.

The results from this work were promising. The resin infused these parts in approximately half the time their current resin system infused the part (Derakane 510-C350). The parts cured in the desired time window. Unfortunately, in a few trials, the resin had a tacky surface due to oxygen inhibition. Therefore, the Navy confirmed our belief that this resin formulation is very sensitive to oxygen inhibition. Overall, the Navy was happy with the infusion and performance of the resin, but would prefer a lower sensitivity to oxygen. As a result, the resin formulation was changed to use Derakane 441-400 as the basis. The old formulation used 65 wt.% CN-151, 15 wt.% MFA, and 20 wt.% styrene. The new resin formulation used 60.6 wt.% Derakane 441-400 resin, 24.6 wt% CN-151 and 15% MFA. The lower CN-151 content noticeably decreased the oxygen sensitivity.

Once the fabrication process was demonstrated and the issues associated with VARTM manufacturing with this system were resolved using these small panels, a large scale demonstration item was manufactured. The low VOC fatty acid resin containing VE/MLau/Sty 65/15/20 was used to make a large scale structure hat-stiffened for the Navy. The hat-stiffened structure is representative of the section that will be used for the Composite Advanced Sail Program and DD(X). The part was prepared by team members at NSWC Carderock to obtain an independent assessment of the resin quality.

The part that was fabricated was a full thickness section of a hat stiffened structure. The part has overall dimensions of 4 ft wide x 10 ft long. The hat section has dimensions of 12" wide x 10" tall. The hat-stiffened area is composed of a low hardness PVC foam. 24 oz E-glass woven roving was used as the reinforcement (Figure 176). Complex bagging geometry was necessary to accommodate the hats (Figure 177). Multiple feed ports were used to decrease injection time (Figure 177).



**Figure 176. Lay-up of hat-stiffened structure showing the PVC foam hats and the E-glass woven roving mats.**



**Figure 177. Lay-up of hat-stiffened structure showing the complex bagging geometry and multiple feed ports and vacuum lines used.**

The CoNap, Trigonox, and HQ contents were added to the resin to have a gel time of approximately 4 hours. The resin successfully and relatively quickly infused the part. The final part quality was excellent (Figure 178). The resin was cured at room temperature and was not post-cured. There were few, if any, voids, and the surface was smooth and non-tacky. Furthermore, even without post-cure, the part did not smell of styrene because all of the styrene cured into the resin. Therefore, this work gives further evidence toward the fact that this resin can be used as a drop-in replacement for commercial vinyl ester systems while significantly reducing VOC emissions without compromising processability. However, mechanical properties of these large-scale structures need to be evaluated to ensure that the properties of these large scale structures are sufficient. Yet, based on small-scale composite testing, we would expect the low VOC resin properties to behave favorably relative to composites made using commercial resins.



**Figure 178. Hat-stiffened structure showing the final hat-stiffened structure and a close-up of the hat-stiffened area.**

### **3.2.6 Novel Styrene Suppressant Systems**

We propose to add small amounts of surface-active dendritic polymers that can react into the polymer matrix to suppress styrene emissions. The surface-active nature should allow these molecules to self-assemble into a vapor barrier to reduce styrene emissions. Commercial petroleum-based dendritic polymers and triglyceride-based dendrimers were used to achieve these goals. The benefits of highly branched systems, such as dendrimers and hyperbranched polymers, include low viscosity, high solubility, and a large number of end-groups per chain. The resulting properties of the polymers are dominated by the end-groups, which provide the most accessible route to developing novel styrene suppressant systems. Commercial dendritic systems are already established and are fairly inexpensive. However, these systems have to be modified to enable them to react into a polymer network and preferentially migrate to the surface. Triglycerides are first generation dendrimers. Yet, methods for making higher generation dendrimers from triglycerides have not been established. On the other hand, there

already exist commercial methods and products enabling them to react into a polymer network. Functionality that induces preferential migration to the surface will be added in a similar manner as for the commercial petroleum-based dendritic polymers.

Recent work has also revealed the potential of highly branched polymers to function as switchable surfaces. As detailed in Patent WMRD-P-02-007 [57], blends of linear polyesters and partially fluorinated polyethyleneimines were shown to present hydrophobic groups at the surface prior to contact with water. After exposure to water, the end-groups flipped, presenting the more hydrophilic backbone of the polymer. In this way we envision using partial end-group fluorination to transport branched polymers to the surface of a VE resin system. Once there, the polymers may act as a barrier against styrene emission. Once exposed to a different material (e.g. a protective coating or adhesive layer), the polymer may undergo a surface switching, exposing a more compatible interface. In this fashion macromolecular styrene suppressants may out-perform the current technology (e.g., paraffin based, Styrid-type suppressants).

Dendrimer structure, molecular weight, and functionality should affect the ability of surface active dendrimers to reduce the styrene emissions from VE resins. These effects are presented below.

### **3.2.6.1 Commercial Petroleum-Based Dendritic Systems**

#### *3.2.6.1.1 Synthetic Routes*

To begin our investigation of branched polymer modifiers, we identified potential commercial sources. It was found that BASF produces a highly branched polyethyleneimine (PEI) trade named Lupasol, and Perstorp produces the Boltorn series of hyperbranched polyesters. Both of the polymers possess reactive end-groups. Lupasol polymer chains are amine terminated while Boltorn chain ends are functionalized with hydroxyl groups. Potential routes for the preparation of modified polymers are shown in Figure 179.

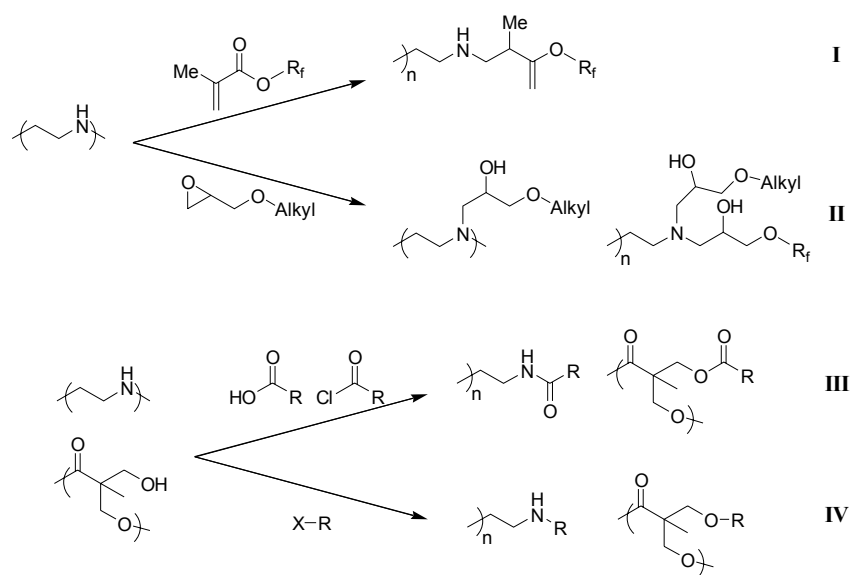


**Figure 179. Potential methods of end-group modification. Routes I (Michael addition) and II (epoxide opening) are more suited to the PEI end-groups, while routes III (acyl condensation) and IV (halide displacement) should be applicable to either system.**

The routes shown in Figure 179-I and Figure 179-II represent very facile reactions. The double bond of a methacrylate or acrylate is very susceptible to nucleophilic attack by primary amines, dubbed a Michael addition. The reaction proceeds rapidly, works even in the absence of solvent, and the extent of reaction can be quantified using infrared spectroscopic techniques. While the Michael addition has been observed to proceed with secondary amines, the rate of the reaction decreases by more than an order of magnitude. The Michael addition may therefore be used to functionalize a branched polymer almost exclusively at the end-groups.

The ring-opening of an epoxide is very rapid for both primary and secondary amines. As a result, a greater degree of substitution may be predicted using epoxies to install end-group functionality. In addition, they make a nice complement to the Michael addition chemistry and permit the preparation of polymers with mixed end-group composition.

The reactions shown in Figure 179-III and Figure 179-IV should provide additional routes to functionalize the Lupasol PEIs, and should also provide means to make modified Boltorn polyesters. The attachment of an acid chloride to an amine or alcohol is one of the classic methods of amide or ester formation, respectively. The tertiary amines (branch points) of the Lupasol PEIs may preclude the use of this chemistry for their modification, as they will likely condense HCl salts in the backbone of the polymer. The Boltorn hyperbranched polymers should form esters very easily, and similar modifications have been reported in the literature.

If the acid chlorides prove difficult to handle or salt condensation becomes a paralyzing issue, alternate modes of carboxylic acid activation may be employed to achieve the same functional group preparation. The use of coupling agents such as DMAP and DCC will allow the amide

formation with dicyclohexyl urea condensation instead of HCl salts. The main question to be answered about ester/amide formation is which route will yield easier polymer isolation.

The substitution of end-groups by nucleophilic displacement of an alkyl halide will also be attempted, as shown in Figure 179-IV. The chemistry involved is not as facile as the other routes, but the successful development of the approach should allow for a very wide selection of functionalities for the polymer end-groups.

There exists a large assortment of candidate groups to attach to the periphery of the branched polymers. Chief among them is the inclusion of fluorinated end-groups that should provide the enthalpic driving force to bring the suppressant system to the surface of the resin. We are also investigating long aliphatic chains, as they should reduce styrene emissions by reducing the permeability of the resin surface. Since this type of sealing approach has been demonstrated with suppressants like Styrid, it has the greatest chance of success. Other potential sealing groups include functionalized silanes, which would provide an alternative to the aliphatic end-groups.

We have already made great strides to functionalize the periphery of the branched polymers, Lupasol and Boltorn. Both the Michael addition and ring-opening of epoxide have been successfully carried out. The Zonyl-TM fluoro-surfactant from DuPont provides an inexpensive Michael acceptor for the nucleophilic amine to attack. We have functionalized Lupasols with fluorinated chains up to 50% by weight.

The Heloxy line of epoxy modifiers from Resolution Performance Products proved to undergo rapid quantitative reaction with Lupasol PEIs. They have been incorporated up to ca. 80% by weight, which is very near the theoretical limit for loading of the polymer.

The other routes to modified polymers are also currently being explored. The search for effective reaction conditions is being facilitated through the use of a heated reaction block and oscillatory shaker table. The reaction block consists of 63 wells sized to accommodate 40 mL disposable vials. The block is arranged such that it has three layers. The bottommost layer is the heated portion. An external controller regulates heating, and feedback is provided through the use of a thermocouple. The top layer of the block is a cooling zone, and is equipped with cut outs to allow for coolant fluid circulation. Bridging the heating and cooling zones is a thin insulating layer, which provides good thermal separation between the two layers.

Because of the 3-zone design of the reaction block we can investigate a wide range of reaction conditions. The cooling zone allows us to reflux low boiling solvents without danger of over-pressurization of the reaction vials. The use of vials to scout reactions also saves greatly in terms of time and material requirements. Instead of using several oil baths and several condensers to search out reaction conditions (e.g. solvent, base, catalyst, nucleophile, etc.) many parameters can be varied at the same time, allowing us to use a semi-combinatorial approach to method development. In some cases, the capacity of the vials is also sufficient for significant material generation.

In the preparation of fluorinated Lupasols via Michael's addition with Zonyl fluorosurfactants, several multi-gram batches were prepared in-parallel. The spontaneous nature of the reactions and the lack of solvent permitted approximately 6 g of material to be reacted in a single vial. If necessary, the reaction block could likely be used to prepare samples of twice that size. The reaction block has therefore proven its value in both method development and sample preparation.

### 3.2.6.1.2 Modification of Hyperbranched Polyethyleneimines

The polyethyleneimine (PEI) system we began investigating has shown some promise as a platform for the preparation of multifunctional materials. We had previously shown the reaction of the PEI with methacrylated perfluorinated chains as well as reaction with aliphatic epoxy monomers. In addition, we have generated mixed end group polymers with both perfluorinated and aliphatic chain ends. Details of the polymer modification have been included in Figure 180.

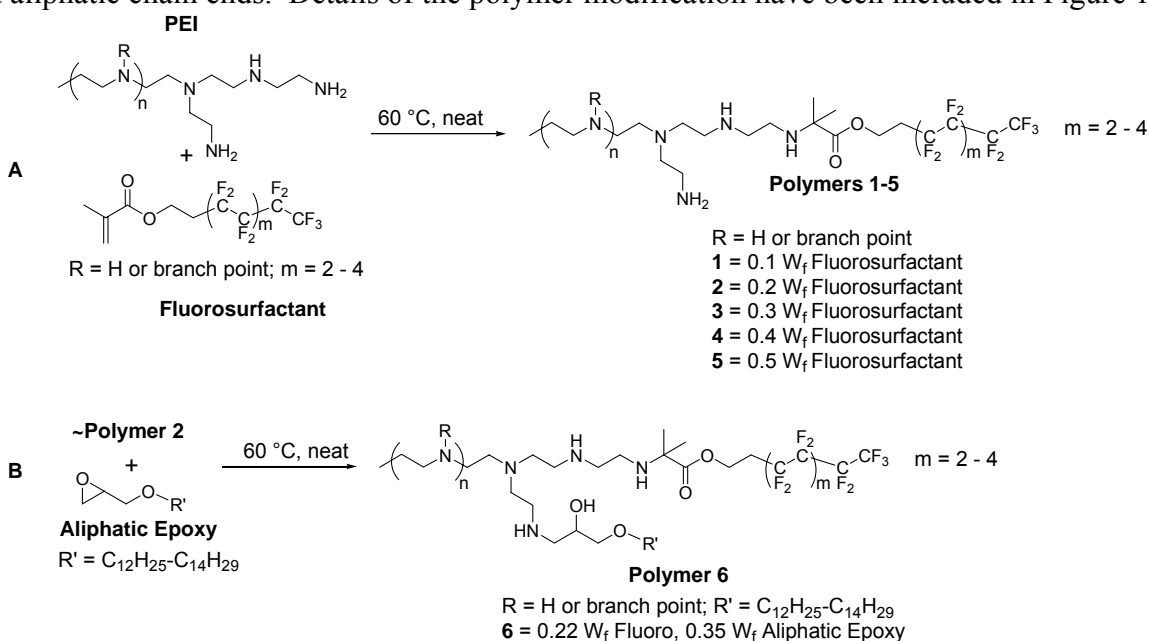


**Figure 180. Synthetic scheme for modification of branched PEIs**

The mixed end group PEIs were developed primarily to enhance the solubility of the fluorinated polymer in a range of organic solvents, including styrene. Fluorinated PEIs exhibited very poor solubility in common organic solvents. The addition of the aliphatic groups compatibilized them with a range of solvents, and made them mostly or fully soluble in solvents ranging from tetrahydrofuran to water.

Full reaction of the perfluorinated groups and aliphatic groups was confirmed by Fourier transform infrared spectroscopy (FTIR) and with proton nuclear magnetic resonance spectroscopy ( $^1\text{H}$  NMR). The reaction of the methacrylate group was followed by monitoring the IR absorbance of the carbonyl group ( $\text{C}=\text{O}$ ). The group has a strong characteristic absorption at ca.  $1727\text{ cm}^{-1}$ . Upon reaction via the Michael addition, the conjugation of the vinyl and carbonyl groups is broken and the absorption shifts to ca.  $1736\text{ cm}^{-1}$ . Full reaction of the vinyl

group was further supported by analysis with  $^1\text{H}$  NMR, which showed an absence of vinyl proton resonances in the spectrum.

A similar method of analysis was adopted for the reaction of the aliphatic epoxy groups. The characteristic IR absorption of the epoxy ring is at ca.  $916\text{ cm}^{-1}$ . Upon reaction, this relatively strong signal disappeared. Further analysis using  $^1\text{H}$  NMR confirmed the reaction of the epoxy group, as the characteristic signals attributed to the 3-membered ring disappeared after reaction. The sensitivity of  $^1\text{H}$  NMR is sufficient that ca. 1-2% of an impurity or unreacted component could be observed. The polymers were therefore considered fully reacted, and were evaluated without additional purification steps.

Traditional polymer purification techniques were not viable with the current PEI systems. Typical protocols involve the precipitation of either the polymer or impurity from a concentrated solution. The phase change allows the physical separation of the desired product. The PEI materials were highly viscous oils or gel-like materials if they contained a high proportion of perfluorinated surfactant. The modified polymers also appeared off-white to light yellow in color, and were more turbid than their parent PEI polymer. The resulting appearance likely arises from micro phase segregation in the material, and is common when considering highly amphiphilic materials.

An extension of this synthetic methodology has also been carried out using alternate methacrylated chains (Figure 181). A poly(dimethylsiloxane) (or PDMS) with alcohol end groups was obtained from commercially available sources. The chain ends of the PDMS were modified with methacrylic acid to form esters, giving the PDMS potentially two sites that would be active to Michael addition chemistry. The esterification was performed at room temperature to preserve the vinyl groups of the methacrylic acid. The condensation agents were 4-(dimethylamino)pyridinium 4-toluenesulfonate (DPTS) and dicyclohexylcarbodiimide (DCC), an acid activating group and condensation agent, respectively. The dicyclohexyl urea (DCU) condensation side-product was isolated by filtration in several steps, leaving primarily PDMS with methacrylate ester end groups. The methacrylated PDMS was then reacted with partially fluorinated PEIs, to give a mixture of products. The PEI chains were present in great excess, so the statistical distribution of products is predominantly represented by a single PDMS chain reacted with two different PEI chains, and each PEI chain reacted with a single PDMS chain. While the adoption of this type of modification can lead to cross-linking of the PEI backbone, it is unlikely at the current levels of loading. This system could be viewed essentially as an  $\text{A}_2\text{-B}_{20+}$  system, providing several routes for cross-link formation. The high molecular weight of the PDMS base polymer ( $M_n \sim 4500\text{ g/mol}$ ) coupled with the relatively low mass of the PEI backbone (ca.  $1300\text{ g/mol}$ ) and the partial consumption of its reactive end groups by the fluorosurfactant resulted in an off-white turbid material with good solubility in organic solvents. The performance of this material will be discussed in the following section.

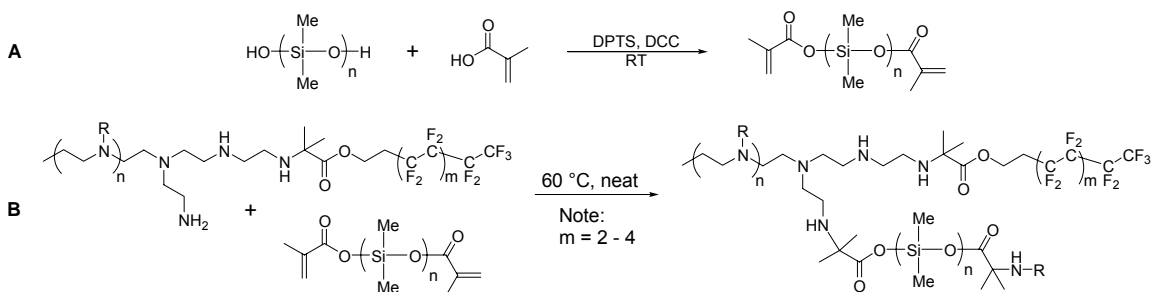


**Figure 181. Preparation of PEI-PDMS suppressants.**

### 3.2.6.1.3 Modification of Hyperbranched Polyesters

The second dendritic polymer system we have investigated is the polyester system with hydroxy end groups. Several attempts were made to functionalize the polymer through standard nucleophilic displacement of alkyl halides by the deprotonated polyester. This method is currently disfavored, as several difficulties arose. The largest difficulty remains the solubility of the polymer after deprotonation, and the susceptibility of the polymer backbone to hydrolysis from adventitious water. The multi-site reaction block allowed the rapid screening of a range of solvent-base combinations in an attempt to modify the polymer using alkyl halide reagents. Solvents such as tetrahydrofuran, chloroform, *N,N*-dimethylacetamide, *N*-methyl pyrrolidinone, *N,N*-dimethyl sulfoxide, *N,N*-dimethyl formamide were evaluated as media for the reaction of the polymer with bases such as potassium hydroxide, sodium hydroxide, imidazole, and potassium carbonate. The relatively high steric hindrance of the polymer backbone coupled with the low solubility of the salt in each of these solvents resulted in little reactivity with representative alkyl halides (e.g. bromooctane). Furthermore, the susceptibility of the polymer backbone to hydrolysis was a deterrent to letting the reaction proceed for extended times (< 48 h). In the future, this method may be re-visited after a dry solvent system is installed in the lab and suitable phase transfer catalysts are obtained (e.g. 18-crown-6 for  $K^+$ , 15-crown-5 for  $Na^+$ , tetrabutylammonium iodide as general catalyst) to enhance the solubility and reactivity of the polymer system.

Fortunately, an alternative method of end group modification has been shown in the literature[58]. It is somewhat more limiting in scope, but allows the preparation of the modified polyester in good yield without solvent. The melt condensation of the polyester has proven to be a versatile technique for the preparation of modified hyperbranched polyesters. The general scheme employed is shown in Figure 182, and is straightforward in its application. The approach has also shown good results for the incorporation of multiple functional groups onto the polyester core.

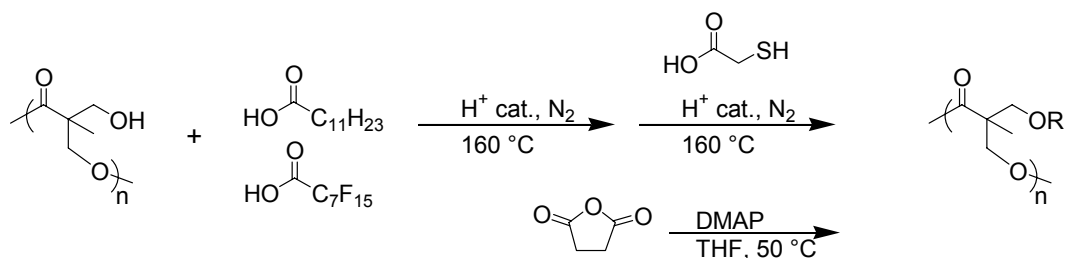


**Figure 182. Melt condensation for modified hyperbranched polyesters. Boltorn HBP is first functionalized with dodecanoic and perfluorooctanoic acids. Thioacetic acid may be added to incorporate thiol end groups, or the polymer may be isolated and functionalized with ring-opened succinic anhydride in a second step to generate acid end groups.**

The largest difficulty of modifying the polyester core arises from its increased backbone stiffness and increased molecular weight due to modification. As a result, the reaction block method of modification is not suitable for the preparation of the polyester, because the melt is too viscous to mix efficiently on the shaker table or by vortex mixer. To obtain good homogeneity, the polymer melt is mixed mechanically. On the small scale and with the lower molecular weight cores, this is accomplished with a magnetic stir-rod. Larger sample preparation and higher molecular weight cores require shaft driven mechanical mixing.

The other difficulty encountered with the melt modification of the hyperbranched polyesters arises from incompatibility of the polymer melt with some potential acids for end group modification. Acids with thermally unstable chain ends would be unsuitable for modification in this fashion (e.g. methacrylic acid) because of the high reaction temperatures involved (160°C). Also, the polar nature of the polyester core means that less polar acids have difficulty reacting into the system (e.g. perfluorinated acids, aliphatic acids longer than ~C<sub>14</sub>).

The approach used to circumvent these limitations is the partial reaction of the polyester's end groups with a compatibilizing end group, typically dodecanoic acid. The aliphatic chain reduces the viscosity of the polymer melt but is sufficiently soluble to react onto the polymer end groups. The resulting polymer is then sufficiently miscible such that long aliphatic acids (up to ~C<sub>22</sub>, behenic acid) or perfluorinated acids may be reacted onto the polymer. One drop of concentrated sulfuric acid is used to catalyze the reaction.

Polymers prepared in this fashion resulted in highly viscous oils or amorphous solids, depending upon the characteristics of the end groups attached. Examples of attached acids include the aliphatic acids with an even number of carbons from decanoic to behenic acid (C<sub>10</sub>-C<sub>22</sub>), the perfluorinated acids with an even number of carbons ranging from octanoic to hexadecanoic acid (C<sub>8</sub>-C<sub>16</sub>), and aromatic chain ends such as pyrene butyric acid (odd number acids are produced to a much lower extent in nature, and were not used strictly based on cost issues). Lower molecular weight acids could likely be incorporated in this fashion (e.g. acetic acid, benzoic acid), but would be better suited to alternate routes that operate below their vaporization temperatures.

Polymer analysis was performed using predominantly <sup>1</sup>H NMR. The complete attachment of acids to the polymer was determined by observing the shape and characteristics of the peaks

arising from the attached acid. Unreacted acids could be observed as sharp peaks with fine structure (e.g. doublet, triplet) while the covalently attached acid exhibited a broadened and slightly upfield shifted signal. The methylene group  $\alpha$  to the carbonyl proved to be the most isolated and well-resolved signal, so it was examined closely to confirm full reaction. The reaction of the perfluorinated acids is largely confirmed by examination of the analogous aliphatic acid, as our current capabilities do not extend to  $^{19}\text{F}$  NMR spectroscopy. The phase segregation behavior of the polymers has been consistent with covalent attachment to the perfluorinated acids.

#### *3.2.6.1.4 Styrene Suppression Efforts*

The commercially available styrene suppressant Styrid has been evaluated in our macro-TGA system, and has shown a high degree of VOC suppression after the formation of a surface skin. Styrid is a suspension of translucent white flakes in organic solvent, which is then mixed into a resin mixture to allow the formation of skin on the surface. Mass spectroscopy analysis of Styrid indicated that it is a mixture of substituted benzene rings (solvent), medium chain length alcohols (e.g. tridecanol), and various long chain hydrocarbons. The mass percentage of solids in the system is ca. 45%, meaning that a low proportion of solids is actually required to generate the skinning effect. According to the company website, Styrid may be incorporated as low as 0.6% by weight to provide the benefits observed[59]. Figure 183 shows the point of skin formation as a function of suppressant loading. The optimal loading of Styrid lies between 0.59% to 0.87% by mass, and increased loading does not significantly shift the onset of the suppression effect. However, the period of time required for skin formation is crucial, as it is during this initial period that styrene emission is greatest in systems undergoing cure. Unfortunately, Styrid did not affect the initial mass loss rate. Furthermore, the time scale for cure is typically less than 1 hour. Yet the time scale for the formation of the elbow is approximately 7 hours for the sample with Styrid. This indicates that Styrid does not reduce the evaporation rate of styrene during the typical cure time of vinyl ester resins. On the other hand, suppressant manufacturers claim that suppressants are most effective during cure. Therefore, cure studies using suppressants must also be studied.

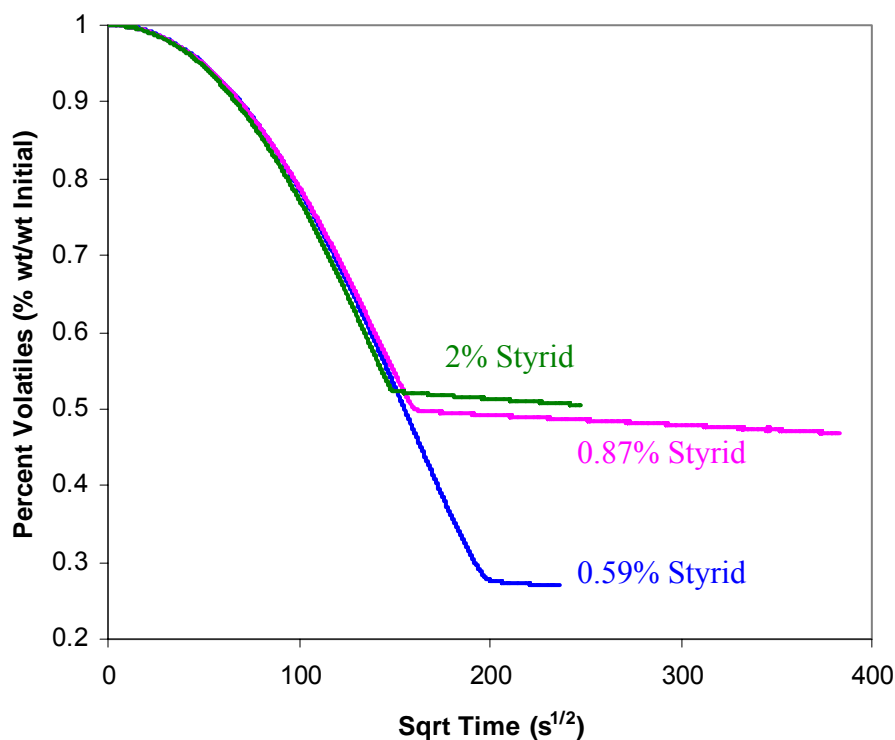


**Figure 183. VOC Suppression as a function of Styrid concentration in 1:1 styrene-VE formulation.**

Several suppressant candidates have been screened using the macro-TGA to evaluate VOC emission drop-off. Representative PEI-based candidates were tested, whose composition is shown in Table 56. The polymers were prepared as described in the preceding section, and were evaluated using a 1:1 styrene:828 vinyl ester resin formulation. The mass of the constituent elements of the polymers are represented relative to the mass of the PEI polymer core.

**Table 56. Composition of PEI-based suppressant candidates. A (+) indicates styrene suppression, (++) indicates better styrene suppression, and (-) indicates a formulation that increases styrene emissions.**

Polymer	Eq. Wt. PEI	Eq. Wt. Perfluoro	Eq. Wt. Aliphatic	Eq. Wt. PDMS	Effect
None	-	-	-	-	Baseline
PEI-Perfluor	1	0.11	0	0	+
PEI-Mixed	1	0.40	0.83	0	+
PDMS-OH	0	0	0	1	-
PEI-PDMS-Perfluoro	1	0.20	0	0.40	++

As an example, for the PEI core functionalized with perfluorinated chains (PEI-perfluor), if 1 g of PEI core was prepared, 0.11 g of the perfluorinated surfactant was reacted onto the polymer chain. The polymers were then mixed with the styrene-VE solution, and were dissolved or dispersed via extended mixing. Hyperbranched PEI with only perfluorinated groups was almost

insoluble in the styrene solvent, and at best it formed a homogenized dispersion. Addition of aliphatic chains improved the solubility to allow almost full solubility. Both the hydroxy terminated PDMS and the PEI-PDMS were fully soluble in styrene.

The results of the macro-TGA analysis of the PEI based suppressants are shown in Figure 184. The PEI polymers alone had little impact upon the total VOC emission of the sample. The PEI with slight perfluorination (PEI-Perfluor) was tested to determine if the PEI would hydrogen-bond sufficiently at the surface of the solution to provide any barrier properties. Negligible effect on VOC loss was observed. The use of more heavily perfluorinated PEIs has been precluded due to their insolubility in styrene and inability to form homogenized dispersions. While more soluble due to the attached aliphatic chains, the mixed end group PEI (PEI-mixed) should also have had sufficient residual amines free for hydrogen bonding. The results suggest that further reaction with the aliphatic epoxies may increase the barrier properties of the PEIs slightly, but these may not be the preferred end groups for reducing styrene emissions.

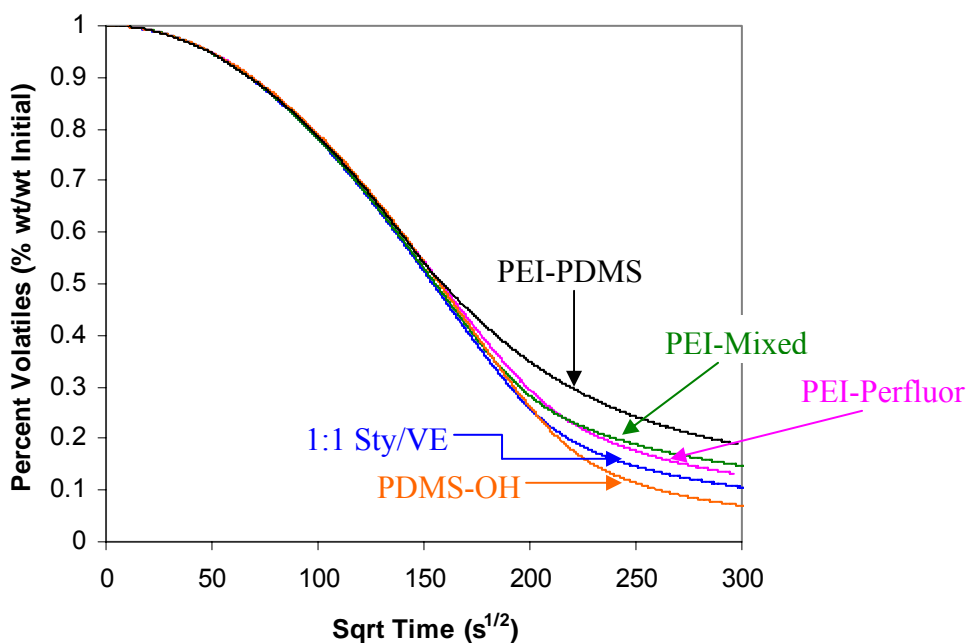


**Figure 184. PEI-based suppressant candidates**

The PDMS based PEIs were also investigated, and have shown promising initial results. The hydroxy-terminated PDMS (PDMS-OH), when dissolved in the styrene-VE solution, has no positive impact upon the rate of styrene emission and appears to change the dynamics of the resin, such that more styrene was evaporated at a given time than for the equivalent styrene-resin baseline system. The siloxane attached to a partially perfluorinated PEI (PEI-PDMS-Perfluoro), however, has generated a compound which has demonstrated a real reduction in styrene emission. After ca. 28 h, the PEI-PDMS suppressant had reduced total VOC emission by ca. 8.2%. Relative to VE/styrene with no suppressants, the PDMS-based PEI reduced the evaporation coefficient by 70% after 20 hrs.

We have looked at increasing the loading of the PDMS on the same PEI, and have found that with the current PEI core ( $M_w = 1300$  g/mol) and the current loading level of perfluorinated chains (0.2 equiv), additional PDMS loaded onto the PEI reduced the magnitude of the styrene suppression. We are currently investigating variation of the PEI core size and the extent of perfluorination in an effort to optimize the VOC suppression by this system.

In addition, the polyester based hyperbranched polymers have been investigated as styrene suppressants. They have the added benefit of better compatibility with the VE resin and increased thermal stability when compared to the analogous PEI systems. The primary end groups used for the modification of the polyester core were aliphatic chains of varying lengths. In some cases, the perfluorinated chains were attached to increase the driving forces for surface segregation. The motivation thus far has been to increase the aliphatic character so that these HBPs would mimic the composition of and possibly the styrene suppression mechanism of Styrid. Ideally these polymers would function as suppressants while maintaining good solubility, so they would not be filtered during infusion into composite weaves. Representative compositions are reported in Table 57.

**Table 57. Composition of polyester based suppressant candidates**

Polymer	End Group 1	Mole Fraction	End Group 2	Mole Fraction
C12	Dodecanoic Acid	0.8	-	-
C12 & C22	Dodecanoic Acid	0.25	Behenic Acid	0.55
C22 & C8F15	Behenic Acid	0.83	Perfluorooctanoic Acid	0.1
C22	Behenic Acid	0.93	-	-

The effects of these additives with respect to styrene suppression are shown in Figure 185, along with comparison to using unreacted behenic acid as a suppressant. Performance of the samples across the board have been disappointing, with no perceptible influence on VOC loss at early times, and only ca. 10% change in total VOC loss after 28 h. Relative to VE/styrene with no suppressants, the behenic acid modified Boltorns reduced the evaporation coefficient by one order of magnitude after 20 hrs. The compositions shown here indicate that long chain end groups suppress styrene more efficiently than short aliphatic end groups. Additionally, behenic acid used as suppressant outperformed the modified hyperbranched polymers. Hyperbranched polyesters modified with long chain aliphatic groups have exhibited low solubility that has been a concern for their efficiency as styrene suppressants. All of the polymers incorporating the behenic acid moiety and the behenic acid itself were not fully soluble in the styrene-VE solution. At this time it is unclear if limited solubility is a benefit for the suppression of styrene emission or if more fully soluble polymers might form a denser phase of hyperbranched polymers near the solution surface.

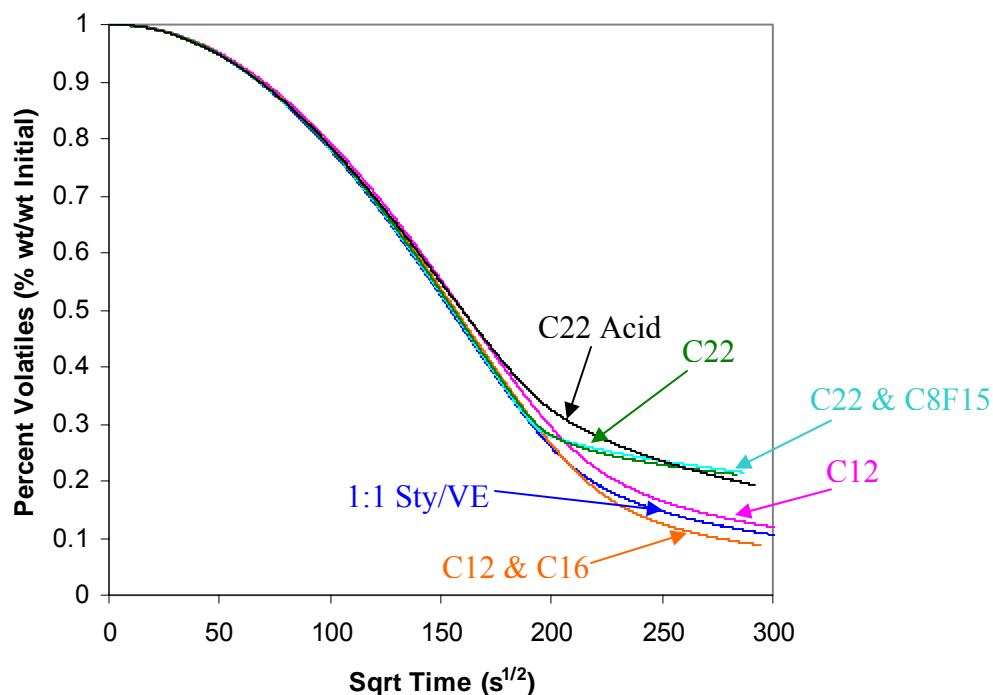


**Figure 185. Emissions performance of polyester based suppressant candidates at 2% loading.**

Currently, we are attempting to address this issue by investigating new synthetic targets and new formulations of HBPs. Synthetically, we are attempting to make targets with a wider range of aliphatic groups (e.g. C<sub>12</sub>, C<sub>16</sub>, C<sub>18</sub>, C<sub>22</sub> all on one core) with the expectation that mixed end group systems will frustrate the crystallization of the aliphatic chain ends, enhancing solubility. We are also trying to increase the level of perfluorinated chains incorporated onto the polymer core, and we have only recently begun the investigation of polyester cores of varying molecular weight. A similar approach is in progress with respect to the formulation of HBPs for suppression. Mixed polymers, each with a different end group, will be prepared to mimic the compositional makeup of Styrid. Additionally, higher molecular weight hyperbranched polymers will be used and modified to see the effect of core molecular weight on styrene suppression.

The dendritic polymer based suppressants we have investigated were designed to segregate to the surface of the resin and combine to form an amorphous top layer. As an alternative mechanism of suppression, additives that were reactive or could reasonably be expected to be responsive to their environment were also developed. It was hoped that by changing the mode of operation that more efficient materials could be discovered. Our previously reported materials have remained our best additives. Hyperbranched polyethyleneimines functionalized with short perfluorinated and long polydimethylsiloxane chains exhibited the best performance of the PEI-based materials. Hyperbranched polyesters functionalized with relatively long aliphatic chains remained the best materials we have developed, though their performance lags that of commercially available VOC suppressants.

The suppressants designed to form an amorphous surface layer were pursued because some of the hyperbranched polyesters with long aliphatic chains had poor solubility in styrene. The polymers would eventually soften and disperse, given sufficient time, but it was feared that heterogeneous surface coverage was achieved because of the crystallization of the long aliphatic chain ends of the HBP. To frustrate crystalline packing, mixtures of HBPs with singular end group compositions were mixed together and the resulting HBP mixture was used as the suppressant. Very little deviation from the control sample was observed.

The higher reactivity of the polyethyleneimine (PEI) scaffold lent itself to investigation of alternative functionalities. An array of acrylate and methacrylate based monomers were obtained from Sartomer. These were combined with the current Michael addition chemistry to functionalize the PEI scaffold with both perfluorinated and potential blocking groups. Figure 186 provides an illustration of representative monomers employed as end groups. These PEI materials, when combined as 2% additive in a 1:1 styrene-vinyl ester resin solution, slightly reduced VOC emissions at long time scales (~ 2.5% VOC reduction after 20h at 40°C). These results pale in comparison to our previously reported suppressants (ca. 8-11% VOC emission reduction after 20h and 40°C). The norbornyl acrylate end group (top functionality, bicyclic system) was selected because it is a large bulky group that fills space while frustrating packing. It was hoped that the sterics of the group would inhibit VOC loss. The bottom three groups are relatively polar groups based on ethylene or propylene glycols. It was hoped that the polarity mismatch would inhibit VOC emission, though the results of our experiments have not yet supported that approach.

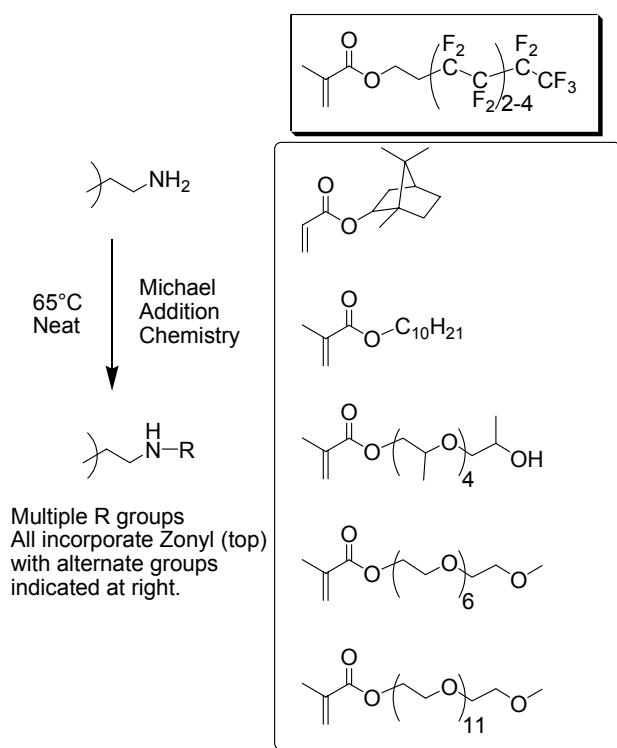


**Figure 186. New end groups for PEI scaffolds.**

In an effort to further explore the use of amorphous materials for VOC suppression, we have leveraged research efforts from an Army Research Office sponsored MURI (Multi-University Research Initiative) program involving Virginia Tech, Penn State, and Cornell University. The Macromolecular Architecture for Performance MURI (MAP-MURI) is concerned with the development of macromolecular architectures (e.g. hyperbranched or topologically distinct) macromolecules that provide some measurable benefit when used in applications. Professor Geoffrey Coates and coworkers have developed several novel catalyst systems for the polymerization of polyolefins, and have generated hyperbranched polypropylene. One sample was obtained for testing on the supposition that while more soluble, the hyperbranched polypropylene would exhibit the barrier properties of its linear analog. The results obtained for this additive are shown in Figure 187. Note that two replicates are included in the plot, the first trial with the additive showed potential to change the slope of the VOC loss curve at early times. The following trial was undertaken in an attempt to confirm the result. As evidenced by the figure, when temperatures remained constant, the effects of the additive were negligible. The change in slope shown in the first trial is attributed solely to the  $\sim 1^\circ\text{C}$  temperature variation observed. While not yet successful, we anticipate receiving additional samples for testing and remain hopeful that they may provide enhanced properties with more tuning.

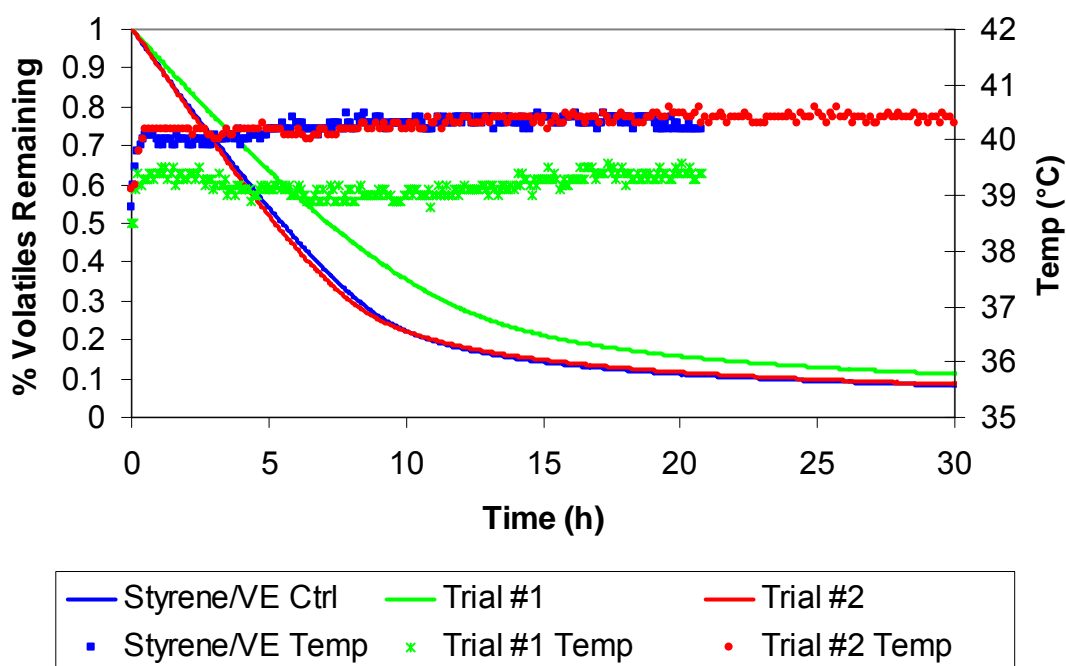


**Figure 187. Emissions as a function of time from a VE/Styrene 50/50 resin showing that HB-polypropylene is not an effective suppressant and temperature control is paramount.**

We have also been investigating the use of reactive components as additives, focusing on two component systems where the **A** and **B** components can react to form covalent bonds. The rationale is that covalent bond formation will promote the generation of a robust film at the surface of the resin. Our typical **A** component has been a hyperbranched PEI functionalized with perfluorinated groups and aliphatic chains. Residual N-H bonds in the polymer backbone or at the chain ends provide sites for the reaction of **B** component onto the HBP.

Our work in this area has centered upon the use of a trifunctional epoxy as the **B** component, produced by Resolution Performance Products. The combination of the hyperbranched polymer and the castor oil derivative initially gave a very promising result, as shown in Figure 188. The reactive system showed significant deviation from the control samples, and more importantly it appeared to change the slope of the styrene emission from very early times. Attempts were made to reproduce the results initially observed (trials Core = 800 g/mol, A-C). However, the positive result appears to have been caused by an aberration in the heating elements of our Macro-TGA oven. A shift of ca. 1.2°C seems to have accounted for the variations in VOC loss, as indicated by the average temperature labels in Figure 188. The slopes of the VOC loss track precisely with the average temperatures of the runs, indicating that the bi-component additive system had little influence on the overall VOC loss. The influence of the HBP core molecular weight was probed also, as indicated by the molecular weights of the HBP core in the figure labels. This series of samples had core molecular weights varying from ca. 800 g/mol to ca. 2000 g/mol; translating to degrees of polymerization of ca. 18 to ca. 47. Other composition ratios were probed for the bi-component additive system, investigating a range of stoichiometries with either the N-H or epoxy functionality in excess. In all cases, insignificant deviation from the control samples were observed, indicating that this route to VOC suppression with this pair of components is unlikely to yield effective styrene suppression.

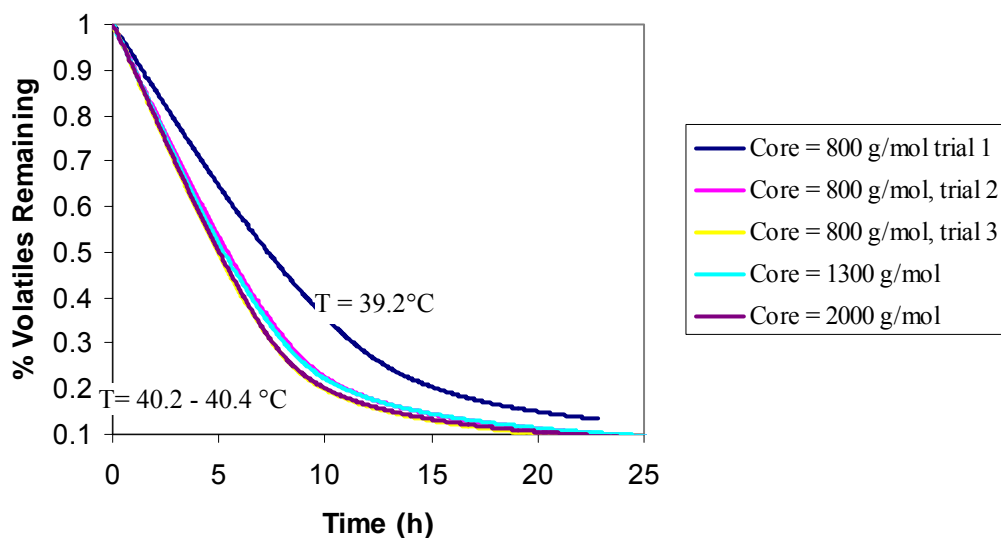


**Figure 188. Results of two component suppressant efforts. Trials with 2 component additives showed greater dependence upon oven temperature than additive composition (e.g. component A molecular weight variation).**

An alternative approach to enhancing VOC loss with dendritic additives has been proposed, using strong associations to cause a transient barrier to form on the resin surface. Suggested functionalities for these applications include hydrogen bonding donor-acceptor groups and spontaneous self-reactive groups, such as thiols. Figure 189 shows these functionalities and how they may be expected to interact. These hyperbranched polymers were prepared using our hyperbranched polyester scaffold, due to the compatibility of available functional groups with these chemistries. The reaction schemes used to functionalize the HBPs are shown in Figure 179. The requisite aliphatic groups were added to enhance the solubility of the HBP through

melt condensation techniques. Thioacetic acid was then added to the reaction to condense onto the HBP, resulting in a thiol-modified HBP. The material was characterized by  $^1\text{H}$  NMR, and clear resonances for the installed thiol were observed. The HBP also appears to absorb or chelate gold nanoparticles, further supporting the presence and availability of the thiols for further reaction.

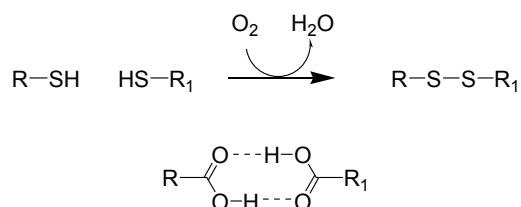


**Figure 189. Disulfide bond formation (top) and carboxylic acid.**

Acid groups were attached to HBP that had been isolated from the melt condensation with only aliphatic and residual hydroxyl (-OH) groups on the periphery. The HBP was dissolved in THF and N,N-dimethylaminopyridine, a well-known activator of carbonyl groups, was used to catalyze the ring-opening of succinic anhydride by the hydroxyl groups. The resultant material was purified by extraction, and the ring-opened acid was observed on the HBP via  $^1\text{H}$  NMR.

These HBPs were evaluated for VOC suppression characteristics using our standard 1:1 styrene-vinyl ester resin solution with 2% additive composition. These candidates exhibited no appreciable suppression. The underlying reason for the performance of these materials could be related to sterics (e.g. HBP scaffold hindering intermolecular interactions) or it could be a conformational issue. If the HBPs are in a poor solvent condition, they could simply have most of their polar chain ends buried in the interior of the HBP, leaving the nonpolar dodecanoic or perfluorinated chain ends in the styrenic liquid phase.

### 3.2.6.2 Triglyceride-Based Dendritic Systems

#### 3.2.6.2.1 *Preparation of Fluorinated, Acrylated Triglycerides*

Triglycerides are first generation dendrimers. Although we hypothesize that increases in the molecular weight of the dendritic polymer should reduce the styrene emissions, first generation dendrimers should also be tested because they are inexpensive and simple to prepare, especially in the case of triglyceride-based dendrimers. Epoxidized soybean oil was chosen as the starting material for this study because it is the least expensive commercially produced epoxidized oil. In addition, it has sufficient epoxide functionality (4 epoxides per triglyceride) for adding both acrylate functionality and surface-active functionality. Epoxidized linseed oil (~6 epoxides/triglyceride) can be used in the future. However, this oil has a greater tendency for epoxy homopolymerization, which will produce undesired structures for this study. There are a number of ways of attaching vinyl functionality to triglycerides[60]. We have initially chosen to add acrylic acid to the triglycerides to enable triglyceride-based dendrimers to polymerize with the VE resin. The addition of acrylate functionality has been studied extensively, the synthesis procedures are well known, and the starting material (epoxidized oils) are inexpensive and commercially produced. In addition, the methods we foresee to producing higher generation

dendrimers make use of epoxidized oils. As for the commercial dendrimers, the addition of fluorinated chains should make the triglycerides surface-active. The simplest method for adding fluorine functionality is to add a fluorinated acid to the epoxide groups of the triglycerides.

Epoxidized soybean oil with 4 epoxides per triglyceride, as measured with NMR [61], was reacted with both perfluorooctanoic acid (completely fluorinated, 8-carbon atom acid) and acrylic acid. 1 wt% AMC-2 was added to the epoxidized oil to catalyze the acid-epoxy reaction and prevent epoxy homopolymerization [4]. Hydroquinone in the amount of 0.0033 g/ml was added to the oil to inhibit free radical polymerization of the acrylic acid [62]. Perfluorooctanoic acid in the amount of 1 group per triglyceride was first added to the epoxidized oil and reacted at 75°C for 1 hour. Then, 3.1 moles of acrylic acid per mole of epoxidized oil was added to the reaction mixture. The reaction was allowed to run for an additional 5 hours. To remove inhibitor and any unreacted acid, the reaction mixture was ether extracted [45]. The mixture was dissolved in diethyl ether and poured into a separatory funnel. Distilled water was added to remove some of the acid from the ether phase. The layers were allowed to separate, and the water layer was discarded. This step was repeated three times. An aqueous solution of saturated sodium bicarbonate was added, which was then shaken to ensure good mixing. The contents were allowed to separate into oil and water layers. The aqueous layer was discarded. Sodium bicarbonate washes were repeated, if necessary, until the pH of the water layer was neutral or alkaline, as determined by pH paper. The ether solution was washed with saturated aqueous sodium chloride to remove water from the ether phase and dried over anhydrous sodium sulfate. The ether was evaporated away at room temperature. NMR confirms the presence of 3 acrylate groups and 1 fluorinated chain on average per triglyceride. Thus, a triglyceride with both anchor and buoy functionality was prepared. Other monomers will be prepared and further studies to determine the ability of this monomer to reduce styrene emissions will be performed in the near future.

#### *3.2.6.2.2 Triglyceride-Based Dendritic Polymers*

There are a number of methods for producing dendrimers. Many of these are time-consuming and require very careful chemistry. The cheapest and easiest way to synthesize triglyceride-based dendrimers is through AB<sub>2</sub> monomers. These monomers have one A group, two B groups, and A and B add to each other when they react. So far, two possible synthetic routes have been hypothesized (Figure 190).

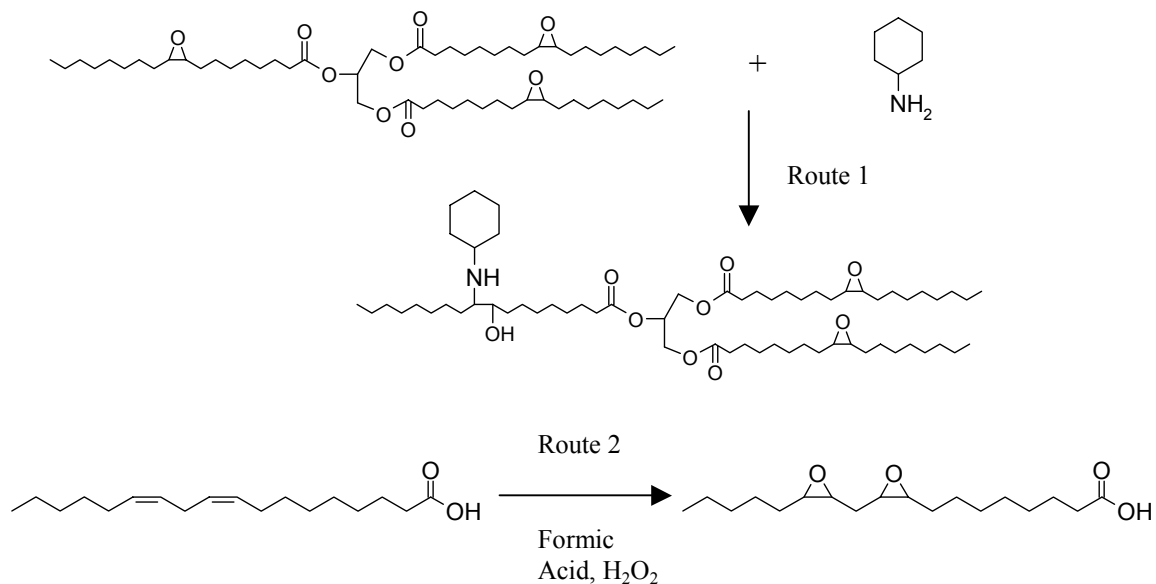


**Figure 190. Potential methods of producing AB<sub>2</sub> monomers from triglycerides and fatty acids. In Route 1, epoxidized triglycerides are modified with cyclohexyl amine. In Route 2, linoleic acid is reacted to form epoxidized linoleic acid.**

In Route 1, a tri-epoxy triglyceride is reacted with a primary mono-amine. The two remaining epoxide groups can react with secondary amines attached to other triglycerides to form a dendritic structure. In order to form a perfect dendrimer, we must start with a tri-epoxy triglyceride and only 1 primary amine should react with a given triglyceride. Olive oil, canola oil, and genetically engineered high oleic soybean oil are excellent candidates as starting materials because of their high likelihood of having one unsaturation site (and thus one epoxide) per fatty acid. In this work so far, epoxidized soybean oil was used because it is inexpensive and readily available. Cyclohexylamine is an excellent candidate as the mono-amine because its primary amines are much more reactive than its secondary amines [63]. Therefore, stable AB<sub>2</sub> monomers can be prepared, which can later be polymerized into dendrimers.

Epoxidized soybean oil was reacted with cyclohexylamine in the stoichiometric amount. The reaction was performed at 60°C initially, but because the sample viscosity remained very low, the temperature was increased to 90°C. After 1 week of reaction, the reaction mixture became fairly viscous, but did not gel. If complete reaction were to occur, this reaction mixture should gel because of the excess epoxides and the high likelihood of having at least two or more epoxides on the same triglyceride reacting with primary epoxides. SEC was run on the sample to determine if the molecular weight of the triglycerides increased. Unfortunately, no change in the SEC chromatograph was observed. Therefore, epoxidized soybean oil was then reacted with cyclohexylamine at 90°C for 1 week in the presence of 1 wt.% phenol, which catalyzes this reaction [63]. The viscosity of the sample increased much more rapidly than for the case without phenol. In addition, small gel-like particles were observed in this reaction mixture. However, the samples have not been analyzed with SEC to determine their molecular weight. More work will be done to characterize and improve the synthesis of these dendrimers.

In Route 2, linoleic acid, a fatty acid rather than a triglyceride, was used as the starting material and was epoxidized. The monomer has 1 acid group and two epoxide groups, and is thus an AB<sub>2</sub> monomer. The AMC-2 catalyst can be used to inhibit epoxy homopolymerization, while catalyzing the acid-epoxy reaction. Current results only prove that epoxidized linoleic acid was successfully produced. Unfortunately, our source of linoleic acid was poor, so that the epoxide functionality was less than 2 (~1.4 epoxides/fatty acid), as determined by NMR [61]. Pure linoleic acid can be used, but this acid is fairly expensive. Alternatively, safflower oil, which has a very high linoleic acid content, can be broken down into its fatty acids and used as an inexpensive source of linoleic acid. However, imperfections in the resulting dendrimer will be produced due to the presence of saturated, mono-unsaturated, and tri-unsaturated acids.

Initial efforts to make hyperbranched polymers from fatty acids were not successful. The epoxidized linoleic acid was reacted with itself and with 1 wt.% epoxidized soybean oil for times as long as 2 weeks. Although FTIR results indicated that all epoxide groups were reacted, SEC results did not show the presence of polymer for the most part. A peak representing higher molecular weight oligomers did appear, but most of the reaction contents were still monomers. On the other hand, when epoxidized soybean oil was polymerized along with the epoxidized linoleic acid, higher molecular weight polymers were achieved (Figure 191). However, a substantial portion (~15 wt%) was still monomer, and the polymer molecular weight is still fairly low (< 5000 g/mol).

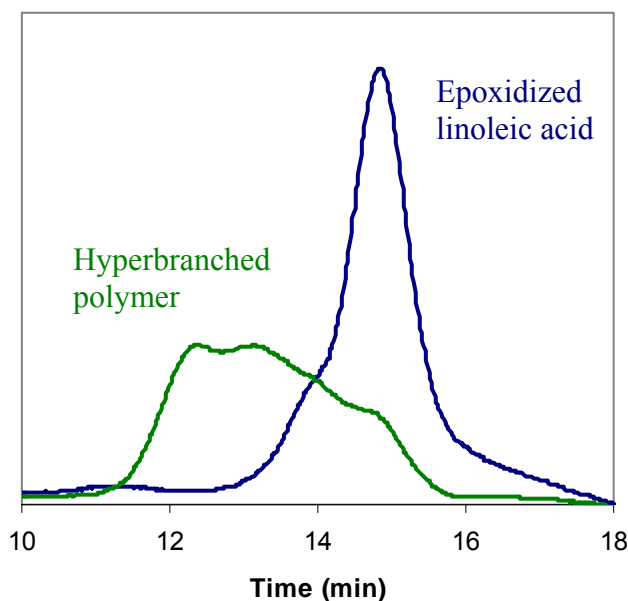


**Figure 191.** The SEC traces of epoxidized linoleic acid compared to that of hyperbranched polymers derived from epoxidized linoleic acid and epoxidized soybean oil.

### 3.3 ENVIRONMENTAL IMPACT AND COST SAVINGS ANALYSIS

#### 3.3.1 Direct Cost

The pertinent factors influencing the commercial production of any VE monomer include the costs of raw materials, synthetic requirements for preparation (e.g. reaction conditions, controls,

and purification requirements), and transportation costs and requirements. The methacrylated fatty acid monomers (MFA's) have been examined using these data to determine projected costs of production and to determine final price points for formulated resins.

### 3.3.1.1 Raw Material Costs

Raw materials costs were calculated by calling suppliers and obtaining up-to-date pricing for the desired components at bulk-order pricing. Most of the suppliers had minimum quantity orders, including one with an order requirement of 40,000 lbs. Another variable was the method of delivery. Materials delivered in 55 gallon drums were generally \$0.10 - \$0.15 per pound more expensive than those delivered in bulk fashion (e.g. rail car or truck-load). For comparison purposes, costs are listed for 55 gallon drum scale or similar whenever possible. The quoted prices were determined in December, 2005 (Table 58).

**Table 58. The quoted price for a given volume scale for various chemicals relevant to the production of bimodal vinyl esters and fatty acid-based vinyl esters.**

Chemical	Price	Volume Scale	Company
<b>Fatty Acids</b>			
Light cut fatty acids	\$1.15/lb	440 lb bag/drum	Twin Rivers Technology (P&G)
Lauric Acid	\$0.65/lb	440 lb bag/drum	Twin Rivers Technology (P&G)
Myristic Acid	\$0.75/lb	440 lb bag/drum	Twin Rivers Technology (P&G)
<b>Vinyl Esters</b>			
Derakane 411-350	\$2.18/lb	55 gal drum	Ashland Chemical Company
Derakane 441-400	\$2.55/lb	55 gal drum	Ashland Chemical Company
CN-151	\$4.15/lb	440 lbs	Sartomer
<b>Epoxy Resin</b>			
Epon 828	\$2.18/lb	55 gal drum	Ashland Distribution Company
Epon 1001F	\$2.22/lb	55 gal drum	Ashland Distribution Company
Epon 1004F	\$2.22/lb	55 gal drum	Ashland Distribution Company
Epon 1007F	\$2.22/lb	55 gal drum	Ashland Distribution Company
Epon 1009F	\$2.22/lb	55 gal drum	Ashland Distribution Company
<b>General Chemicals</b>			
Styrene	\$0.68/lb	45,000 lb truck load	Dow Chemical Company
Methacrylic Acid	\$3.96/lb	55 gal drum	Sigma-Aldrich Development and Manufacturing Scale Department
Glycidyl methacrylate	\$4.34/lb	55 gal drum	Dow Chemical Company
AMC-2 Catalyst	\$32.03/lb	55 gal drum	Aerojet Fine Chemicals

The cost of the fatty acids seems exceptionally high. These chemicals are produced in a similar manner relative to biodiesel. The cost of biodiesel is ~ \$2/gallon or \$0.30/lb. Considering the inexpensive chemicals and similar purification procedures, we would expect the cost of fatty acid monomers to be ~ \$0.30/lb. We believe the prices quoted to us have a considerable mark-up that would be omitted for a company producing these fatty acid monomers on a large scale.

### 3.3.1.2 Estimated Resin Costs

#### 3.3.1.2.1 *Fatty Acid-Based Resin Costs*

The rough estimate for monomer production costs and system formulation, as suggested by R. Moulton of Applied Poleramics Inc., is to use a multiplier of raw material costs for the target price. For monomer generation, it was suggested that 2x is a suitable target price. One benefit of the MFA preparation is that the resultant material will be a DOT non-regulated material, reducing shipping costs.

Using lauric acid, myristic acid, and a light cut of fatty acids (C8-C10 mixture) as the basis for cost analysis, we can estimate the influence of molecular weight on pricing for the final product (Table 59). Note that the chain lengths of the fatty acids results in different weight fractions used for the monomer preparation. For example, to generate 1 lb of monomer from the light cut, lauric, and myristic acids requires differing quantities of glycidyl methacrylate for each fatty acid. At 0.5 wt.% loading levels, the catalyst adds \$0.17 per pound to the materials cost, and about \$0.34 per pound at 1% loading. Other less expensive catalysts can be used, such as triphenyl phosphine/triphenyl antimony. These catalysts would only add ~ \$0.05/lb to the final cost.

**Table 59. The projected cost of MFA monomers on the small production scale.**

Net Wt.	Fatty Acid	Mass FA	Mass GM	Materials Cost	Small Scale Price
1 lb	Light cut	0.527	0.473	\$2.71/lb	\$5.42/lb
1 lb	Lauric	0.585	0.415	\$2.23/lb	\$4.46/lb
1 lb	Myristic	0.616	0.384	\$2.18/lb	\$4.35/lb

At the laboratory scale, the reaction is typically executed in a jacketed reactor with cooling, to control the exotherm as the reagents undergo addition. The chemistry employed is facile and robust, requiring no inert environments and demonstrating independence from atmospheric moisture. On a small batch-scale production level, the material could be prepared in drums, undergoing reaction at room temperature after mixing. Production at this stage would be limited to several drums per week, resulting in about 250 gallon capacity per week. Including catalyst at 0.5 wt.% loading, the lauric acid based FA monomer could be delivered to customers for ca. \$4.46/lb, including shipping and production costs (using 2x multiplier for raw materials cost) (Table 59). Following the production of the monomer, it will be incorporated into VE formulations before being shipped out to the marketplace.

The price can be reduced significantly through a few means. First, larger scale facilities are less likely to have a substantial mark-up in the cost of the fatty acids. This would reduce the materials cost of the resin by ~\$0.30/lb. The use of the less expensive catalyst package would reduce the materials cost by another \$0.12/lb. Finally, when production is scaled-up to the size of specialty monomers, or especially commodity chemicals, the price would drop due to economy of scale. Overall, we'd expect that the chemical industry could produce these monomers for less than \$2/lb. Although the price is considerably higher than that of styrene,

these fatty acid monomers would be less expensive than glycidyl methacrylate, and other possible petroleum comonomers with costs of \$3-\$5/lb.

The most successful resin formulation based on this work is the VE/MFA/Sty 65/15/20. This resin formulation can be prepared using Derakane 441-400 as the basis and adding MFA and pure VE to reduce the styrene content to 20 wt.% while maintaining 65 wt.% VE. This formulation uses 60.6 wt.% Derakane 441-400, 24.4 wt.% pure VE (CN-151) and 15.0 wt.% MFA. Based on the component costs, the price of the resin formulation as made from a small manufacturer, such as Applied Poleramics, Inc., was estimated (Table 60). The price factors in a 2x multiplier for the MFA costs. The first price column uses the cost for all of the components to determine the price. According to the quoted prices for Derakane resins and their styrene contents, the cost of pure VE was calculated to be \$3.4/lb. Rather than using the marked-up price for CN-151, the cost for Derakane VE resins was assumed for the second price column. The costs for the resins are approximately 18-32% greater than the cost of Derakane 441-400. Considering the 40% reduction in emissions relative to Derakane 441-400, it is possible to find a market for these resins. However, for large-scale DoD impact, the cost of these resins would need to be reduced.

**Table 60. The estimated prices for VE/MFA/Sty 65/15/20 resins as produced from a small scale manufacturer.**

Methacrylated Fatty Acid Used in Resin Formulation	Estimated Price for VE/MFA/Styrene 65/15/20	
	Based on all component costs (CN-151 included)	Based on Derakane VE costs (CN-151 excluded) and other chemical costs
Light cut	\$3.37/lb	\$3.19/lb
Lauric acid	\$3.23/lb	\$3.04/lb
Myristic acid	\$3.21/lb	\$3.03/lb

Based on the component costs, the price of the resin formulation as made from a large resin manufacturer can be estimated without the large mark-up in price for the MFA monomers (Table 61). Interestingly, the estimated resin prices are only slightly above the cost of Derakane 441-400. Furthermore, if the MFA monomers can be produced at a large scale, dropping their price to ~\$1.50/lb (third price column), the cost difference between Derakane 441-400 and our low VOC formulation is only \$0.05/lb while reducing emissions by 40%. Based on these numbers, we would expect that the use of these resins is economically viable and would be considered for use in most DoD vinyl ester applications.

**Table 61. The estimated prices for VE/MFA/Sty 65/15/20 resins as produced from a large scale VE manufacturer for a number of assumptions of the economy of scale.**

Methacrylated Fatty Acid Used in Resin Formulation	Estimated Price for VE/MFA/Styrene 65/15/20		
	Based on all component costs (CN-151 included)	Based on Derakane VE costs (CN-151 excluded) and other chemical costs	Economy of scale projection (\$1.50/lb MFA)
Light cut	\$2.96/lb	\$2.78/lb	\$2.60/lb
Lauric acid	\$2.89/lb	\$2.71/lb	\$2.60/lb
Myristic acid	\$2.88/lb	\$2.70/lb	\$2.60/lb

### 3.3.1.2.2 Bimodal Blend Resin Costs

The vinyl ester preparation reaction is a well known reaction, and is relatively simple though it does require the use of elevated temperatures and cooling coils to prevent thermal runaway and gelation. On a small batch-scale production level, the material could be prepared in drum reactors. Production at this stage would be limited to several drums per week, resulting in about 250 gallon capacity per week. AMC-2 catalyst loading of 0.5 wt% was found to be sufficient for this reaction. Once the methacrylation reaction is finished, the resin will be mixed while hot with styrene in the proper ratios to produce the bimodal vinyl ester resin.

The raw material costs were used to estimate the price of the bimodal resin (Table 59). Considering that each 100XF resin used requires different methacrylic acid contents, the costing was determined for all four 100XF blends at two different styrene contents (Table 62). The resin cost is only a little over \$2/lb. Therefore, it is feasible that this resin formulation would be used in industry because a lower estimate for its price is in line with current commercial resin prices. Table 63 uses the 2x multiplier for raw materials cost to determine the price a small manufacturer would sell the resin. This cost of over \$4/lb is an upper estimate to the resin price. It is expected that larger manufacturers should be able to reduce this price to \$3/lb or lower because of the economy of scale. Based on these numbers, bimodal vinyl esters are also economically feasible alternatives to current commercial resins and we would expect them to be considered for use in most DoD vinyl ester applications.

**Table 62. Lower bound estimate (large scale manufacturer) for the cost of bimodal vinyl ester resins.**

Cost per Pound (\$/lb)				
Formulation	Epon 1001F	Epon 1004F	Epon 1007F	Epon 1009F
75/25 + 35% styrene	2.18	2.17	2.15	2.15
75/25 + 30% styrene	2.27	2.25	2.24	2.24
65/35 + 35% styrene	2.16	2.13	2.11	2.11
65/35 + 30% styrene	2.24	2.22	2.20	2.20

**Table 63. Upper bound estimate (small scale manufacturer) for the cost of bimodal vinyl ester resins.**

<b>Cost per Pound (\$/lb)</b>				
<b>Formulation</b>	<b>Epon 1001F</b>	<b>Epon 1004F</b>	<b>Epon 1007F</b>	<b>Epon 1009F</b>
75/25 + 35% styrene	4.37	4.33	4.30	4.30
75/25 + 30% styrene	4.54	4.50	4.48	4.48
65/35 + 35% styrene	4.32	4.26	4.22	4.22
65/35 + 30% styrene	4.49	4.44	4.40	4.39

### 3.3.2 Indirect Cost Analysis

An initial analysis of military platforms has been completed in order to determine potential use applications of new VE resin technologies. Among the factors influencing resin selection are performance requirements including thermal limits and resin durability in harsh environments. Because of the complex nature of end-use for military composites, it is difficult to narrow applications to focus on only select resin systems. In our effort, however, we can conclude that cost is a substantial driver to resin selection for both the naval surface warfare structures and for the Army Future Combat Systems.

Additionally, an even greater cost restriction is observed in Army composite replacement platforms, where composite structures are being implemented as corrosion resistant replacement parts in legacy platforms. Among the platforms scheduled to see composite replacement parts in the near term are Army transport vehicles, such as HMMWV hoods and doors, M939 hoods and cargo floors, and M35-A2 and M35-A3 hoods, doors and fenders. The total volume of replacement components in these military platforms approaches \$20M annually, which if replaced with low-cost VE resins, as is currently proposed in designed technologies, could result in substantial increases in pollution from military fielded structures.

Besides raw material costs, composite fabrication results in other costs to the DoD. Because of the NESHAP regulations, HAP emissions from current composite resins would need to be captured and removed from the air in manufacturing facilities. These costs would introduce the capital costs of installing hood and other emissions capture devices [64], which is approximately ~\$1M/site. In addition, the cost of installing scrubbing devices to remove the emissions from the air would be an additional ~\$1M/site. The operating and maintenance costs for these devices would be approximately ~\$200k/site/yr. Additionally, emissions monitoring would need to be performed in each of these facilities costing again ~\$200k/site/yr.

Rather than using vinyl ester resins, epoxy resins can be used for most composite applications. Epoxy resins have only ~ 2-10% HAP content, and therefore would not require the acquisition of the large and expensive capital equipment to capture and treat emissions. However, epoxy resins cost ~\$8/lb, which is 370% more than that of Derakane 411-350 and would still require the manpower and costs associated with emissions monitoring.

The low VOC resins developed in this work would also still require VOC emissions monitoring at ~\$200k/site/yr. Also like epoxy resins, these low VOC VE resins would not require the expensive capital equipment for emissions capture and treatment. Even at a price of \$3/lb, the

use of these low VOC resins would make financial sense relative to epoxy resins because of their lower cost per pound (Table 64). The use of ~100,000 lbs resin per year was assumed for comparison purposes. This amount of resin is the expected annual amount for HMMWV composite hood replacements. Based on this relatively small production volume, the capital costs for HMMWV hood production alone should be ~\$500k, with annual operating costs of ~\$200k. Assuming the low VOC resin will cost ~\$3/lb (bimodal or fatty acid-based VE) and the Derakane resin costs ~\$2/lb, Table 65 shows that the higher resin costs for the low VOC resins are more than offset by the capital and operating expenses required for the standard VE/UPE resin. As a result, return on investment (ROI) should occur in ~2.5 yrs. These results show that it is clearly in the best interest of the DoD to switch to low VOC resins to reduce costs, while also reducing emissions and improving properties.

**Table 64. Costs over 10 years for epoxy resins for production of HMMWV hoods (~100,000 lbs resin/yr) relative to using low VOC resins.**

<b>Cost</b>	<b>Epoxy Resins</b>	<b>Low VOC VE</b>	<b>Cost Benefit of Low VOC VE</b>
Emissions monitoring	\$200,000	\$200,000	\$0
Emissions Capture (capital)	\$0	\$0	\$0
Emissions Capture (operating)	\$0	\$0	\$0
Emissions Treatment (capital)	\$0	\$0	\$0
Emissions Treatment (operating)	\$0	\$0	\$0
Resin Cost	\$8,000,000	\$3,000,000	\$5,000,000
<b>Total=</b>	<b>\$8,200,000</b>	<b>\$3,200,000</b>	<b>\$5,000,000</b>
<b>ROI=</b>			<b>0 yrs</b>

**Table 65. Costs over 10 years for standard VE resins for production of HMMWV hoods (~100,000 lbs resin/yr) relative to using low VOC resins.**

<b>Cost</b>	<b>Standard VE</b>	<b>Low VOC VE</b>	<b>Cost Benefit of Low VOC VE</b>
Emissions monitoring	\$200,000	\$200,000	\$0
Emissions Capture (capital)	\$250,000	\$0	\$250,000
Emissions Capture (operating)	\$1,000,000	\$0	\$1,000,000
Emissions Treatment (capital)	\$250,000	\$0	\$250,000
Emissions Treatment (operating)	\$1,000,000	\$0	\$1,000,000
Resin Cost	\$2,000,000	\$3,000,000	-\$1,000,000
<b>Total=</b>	<b>\$4,700,000</b>	<b>\$3,200,000</b>	<b>\$1,500,000</b>
<b>ROI=</b>			<b>2.5 yrs</b>

A cost comparison to metal structures was not performed. In general, it was assumed that the switch to composites from metal structures is done to address a serious materials issue, such as corrosion, or to meet a specification that metal parts cannot meet. In general, the switch from metal to composites is being done to reduce required maintenance, improve force readiness, reduce weight, and improve range and mobility of our forces.

### 3.4 CONCLUSIONS

Styrene emissions from VE resins occur during all phases of processing and fielding of the composite part. Reducing the styrene content in VE resins decreases the processability of and fracture toughness of these resins, and is therefore not an acceptable means of reducing styrene emissions. Styrene emissions can be successfully reduced or eliminated from VE resins by using a bimodal distribution of VE monomers and replacing styrene with methacrylate monomers or fatty acid-based monomers.

Synthetic procedures to produce VE monomers with a narrow molecular weight distribution have been developed. The use of techniques including FTIR, SEC, and NMR to characterize the monomers has been established. The properties of model VE systems and commercial VE resins have been measured, and the effect of VE molecular weight and styrene content were assessed.

A macro-TGA was designed and developed to measure the styrene emissions from commercial and model VE resins. VE resin mass loss as a function of time displayed a characteristic elbow, where the mass loss rate decreased significantly. In addition, initial styrene emission rates were not a function of styrene content. However, the total content of styrene evaporated was a function of styrene content, indicating that styrene emissions can be reduced by using a bimodal distribution of VE monomer. The styrene emissions of commercial resins were assessed. The styrene emission from these resins was regular and can be predicted using mathematical models.

Bimodal blends of vinyl ester monomers have been prepared. These resins result in low resin viscosities and high polymer toughness. Also, these resins use ~20% less styrene, thereby reducing styrene emissions. Furthermore, emission studies showed that overall emissions were reduced as the molecular weight of the vinyl ester monomer increased.

A number of petroleum-based methacrylate comonomers were used in place of styrene in VE resins. Cyclohexyl methacrylate appears to be the best choice as a styrene replacement because its resins have low viscosities, and the polymer properties were similar to VE/styrene resins. Synthetic procedures for preparing fatty acid-based comonomers have been developed because of the potential environmental and economic benefit. Current results show that when fatty acid-based comonomers are blended with styrene, they result in resins and polymers with very good properties. These fatty acid-based resins have excellent fracture properties and have over 50% reduction in VOC emissions. Shorter saturated fatty acid chains, elevated temperature cure, and E-beam cure are all ways of improving the properties of these resins. There are additional ways of modifying fatty acid structure to improve the properties of the resulting polymers, some of which will be tested next year. Unfortunately, current cost estimates of these fatty acid monomers are high because of the high cost of glycidyl methacrylate and the low production levels.

The low VOC composites that have been fabricated have properties that are similar or superior to that of composites made with commercial resins. Also, bimodal-based vinyl esters and mixtures of fatty acids and bimodal blends of vinyl esters can be used to make composites with excellent performance and low VOC emissions.

Commercial styrene suppressants do not decrease styrene evaporation within the time-scale for cure. Therefore, the styrene suppressants developed in this work must segregate to the surface faster to effectively reduce styrene emissions. Multi-functional dendritic styrene suppressants have been prepared. Triglycerides, fatty acids, and commercial dendritic polymers were used. Fluorine functionality has been introduced into the dendritic polymer to induce surface segregation. These suppressants segregate to the surface, but currently they have only reduced styrene emissions to a small degree. The use of suppressants composed of two components that react to form a barrier to styrene evaporation have also been ineffective.

Overall, the program has been successful at identifying critical DoD environmental needs, developing practical solutions to these requirements, and developing candidate resins for reducing VOC emissions from VE resins for military applications. Future work must still be done to further develop these candidate resins and discover new low VOC resin systems. Furthermore, work must be done to ensure that these resins produce good composite parts with good properties.

This program exceeded all originally established goals and accomplished many scientific achievements as well as many other important achievements:

- The novel idea of using fatty acid monomers as styrene replacements in thermosetting resins.
- The development of a number of novel fatty acid monomers for the production of renewable polymers.
- The development of bimodal blends of vinyl ester monomers to improve fracture behavior using low styrene content while maintaining processability.
- A device for measuring styrene mass loss as a function of time and temperature from large samples.
- Improvement in fracture properties of as much as three times relative to commercial resins.
- Improvement in composite mechanical properties.
- Reduction in VOC/HAP emissions by as much as 78%.
- Development of a model to predict the emissions profiles from vinyl ester resins with a fair degree of accuracy.
- A number of Army technical reports (App. B).
- Six published journal publications, and many more in progress (App. C).
- In addition, this project received a number of awards including:
  - SERDP Weapons Platforms Project of the Year Award for SERDP PP-1271, November, 2005.
  - Army Research and Development Award, 2005.
  - Best Resin Technical Paper Award, *Composites 2004*, Tampa, FL, presented by the American Composites Manufacturing Association.

## 4.0 PERFORMANCE ASSESSMENT

### 4.1 PERFORMANCE DATA

Four demonstrations were completed under this Environmental Security Technology Certification Program (ESTCP) effort to assess the efficacy of the +100 additive to reduce particulate emissions from turbine engines. The demonstrations were:

1. Four JT8D-9A engines on T-43 aircraft at Randolph AFB
2. TF33 engine at Barksdale AFB
3. Second TF33 engine at Barksdale AFB (TF33 II)
4. T63 engine at Wright-Patterson AFB

All engines under this demonstration program except the T63 were tested at a minimum of five power settings with and without the +100 additive. PND, particle size distribution, and fuel chemical composition were analyzed. Each engine power setting was held 5 to 10 minutes to ensure steady-state operation and gather sufficient data for statistical analysis. Several size distribution measurements were taken at each power setting to assess particle size consistency throughout the test period. Particulate data for the TF33 and T-43 demonstrations are presented in Tables 66, 67, 68, and in Figure 192. The PND data trends were fairly consistent as a function of engine power except for the abnormally high PND for the cruise power for engine #608 (Figure 5). The large discrepancy may be due to a dilution air leak or an instrument malfunction.

**Table 66. Particle Number Density Data for TF33 Test I.**

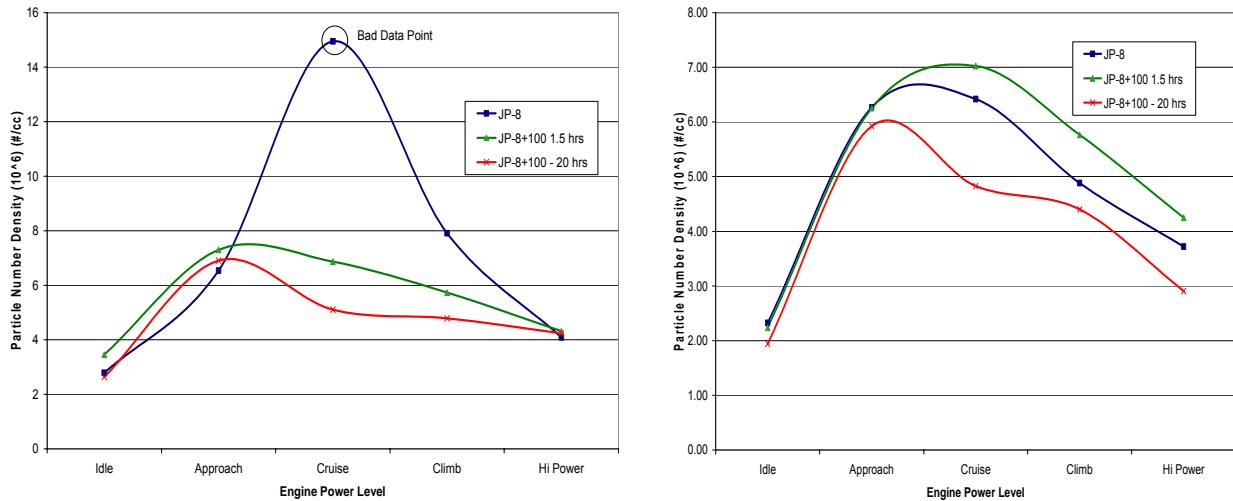
	Engine Power Setting				
	58%	70%	80%	90%	98%
Average JP-8 (#/cm <sup>3</sup> )	20 x 10 <sup>6</sup>	26 x 10 <sup>6</sup>	30 x 10 <sup>6</sup>	44 x 10 <sup>6</sup>	35 x 10 <sup>6</sup>
%error JP-8	11%	11%	11%	6%	28%
Average JP-8+100 (#/cm <sup>3</sup> )	17 x 10 <sup>6</sup>	23 x 10 <sup>6</sup>	26 x 10 <sup>6</sup>	45 x 10 <sup>6</sup>	31 x 10 <sup>6</sup>
%error JP-8+100	18%	17%	20%	21%	12%
%change with additive	<b>-13%</b>	<b>-11%</b>	<b>-14%</b>	<b>2%</b>	<b>-12%</b>

**Table 67. Particle Mean Diameter for T-43 Aircraft Engines Using JP-8 and JP-8+100.**

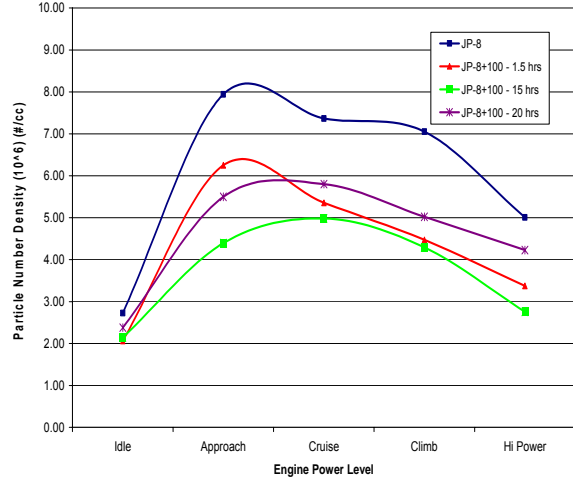
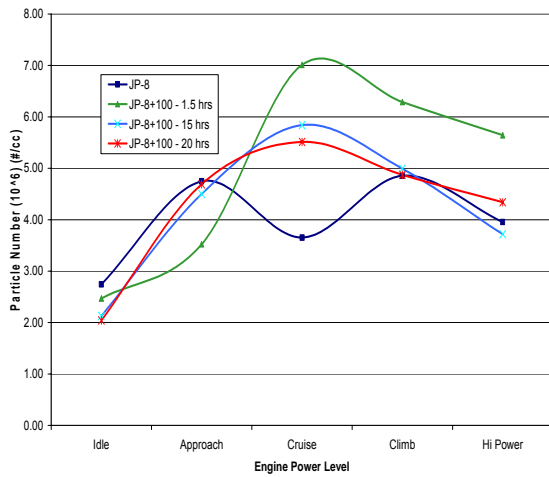
Engine 613				Engine 636			
	Particle Mean Diameter (nm)				Particle Mean Diameter (nm)		
Power level	JP-8	JP-8+100 (20 hrs)	% change	Power level	JP-8	JP-8+100 (20 hrs)	% change
Idle	53.3	55.8	4.6%	Idle	52.0	52.0	0.0%
Approach	68.2	62.3	-8.7%	Approach	70.0	71.0	1.4%
Cruise	82.0	75.0	-8.5%	Cruise	75.0	74.3	-0.9%
Climb	78.0	74.3	-4.8%	Climb	78.0	78.3	0.4%
Hi-Power	83.0	72.8	-12.3%	Hi-Power	83.0	76.7	-7.6%

Engine 608				Engine 607			
	Particle Mean Diameter (nm)				Particle Mean Diameter (nm)		
Power level	JP-8	JP-8+100 (20 hrs)	% change	Power level	JP-8	JP-8+100 (20 hrs)	% change
Idle	50.0	62.8	25.5%	Idle	47.0	58.3	24.1%
Approach	71.0	74.7	5.2%	Approach	62.0	63.0	1.6%
Cruise	74.0	80.3	8.6%	Cruise	71.0	73.0	2.8%
Climb	81.0	80.0	-1.2%	Climb	73.0	74.7	2.3%
Hi-Power	78.0	80.0	2.6%	Hi-Power	66.0	78.0	18.2%



**Figure 192. PND as a Function of Power Setting for T-43 Engines 608 and 636.**



**Figure 193. PND as a Function of Power Setting for T-43 Engines 607 and 613.**

**Table 68. Particle Number Density ( $10^6$ ) for Different Power Settings TF33 Tests II.**

Test Day and Fuel Used	Average or Error (1-Sigma)	58	70	80	90	98
Monday (JP-8 all)	Average	32.9	28.6	30.9	40.2	36.0
Monday (JP-8 all)	Error	38%	59%	64%	49%	66%
Monday (JP-8 first five runs)	Average	27.6	19.6	20.5	29.5	25.2
Monday (JP-8 first five runs)	Error	40%	31%	29%	15%	22%
Tuesday (JP-8 + 100)	Average	23.0	21.7	20.1	25.8	21.2
Tuesday (JP-8 + 100)	Error	15%	16%	25%	17%	15%
Wednesday (JP-8+100)	Average	22.3	19.1	19.1	25.5	20.6
Wednesday (JP-8+100)	Error	7%	7%	7%	5%	10%
Thursday (JP-8+100)	Average	18.6	16.8	16.8	22.2	17.3
Thursday (JP-8+100)	Error	10%	12%	13%	6%	10%

## 4.2 PERFORMANCE CRITERIA

The performance criteria for the demonstration are shown in Table 69. The particle concentration was designated as the only primary criterion because it was considered the most reliable and easier to measure parameter for the demonstration. A 40% or higher reduction was selected to ensure statistical significance based on previous experience. Due to the complexities associated with combustion processes in turbine engines, it was unrealistic to expect a significant reduction in particulate emissions with the additive for all engines and test conditions. Therefore, a 40% or larger reduction in PND for 70% or more of the test conditions was considered reasonable to confirm the reduction in particulate emissions with the additive.

**Table 69. Performance Criteria.**

<b>Performance Criteria</b>	<b>Description</b>	<b>Primary or Secondary</b>
Reduced PM emissions	40% or higher reduction particle number density for 70% for all tests	Primary
Reduced gaseous pollutant emissions	20% reduction in CO, NO <sub>x</sub> and unburned hydrocarbons (UHC) emissions for all test conditions	Secondary
Reduce size of PM	30% reduction in mean particle diameter	Secondary
Reduced amount of PAH	50% reduction in PAH concentration on particulate matter	Secondary
Visibly cleaner engine	Cleaner turbine blades and exhaust	Secondary

**Table 70. Actual versus Expected Performance.**

<b>Performance Criteria</b>	<b>Expected Performance Metric</b>	<b>Performance Confirmation Method</b>	<b>Actual Performance</b>
Reduced PM emissions	Greater than 40% in particle number density for 70% of tests	Average condensation nuclei counter (CNC) measurements and determine uncertainty for each condition	Only one case showed a maximum of 40% reduction in PND.
Reduced gaseous pollutant emissions	20% reduction in CO, NO <sub>x</sub> , and THC for all test conditions	Average gaseous emissions measurements and determine uncertainty for each condition	Additive reduced THC by 15-22% in TF33 & T63 engines. It had statistically insignificant effects on all other gaseous emissions. No effect JT8D engines.
Reduce size of PM	30% reduction in mean particle diameter	Average particle mean size measurements from DMA and determine uncertainty for each condition	Minor reductions in particle mean diameter.
Reduced amount of PAH	50% reduction in PAH concentration on PM	Average concentration of PAHs in particulates and determine uncertainty for each condition	Additive showed no effect on PAH content of particulates.
Visibly cleaner engine	Cleaner hot section/exhaust	Reduced engine maintenance. Compare images (photos) before and after tests (longer term [tenths of hrs] effect)	Engine maintenance could not be assessed due to short-term use of the additive.

## 4.3 DATA EVALUATION

### 4.3.1 TF33 Tests I at Barksdale Air Force Base

#### 4.3.1.1 Particulate Matter Emissions

PND values for the TF33 were generally between  $2.0 \times 10^7$  and  $5.0 \times 10^7$  particles per  $\text{cm}^3$  with and without the additive. As expected, lower PND values were obtained at the lower power setting, which increased as the engine power was increased until the engine setting of 90%. At maximum power (98%), the particulate level decreased to the values of the 80% power, probably due to higher efficiency (improved soot and volatile particle combustion) at the higher power level. The first 40 tests were conducted with JP-8 and showed very good reproducibility (within 15%) at most power settings. Larger errors were observed at high power and when the engine operated on JP-8+100. Engine operation with the additive initially did not appear to impact the particulate emissions. After run number 70 (5 hrs of use of +100), there appeared to be reductions in PND at the 58, 70, and 80% power test conditions; however, a trend of increases in PND at the 90 and 98% conditions were also observed. It is difficult to assess if there was a time dependent effect with the additive (improved emissions as additive was used) since the reduction was observed only during the last three or four run conditions. The PND data, listed in Table 66, show that there was a reduction in PND for four of the five conditions; however, the calculated error (1-sigma) was higher than the observed reduction, rendering the reductions statistically insignificant. Although at the end of the test program the trends showed reductions in PND for the lower power conditions, the lack of sufficient test runs precluded an acceptable statistical analysis with those data. Longer test times were needed to investigate the long-term effects of the additive on particulate emissions. However, these are usually not practical and introduce uncontrollable factors such as different fuels, atmospheric conditions, and even engine wear and tear that can potentially impact emissions and cloud the real effects of the additive.

Particle diameters were in the 60-115 nm range, thus, significantly smaller than  $2.5 \mu\text{m}$  (particulate matter 2.5 microns or less in diameter [PM<sub>2.5</sub>].) As expected, the particle mean size increased as a function of power setting. Slight reductions in particle diameter with the additive were observed for all conditions tested. The largest reduction at 9% in diameter was observed for the idle condition (58%); however, considering the calculated error for each data set, the differences in particle mean diameter between the fuels are considered statistically insignificant.

### 4.3.2 T-43 Tests at Randolph Air Force Base

#### 4.3.2.1 Particulate Emissions

Average values for the PND data for all four engines as a function of power setting and run time are shown in Figures 5 and 6 above. Precision (repeatability) errors for the PND measurements for most tests were 10-20%. All four engines produced similar PND values and trends as a function of power setting. Values of  $2.0\text{-}3.0 \times 10^6$  particles per  $\text{cm}^3$  were observed for the idle condition, while  $4.0\text{-}8.0 \times 10^6$  particles per  $\text{cm}^3$  were common for the mid-power levels. At the higher power setting, the values decreased to  $3.0\text{-}5.0 \times 10^6$  particles per  $\text{cm}^3$  for most conditions. Comparison of particulate emissions between the engines operating with JP-8+100 and the baseline fuel showed no consistent trend. For engine 613, an average reduction of approximately

40% in PND with the +100 additive was observed for all power conditions. Also, significant variation in the PND was observed as a function of time but with no clear trend. For engines 608 and 636, there also appears to be a slight reduction in PND for the engines operating for 20 hrs with the additive; however, there was also an increase in PND for engines 607 and 636 after a 1.5 hour JP-8+100 use. The latter could be the result of increased particulate emissions as the engine was cleaned with the additive; however, these results were inconsistent with all engines and power settings. Longer test times with the +100 additive could have shed light into the additive's long-term effects on emissions.

Listed in Table 67 are the average mean particle diameters for the engines, fuels, and conditions tested. The particle diameter is an important parameter since its relation to mass is to the third power. Mean particle diameters for the four JT8D-9 engines varied from 50 to 83 nm, with the smallest particles at the idle condition and the largest at one of the three highest power settings. The small mean particle diameter at idle may be partly the result of large concentrations of volatile particles resulting from uncombusted or partially combusted jet fuel. Separation of volatile and nonvolatile particles was not performed in this study. For engine 613, reductions in the particle size were observed with the additive for all conditions except idle. For two of the four engines (607 and 608), there were increases in particle size with the additive ranging from 1.6 to 25%, with the largest increases occurring at the low power setting (idle). Negligible changes in particle size were observed for engine 636. From these results, it is clear that the impacts of the +100 additive on engine particulate emissions cannot be generalized since they differ significantly depending on engine and test conditions.

### **4.3.3 TF33 Tests II at Barksdale Air Force Base**

#### **4.3.3.1 Particle Emissions**

Average particle concentration values for each test condition per day with their respective one standard deviation errors are shown in Table 65. The engine was operated with JP-8 for the first 40 test runs and subsequent tests with JP-8+100. A significant increase in PND with the continuous use of JP-8 was observed. This sharp increase in particle loading with JP-8 is not well understood, and it could be due to several factors, including progressive fouling of fuel nozzles, slight differences in engine operating conditions, changes or uncertainties in dilution flows, unknown instrumentation artifacts, or a combination of these. Addition of the +100 additive appeared to have reduced the PND to their original levels with JP-8. Subsequent use of JP-8+100 increased particulate emissions which then stabilized to values between  $15.0 \times 10^6$  to  $25.0 \times 10^6$  for all the conditions tested.

The effects of the additive on particulate mass were insignificant at the lowest three power settings. At full power, there appeared to be an increase in particulate mass with the additive; however, a T-test analysis revealed that it was statistically insignificant. The only power setting that showed statistically significant reductions in particle mass sample averages was at the 90% setting. Approximately 30% reduction in particulate mass emissions was observed at the 90% condition.

#### **4.3.4 T63 Tests at Wright-Patterson Air Force Base**

##### **4.3.4.1 Particle Emissions**

PND data as a function of test time for the cruise condition during the long-duration T63 tests show that the PND increased by nearly 50% from 13 to 48 hrs of operation with JP-8. This is believed to be the result of fuel nozzle fouling, which potentially caused non-uniform fuel spray and eventual degradation of the combustion performance. Continuous use of the baseline fuel did not further degrade/increase engine particulate emissions. After 87.5 hrs of test time, JP-8+100 was used. The +100 additive did not effect a change in PND until after 40 hrs of use in which a marginal reduction of 15% was observed. Further use of the additive had negligible effect on the PND.

The particle size distributions show that the mean particle diameters for the baseline and +100 fuels were very similar for all test runs. The concentration of particles peaked at the 88 hr mark and decreased slowly with use of the additive. Consistent with the PND data, negligible differences were observed between the 129- and 175-hr size distribution and trends, thus no changes in mass occurred during this time period.

#### **4.4 TECHNOLOGY COMPARISON**

As discussed in Section 4.1, Performance Data, the impact of the +100 additive on engine emissions is highly dependent on engine condition and technology. However, for most test cases evaluated, the +100 additive was ineffective in reducing particulate matter emissions relative to JP-8. Long-term evaluations of the additive are recommended to assess its ability to keep fuel nozzles and other engine components clean, in order to quantify the effects of a potentially cleaner engine on emissions.

*This page left blank intentionally.*

## 5.0 COST ASSESSMENT

### 5.1 COST REPORTING

The operational costs for the +100 additive conversion of the T-43 and B-52 aircraft at Randolph AFB and Barksdale AFB, respectively, are mostly due to the cost of the additive. All other potential costs are considered relatively low. A summary of these operational and the implementation costs is presented in Table 71.

**Table 71. +100 Additive Operational and Implementation Costs for T-43 and B-52 Aircraft.**

Aircraft/Air Force Base	Direct Costs			
	Start-Up		Operation and Maintenance	
	Activity	\$ Dollars	Activity	\$ Dollars
T-43/Randolph AFB	Additive Injection System	\$ -	*Additive per yr (Based on 3.6 million gallons JP-8)	\$18,200
	Defuel Trucks			
	Additive Storage Tanks	\$15,000		
	Installation	\$ -		
	<b>Total</b>	<b>\$15,000</b>		<b>\$18,200</b>
B-52/Barksdale AFB	Training Operators	\$6,000	*Additive per yr (Based on 41.6 million gallons JP-8)	\$208,000
	Additive Injection System	\$52,500		
	Defuel Trucks	\$145,000		
	Storage Tanks & Misc	\$15,000		
	Site Verification	\$11,250		
	Installation	\$21,000		
	Travel & Mobilization	\$13,000		
	<b>Total</b>	<b>\$263,750</b>		<b>\$208,000</b>

\*Additive cost based on average annual fuel consumption multiplied by \$0.005 per gallon JP-8 fuel.

### 5.2 COST ANALYSIS

Based on experience with fighter and cargo aircraft presently using the +100 additive, reduced coking of fuel nozzles and therefore reduced engine maintenance due to fuel nozzle and combustor anomalies are expected with the use of the additive. However, for this demonstration the aircraft or engines were operated with the additive for only 1 week, which did not allow a long-term (several years) assessment on the maintenance benefits of the additive. Since these benefits are highly dependent on engine type and operation, it is impossible to properly estimate potential cost savings in maintenance (e.g., time between engine overhauls) and increased engine life caused by the additive without a long-term study. Since consistent benefits in emissions were not observed in this program, the additive appears to offer no cost benefits in these platforms.

### **5.2.1 Implementation Costs for B-52 Aircraft at Barksdale AFB**

A study conducted by Mr. Ozzie Pinkham of C4e Inc. (on contract with AFRL/PRTG) identified four options for the implementation of the +100 additive at Barksdale AFB for use in the B-52 aircraft. Options and associated costs are described in Appendix A of the final report.

### **5.2.2 Implementation Costs for T-43 Aircraft at Randolph AFB**

Based on discussions with base officials, there is no cost for implementation of the +100 additive on the T-43A trainer aircraft at Randolph AFB. Since the base already operates smaller trainers (e.g., T-37s and T-38s) with JP-8+100, the infrastructure required to support the additive use in the T-43 aircraft (additive injection carts, refueler trucks, etc.) is already in place. Costs associated with the increased workload as the result of additive injection are expected to be minimal. An additional defueling truck might be required to facilitate the aircraft defuels. The use of the additive may actually simplify on-base defueling operations since there will no longer be a need to have separate defueling tanks for JP-8 and JP-8+100. Details on the implementation of the additive for T-43 planes at Randolph AFB are discussed in Appendix B of the final report.

## **5.3 COST COMPARISON**

As previously mentioned, use of the +100 additive on these platforms is expected to provide benefits on reduced engine maintenance due to cleaner fuel nozzles and hot section parts. These benefits, however, could not be demonstrated in this program due to the short duration of the demonstration. Benefits in emissions were inconsistent and highly dependent on engine and engine condition. Since benefits were not observed in this study, a cost comparison of the +100 additive with conventional technologies (e.g., engine retrofits) is not warranted.

## **6.0 IMPLEMENTATION ISSUES**

### **6.1 COST OBSERVATIONS**

The relatively low cost of the additive at \$0.005 per gallon of fuel is expected to decrease due to increased additive production if used in these and other cargo or bomber aircraft.

### **6.2 PERFORMANCE OBSERVATIONS**

Detailed performance observations are discussed in Section 4.

### **6.3 SCALE-UP**

Full-scale implementation of the +100 additive on the T-43 or B-52 aircraft will require approval from the aircraft manufacturer, SPO, and base and/or unit commander. The implementation costs listed in Table 68 are estimates based on previous experience on implementing the additive at other bases.

### **6.4 OTHER SIGNIFICANT OBSERVATIONS**

Technical challenges, mostly associated with the additive disarming of filter coalescers, will adversely affect the implementation of this additive on any large aircraft. More details are provided in Section 2.4. Implementation of newly developed filter coalescers should alleviate most of these concerns.

### **6.5 LESSONS LEARNED**

Although the effects of the +100 additive on engine particulate emissions were inconsistent, the additive was observed to have no detrimental effect on the emissions or performance of the engines tested. Longer duration tests are required to determine the potential of the additive to reduce engine maintenance and prevent degradation of engine emissions.

### **6.6 END-USER/ORIGINAL EQUIPMENT MANUFACTURER (OEM) ISSUES**

A study conducted by C4e Inc. to investigate the feasibility of converting the existing fleet of T-43A aircraft at Randolph AFB to JP-8+100 was completed. The study showed that defueling operations with this aircraft were not a major issue since defuels were minimum and usually occurred on station. Therefore, there appear to be no major issues to the implementation of the additive in the T-43. However, further coordination and acceptance from the aircraft SPO and Boeing will be required before the AETC grants the approval to convert the T-43 fleet to use the +100 additive.

Implementation of the +100 additive on the B-52 is more challenging since the aircraft lands in bases not equipped to handle the additive. High blend back ratios (currently set at 100 gallons JP-8 per gallon of JP-8+100) have been established to prevent the filter problems. This complicates the implementation of the additive in locations not equipped (e.g., defuel tanks and refueling trucks) to handle these highly demanding defueling and blending operations. Additive

implementation on the B-52 will need to be approved by the airframer (Boeing), the Air Force Petroleum Office (AFPET), the B-52 SPO, and base officials.

Based on this demonstration, the increased cost and logistics burden associated with using the +100 additive in these platforms cannot be justified since no clear (or sufficient) benefits in emissions were observed. However, a more extensive program should be established on these aircraft to study the potential benefits of the additive on reduced engine maintenance, as has been observed in other platforms.

## **6.7 APPROACH TO REGULATORY COMPLIANCE AND ACCEPTANCE**

Based on the results from this demonstration, the +100 additive will not greatly influence the PM emissions from turbine engines and therefore will not help meet regulatory requirements for particulate matter. Additional research is recommended for the assessment of the additive on unburned hydrocarbons since reductions in these volatile organic compounds (VOC) were observed in two types of engines.

## 7.0 REFERENCES

1. Corporan, E., and O. Monroig. "Reduction of Particulate Emissions in Turbine Engines Using the +100 Additive," Final Report - ESTCP Project No. PP-200121, June 2005.
2. Corporan, E., M.J. DeWitt, O. Monroig and M. Wagner. "Influence of Fuel Chemical Composition on Particulate Matter Emissions of a Turbine Engine," GT2004-54335, Proceedings of ASME Turbo Expo 2004, Vienna, Austria, 2004.
3. Dockery, D. W., J. H. Ware, B. G. Ferris, Jr., F. E. Speizer, N. R. Cook, and S. M. Herman. "Change in Pulmonary Function in Children Associated with Air Pollution Episodes," *J. Air Poll. Control Assoc.* 32:937-942, 1982.
4. Environmental Protection Agency. EPA's Revised Particulate Matter Standards. <http://www.epa.gov/ttn/oarpg/naaqsfm/pmfact.html>, July 17, 1997.
5. Harrison III, W.E., "Aircraft Thermal Management: Report of the Joint WRDC/ASD Aircraft Thermal Management Working Group," WRDC-TR-90-2021, February 1990
6. Heneghan, S.P., S. Zabarnick, D.R. Ballal, and W.E. Harrison III. "JP-8+100: The Development of High-Thermal-Stability Jet Fuel," *Journal of Energy Resources Technology*, Vol. 118, pages 170-179, September 1996.
7. Howard, R. P. et al. "Experimental Characterization of Gas Turbine Emissions at Simulated Flight Altitude Conditions," AEDC-TR-96-3, September 1996.
8. Kalt, D.H., S. Zabarnick, S.D. Anderson, and P.D. Liberio. "Fuel and Fuel System Materials Compatibility Test Program for a JP-8+100 Fuel Additive Package," AFRL Tech Report No. AFRL-PR-WP-TR-2000-2021, March 1999.
9. Kinkead, E.R., R.E. Wolfe, M.L. Feldmann, H.F. Leahy, and W.W. Jederburg. "Acute Toxicity Evaluation of JP-8 Jet Fuel and JP-8 Jet Fuel Containing Additives," AFMC Tech Report No. AL/OE-TR-1996-0136, February 1996.
10. Landau, M., et al. "Jet Aircraft Engine Exhaust Emissions Database Development—Year 1990 and 2015 Scenarios," NASA Contractor Report 4613, July 1994.
11. Lippmann, M., and P. J. Liroy. "Critical Issues in Air Pollution Epidemiology," *Envir. Health Perspec.* 62:243-258, 1985.
12. Liscinsky, D.S., M.B. Colkett, D.J. Hautman, and B. True. "Effect of Fuel Additives on Particle Formation in Gas Turbine Combustors," AIAA 2001-3745, AIAA Joint Propulsion Conference 2001.
13. Niedzwiecki, R. "Aircraft Technology and its Relation to Emissions," Chapter 7 of Report of The Intergovernmental Panel on Climate Change, IPCC, 1998.

14. SAE AIR 5892 “Nonvolatile Exhaust Particle Measurement Techniques,” SAE Publications, Society of Automotive Engineers, 2004.
15. Schwartz, J., “Particulate Air Pollution and Chronic Respiratory Disease,” Environ. Research 62:7, 1993.
16. Thompson, A. M., “Atmospheric Effects of Aviation: First Report on the Subsonic,” NASA Reference Publication 1385, 1996.
17. Universal Technology Corporation (UTC) and C4e, Inc., “Study of JP-8+100 Impact on C-130 Aircraft at 123 AW, KY ANG,” September 2000.
18. Wilson R., and J. Spengler. “Particles in Our Air Concentrations and Health Effects,” Harvard University Press, 1996.

## APPENDIX A

### POINTS OF CONTACT

<b>Point of Contact Name</b>	<b>Organization Address</b>	<b>Phone/Fax/E-Mail</b>	<b>Role in Project</b>
Edwin Corporan	AFRL/PRTG 1790 Loop Road, N WPAFB, OH 45433	edwin.corporan@wpafb.af.mil	Principal Investigator
Keith O. Legg	Rowan Technology Group 1590 South Milwaukee Ave, Suite 205 Libertyville, IL 60048	Phone : (847) 680-9420 Fax: (847) 680-9682 klegg@rowantechnology.com	
Orvin Monroig	AFRL/PRTG 1790 Loop Road, N WPAFB, OH 45433	orvin.monroig@wpafb.af.mil	Co-principal Investigator
Bruce D. Sartwell	Naval Research Laboratory Code 6170 4555 Overlook Avenue, SW Washington DC	Phone: (202) 767-0722 Fax: (202) 767-3321 sartwell@nrl.navy.mil	
Phil Whitefield	University of Missouri-Rolla G-7 Norwood Hall 1870 Miner Circle Rolla, MO 65409-0430	pwhite@umr.edu	Aircraft Particulate Measurements

*This page left blank intentionally.*